2013-02-20

Field studies of snowpack stress and deformation due to surface loads and temperature effects

Exner, Thomas

Exner, T. (2013). Field studies of snowpack stress and deformation due to surface loads and temperature effects (Unpublished doctoral thesis). University of Calgary, Calgary, AB.
doi:10.11575/PRISM/16284
http://hdl.handle.net/1880/49416
doctoral thesis

UNIVERSITY OF CALGARY

Field studies of snowpack stress and deformation due to surface loads and temperature effects

by

Thomas Exner

A THESIS
SUBMITTED TO THE FACULTY OF GRADUATE STUDIES
IN PARTIAL FULFILMENT OF THE REQUIREMENTS FOR THE
DEGREE OF DOCTOR OF PHILOSOPHY

DEPARTMENT OF GEOSCIENCE

CALGARY, ALBERTA

APRIL, 2012

Abstract

Snow surface loads such as skiers and snowmobiles are the triggers of the slab avalanche in many avalanche accidents. In most cases a cohesive slab overlies a weaker layer. Slab avalanche release strongly depends on stresses reaching the weak layer. Daytime snow temperature changes also can have a substantial impact on the release process of natural and human-triggered slab avalanches. Daytime variations of the near-surface layers affect the stiffness and the creep of the upper snowpack on a slope.

For this study, a method was developed to measure normal stresses in the snowpack due to surface loads. These surface loads were skiers and snowmobiles in field experiments and metal weights in cold lab experiments. During the outdoor skier stress experiments and the cold lab studies the effect of warming and cooling of the near-surface layers and the effect on normal stress distribution was investigated. The impact of daytime heating of the near-surface layers on snowpack creep was monitored in field experiments.

Overall, normal stresses due to surface loads penetrated deeper into the snowpack with warming of the near-surface layers or decreasing layer stiffness. Snowmobiles affected the snowpack over a larger area and stresses penetrated the snowpack deeper than for skier loads. In the case of the skier loads the bending of the skis appeared to have a considerable effect on the normal stress distribution. Creep of the near-surface layers accelerated with solar daytime warming and also affected layers below the warming front.

Acknowledgements

First of all I would like to express my sincere gratitude to my supervisor and mentor, Bruce Jamieson, whose guidance majorly contributed to this thesis. Bruce allowed all the freedom and flexibility that was needed and his much-appreciated support was always at hand whenever required.

For their tireless effort collecting the field data, their friendship and company I am grateful to my fellow graduate students, field technicians and all others who assisted with field work: Dave Gauthier, Catherine Brown, Cora Shea, Mike Smith, James Floyer, Cam Ross, Laura Bakerman, Catherine Johnston, Willy Rens, Jordan Stiefvater, John Freeman, Christoph Hummel, Jacqui Coward. For assisting with data analysis of the snowpack creep experiments I would like to thank Kisa Elmer.

The Avalanche Control Section at Glacier National Park provided valuable field support and guidance. Many thanks to Bruce McMahon, Jeff Goodrich, Eric Dafoe, Johann Schleiss, Jim Phillips, Dean Flick, Mark Harrison, Luc Beaulieu. Additionally, I would like to extend my gratitude to Mike Wiegele and his staff at Mike Wiegele Heli-Skiing for fieldwork support at the Blue River field station.

Numerous guides and avalanche forecasters kindly shared their knowledge and experiences on warming related avalanches. Thanks a lot for this invaluable practical input.

Thanks are also due to the staff at the Engineering Machine Shop at the University of Calgary for their help to design and build field equipment.

For proofreading and reviews of the manuscript, which certainly helped to improve its quality, I am grateful to Bruce Jamieson, Masaki Hayashi, Shawn Marshall, Tom Brown, Howard Conway, Mike Smith, Cora Shea, Jacqui Coward, Mike Conlan, Ryan Buhler, Scott Thumlert, Sascha Bellaire, Carola Weber and Tanis Marshall.

For financial support, I am indebted to the Natural Sciences and Engineering Research Council of Canada, HeliCat Canada, the Canadian Avalanche Association, Mike Wiegele Helicopter Skiing, Teck Mining Company, Canada West Ski Areas Association, the Association of Canadian Mountain Guides, Backcountry Lodges of British Columbia, and the Canadian Ski Guides Association.

Bruce Edgerly and team from Backcountry Access generously supported our field work with avalanche safety and backcountry gear.

Special thanks to Ron, Karin and Louis for their friendship, great support and encouragement during overwhelmingly busy office hours and the final stages of this thesis. Jacqui, thanks for sharing your time and love, and your encouragement.

Last but not least my cordial gratitude goes to my parents and brother for their understanding and great support during all my endeavours in live.

Table of Contents

List of Tables

List of Figures

List of Symbols and Abbreviations

2D	Two dimensional
ASARC	Applied Snow and Avalanche Research University of Calgary
CAA	Canadian Avalanche Association
FEM	Finite element model
HSL	Hard slab
ICSSG	International Classification of Seasonal Snow on the Ground
n/a	Not available
SSL	Soft slab
WL	Weak layer

General

C	Capacitance
d	Spacing between capacitor plates
V	Voltage
P	Point on snow profile
Q	Activation energy
R	Gas constant
x	Horizontal distance
z_n	Snow depth at point P_n
z_{n+1}	Snow depth at point P_{n+1}
α	Deformation angle
γ	Constant

Skier stress

BI	Skier bending index
ΔBI	Change of BI during warming/cooling
SP	Ski penetration under the centre of the ski boot
SP_{Tip}	Ski penetration under the ski tip
SP_{Tail}	Ski penetration under the tail of the ski
z_{eff}	Actual depth of stress sensor below ski factoring in ski penetration and compaction

Snowpack

HS	Total snowpack height
t	Duration of temperature event
T_{max_surf}	Max. snow temperature (beginning of cooling or end of warming) at snow surface

T_{max10}	Max. snow temperature (beginning of cooling or end of warming) at 10 cm snow depth
T_{min_surf}	Min. snow temperature (beginning of warming or end of cooling) at snow surface
T_{min10}	Min. snow temperature (beginning of warming or end of cooling) at 10 cm snow depth
z	Snow depth (vertical)
ΔHS	Settlement
$\Delta HS/\Delta t$	Settling rate
ΔT_{10}	Snow temperature increase/decrease during warming/cooling at 10 cm snow depth
$\Delta T_{10}/\Delta t$	Warming/cooling rate at 10 cm snow depth
ΔT_{surf}	Snow temperature increase/decrease during warming/cooling at snow surface
$\Delta T_{surf}/\Delta t$	Warming/cooling rate at snow surface
ρ	Snow density
φ	Slope angle (against horizontal)

Mechanical properties and fracture mechanics of slab and weak layer

a_c	Critical crack size (shear model)
E	Youngs modulus
E'	Effective stiffness/modulus
G'	Shear modulus
G_{II}	Fracture energy in shear
G_o'	Reference shear modulus
H	Slab thickness (slope normal)
h	Slab thickness
K_{Ic}	Fracture toughness (critical stress intensity) in tension
K_{IIc}	Shear fracture toughness (critical stress intensity) in shear
r_c	Critical crack size (collapse bending wave model)
v_{lp}	Slope parallel component of snowpack creep
w_f	Specific fracture energy
γ	Shear strain
$\dot{\gamma}$	Shear strain rate
ν	Poisson ratio
σ	Normal stress
σ_{10}	Normal stress at 10 cm snow depth
σ_{40}	Normal stress at 40 cm snow depth

σ_{init}	Normal stress at beginning of warming or cooling
σ_o	Normal stress at surface below surface load
τ	Shear stress
$\dot{\tau}$	Shear deformation rate
τ_g	Bulk shear stress ('far field' stress)
τ_p	Peak shear stress at perimeter of (imperfection/flaw)
τ_r	Residual shear stress

Snow surface energy balance

G	Ground heat flux
H_S	Sensible turbulent heat flux
H_L	Latent turbulent heat flux
H_P	Energy flux due precipitation and blowing snow
$L\downarrow$	Incoming short-wave radiation
$L\uparrow$	Outgoing short-wave radiation
$S\downarrow$	Incoming long-wave radiation
$S\uparrow$	Outgoing (reflected) long-wave radiation
T_{avg}	Average snow temperature
T_{surf}	Snow temperature at snow surface
T_{10}	Snow temperature at 10 cm depth
T_{20}	Snow temperature at 20 cm depth
T_s	Snow temperature
T_a	Air temperature
T	Temperature of slab
T_s	Sensor temperature

Snowpack creep

Δc	Total snowpack creep
Δs	Slope parallel displacement
Δv	Difference of slope parallel displacement speed between two layers
Δx	Horizontal displacement
Δz	Vertical displacement
v_n	Layer-parallel component of creep speed at point P_n
v_{n+1}	Layer-parallel component of creep speed at point P_{n+1}
v_{lp}	Layer-parallel displacement speed

Statistics and error analysis

a	Coefficient of fits functions

b	Coefficient of fits functions
c	Coefficient of fits functions
d	Coefficient of fits functions
n	Sample size
r	Pearson linear correlation coefficient
r_s	Spearman rank correlation coefficient
SE	Standard deviation
R^2	Coefficient of determination
SSE	Sum of squares due to error
e_{conv}	Error due to conversion of voltage to stress
e_{tcorr}	Error due to temperature correction
e_{avg}	Error due to averaging the stress signal
e_z	Error due to manual measurement of sensor depth
e_{tot}	Total error

CHAPTER 1

Introduction

Every year winter puts a blanket of snow over large populated areas in mountain landscapes all over the world. This brings great enjoyment to many winter enthusiasts, but also can cause dangerous snow avalanche conditions threatening property, infrastructure and lives. Worldwide, avalanches claim the lives of more than 350 people per year (ICAR, 2010; Podolskiy and others, 2009). The majority of avalanche accidents in the western world, most of which occur in North America and Europe, are due to recreational activities. In other parts of the world, where avalanche risk mitigation programs are less developed, for example in parts of South America and Asia, larger catastrophic avalanches are still the main cause for the loss of lives and damage to infrastructure of dwellings and work places (Podolskiy and others, 2009; Gallardo, 2003).

Snow avalanches do not pose the same threat as other natural disasters, such as floods, earthquakes, tropical storms, droughts, and volcanic hazards in terms of the number of people affected and direct costs (McClung and Schaerer, 2007, p. 14). Those catastrophic events are rare, sometimes unforeseen and unavoidable. In heavily populated areas of the European Alps and parts of North America, where winter tourisms is a major economical factor, the threat of snow avalanches as the major frequent natural hazard, needs to be dealt with on almost a daily basis during the winter months.

In Canada, the average number of deaths due to avalanches rose in recent years to 15 per year due to rapidly rising numbers of recreational winter backcountry activities (Jamieson and Stethem, 2002). In British Columbia, the direct revenue of the helicopter and cat ski industry alone is approximately $100 million per year (HeliCat Canada, 2002), which makes for approximately a third of the downhill ski industry. The average estimated costs for avalanche risk mitigation measures in Canada, mostly for transportation corridors, are approximately $12 million per year (Jamieson and Stethem, 2002).

Some of the factors that contribute to avalanching such as large new snow amounts and the redistribution of snow due to strong winds are fairly obvious and can be recognized with a small amount of awareness. Others are more subtle and not as easy to recognize, but can tip the balance from an enjoyable day in the mountains to an avalanche tragedy. Deteriorating avalanche conditions due to daytime warming of the snowpack is one of those subtle changes, which can be hard to recognize. de Quervain (1966) described the effect of temperature on snowpack stability as one of the most challenging aspects of avalanche forecasting.

In many cases, the conditions that led to an avalanche accident were foreseeable and most avalanche victims triggered the avalanche themselves (Jamieson and others, 2010, p. 31). Thus, the release of an avalanche is not a random event, although, the complex interaction of snowpack and weather conditions are at times very difficult to interpret. In most countries, where backcountry recreation in avalanche terrain has gained popularity, public avalanche forecasting services provide valuable information to make backcountry users aware of current avalanche conditions. An effective avalanche forecast requires a sound theoretical background and extensive practical experience. According to Hogarth (2001) avalanche terrain can be described as a ‘wicked’ learning environment, since feedback is not always immediate; however, it can be fatal when it is. Therefore, it is in the best interest of all winter backcountry users to be able to make informed decisions before enjoying the great many benefits of the mountains in the winter.

This thesis aims to enhance the understanding of the slab avalanche release process and to assist avalanche professionals and recreationists alike in their decision-making processes. In particular, the focus of this thesis is on the impact of skiers and snowmobiles on the snowpack as potential slab avalanche triggers and the effects of (daytime) snowpack warming and cooling on the slab avalanche release process.

1.1 Overview of thesis chapters

Sections 1.2 to **1.7.** provide an overview of necessary background knowledge for the comprehension of this thesis, such as general properties of snow as a material, the energy balance of the snow surface with respect to important warming sources, and an overview of the state of the art of slab avalanche fracture mechanics. The specific goals and objectives of the thesis are outlined in **Section 1.8.** The current state of knowledge of the interaction of (daytime) snowpack temperature changes and snowpack stability, and the additional stress distribution due to surface loads is reviewed in **Chapter 2**. Field methods for snow characterization and general methods for data analysis are introduced in **Chapter 3**. Field methods and analyses procedures that only apply for specific experiments are described in the methods sections of the appropriate chapter. The stress measurement technique, which was developed for this thesis and applied for the skier, snowmobile and cold lab experiments is introduced and evaluated in **Chapter 4**. **Chapter 5** analyses the stress distribution under skiers and its changes due to temperature variations in field experiments. The dynamic impact on the snowpack of snowmobiles, in comparison to skier loads is investigated in **Chapter 6.** The effect of temperature variations on the stress distribution due to surface loads (metal weights) is examined under controlled experimental conditions in cold lab studies in **Chapter 7**. **Chapter 8** explores the effect of solar warming on creep of the near-surface layers of the snowpack in field studies using time-lapse photography. **Chapters 9** summarises the findings of this thesis and puts them into perspective for practical applications and points out the limitations of these studies. It also provides an outlook for further investigation on this topic.

1.2. Basic properties of snow

Snow is a fascinating material with unique properties, which are different from those of most other materials. Mellor (1975) stated ‘there is no material of engineering significance that displays the bewildering complexities of snow’. More recent studies confirmed the uniqueness of snow as a material. For example, Kirchner and others (2002) concluded ‘with its extraordinary low values of K_{Ic} and K_{IIc} (fracture toughness in tension and shear) snow is one of the most brittle materials known to man’. Below, some of the characteristics of deposited seasonal alpine snow, which are relevant for this thesis, are introduced.

Highly porous: The smaller portion of the volume of snow consists of a solid ice matrix. The remainder is pore space filled with air and water vapour. Depending on snow density, typically between 30 and 550 kg m^{-3} for dry snow, the porosity of snow ranges from approximately 40 to 97 % of the snow volume (McClung and Schaerer, 2006, p. 75). This is the reason why the description of snow with theories for solid materials is limited. More recent studies treated snow as a foam of ice (Kirchner and others, 2001) or a bonded granular material (McClung, 1981), which is likely closer to the real structure of snow as a material. The number and size of inter-granular bonds within the ice matrix basically determine mechanical and thermal properties of snow.

Visco-elastic, rate dependent deformation: Since the matrix material of snow is ice, the mechanical properties of ice also qualitatively apply, but on a different scale. For example, the tensile strength and fracture toughness of ice are approximately 100 times greater than those of snow at densities around 200 kg m^{-3} (Petrovic, 2003). The deformation of ice basically comprises three processes (Sinha, 1978), which also describe the rheological behaviour of snow in a similar way (Chandal and others, 2007):

(1) Direct elastic deformation (*independent of temperature* and *recoverable)*

(2) Delayed elastic deformation (*highly temperature dependent* and *recoverable*)

(3) Viscous flow (also *highly temperature dependent* but *irreversible*)

The deformation behaviour of snow strongly depends on strain rate. Small strains at fast strain rates usually lead to elastic deformation and eventually to

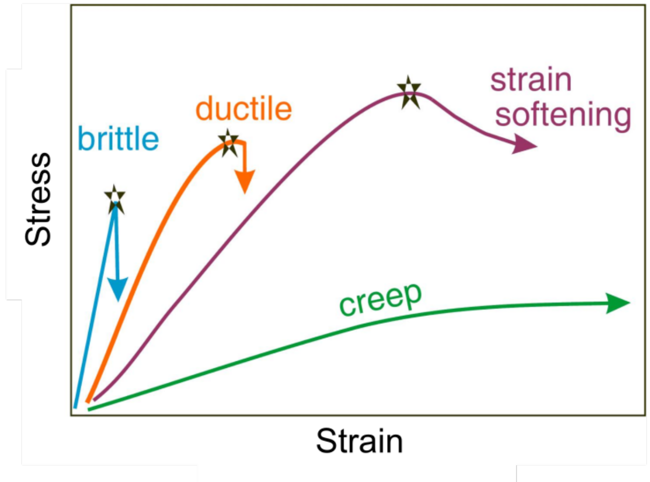

Figure 1.1. Deformation behaviour of snow **(**After Schweizer and others, 2003)

brittle fracture (Figure 1.1). Slower strain rates allow larger deformation, which is usually viscous (ductile) due to rearrangement of the matrix of the ice material. The transition from brittle to viscous (ductile) behaviour takes place at strain rates of approximately 10^{-4} to 10^{-3} s^{-1}. (Fukazawa and Narita, 1993; Schweizer, 1998). At the strain rates at which snow exhibits strain softening, snow still fails from an engineering point of view (peak on the stress strain curve). During strain softening, with increasing deformation, stress decreases to a residual value (Figure 1.1). Fracture does not occur in this case, which can be explained by the rate of breaking and re-welding of bonds in the ice matrix. Creep occurs at strain rates below those of the strain softening case. Snow is also referred to as a quasi-brittle material, implying a small zone of mostly elastic deformation until brittle fracture for high strain rates. Most concepts to explain fracture propagation treat snow as a linear elastic (brittle) material (Sigrist, 2006, p.15-33). Presumably, fracture processes during propagation happen well above the ductile to brittle transition. For other applications, such as failure initiation in direct action avalanches, and settlement and densification (creep), snow is regarded as a viscous (ductile) material. Furthermore, the failure strength also depends on deformation rate. From slow (10^{-7} s^{-1}) to fast (10^{-2} s^{-1}) deformations, failure strength decreases by a factor of 10 (Schweizer, 1998). Fast deformation rates are reached for example due to rapid skier loading; gradual loading due to accumulating new snow causes slow deformation rates.

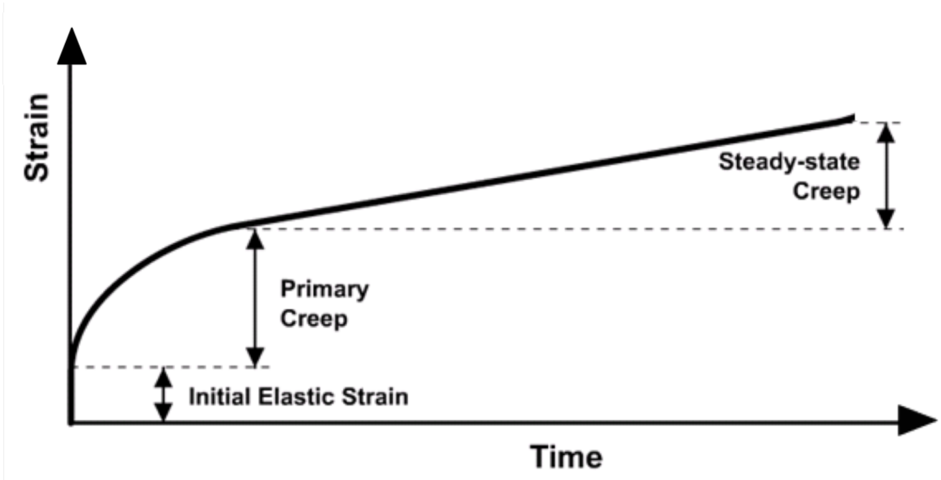

Figure 1.2. Schematic of creep behaviour of snow (After Chandal and others, 2007).

Snow creep, at slow strain rates, similarly to the deformation behaviour of ice exhibits the same stages of deformation: initial elastic strain, primary creep (delayed elastic), and steady state creep (viscous) (Figure 1.2). Usually, strain rates for snow creep are well below those for ductile to brittle transition. Nevertheless, during the onset of creep (elastic strain and primary creep) at high temperatures (close to the melting point) strain rates are considerably higher. This and stress concentration at a layer interface with different stiffness may lead to ductile to brittle transition (Habermann and others, 2008). Secondary or steady state creep usually leads to settlement and strengthening of the snowpack.

High temperature material: Considering that the absolute temperature of seasonal snow is mostly within 5 – 10% below its melting point (273.2 K), snow is considered and shows characteristics of a high temperature material – thermodynamic and diffusion processes gain importance close to the melting point (Spear and others, 2010). In particular, in snow with its high porosity those processes become extremely important for snow metamorphism when temperatures approach the melting point. Additionally, at temperatures above approximately -5 to -7˚C pre-melting phenomena, such as grain boundary slip affect the mechanical properties of snow (Petrenko and Witworth, 1999). The temperature dependence of the mechanical properties of snow is reviewed in more detail in Section 1.3.

Metamorphism: As soon as snow deposits on the ground it undergoes constant changes. Creep (settlement and densification) rearranges the number and size of bonds (McClung and Schaerer, 2006, p. 75). Since the snowpack is almost always subjected to a temperature gradient, between the ground and the snow surfaces, vapour transport processes constantly change the matrix of the ice material. Usually, at vertical temperature gradients of approximately less than 5 to 10 $^{\circ}C\,m^{-1}$ rounding (equilibrium metamorphism) increases strength and density (Colbeck, 1997; Armstrong and Brun, 2008, p. 29). At higher temperature gradients faceting (kinetic growth metamorphism) occurs which can cause of loss of strength (McClung and Schaerer, 2006, p. 57). The increasing number and size of bonds due to pressure sintering is an important, rapid, process when snow is subjected to external surface loads or more load due to precipitation (Szabo and Schneebeli, 2007).

Good insulator: Snow is an excellent thermal insulator due to its low thermal conductivity. Most of the heat is transported through the ice lattice. The thermal conductivity of ice at -10˚C is approximately 2.3 $W\,m^{-1}\,K^{-1}$ and that of air, which takes up most of the volume of snow, only 0.023 $W\,m^{-1}\,K^{-1}$ – two orders of magnitude less (Sturm and others, 1997). Due to the low thermal conductivity surface warming only slowly penetrates the near-surface layers of the snowpack. Usually, daytime warming only affects the top 20 – 30 cm. The main contribution, however, to warming of the near-surface layers is due to absorption of short wave radiation (see Section 1.7). Typical values for the effective thermal conductivity of snow, for a density range of 150 – 300 $kg\,m^{-3}$, are approximately 0.1 – 0.3 $W\,m^{-1}\,K^{-1}$ (Sturm and others, 1997).

1.3 Slab avalanche release

Generally, avalanches are masses of falling snow, ice, soil or rock. Depending on their type of release, snow avalanches can be classified as loose snow and slab avalanches (McClung and Schaerer, 2007, p. 73). Loose snow avalanches start at

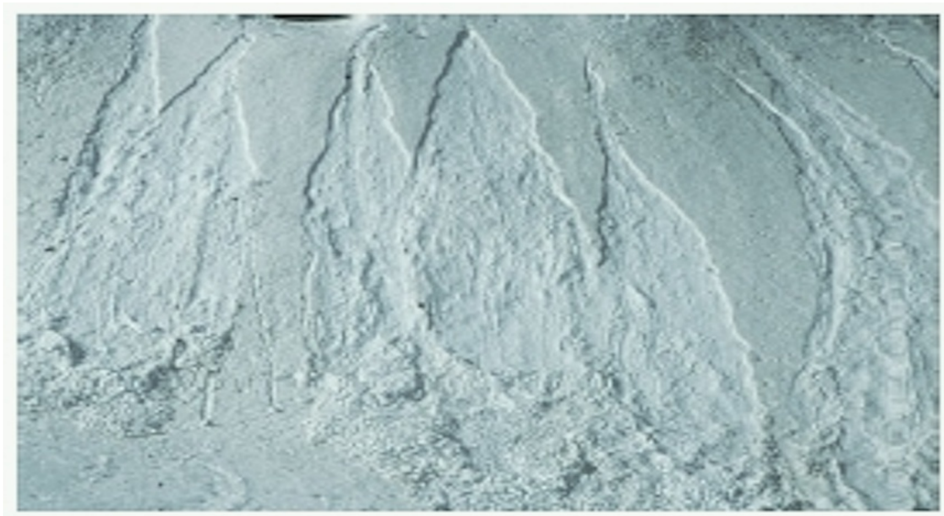

Figure 1.3. Loose snow avalanches with characteristic point releases. (Photo: www.slf.ch)

the snow surface in snow of low cohesion and can be either dry or wet (Figure 1.3). They rarely reach a size and mass that is dangerous to backcountry users. Most human triggered recreational avalanches and also most large catastrophic avalanches are dry slab avalanches, where a large cohesive block (slab) of snow detaches from the surrounding snowpack and glides downward (Figure 1.4). This thesis is concerned with dry slab avalanches.

1.3.1 Ingredients of a slab avalanche

Layered snowpack: The seasonal snowpack is usually characterized by its layered structure that reflects the various influences of weather and terrain characteristics. Observations show that slab avalanches almost always fracture at an interface between two adjacent layers with different properties, such as grain size and type, density and hardness (Schweizer, 1993; Colbeck, 1991). In most cases, a cohesive slab overlies a weaker layer with poor bonding and low strength, where fractures can occur and propagate (Figure 1.5).

Slope angle: Dry slab avalanches occur most frequently between slope angles of 30° to 45° (*Perla,* 1975) and in rare cases have been observed at and below 25°. The slope angle must be steep enough to exceed friction at the base after the slab

a.

b.

Figure 1.4. Examples of slab avalanches: **(a)** accidentally triggered by a skier, **(b)** large, destructive slab avalanche released by explosives. (Photos: (a) T. Exner, (b) www.slf.ch)

has been detached from its surroundings (van Herwijnen and Heierli, 2009). The friction between the bed surface and the overlying slab depends mainly on the snow microstructure at the interface.

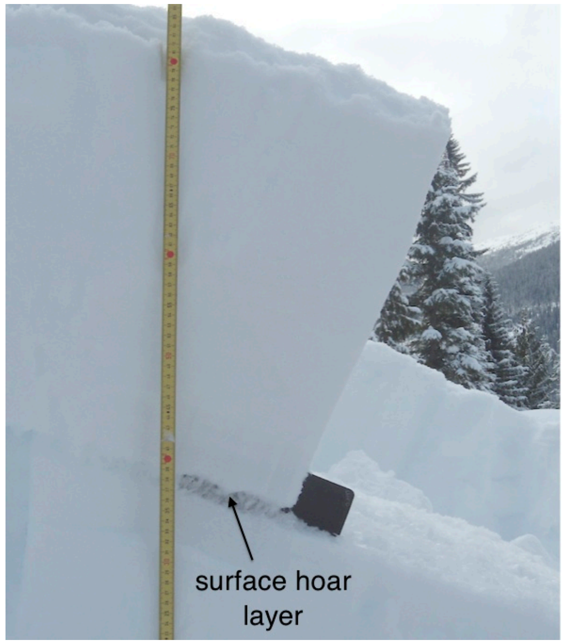

Figure 1.5. Cohesive slab over a layer of buried surface hoar, which is known as one of the most reactive weak layers. (Photo: ASARC)

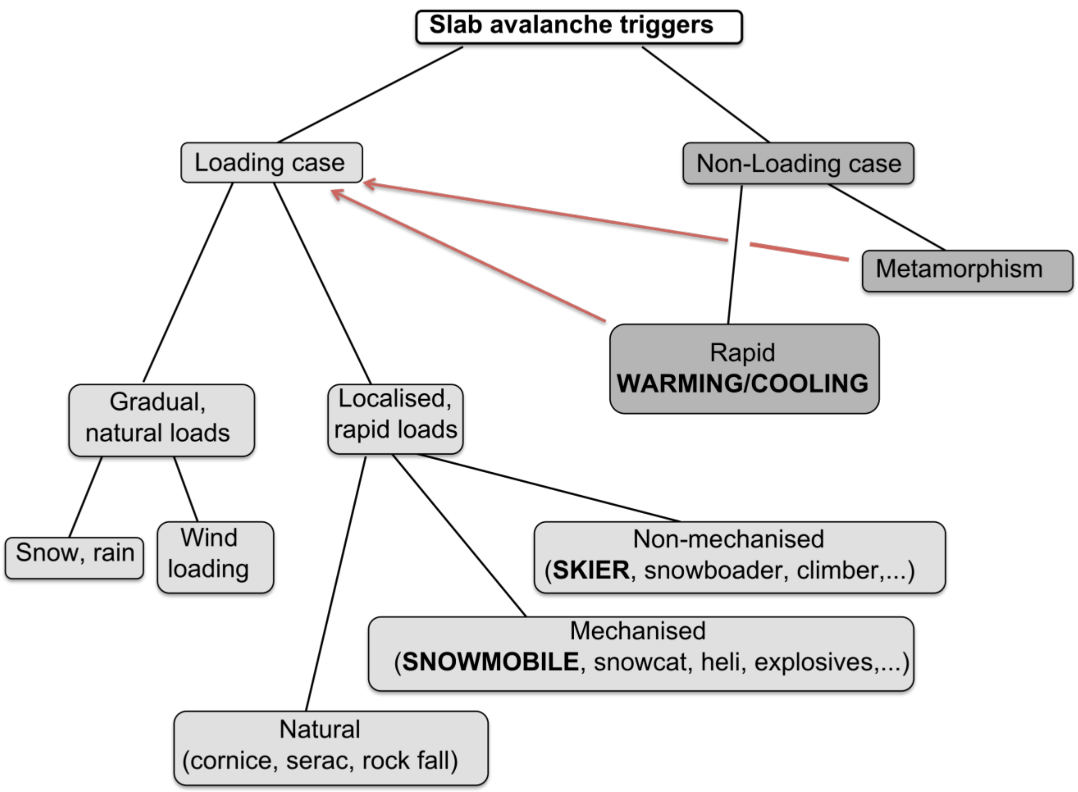

Figure 1.6. Overview of slab avalanche triggers. Warming/cooling can be triggers themselves, but also contribute to easier triggering in the loading case category. The bold and capitalised triggers are subject of this thesis.

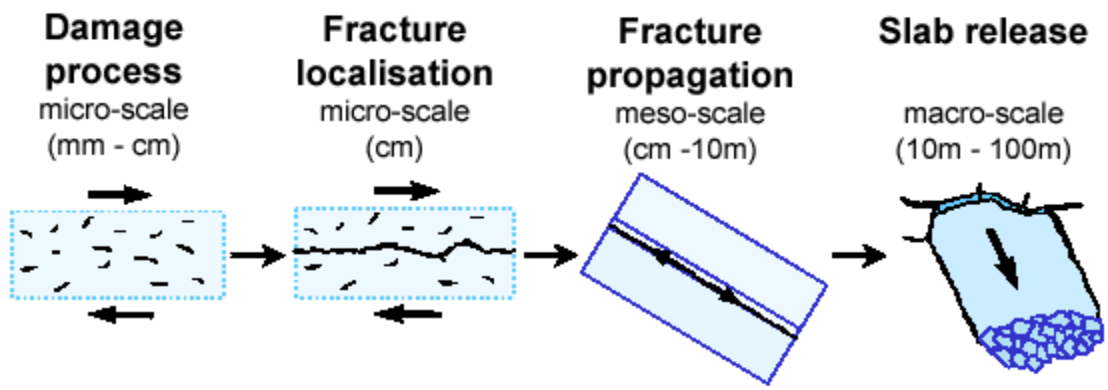

Figure 1.7. Schematic of fracture evolution and slab avalanche release (Schweizer and others, 2003; reproduced with permission from J. Schweizer).

Slab avalanche triggers: Slab avalanches release either by adding more load to the snowpack (*loading case*) or due to internal changes of the mechanical properties of the slab/weak layer combination (*non-loading case*) (Figure 1.6). The loading case can be divided in widespread, gradual loading due to snow, rain and snow redistribution by wind, and localized rapid loading due to surface loads such as skiers, snowmobilers, cornice fall or explosives. Slab release without an external additional load requires either snow temperature variations (Tremper, 2008, p. 50) or deterioration of the weak layer to destabilise the snowpack.

Examples for the latter are faceting on or below crusts (Jamieson, 2006) or the development of depth hoar close to the ground driven by strong temperature gradients (Hirashima and others, 2008). In addition, these internal changes provide more suitable conditions for surface loads to act as a trigger. This thesis is concerned with the localized loads of *skiers* and *snowmobiles*, and the effects of *snow temperature changes* on the natural release process.

Fracture propagation: Figure 1.7 demonstrates the development of a weak layer failure leading to avalanche release. The failure starts with the damage process on the scale of inter-granular bonds, followed by a larger localized fracture that propagates along the weak layer/slab interface (Schweizer and others, 2003). The propagating fracture, which is driven by released energy from the slab/weak layer system is the most important prerequisite for slab avalanche release. A more

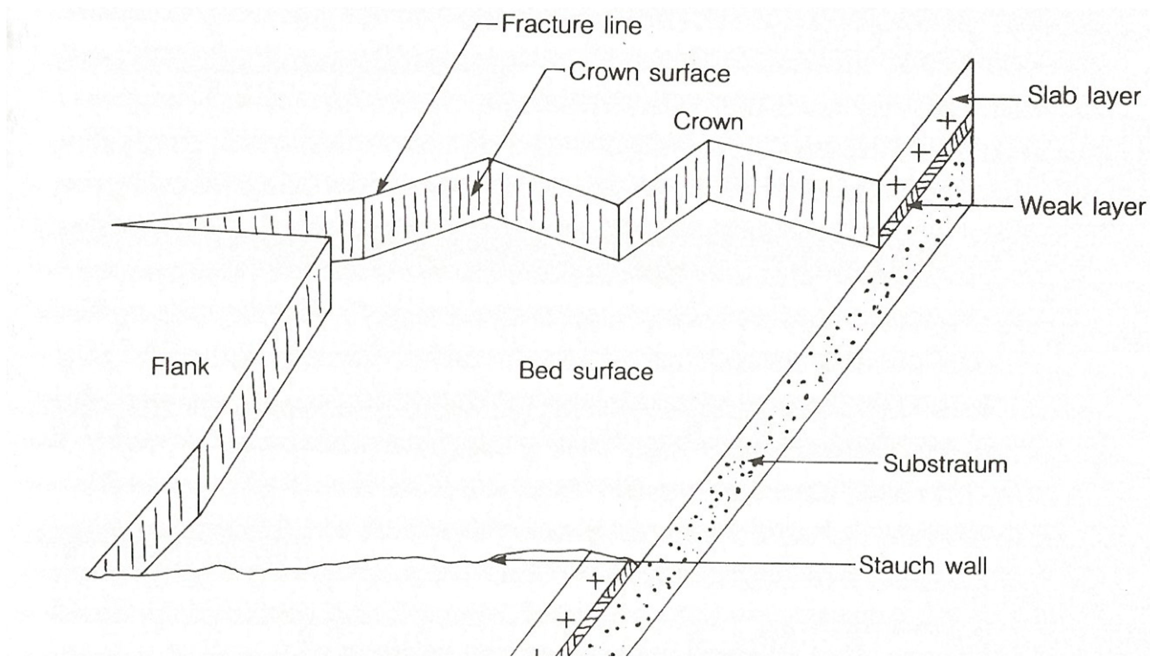

Figure 1.8. Start zone characteristics of a slab avalanche (After Gray and Male, 1981, p. 483)

detailed overview of the current state of the art of slab avalanche fracture mechanics is given in Section 1.4.

Release sequence: A slab avalanche can release after the slab is completely separated from the surrounding snowpack and the slope is sufficiently steep to overcome basal friction and lateral support at the flanks and the stauchwall (Figure 1.8). To detach the slab, fractures occur in tension at the upper boundary (crown), mostly in shear at the sides (flanks) and in shear and/or collapse in the weak layer at the base of the slab above the bed surface (de Quervain, 1966; Birkeland and others, 2009). Nowadays, it is commonly agreed on that the basal fracture occurs first, followed by the crown fracture, then flank and stauchwall fracture (Schweizer, 1999). Observations that most crown fractures appear to be approximately slope normal is regarded as evidence that the basal fracture precedes the crown fracture. The crown fracture can only show the perpendicular shape if the stress has only a slope parallel component at the moment when the crown fractures (Perla, 1970, 1975). During the propagation of the fracture in the weak layer the tensile stress in the overlying slab increases until crown fracture occurs.

1.4 Slab avalanche fracture mechanics

This section provides an overview of the current understanding of slab avalanche fracture mechanics. A detailed review would be beyond the scope of this background section. The reader is referred to Gauthier (2007) and Sigrist (2006) for a detailed practical and theoretical background of slab avalanche fracture mechanics. Slab avalanche fracture mechanics is basically concerned with the process of initiation and propagation of the basal fracture at the slab/weak layer interface.

1.4.1 Fracture initiation

Fracture initiation by rapid localised loads (Figure 1.6) is usually described by a stress – strength approach (Foehn, 1987). Rapid, localised loads, such as humans, cornice fall and explosives usually cause a brittle fracture once the additional applied stress exceeds the strength (in shear and/or compression) of the weak layer; in other words, if the additional deformation in the weak layer is sufficient to cause a localised (brittle) fracture. Once shear/compressive strength in the weak layer is exceeded does not necessarily mean that a fracture will propagate. Figure 1.9 gives an example of a skier-induced weak layer fracture that did not propagate. Whether a fracture will propagate depends if the slab/weak layer system can provide the energy to drive the fracture without any external forces.

For spontaneous slab avalanches, stress may exceed strength by slow gradual loading due to precipitation or changes of the mechanical properties of the slab weak layer system. The latter can be achieved by either rapid temperature changes or deterioration of the weak layer (Schweizer and others, 2003). A commonly accepted model for the initiation of a basal shear fracture is the growth of a flaw or imperfection within the weak layer to critical size (McClung, 1979; Bader and Salm, 1990). Basically, within the imperfection or flaw the weight of the slab cannot be fully supported, therefore higher stresses occur at the perimeter of the imperfection (Figure 1.10). Further gradual loading, for example by snowfall, leads to initial shear failure. Strain softening may further increase the size of the

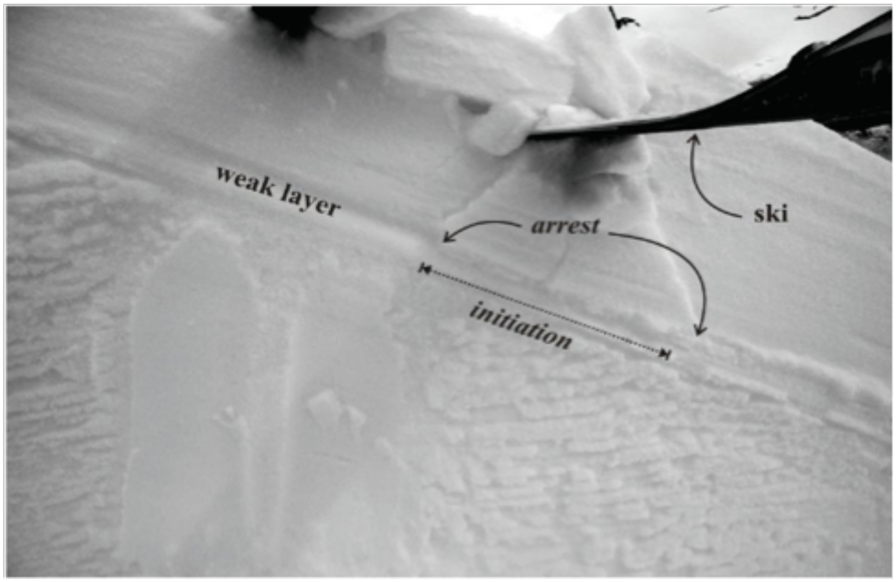

Figure 1.9. Fractured weak layer due to a skier. The stress due to the skier exceeded weak layer strength, but the initiated fracture arrested. (After Gauthier, 2007)

imperfection. Consequently, stress concentration at its sides increases until a point when ductile to brittle deformation occurs.

The initiation of a fracture can also be viewed as the competition between bond fracturing and bond welding rate in a creeping snowpack (Schweizer, 1999; Louchet, 2001). When the rate of bond fracturing exceeds the rate of bond healing (welding) a damage zone may accumulate, due to the variability of the snow microstructure, to failure localisation, which may eventually lead to rapid fracture propagation (Figure 1.7).

1.4.2 Fracture propagation

Basically, two concepts describe the propagation of an initial basal fracture. Those are distinguished by the source that provides the energy to drive the fracture or to overcome fracture resistance, which is the work needed to create the new fracture surface.

Shear fracture propagation: The driving force for shear fracture propagation originates from stored elastic energy of the unsupported slab while the flaw size is increasing (Schweizer, 1999) (Figure 1.10). This process requires a slope angle steep enough to overcome friction at the base of the slab. The amount of available elastic energy increases with the growth of the imperfection. The released elastic energy needs to be sufficient to overcome fracture resistance – the energy needed to create the new fracture surface. The energy condition that needs to be met for propagation is usually described by the critical size (a_c) of the initial crack (Kirchner, 2002):

$$a_c = \frac{1}{\pi}\left(\frac{K_{IIc}}{\tau_g}\right)^2 \tag{1.1}$$

with K_{IIc}: Fracture toughness in shear

τ_g: Bulk shear stress (far field stress)

Once the initial crack reaches critical size the stress intensity at the crack tip (K_{IIc}) is high enough to drive (propagate) the fracture. The critical stress intensity is also called fracture toughness (McClung, 2009):

$$K_{IIc} = \sqrt{E'G_{II}} \tag{1.2}$$

with E': Effective modulus

G_{II}: Fracture energy in shear

So far, the critical crack size has only been a theoretical concept since it has not been possible yet to measure it before a slab avalanche release. However, fracture laboratory experiments on snow samples yielded experimental clues on the size of the critical crack length (McClung, 2011). In general, it is commonly assumed that the critical length ranges between 0.1 and 10 m. For slow growth of the shear band the initial flaw is estimated to be between 0.1 and 1 m (Schweizer, 1999; Kirchner and others, 2002), for fast growth between 1 - 10 m. For the case of rapid localised loads (e.g. skier-triggering) the initial crack size necessary for rapid crack growth is basically within the order of the slab thickness (McClung and Schweizer, 1999; Schweizer and others, 2003).

The shear model also explains interface fractures, for example when the slab overlies a crust and no collapsible weak layer is present. However, field

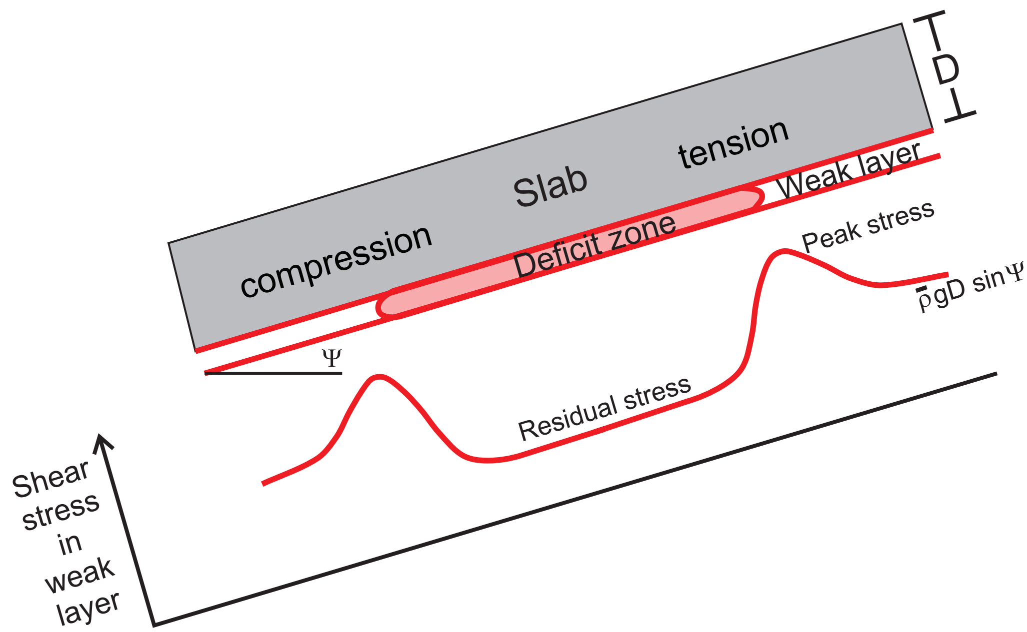

Figure 1.10. Schematic of the shear stress distribution due to an imperfection (deficit zone) in a weak layer. (After McClung, 1981, Palmer and Rice, 1973)

experiments showed that most layers showed at least a slight collapse (van Herwijnen, 2005). Since the shear fracture model draws its energy from gravity due to the slope angle it does not explain propagating fracture in low angle or level terrain. Field observations have shown that in particular collapsible weak layers can propagate a fracture over large distances in flat terrain.

Weak layer collapse and bending wave: Many weak layers consist of collapsible crystal types, such as surface hoar and faceted grains, which can range in thickness from below 1 mm to over 1 cm (van Herwijnen and Jamieson, 2005). Once the layer is locally collapsed by compressive failure, for example by a skier, the release of potential and elastic energy of the resulting bending wave provides the force to drive the fracture. The propagation of the bending wave is independent of slope angle (for slope angles important for slab avalanche release). In flat terrain, fractures can propagate over long distances (up to several hundreds of meters) and are purely driven by a bending wave (Figure 1.11) (Johnson and others, 2004; Heierli and Zaiser, 2008). The thickness and flexural rigidity of the slab determine the size of the initial crack necessary to propagate the fracture. The critical crack size (r_c) is given by (Heierli and Zaiser, 2008):

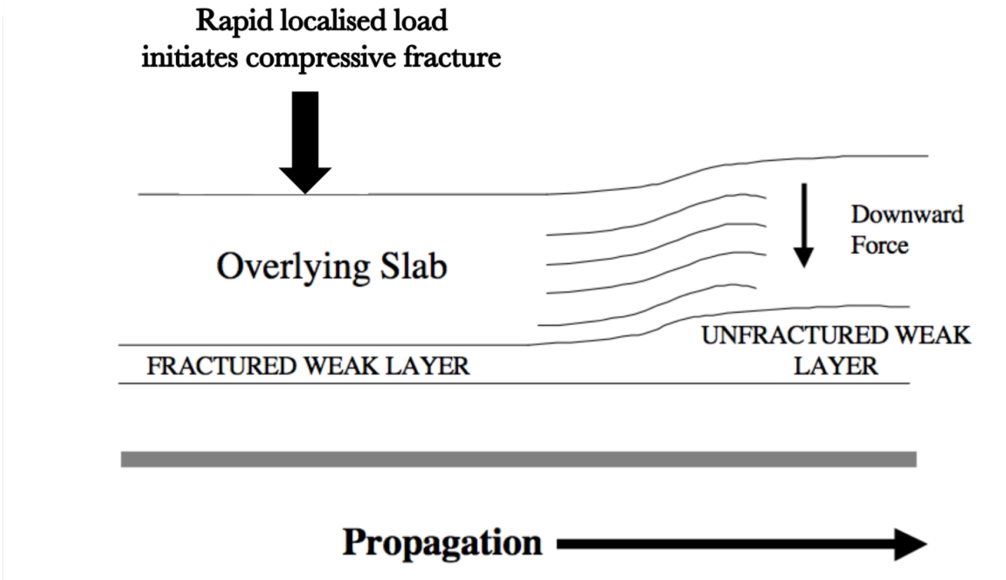

Figure 1.11. Schematic of a bending wave triggered by compressive fracture, propagating the weak layer fracture (After Johnson et al., 2000)

$$r_c = \frac{4}{\pi\gamma}\frac{w_f E}{(\rho g h)^2} \tag{1.3}$$

with E : Young's modulus of the slab

w_f : Specific fracture energy

ρgh: Weight of the slab

γ: Constant (dimensionless)

Shear vs. Collapse: The contribution of each process to fracture propagation depends on the type of the weak layer and slope angle. With increasing slope angle, fractures in shear become the dominating process for propagation. Sigrist (2006) calculated the ratio of energy release by a shear fracture to a compressive fracture (bending wave) depending on slope angle (Figure 1.12). Above a slope angle of approximately 55° the fracture is completely dominated by shear. At slope angles around 38°, where most slab avalanches occur (*Perla*, 1975), the bending component is about 1.5 times higher than the shear component.

Herwijnen and Jamieson (2005) conducted field experiment with high-

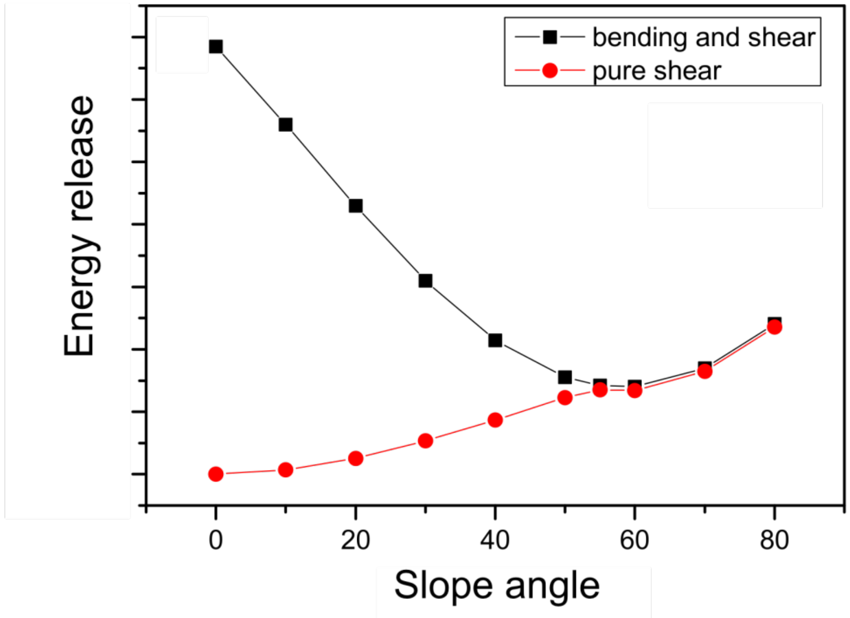

Figure 1.12. Energy release rate depending on slope angle of pure shear propagation and bending and shear (After Sigrist, 2006)

speed cameras and observed a drop of the weak layer independent of slope angle and thickness. This indicates the importance of the compressive fracture as a source of energy for fracture propagation. On the other hand there is evidence from a lab study by Borstad and McClung (2008) that collapse is preceded by weak layer parallel shear. Overall, it seems plausible that a combination of both, shear fracture and bending wave model, come closest to describing the actual fracture process.

1.5 What is snowpack stability?

According to the definition of the Canadian Avalanche Association (CAA, 2007), snowpack stability is the likelihood of avalanches not to release. From a fracture mechanical point of view, stability (or instability) is determined by the ease of how a fracture is initiated and by the propagation propensity of an initiated fracture. A snowpack can be extremely unstable (bonding between layers) in terms of the ease of initiating a fracture, but if the fracture does not propagate, slab avalanche release is very unlikely. On the other hand, fracture propagation propensity may be

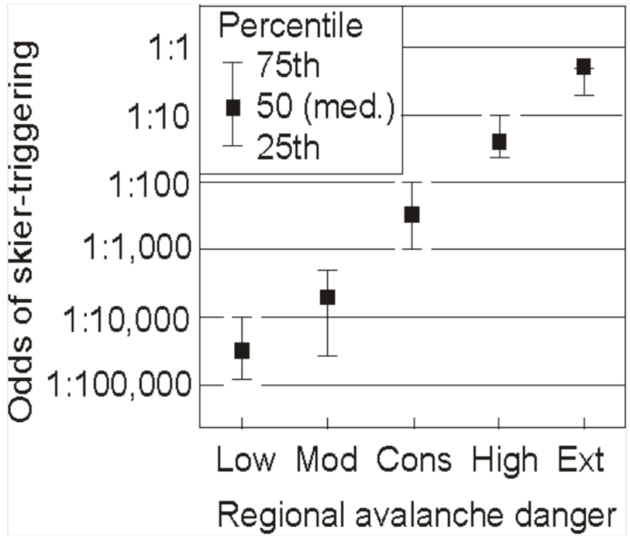

Figure 1.13. The odds of skier-triggering depending on the regional avalanche danger rating (Jamieson and others, 2009; reproduced with permission from B. Jamieson)

high, but due to the depth of the weak layer, fracture initiation due to surface loads is very unlikely. The situation of a thick cohesive slab overlying a layer with high propagation potential is usually referred to as ‘bridging’. If a fracture is initiated insuch a case, consequences of the resulting large slab avalanche are usually high.

The factors that are used to assess instability can be classified in three categories (McClung, 2002b). The following very general classification equals increasing direct evidence of instability with increasing class number:

Class I: Meteorological factors (precipitation, temperature, wind speed and direction, etc.)

Class II: Snowpack structure (layering, depth and type of weak layer, etc.)

Class III: Direct evidence of instabilities (recent avalanches, whumpfing, positive results from instability tests)

Overall, instabilities and resulting avalanches are rare. Most of the time, snowpack stratifications are in a stable state. An estimation of the odds of skier-triggering by leading avalanche experts in North America (Jamieson and others, 2009) helped to quantify the usually qualitative and probabilistic nature of avalanche danger/instability forecasts (Figure 1.13). For example, when the danger is rated *considerable experts expected that* one in approximately 100 to 1000 avalanche start zones release when skied without any expert route selection.

1.6 The role of avalanche forecasting

Avalanche forecasting is the art of assessing and predicting the temporal and spatial variation of instabilities in the snowpack (McClung, 2002a). In particular, forecasters assess and communicate the avalanche danger level (Figure 1.14a) and specify the likelihood of human triggering or spontaneous release of avalanches with respect to the approximate location of occurrence, and type and size of the expected avalanche. An example of a forecast 'considerable' danger level and the specification of the avalanche problem is provided in Figure 1.14b.

The distribution of instabilities cannot be measured, seen, or predicted by numerical physical models in a deterministic way. Therefore, avalanche forecasters rely on their experience and local knowledge combined with a sound theoretical background. 'The implication is that snow-avalanche forecasting is a risk-based or probabilistic process rather than a question of analytical estimates based on known quantities' (McClung and Schaerer, 2007, p. 81). LaChapelle (1980) describes avalanche forecasting as a complex process that to a large extent is based on experience and theoretical knowledge of the forecaster, but an intuitive component is also involved, which is very hard to reduce.

In particular, local terrain characteristics seem to have a strong influence on how weather factors affect avalanche conditions. Public avalanche forecasts usually cover a large area that cannot cover all local deviations from the general regional forecast. Thus, scale is a major issue in avalanche forecasting. It is the nature of the problem that the regional forecast mostly provides average conditions. Locally, on the drainage scale, the regional forecast can deviate by a full danger level, in rare cases by two levels (Bakermans and others, 2010). Ultimately, backcountry travellers have to decide on a slope scale if a specific slope is stable or not.

a.

Avalanche danger is determined by the likelihood, size and distribution of avalanches.				
Danger Level		**Travel Advice**	**Likelihood of Avalanches**	**Avalanche Size and Distribution**
5 Extreme	4 5	Avoid all avalanche terrain.	Natural and human-triggered avalanches certain.	Large to very large avalanches in many areas.
4 High	4 5	Very dangerous avalanche conditions. Travel in avalanche terrain not recommended.	Natural avalanches likely; human-triggered avalanches very likely.	Large avalanches in many areas; or very large avalanches in specific areas
3 Considerable	3	Dangerous avalanche conditions. Careful snowpack evaluation, cautious route-finding and conservative decision-making essential.	Natural avalanches possible; human-triggered avalanches likely.	Small avalanches in many areas; or large avalanches i specific areas; or very large avalanches in isolated area
2 Moderate	2	Heightened avalanche conditions on specific terrain features. Evaluate snow and terrain carefully; identify features of concern.	Natural avalanches unlikely; human-triggered avalanches possible.	Small avalanches in specifi areas; or large avalanches in isolated areas.
1 Low	1	Generally safe avalanche conditions. Watch for unstable snow on isolated terrain features.	Natural and human-triggered avalanches unlikely.	Small avalanches in isolated areas or extreme terrain.

b.

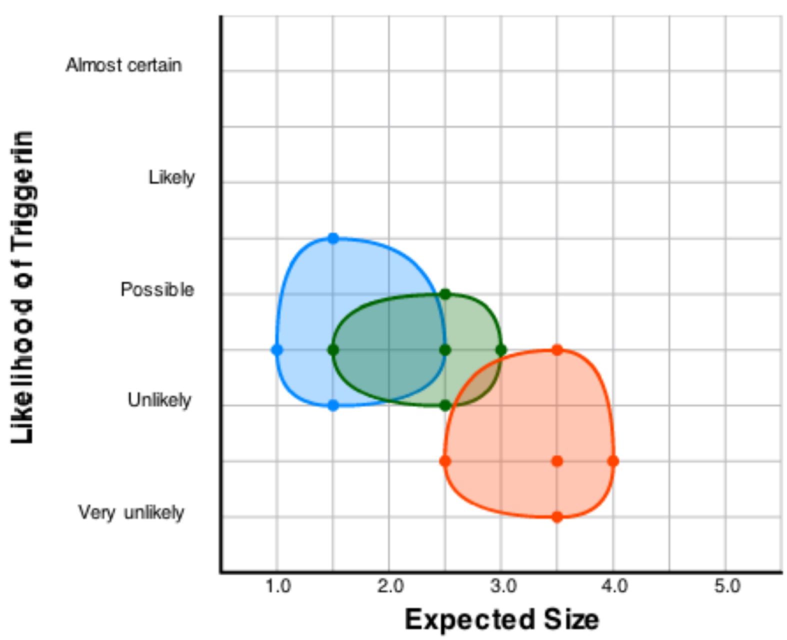

Figure 1.14. (a) North American public avalanche danger scale (Statham and others, 2010), **(b)** Example of a day with *considerable* avalanche hazard. In this case it was possible to trigger wind-slab with an expected size of 2.5 (blue area). A deeper less reactive weak layer (facets on crust) was expected to produce large avalanches up to size 4 once triggered (red area) (www.avalanche.ca; retrieved August 2010).

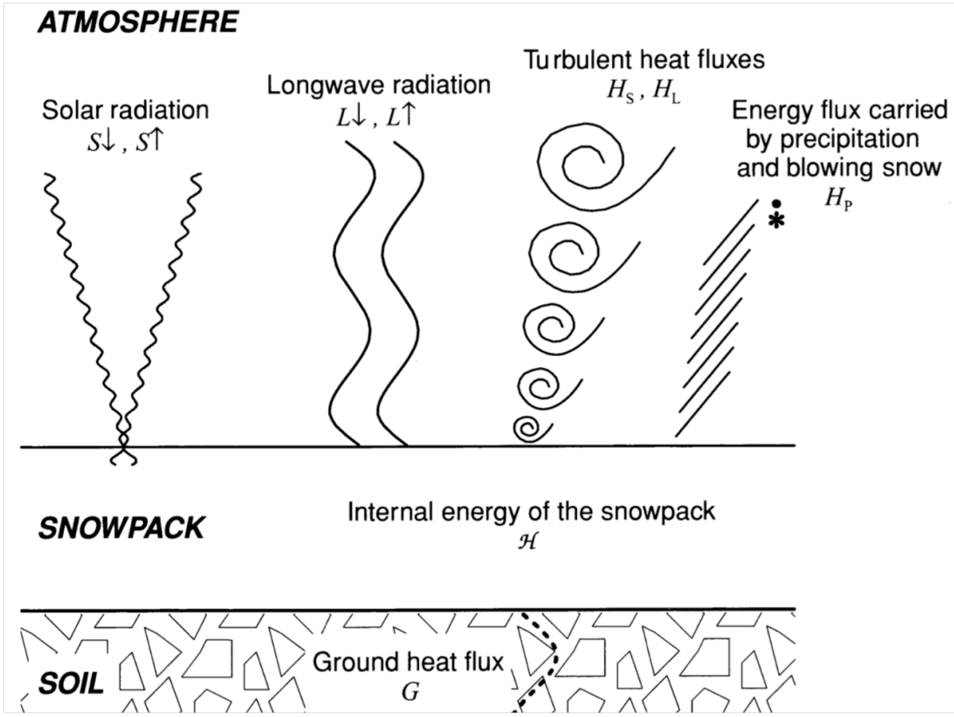

Figure 1.15. Energy balance of snow surface. (King and others, 2008; reproduced with permission from J. King)

An improvement of the understanding of the interaction of weather and snowpack conditions greatly assists avalanche forecasters to increase the accuracy of public forecasts and helps professionals and recreationists alike to make the ultimate decision when assessing the stability of a single slope.

1.7 Heat sources of the snowpack

The schematic in Figure 1.15 provides an overview of all energy sinks and sources of the snowpack that contribute to its internal energy (temperature). The ground heat flux (G) keeps the lower boundary of the snowpack mostly at, or within a few degrees just below the melting point. This property, of most seasonal snowpacks, maintains a vertical temperature gradient since the snow surface is most of the time below the 0˚C during dry snowpack conditions. The vertical temperature gradient is the most important driving force of snow metamorphism.

All other exchange processes take place in the near-surface layers. These are the radiation balance (short-wave (S) and long-wave (L) radiation), turbulent exchange of sensible (H_S) and latent heat (H_L), and input due to precipitation and blowing snow (H_P).

The albedo of snow, which controls the energy input due to solar radiation, strongly depends on the age and condition of the snow surface. Freshly fallen snow shows albedo values of up to 0.95, which means only 5 % of the incoming solar radiation is absorbed. Within a few days, the albedo can drop to 0.50, causing a five-fold increase in absorbed solar energy (King and others, 2008, p. 55) (Gray and Male, 1981, p. 323). The slow process of thermal conductivity does not limit the depth penetration of solar energy. Incident solar radiation instantly warms the surface layers at the depth where the penetrating radiation is absorbed. Therefore, solar radiation is the most efficient heat source for rapid warming processes.

Snow almost behaves like a perfect black body with an emissivity of 0.98. That means it absorbs all of the long-wave radiation of the atmosphere and emits the maximum thermal radiation that is allowed by the surface temperature (King and others, 2008, p. 58). This, for instance, accounts for most of the rapid cooling of the snow surface, which greatly contributes to the formation of weak layers such as surface facets and surface hoar.

Clouds, in particular when thin and at mid to higher level altitudes, can intensify the effect of solar warming. Reflection of solar radiation and long-wave radiation contributes to a considerably higher energy input into the snowpack. This greenhouse effect is well known from field observations, in particular on calm days when turbulent energy exchange (cooling due to wind) is minimal.

The turbulent heat exchange, on windy days, greatly contributes to either cooling or warming the near-surface layers. On clear, calm and cold winter days solar warming can considerably warm the surface layers. Under windy conditions the negative turbulent energy transport counterbalances the solar energy input. During many field days for this thesis, the expected (forecasted) snowpack warming was prevented due to the cooling effect of wind and thick clouds. On the other hand, warm winds (when considerably warmer than the snow surface) have the potential to rapidly warm the near-surface layers.

1.8 Thesis objectives and goals

This thesis aims to contribute to a better understanding of the slab avalanche release process. In particular, deformation in the snowpack caused by external surface loads and surface warming and cooling effects were considered. Before this work, only a limited number of studies addressed the sub-surface deformation under surface loads and its temperature induced variations (Section 1.2.2 and 1.3.7). For relevant and realistic surface loads, skier and snowmobiles were chosen for the field experiments. Plausible concepts to explain stability changes due to surface warming are known, but field data to support those are rare. A major part of the thesis is dedicated to shed more light on the quantitative effect of temperature on stability of a dry snowpack in field studies. The following list states the objectives of this thesis and the original approach for each subtopic:

- *Develop a method to measure additional normal stresses due to static and dynamic surface loads in a natural snowpack.* The method needed to be field portable, easily repeatable and able to capture stress changes due temperature variations of the near-surface layers. No such method was available prior to this research.

- *Measure the effect of snow temperature variations on the normal stress distribution below static and dynamic skier loads.* This effect has never been verified in systematic field experiments, although it has been calculated for limited cases by theoretical and analytical methods.

- *Compare the measured static and dynamic normal stress distribution in the snowpack due to skiers and snowmobiles.* The impact of snowmobiles on the snowpack before this study had only been speculative. No studies, either analytical or experimental, were available to estimate normal snowpack stresses under snowmobiles.

- *Conduct cold lab experiments to study the effect of snow temperature variations on the stress distribution below static surface loads.* This original lab study was intended to gain more insight on the impact of snowpack temperature changes under controlled lab conditions in addition to the outdoor experiments.

- *Study the effect of rapid solar warming on snowpack creep in the near-surface layers in field experiments*. Field observations and experience strongly hinted at the destabilising effect of rapid solar warming, but no field data were available to confirm these observations.

To summarise, a fieldwork-based and experimental approach was chosen to verify and complement partially known concepts of the impact of snowpack temperature changes on the deformation behaviour of snow due to various surface loads under realistic natural conditions. Previous theoretical approaches and laboratory studies yielded essential knowledge under idealised and controlled environments. Ultimately, however, the subject of this thesis needs to be studied under realistic natural conditions with all its complicating factors.

CHAPTER 2

Current state of knowledge

All of the experiments that were conducted for this thesis were either concerned with

- normal stresses in the snowpack due to static and dynamic surface loads,
- the impact of stiffness changes of the near surface layers on the stress distribution due to daily snow temperature variations,
- or the deformation (creep) of the snowpack due rapid warming.

To provide the reader with a comprehensive overview of relevant studies and knowledge, it appeared practical to divide this literature review chapter in two core topics:

- Stresses in a layered snowpack due to surface loads (Section 2.1)
- Effect of warming of the near surface layers on snowpack stability (Section 2.2)

The following pages present the current state of knowledge relevant to the two topics, which was gained from published empirical, theoretical, laboratory, modelling, statistical, and field-experimental investigations.

2.1 Stresses in a layered snowpack due to surface loads

2.1.1 Analytical and numerical studies

Boussinesq (1885) first provided the analytical foundation of the stress distribution below surface loads in a homogenous material approximated as an elastic half space. Under this assumption, stress distribution is independent of the stiffness of the material. The effect of a layered material on stress distribution due to surface loads has long been studied in other disciplines of engineering such as pavement design (Burmister, 1945). Das (2008) provided a comprehensive overview of the stress distribution problem in layered materials or general engineering problems.

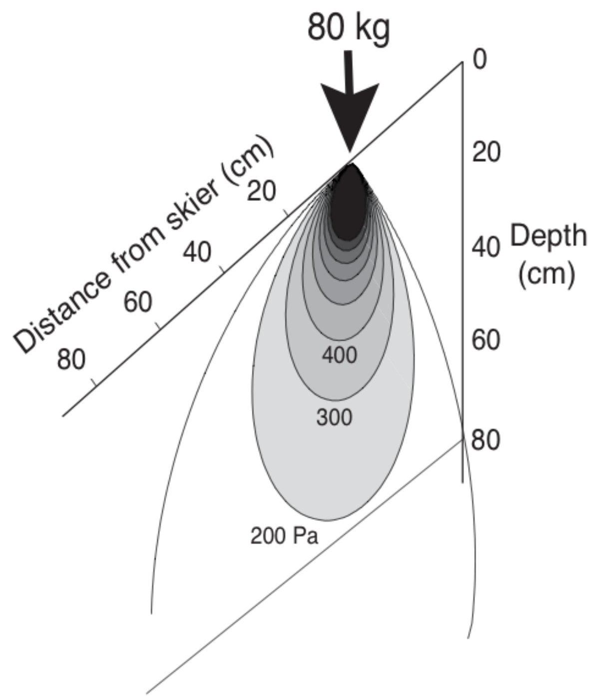

Figure 2.1. Calculated additional shear stresses due to a skier approximated as a line load. Contours are in Pa. (After Föhn, 1987)

The concept of Boussinesq was first applied by Salm (1977) to calculate additional stresses in a horizontal and inclined snowpack below a uniform static line load. According to Salm's results, normal and shear components of stresses rapidly decrease vertically below and horizontally to the sides of the load. The bulb of shear stress and the horizontal component of normal stress are wider than the vertical normal stress further away from the load. Föhn (1987), also based on Boussinesq's approach, calculated the additional shear stresses below skiers, climbers, snow machines and explosives on a slope. Shear stresses decrease with depth in a non-linear way (Figure 2.1). At a depth of 80 cm the additional shear stress due to a static skier load decreases to approximately 4 % of the surface value. Foehn approximated the surface loads as either static line or band loads. At 50 cm below the snow surface the weight of a climber, approximated as a point load, stresses the snowpack about three times more than the weight of a skier. The force due to a snow machine (snow cat) stresses the snowpack approximately seven times more and explosives, depending on the height of detonation above the snowpack, approximately 17 – 30 times more. Backcountry users such as climbers, snow-shoers, and hikers apply their load over a considerably smaller surface area to the snowpack. The resulting stresses increase significantly and penetrate deeper into the snowpack.

Curtis and Smith (1974) and Smith (1972) conducted FEM calculations on shear stresses within a layered snowpack with varying thickness and changing slope angles. The impact of surface loads was not included. Both studies confirmed the effect of layers with varying stiffness on stress distribution.

Johnson (1980) investigated the dynamic impact of explosives by FEM modelling. He pointed out that differences in stiffness of layers have a substantial impact on penetration of stress waves into the snowpack. Colbeck (1991) also pointed out the importance of layer stiffness for the slab avalanche release process and the stress distribution due to surface loads.

Schweizer (1993) investigated the shear stress distribution due to static skier loads in snow as a layered material by analytical and FEM calculations for different snowpack profiles. He concluded that additional shear stresses due to skiers in the near-surface layers are comparable to shear strength in weak layers. Hard surface layers tend to prevent skier stresses from penetrating into deeper potential weak layers – a process that is referred to as 'bridging' and therefore increases snowpack stability. Peaks in stress gradient at the transition from harder to softer layers are responsible for fracture initiation at those interfaces.

McClung and Schweizer (1999) conducted a mathematical analysis of the skier's impact on snowpack stability and the skier stability index. They concluded that most previous studies on the (static) stress impact of a skier were limited and that future studies needed to include dynamic effects for a more realistic approach. For a slab with ρ = 200 kg m^{-3}, a skier's weight of 70 kg on 1.70 m long skis on a 35˚ steep slope, the additional skier shear stress until a depth of approximately 30 cm was larger than the shear stress due to the weight of the slab. The skier stress rapidly decreases with depth, whereas the contribution of the slab increases. They concluded that the additional shear stress due to a static skier is negligible compared to the shear strength of weak snowpack layers at depths below approximately 1 m. However, this does not mean that skiers are not able to trigger slab avalanches with more than 1 m thickness. A fracture initiated in an area where the slab is thinner than 1 m often propagates in deeper areas and therefore can release large slab avalanches.

Wilson and others (1999) confirmed the results from previous studies by FEM modelling of the stress impact of a skier. The main results of their study on the effect of warming of the near-surface layers are presented in Section 2.2.3. Further FEM studies by Jones and others (2006) contributed to the understanding of skier-induced shear stresses in weak layers below slabs of different stratification (thickness and stiffness) over a bed surface of different stiffness. They pointed out that stiffer bed surfaces lead to stress concentration in the weaker layer above and therefore contribute to instability of slab/weak layer combinations.

Habermann and others (2008) modelled stresses and deformation, using the FEM method, in weak layers for a static skier load below a multi-layered slab, characterized by varying stiffness, over a bed surface with different stiffness. Stiff layers within the slab always reduce stresses in the weak layer, whereas stiffer bed surfaces increase additional stresses in weak layers. Depending on slab properties, shear stresses in the weak layer can vary by a factor of two.

Recent laboratory experiments by Reiweger and Schweizer (2010) suggested that shear strain concentration in buried surface hoar layers can be up to 10 – 100 times higher than the global strain. This confirms the importance of stress concentrations at the transition of layers with different stiffness.

2.1.2. Field studies

Gubler (1977) conducted field tests on the effectiveness of explosives for avalanche release. Moist and wet snow strongly attenuated the pressure wave induced by the detonation. The effective zone was basically reduced to the crater area.

Schweizer and others (1995), and Camponovo and Schweizer (1996) first measured the static and dynamic impact of a skier on the snowpack in field experiments by burying load cells prior to skier loading. Their results confirmed that

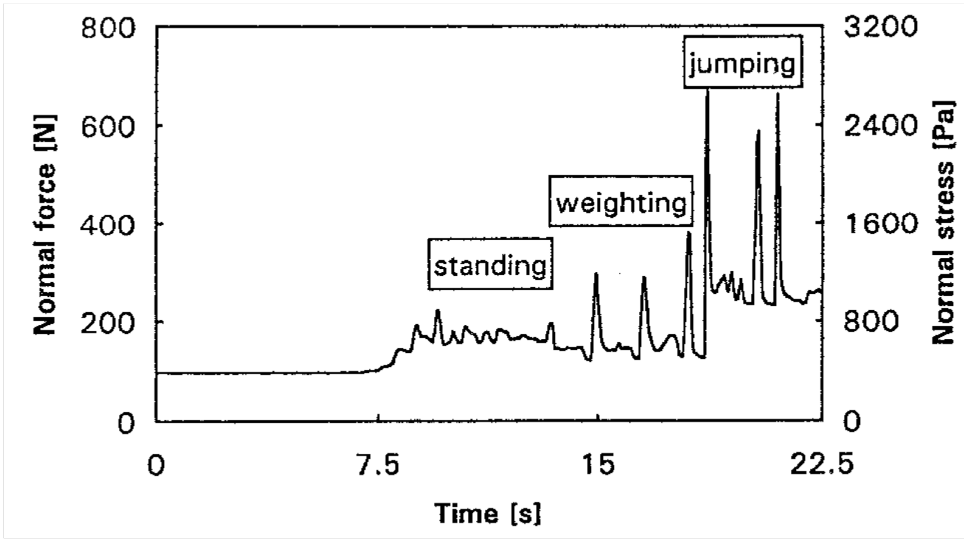

Figure 2.2. Normal forces and stresses 24 cm below the snow surface for the loading steps of standing, knee drops and jumping. (Schweizer and others, 1995; reproduced with permission from J. Schweizer)

forces applied by a skier decrease with snow depth and that snowpack conditions of the surface layer have an important impact on stress penetration (Figure 2.2).

Stiffer, harder layers spread out the load more laterally, whereas softer layers allow deeper stress penetration (Figure 2.3). Based on similar field studies and calculations, Schweizer and Camponovo (2001) found that the additional skier stress in the snowpack does not reach beyond 1 m to the side and that at a depth of 1 m stresses reduce below values that could affect weak layers. The loading step of knee drops is comparable to a skier performing downhill turns.

A current field study by Thumlert and others (in prep.) on the dynamic impact of snowmobiles and skiers suggests that snowmobile forces can be up to a factor of five higher compared to those of a skier.

2.1.2.1 Surface stresses under skis

Lind and Sanders (2003, p. 65) pointed out the problem of stress distribution on the snow surface along a ski, which is influenced by many factors such as snow and ski stiffness. Kaps and other (2000) modelled the pressure distribution under skis during carved turns. As part of their studies they calculated the stress distribution along the ski for two skis with different stiffness during straight skiing on a hard

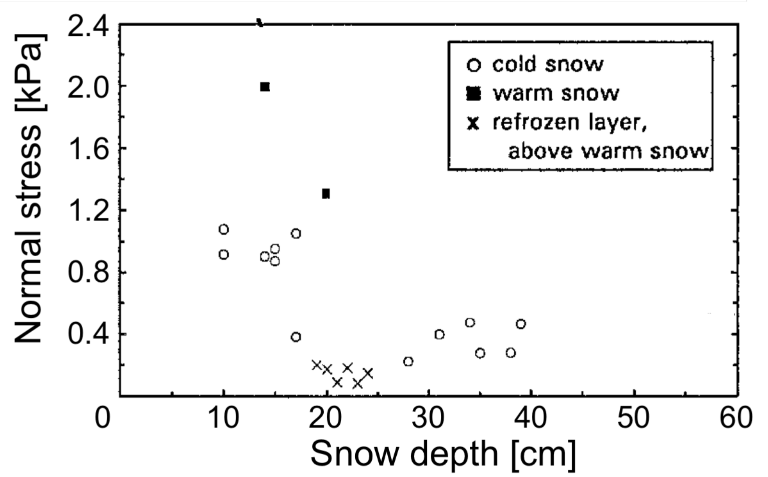

Figure 2.3. Normal stresses for the loading step of weighting (knee drops) for various snowpack conditions. (Schweizer and others, 1995; reproduced with permission from J. Schweizer)

snow surface, which yielded a considerably different stress distribution. Maximal peak values up to 12.5 kPa occurred. Scott and others (2007) and Piziali (1972) actually measured the pressure distribution for straight skiing and performing turns. Stresses during a turn are more equally distributed along the skis compared to straight skiing. Peak stresses during a turn were lower compared to straight skiing. Measured stresses by Piziali (1972) for straight skiing were by up to a factor of four higher than calculated peak stresses by Kaps and others (2000).

2.1.3. Summary

Analytical, numerical and field studies are in agreement that additional stresses due to surface loads decrease with snow depth and that layering of the snowpack (varying stiffness) has an important effect on stress and deformation distribution.

Generally, the majority of research on snowpack stability thus far was concerned with the spontaneous release of avalanches. However, avalanche statistics show that most avalanches accidents are recreational where the victim was often the trigger (Jamieson and others, 2010, p.31). To date, only a very limited number of field studies are available to confirm the results from theoretical and analytical studies on human (skier) triggering of slab avalanches.

Furthermore, the distribution of the skier’s weight along the ski due to bending of the ski has not been taken in to account yet in terms of the slab avalanche trigger process. It is known from measurements of the stress distribution along skis that peak stresses decrease with increasing ski bending during a turn (Section 2.1.2).

Before this study, the impact of snowmobiles on the snowpack has only been speculative. The increasing number of snowmobile avalanche accidents requires the inclusion of snowmobiles as a frequent trigger. Presumably, the larger weight and the higher speed of travel affect the snowpack in a much different way than other backcountry users such as skier, snowboarders or climbers.

Generally, the weight of a human avalanche trigger (e.g. skier, climber, snowmobile) is negligibly small compared to the mass of snow that is set in motion after an avalanche release with up to many hundreds of tons of snow. These surface loads, merely provide the initial input. It strongly depends on the depth penetration and surface area that is affected by this initial ‘disturbance’ and the slab/weak layer properties if the initial fracture can be sustained and propagate to release a slab avalanche.

2.2. Impacts of warming of the near surface layers on snowpack stability

This section presents a review of the current state of knowledge of the effects of snow temperature changes on snowpack stability. Important warming sources have already been discussed in Section 1.7. In particular, the effects of warming on two particular parts of slab avalanche release, fracture initiation and propagation, are reviewed. From experience and observations it is known that in fairly rare cases rapid cooling is reported to trigger slab avalanches (Goddard, pers. comm.). For the sake of clarity it should be noted that this literature review of warming effects on snowpack stability refers to short-term temperatures changes within a time span ranging from less than a few hours to multiple days in certain cases. Other long-term warming effects that exceed this time range, such as seasonal and global warming effects on avalanche activity, are not considered here.

Many textbooks on avalanche safety acknowledge surface warming of the snowpack, in particular strong and rapid warming as a factor that can cause instability (Jamieson, 2000; Tremper, 2001; McClung and Schaerer, 2006; Munter, 2009). However, in most of these books the effect of warming is not quantified but rather described in qualitative terms. When considering the effect of warming on instabilities many tend to think more about spring conditions (moist and wet snowpack) and less about warming effects during cold days while the snowpack is still dry. This fact was confirmed in a survey amongst avalanche workers on the warming effect on snowpack stability. Actual snowpack and air temperatures of warming induced instabilities were colder than those perceived by avalanche workers in many cases (Exner, 2006).

2.2.1. Results from accident statistics and observations

Statistical analyses of avalanche accidents in western Canada (Jamieson and Geldsetzer, 1996; supplemented with data from the CAA, 2003) showed that 70% of over 1000 recreational avalanche accidents occurred between noon and 4 pm. During this time period daytime temperatures are usually highest and the misleading conclusion could be drawn that this is strongly correlated to snow slab instability. Experience shows that during that time, most recreationists are in avalanche terrain and thus act as the main trigger themselves rather than the daytime warming effect. In 4% out of 65 accidents, the temperature from the previous day increased between 3° and 8°C. Of these 65 accidents, 86% exhibited only minor temperature changes between -2.5° and +2.5°C, suggesting that air temperature warming often does not have a significant influence on stability changes.

Jamieson and Geldsetzer (1999) surveyed 153 avalanche workers in Canada on weather, snow pack and terrain characteristics from unexpected avalanches. The results regarding air temperature conditions showed an increase from the previous day of 5° to 10° C in 6 % of cases. In 69 % of the 153 people surveyed, the temperature rose by 1° to 5°C. The temperature increased rapidly in the last three hours by more than 5°C in 5 % and in 44 % the increase was between 1°and 5°C. In all others cases, the temperature remained steady or decreased. In 73 % the air temperature ranged between –10° and 0 °C, and 11 % showed air temperatures above 0°C. Other factors contributing to avalanching were not ruled out in these temperature considerations. This might reduce the percentage of avalanches occurring at the same time as warming. These results are in agreement with the statistics from the CAA (2003).

Harvey and others (2002) analysed over 1000 recreational avalanches accidents in the Swiss Alps between 1970 and 1999. On 24 particular days, 4 or more avalanches occurred on a single day. These 128 days were defined as avalanche days. According to factors contributing to avalanching, these days, were divided into five clusters sorted by the temperature difference to the previous day (Figure 2.4). Only Cluster 1 (20 % or 23 accidents) exhibited a temperature increase of approximately 2° to 5°C. In all others clusters, temperatures dropped from the previous day. The mean morning temperatures at 2000 m with -6°C were highest in Cluster 1. This yields a considerable percentage of avalanches in which warming appeared to be the only factor contributing to avalanching.

Bakermans (2006) showed that direct solar radiation is the dominant factor for near surface daytime warming. Thus, the results from the CAA (2003), and Jamieson and Geldsetzer (1999) might not be conclusive, since the radiant increase of near surface temperatures was not taken into account. Furthermore, the influence of other factors such as new snow loading and drifting snow was not ruled out, which might even decrease the number of days in which warming was the significant factor. In contrast to the Canadian studies, the statistics from Swiss accident data from Harvey and others (2002) yielded that warming was the only contributing factor that lead to avalanching in 20 % of 128 cases. Different weather patterns and snow pack characteristics of the European Alpine and Western Canadian snow climate and different methods of analyses might have contributed to the variations in the results.

In 23 (25%) of 91 fatal avalanche accidents in Canada (between 1996 and 2007) critical warming appeared as a contributing factor (Jamieson and others,

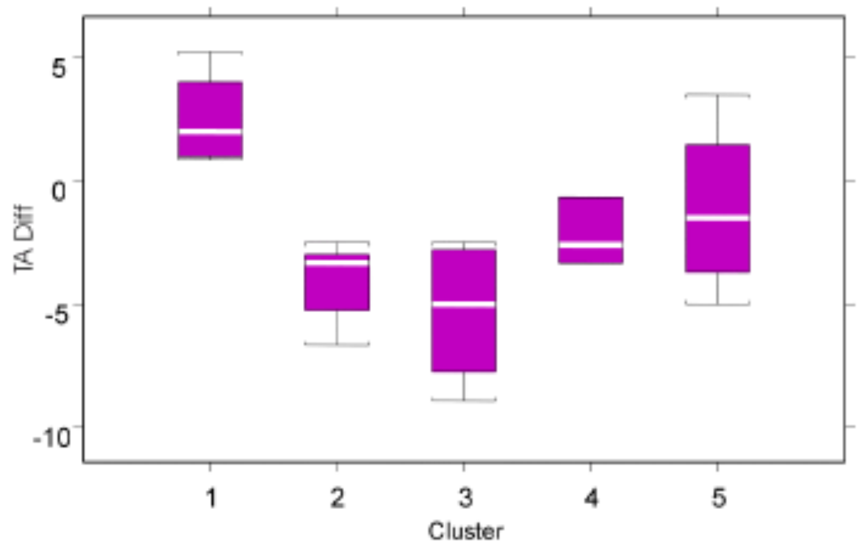

Figure 2.4. Temperature difference to the previous day of recreational avalanche accident for five clusters: Cluster 1: Temperature rise since previous day, insignificant amount of new snow and low winds; Cluster 2: Lots of new snow during previous days and cold temperatures; Cluster 3: Weak snow cover, moderate amount of new snow, moderate winds and cold temperatures; Cluster 4: Strong winds; Cluster 5: Largest amounts of new snow, moderate winds and weak snow cover. (Harvey and others, 2002; reproduced with permission from S. Harvey)

2010, p. 26). Critical warming was defined as 'either a recent rapid rise in air temperature to near 0˚C, or wetting of the upper snowpack due to strong sun, above-freezing air temperatures or rain' (p. 420). In 13 cases (11%) that showed signs of critical warming, no recent loading due to wind or precipitation was observed.

2.2.1.1 Low density snow and rapid solar warming

According to a survey that was conducted amongst 35 experienced avalanche practitioners in western Canada, numerous reports of slab avalanches where solar warming contributed to instability followed a similar pattern (Exner and Jamieson, 2008). In all of these cases, obvious signs of instability (shooting cracks, whumpfing and skier-triggered avalanches) developed during a short period of strong solar warming after the snowpack initially appeared to be stable and no obvious weak layer was observed. A few of these cases were reported by helicopter and cat ski operations, where a run was skied several times during the warming period. Snowpack observations ranged from no signs of instability on the first run to shooting cracks and triggered slabs within hours on the following runs. The following list summarises conditions which were reported in a number of incidents.

- *East to south-east facing slopes (35-40° slope angle)*
- *Air temperatures well below zero (in the -8° to -15°C range)*
- *Clear skies, strong solar radiation in the morning hours in March or April*
- *First sunny day after a storm*
- *Cold, low density near surface layer*
- *No signs of warming (snow surface still dry)*
- *Initially stable snowpack, no obvious weak layers*

In the winter season of 2007/08, a number of natural slab avalanches released in January above ice climbs in the Canadian Rocky Mountains (Rockies) on steep sunny aspects. Most of these avalanches released in the first few days after a storm on a sunny day with air temperatures well below zero. Perhaps the combination of the weak snowpack in the Rockies this winter and still sufficiently strong solar radiation on steep sunny aspects was a factor in releasing these avalanches. Given the weak, unstable snowpack, even the low January sun provided enough warming to act as a trigger. In the springtime it is more common for avalanches above ice climbs to start as moist point releases and then eventually trigger a deeper weak layer and release a slab avalanche (Exner and Jamieson, 2008).

2.2.2. The warming effect in (statistical) forecast models

Air and snow temperature parameters are included in many statistical avalanche forecasting models. In most cases these parameters did not contribute significantly to avalanche hazard or avalanche activity.

In an expert system approach to forecast avalanche hazard (Schweizer and Foehn, 1996) air temperature, daytime warming and the three-day sum of maximum temperature were not considered major parameters when evaluated according to logical importance. Davis and others (1999) correlated storm and weather factors with avalanche activity. Minimum and maximum air temperature did not prove to be of any predictive merit. All air temperature parameters (min, max, previous day) in a study by Jones and Jamieson (2001) only yielded non-significant correlations with skier-triggered avalanches. Jamieson and others (2009) correlated local weather and snowpack observations with the regional and local avalanche danger. Temperature parameters such as daytime warming, temperature change within the last 24 hours and above freezing temperatures all showed insignificant correlations. Only temperature above freezing was significantly correlated with the local danger, but with a low correlation coefficient.

2.2.3 Depth of weak layers affected by surface warming

Usually, surface warming is most efficient as an avalanche trigger on relatively thin slabs consisting of low-density new snow (McClung and Schaerer, 2006, p. 97). McClung (1996) concluded that the daytime warming temperature effect on a weak layer is mostly not relevant since typical daytime warming usually does not reach the weak layer. Daytime warming only increases the temperature of the top 20 – 30 cm of the snowpack. The average weak layer depth of the typical skier triggered avalanche is approximately 40 - 50 cm (Schweizer and Luetschg, 2001; Schweizer and Jamieson, 2001).

Wilson and others (2001) showed with FEM modelling that the warming front does not have to reach the weak layer for slope-parallel deformation to increase in layers below that are not reached by the warming front. These findings have been confirmed by field experiments by Exner and Jamieson (2008) on the daytime warming effect of snowpack creep of the near-surface layers (see Chapter 8).

Observations showed that surface warming occasionally contributes to the release of deep slab avalanches (Jamieson and others, 2000). In those cases it is assumed that slab thickness in the start zones in very variable. Most likely the fracture is initiated in those thinner areas, for example wind affected, or in weaker zones that comprise faceted grains and depth hoar (Logan, 1993). Also snowpack warming over multiple days may contribute to the release of deeper instabilities (Jamieson and others, 2000).

2.2.4. Direct-immediate and indirect-delayed effects of surface warming

The effect of snow temperature changes on snowpack instability is a highly time-sensitive process (Schweizer and others, 2003; McClung, 1996). Snow stiffness, as the most temperature dependent mechanical property, is regarded as the most important mechanical property of snow that influences snowpack instability (McClung and Schweizer, 1999). Other mechanical properties such as fracture toughness, the energy release rate during the fracture process, and snowpack creep strongly depend on stiffness. Basically, stiffness is determined by the microstructure of the ice skeleton or in particular by the number and size of inter-granular bonds.

The direct elastic deformation is usually described by Young's modulus, which is nearly independent of temperature (McClung, 2003; Section 1.2). To describe the behaviour of snow for rapid, partially inelastic deformation, an effective modulus (stiffness) is applied, which incorporates all three modes of deformation (see Section 1.2) However, the effective modulus mostly comprises the direct and delayed elastic deformation and to a small extent plastic (viscous) deformation (McClung, 1996; Schweizer and Camponovo, 2002).

Assuming that the snow microstructure does not change, it is the temperature dependence of the effective stiffness of the ice matrix that is directly responsible for bulk stiffness changes of snow. The number and size of bonds dictate the bulk stiffness of snow, which usually increases with snowpack creep, settlement and densification (Bartelt and Christen, 1999). These processes are also highly temperature dependent themselves and therefore indirectly influence snow stiffness. Usually, this requires more time than the direct effect of temperature changes on the ice matrix. Accordingly, temperature changes, in particular warming, can be divided into *direct-immediate* and *indirect-delayed* effects on stiffness or snowpack instability (McClung,1996; McClung and

Schweizer, 1999; Schweizer and others, 2003):

Direct-immediate effects: No or negligible changes in snow microstructure of the slab take place. Stiffness is primarily directly controlled by the temperature dependence of the effective stiffness of the ice material of the current lattice. *Direct-immediate* effects usually promote instability, since other processes, that strengthen the snowpack, such as sintering, require more time. Mechanical properties that determine snowpack stability, such as stiffness, strength and fracture toughness (propagation propensity, energy release) are therefore also directly affected (McClung and Schweizer, 1999). In rare cases, however, where the weak-layer is reached by the warming front fracture toughness of the slab weak/layer combination likely slightly increases (McClung, 1996).

Indirect-delayed effects: In this case, slab stiffness changes are mainly controlled by changes in snow microstructure. Rearrangement of the microstructure through settlement (densification) and sintering increases the number, size and strength of inter-granular bonds. The *direct-immediate* effect of snow temperature on stiffness becomes a second order effect in this case, but still takes place. Actually, decreasing stiffness of the ice matrix enables faster settlement, creep and densification and in turn promotes strengthening of the snowpack in the long run. Snowpack stability usually increases due to *indirect-delayed* effects. These processes require time. Temperature has the strongest effect on bonding and creep processes (*indirect-delayed effects*) which are highly time and temperature dependent (McClung, 2003).

2.2.5. Temperature dependence of snowpack strength

Measurements from Bucher (1948) and Roch (1966) showed a decrease of tensile strength of 25 - 75% for increasing temperatures from -10˚C to 0˚C. However, fracture line data from Perla (1976) indicated that bed surface shear strength increased with increasing bed surface temperature. This trend is most likely due to a ‘depth’ effect of the weak layer. Deeper weak layers are usually warmer and have higher shear strength due to the larger mass of the overlying slab (McClung, 1996; Jamieson and Johnston, 1998). Weak layer shear strength decreased by 10 - 15 % with warming weak layer temperatures from -3˚C to close to the melting point, according to field studies from Hoeller (1998). McClung (1996) conducted shear experiments and concluded, in contrast to other studies, that failure strength and strain is nearly independent of temperature. Schweizer (1998) found a decrease of shear strength of 20% with warming from -15˚C to -2˚C also in lab experiments with a shear apparatus.

The decrease in weak layer strength contributes, if the weak layer is affected by warming, to instability, but is not, as was believed for some time, the major cause for stability changes. Temperature effects on slab stiffness and deformation rate seem to be the major contributor to instability of natural slab avalanches (McClung and Schweizer, 1999).

2.2.6 Temperature dependence of effective stiffness

Mellor (1975) reported a decrease of Young's modulus of less than 20% for increasing temperatures from -10˚C to -2˚C from high frequency vibration experiments. Likely, the reported decrease actually contained visco-elastic effects and therefore strictly speaking describes the effective modulus.

McClung (1996) conducted shear frame experiments on snow samples at various temperatures and estimated stiffness from the initial tangent modulus on the stress-strain curve. The tangent modulus increased by approximately a factor of three as snow temperature decreased from -2˚C to -18˚C. McClung concluded that despite the fairly rapid deformation, to some extent, irrecoverable viscous deformation is included in his results on stiffness.

Laboratory experiments from Schweizer (1998) on the effective shear modulus confirmed the temperature dependence of stiffness. Visco-elastic effects and the temperature dependence of the effective stiffness may play a role in slow fracture initiation (spontaneous and artificially/human triggered avalanches) but once a fracture is initiated the propagation behaviour is best described by the quasi-brittle behaviour of snow (McClung, 2003).

Schweizer and Camponovo (2002) conducted dynamic load experiments to

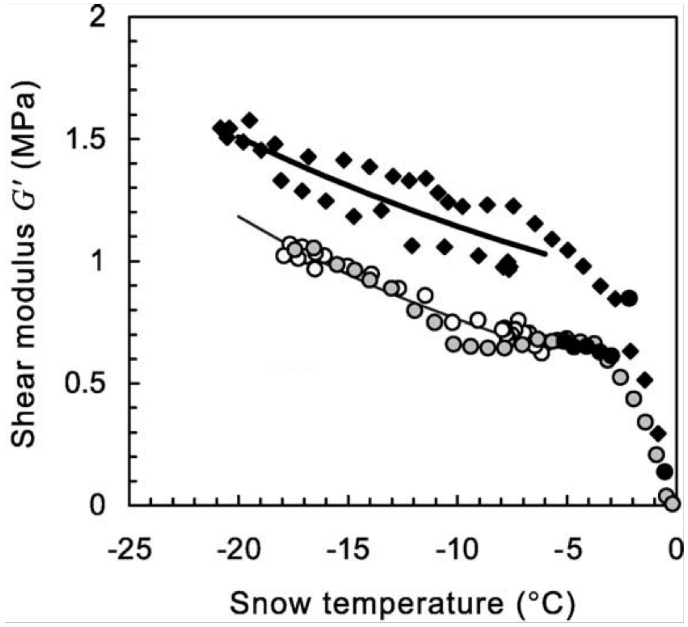

Figure 2.5. Temperature dependence of the effective elastic shear modulus of snow. Solid lines indicate an Arrhenius relationship (Schweizer and Camponovo, 2002; reproduced with permission from J. Schweizer)

determine the temperature dependence of the effective elastic shear modulus of snow samples in a cold laboratory at high strain rates to exclude irrecoverable viscous deformation. The effective shear modulus decreased approximately 50% with warming snow temperatures from -20˚C to about -6˚C following an Arrhenius relationship (Figure 2.5). At warmer temperatures closer to the melting point stiffness decreased even faster. Likely, pre-melting phenomena (grain boundary sliding) were responsible for the faster decrease towards the melting point.

Reuter and Schweizer (2011) measured the stiffness (effective modulus) of the near surface layers with a snow micro-penetrometer in field experiments and calculated the solar energy input into the snowpack from the surface energy balance. Reuter observed a decrease of surface layer stiffness of approximately 50% for a solar energy input of about 300 kJ/m^2, which approximately equals one half hour of exposure to solar radiation in the morning hours on a steep east-facing aspect. The critical cut length necessary to initiate a fracture in Propagation Saw Tests (PST) yielded a weak decreasing trend with the high solar energy input.

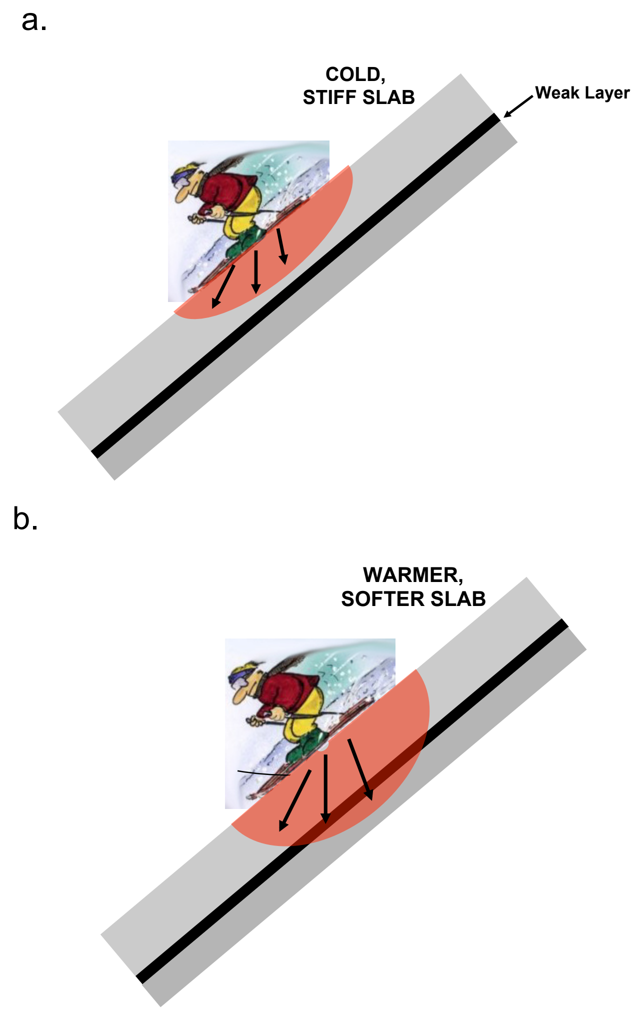

Figure 2.6. The effect of slab temperature on deformation due to a skier load: **(a)** hard, colder surface layer and **(b)** soft, warmer surface layer. (After McClung and Schweizer, 1999)

2.2.7 Effect of warming induced stiffness changes on fracture initiation and propagation

Stiffness, as the most important mechanical property of snow, controls fracture initiation and propagation propensity. In the following pages, the temperature dependence of fracture initiation of spontaneous and human triggered avalanches, and the fracture propagation process are reviewed.

2.2.7.1 Fracture initiation

McClung and Schweizer (1999) argued that stresses and deformation due to a surface load, such as a skier, penetrate deeper into the snowpack and affect a larger area with warming of the near surface layers (Figure 2.6). The temperature dependent delayed-elastic and visco-elastic deformation (effective stiffness) should increase with warming. A fracture in a potential weak layer that was not affected by the deformation due to the surface load as long as snow temperatures were cooler could be initiated after warming.

Wilson and others (1999) showed with FEM modelling that shear stress due to a static skier load increased with warming up to 37% at 50 cm and 51 % at 30 cm weak layer depth. For their studies they assumed a stiffness decrease with warming of 50% according to a temperature increase from -15 to -5˚C (Schweizer, 1998). The increase in shear stress may be sufficient to exceed the strength of the weak layer.

Schweizer and Camponovo (2001) concluded from field experiments that the skier-induced stresses in the snowpack penetrate deeper in warmer surface layers.

2.2.7.2 Propagation propensity (fracture toughness)

McClung (1996) argued that failure toughness, the area under the stress-strain curve to failure, decreases with warming. Less work is needed for warmer snow, with lower stiffness (lower initial tangent modulus) to reach the peak stress, which is nearly independent of temperature according to his shear tests.

McClung and Schweizer (1999), based on measurements from Schweizer (1998) revised the temperature effect on failure toughness. According to Schweizer’s results failure strain increases and failure strength slightly decreases with warming. Consequently, failure toughness shows an increasing trend with warming, which would impede failure initiation. It should be noted here that failure toughness is different from fracture toughness. In an engineering sense failure is defined as the peak on the stress-strain curve. Brittle fracture does not necessarily occur yet. Visco-elastic effects play a major role for failure toughness (fracture initiation), whereas fracture toughness is mainly determined by linear elastic

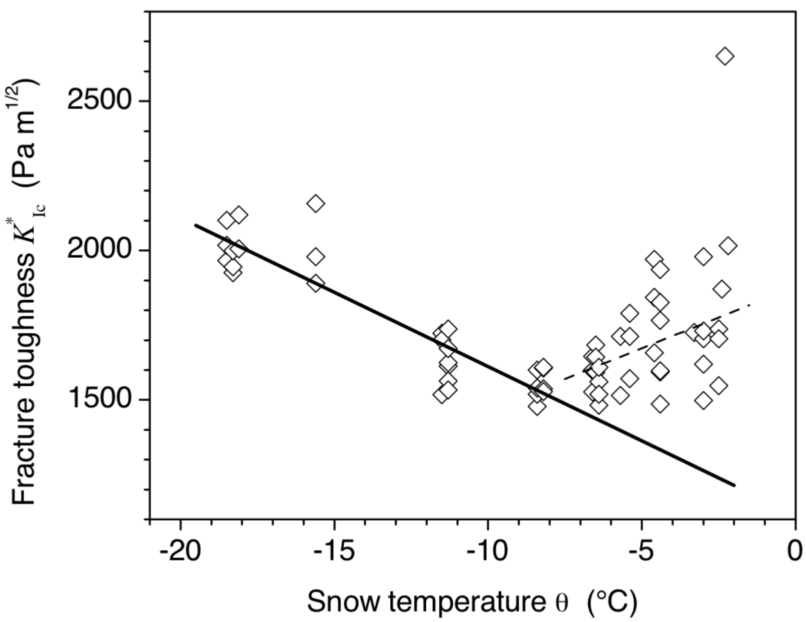

Figure 2.7. Temperature dependence of fracture toughness in tension. (Schweizer and others, 2004; reproduced with permission from J. Schweizer)

deformation (fracture propagation).

Furthermore, McClung and Schweizer (1999) argued, since stiffness decreases with warming, fracture propagation also likely decreases with warming. According to Equation 1.2, fracture toughness (K_{IIc}) is proportional to the square root of the shear modulus (G_{II}).

Schweizer and others (2004) conducted the first experimental study on the temperature dependence of fracture toughness in tension and found a 25% decrease for a 10˚C increase in snow temperature (Figure 2.7). Fracture toughness decreased with rising snow temperatures to about -6˚C, basically following an Arrhenius relationship. For higher temperatures the Arrhenius relationship broke down and fracture toughness showed a slight increasing trend towards to melting point. Pre-melting phenomena at grain boundaries, which are typical for high temperature materials (Spear and others, 2010), may explain this behaviour. Pedrenko and Withworth (1999) reported similar behaviour of ice. Decreasing fracture toughness with rising snow temperatures indicates higher propagation propensity of an initiated fracture.

Most fracture mechanical models are based on linear elastic fracture mechanics (LEFM) in which it is assumed that fracture propagation is a purely elastic (brittle) process. McClung (2009) proposed to describe fracture propagation by an effective fracture toughness, which also includes the fracture toughness of the weak layer and visco-elastic effects.

In most cases, weak layer temperature is not affected by daytime warming (Section 2.2.3). This implies that changes of propagation propensity are mainly determined by warming of the slab. Even if the weak layer is reached by the warming front it is the effective fracture toughness of the slab/weak layer system that controls the propagation process. Reduced stiffness of the slab (more energy available to create a new fracture surface) remains the first order effect over slightly increased fracture toughness of the weak layer (McClung, 2009). It is known from observations, however, that once a weak layer warms up and becomes moist, the effective fracture toughness of the slab/weak layer system increases. Forecasters reported that explosive control is most efficient when the surface layers warmed up, but as soon as the weak layer became moist explosives were not effective (Föhn, 1987).

Simenhois and Birkland (2008) conducted Propagation Saw Tests (PST) on warming days and reported shorter cut lengths to produce a propagating fracture in the test column indicating increasing propagation propensity with surface warming.

Fracture toughness in tension of the slab and slab stiffness appear to be the strongest contributors to effective toughness, which is the major measure to evaluate propagation propensity. Reduction of effective fracture toughness is the primary effect of warming on slab release. In other words, higher elastic energy release rates become available for fracture propagation (McClung, 2009).

2.2.7.3 Temperature effect on critical crack size

The temperature dependence of the critical initial crack size according to the collapse model (Section 1.4.2) can be estimated with Equation 1.3. With the temperature dependent stiffness (E) in the numerator, it follows that decreasing stiffness with warming reduces the critical crack size. In other words, the fracture in a weak layer induced by a skier may become sufficiently large to self-propagate. The critical crack size *(a_c)* derived from the shear model is obtained by combining Equation (1.1) and (1.2):

$$a_c = \frac{1}{\pi}\frac{EG_{II}}{\tau_g^{\,2}} \tag{2.1}$$

The temperature dependence of the critical crack size enters through the stiffness *(E)*. The temperature dependence of the effective shear modulus is given by (Schweizer and Camponovo, 2002):

$$G = G_0^{'}\, e^{-\frac{Q}{RT}} \tag{2.2}$$

with *G_o'*: Reference value for *G*

R: Gas constant

T: Snow temperature

Q: Activation energy

The shear modulus *(G)* can be written in terms of Young's modulus (Das, 2008, p. 57):

$$G = \frac{E}{2(1-\nu)} \tag{2.3}$$

with ν: Poisson's ratio

If stiffness *(E)* decreases with warming snowpack temperature, then according to Equation 1.4, the critical crack size for propagation *(a_c)* is also reduced. Regarding the spontaneous slab release process, existing flaws in a weak layer may become critical and self-propagate.

2.2.8. The warming effect on creep

Snowpack creep is the deformation of the snowpack due to gravitational forces and snow metamorphism (McClung and Schaerer, 2006, p. 75) and can be divided in a slope normal and slope parallel component. Generally, snowpack creep is a viscous irreversible process that usually increases density, hardness (stiffness) and the number and size of bonds. Usually, strain and deformation rates during creep are more than two orders of magnitude too low to induce brittle fracture or strain softening (see Section 1.2). Only the first (elastic) stage of creep may cause strain rates high enough for ductile to brittle transition. On a very short time scale (immediate to hours) if the slope parallel deformation due to increased creep reaches the threshold for ductile to brittle transition, a failure or fracture may be initiated. Rapid warming events may have the potential to accelerate creep (slope parallel) to reach those critical values.

An extensive body of literature is available to describe the creep process of the snowpack (e.g. Mellor and Smith, 1966; McClung, 1984; Olange and McClung, 1990; Abe, 2001). Most of those studies, however, focus on stationary creep as a process that strengthens the snowpack over days and weeks or are concerned with the pressure due to creep on structures and buildings. Only a very limited number of studies exist that examine the initial stages of creep (short term) that may affect the slab avalanche release process.

Voitkovsky and others (1975) pointed out that the highest deformation rates during the creep process occur in the initial stages in particular in low-density snow.

McClung (1979) concluded from field studies and calculations that creep rate increased in the order of 10 – 20 % for warming in low-density snow. That would refer to an increase of 5 - 10 % of the driving force for fracture propagation due to the decrease of Young's modulus.

Conway (1998) measured the increase of shear strain rate in the near-surface layers with an array of glide shoes in the snowpack that were attached to potentiometers during the onset of rain and concluded that warming and the added load due to rain decreased the critical length for propagation by 10 – 20%. Conway also observed that layers that are directly affected by the warming showed increased strain rates. The pure effect of warming could not be separated from the additional load added by the rain.

Louchet (2001) modelled a layered snowpack as an 'open cell foam' of ice.

Creep and deformation was introduced by the rate of bond breaking and welding rate, which are temperature dependent parameters. At higher temperatures the welding rate was assumed to increase. This implies that creep instability at warmer temperatures decreases with other factors being constant. This is in contrast to other approaches and field observations of solar induced slab releases (see Chapter 8). The time-sensitivity of warming effects was not entirely taken into account in this approach.

Trautman and others (2004) determined deformation rates due to creep of up to 1 cm/day for a melting snowpack in the near-surface layers where melt water accumulated. This is potentially related to the release of wet avalanche release.

From laboratory creep studies with snow samples in shear Chandal and others (2007) estimated the temperature dependence of Young's modulus. They concluded that the onset of creep is slightly temperature dependent and mainly depends on density and hardness.

Field experiments from Exner and Jamieson (2009) in fact showed that the slope parallel component of creep due to solar warming accelerated, even below the layers that were directly affected by the warming. The results of this study are presented in detail in Chapter 8.

2.2.9 Summary

Field observations, experience and avalanche accident statistics provided hints that (rapid) warming of the near-surface layers (mostly daytime warming) can be a major factor contributing to both human-triggered and spontaneous slab avalanche release. Many textbooks on avalanche safety acknowledge warming as one of the major factors contributing to avalanching, even though rare in occurrence compared to other factors such as precipitation and snow redistribution due to winds. The effect of surface warming, however, has not received as much attention through scientific studies as the other two. A reason for that may be that warming is not as tangible and obvious as large new snow amounts and blowing and drifting snow due to strong winds. The causes are subtle and mostly invisible, but the effects can be dramatic and fatal (Tremper, 2008, p. 61).

In statistical forecast models the destabilising effect of warming did not prove to be a significant contributing factor. This may stem from the relatively low frequency of warming induced instabilities or that the time scale considered in those models was too large to capture rapid warming effects.

The effective moduli, stiffness in tension and shear, are regarded as the most temperature dependent and most important mechanical properties of snow with regard to snowpack stability. Other mechanical properties and behaviour of snow that play a major role in the slab avalanche release process strongly depend on stiffness. Those are the depth penetration of stresses and deformation due to surface loads, fracture toughness, the energy release rate, and the critical crack size necessary for fracture propagation. Snowpack warming effects that may cause instability have so far been described mostly in qualitative terms. Through a limited number of laboratory studies, however, more is known about the quantitative temperature dependence of the shear modulus and fracture toughness in tension. Field studies to shed more light on the temperature dependence of mechanical properties and instability to this date are rare. Exner and Jamieson (2008) expanded the approach of measuring the additional skier stresses (Section 2.1.2) to 2D measurements and included the effects of temperature and the bending of the skis. This study is presented in detail in Chapter 3.

Amongst other recommendations to comprehensively understand snow avalanche formation, Schweizer and others (2003) in a review on the state of art on snow avalanche formation suggested to address the quantitative effect of surface warming on snowpack stability.

CHAPTER 3

General methods

General methods for snowpack characterisation and data analysis are introduced in this chapter. Specific methods are described in the methods section of each chapter. The stress measurement technique, which was used for the skier stress (Chapter 5), snowmobile (Chapter 6) and cold lab experiments (Chapter 7) is described and evaluated in detail in Chapter 4.

3.1 Study site and areas

The majority of the field studies were conducted in Glacier National Park, BC. Preliminary studies that led to the development of the stress measurement technique described in Chapter 4 were performed in Kananaskis Country, AB (Figure 3.1). Glacier National Park is located in the Selkirk Mountains with its intermountain snow climate (Haegeli and McClung, 2007). The Kananaskis area, as part of the Canadian Rockies shows all characteristics of a continental snow climate.

3.2 Standard methods for snowpack characterisation

Snow as a highly porous, visco-elastic and temperature dependent material is in constant change. Snowpack properties and layering therefore can vary considerably over space and time. This required classification of the snow for each of the experiments conducted for this study in terms of grain shape and size, hand hardness, density, temperature, and moisture content for each layer of interest. The snow classification followed the guidelines of the ICSSG (Fierz and others, 2009), which have been successfully applied by practitioners and researchers for many years. Snowpack layers on a vertical snow pit wall adjacent to the

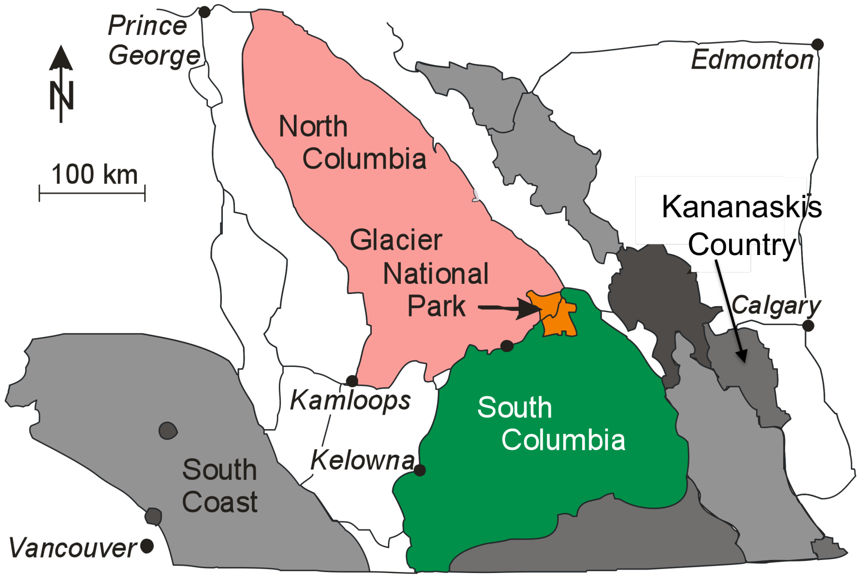

Figure 3.1. Map of study area and sites.

experimental sites were identified by visual and tactile clues and characterised according to the guidelines of the CAA (CAA, 2007). Snow type, hardness and liquid water content can be somewhat subjective depending on observer differences. To ensure preferably objective observations, at the beginning of every field season ASARC staff 'calibrated' snowpack classifications against each other in a week-long field method training.

3.2.1 Grain type and size

The type and size of snow grains for each layer were determined with the help of a crystal screen with 1 to 3 mm grids and an eight-times optical loupe. Main grain shape classes are listed in Table 3.1. Grain size was estimated to an accuracy of approximately a quarter of a millimetre. For grain size classes see Table 3.2.

3.2.2 Hand Hardness

Snow hardness was determined by standard hand hardness tests of each identified layer. The objects (Table 3.3) were gently pushed into the snow pit wall with a force of approximately 10 – 15 N (Fierz and others, 2009). The hand

Table 3.1. Main morphological grain shape classes (After Fierz and others, 2009).

Class	*Symbol*	*Code*
Precipitation **P**articles	+	PP
Decomposing and **F**ragmented precip. part.	⁄	DF
Rounded **G**rains	•	RG
Faceted **C**rystals	□	FC
Depth **H**oar	∧	DH
Surface **H**oar	∨	SH
Melt **F**orms	o	MF
Ice **F**ormations	▮	IF

Table 3.2. Grain sizes (After Fierz and others, 2009).

Term	*Size [mm]*
Very fine	< 0.2
Fine	0.2 – 0.5
Medium	0.5 – 1.0
Coarse	1.0 – 2.0
Very coarse	2.0 – 5.0
Extreme	> 5.0

Table 3.3. Classification of snow hardness (After Fierz and others, 2009; McClung and Schaerer, 2006, p. 77).

Term	*Object*	*Code*	*Strength [kPa]*	*Symbol*
Very low	Fist	F	0 – 1	
Low	4 Finger	4F	1 – 10	⁄
Medium	1 Finger	1F	10 – 100	X
High	Pencil	P	100 – 1000	⁄⁄
Very High	Knife blade	K	> 1000	⋇
Ice		I		▮

hardness test is a measure for push resistance and is fairly subjective since it depends on the operator's definition of 'gentle' and the operator's hand size and objects used. Nevertheless, the test is suitable to record relative hardness differences within one snow profile in a reasonably objective way. For comparing

Figure 3.2. Push gauge with 1 cm^2 disk at tip.

hardness profiles from different observers it is recommended that operators ‘calibrate’ themselves against each other (Fierz and others, 2009).

3.2.3 Penetration resistance

In addition to the hand hardness measurements push resistances with a push gauge and a 1 cm^2 disk were conducted (Figure 3.2). The push gauge was inserted layer-parallel with a spacing of 5 cm, or less for thinner layers. Up to five push resistance measurements per layer were conducted. Push resistance in kPa was calculated from the force reading (N) of the gauge and the surface area of the disk.

The push resistance is a more objective method to determine snow hardness than the hand hardness test. Smaller changes in hardness can be detected and quantified which is not possible with the hand hardness test due to the operator dependent performance. Basically, snow density, the number and size of inter-granular bonds, and snow temperature determine snow hardness (resistance to penetration) or stiffness. Table 3.3 gives an overview how penetration resistance and hand hardness are related. Determining stiffness (Young’s modulus) accurately, which is an important mechanical property, is a complex procedure (Sigrist, 2006, p. 50). For the purpose of this thesis, the change in push resistance was used as an approximate measure for stiffness changes. The push resistance measurements turned out to be sensitive to hardness (stiffness) changes due to temperature variations. Challenges with the push gauge technique arose in warmer snow that started to become moist. 'Ratcheting' (irregular penetration speed) of the probe tip caused unrealistically high force values. Those were excluded from analysis. The accuracy of the push resistance measurements was estimated at 90 % with a confidence of 95 % (Smith, pers. comm.).

3.2.4 Weather data

Meteorological data (air temperature, wind speed and direction, incoming short and long wave radiation) were available from automatic weather stations at the Mt. Fidelity study site (Glacier National Park) for experiments that were conducted in close proximity.

3.2.5 Density

Snow density of each layer thicker than 3 cm was measured by weighing snow samples taken in a aluminium tube of 100 cm^3 volume. The reading of the scale multiplied by ten was recorded as snow density in kg/m^3. In some cases density was averaged over two measurements to minimise the error.

3.2.6 Liquid water content

The liquid water content of the snow was classified according to the guidelines outlined in Table 3.4.

3.2.7 Snow temperature

Snow temperature was measured with an Oakton Acorn hand-held thermistor thermometer. In most cases, the measurements were taken in vertical 5 cm intervals in the top 30 cm of the snow pit wall; below in 10 cm intervals. The maximal depth rarely exceeded 1 m since most experiments were concerned with temperature changes in the near-surface layers. The thermometer was inserted parallel to the layer. The thermometer was shaded from the sun while measuring snow surface temperature and near-surface snow temperature.

Table 3.4. Classification of liquid water content (After Fierz and others, 2009).

Term	*Code*	*Description*	*Approximate water content [vol. %]*	*Symbol*
Dry	D	Snow grains have little tendency to adhere to each other when pressed together, as in making a snowball.	0	
Moist	M	When lightly crushed, the snow has a distinct tendency to stick together.	0 – 3	I
Wet	W	Water cannot be pressed out by moderately squeezing the snow in hands.	3 – 8	II
Very wet	V	Water can be pressed out by moderately squeezing the snow in hands.	8 – 15	III
Soaked	S	The snow is soaked with water.	> 15	IIII

3.3 Methods for data analysis

The majority of the data analysis (basic statistics, regression curves, graphing, image processing) was conducted in Mathworks Matlab (version R2010aSV and R2008bSV) (citation). Curve fitting of measured data points was conducted with the additional Curve Fitting Toolbox.

The 2D contour plots of normal stresses (Chapter 5, 6 and 7) were generated with built-in contour plot functions. The measured data points were linearly interpolated on a finer regular grid and smoothed by using a 2D convolution function.

3.4 Definitions

3.4.1 Stresses

Within the context of this thesis the terms *stress* and *normal stress* are used interchangeably and refer to vertical normal stresses in the snowpack due to

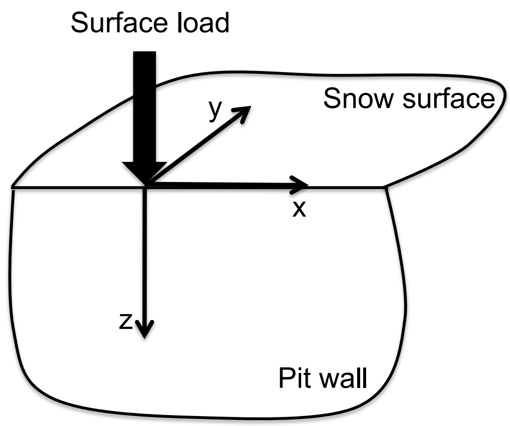

Figure 3.3. Cartesian coordinate system with origin on undisturbed snow surface at the centre of the surface load.

surface loads. Normal stress on the sensor prior to surface loading is subtracted. Other stresses, such as shear stress, are specifically mentioned. Since all experiments were conducted in flat terrain (0˚ slope angle) and the sensor pads were always oriented horizontally, only the vertical component of normal stresses was measured.

Normal stresses in the snowpack relative to measured or calculated surface stresses are referred to as normalised stresses.

3.4.2 Coordinate system

To describe locations within the snowpack a Cartesian x,y,z - coordinate system was chosen. The positive z-axis denotes the direction vertically into the snowpack, the x-axis is pointed along surface load, for example along a ski, and the y-axis across the surface load. The origin of the coordinate system was chosen on the undisturbed snow surface under the centre of surface loads. For example, this was the centre of the ski boot during the skier experiments and the centre of the metal weights in the cold lab experiments. The effective depth z_{eff} is the depth below the ski factoring in compaction of the near-surface layer.

3.4.3 Dry vs. wet snow conditions

With warming temperatures in spring season the snowpack gradually becomes isothermal at 0˚C and loses its cohesion. Wet slab and loose avalanche are more likely, which can be large with huge destructive potential (Tremper, 2008, p.147). Effects of warming on dry slab avalanches are subtler and can easily be underestimated (Exner and Jamieson, 2008). This thesis is concerned with slab avalanche release processes during dry snow conditions. Nevertheless, cases in which only the surface layer started to become moist were still regarded as dry snowpack conditions.

CHAPTER 4

A method to measure normal stresses in the snowpack due to surface loads

4.1 Introduction

Compaction and indentation of the snowpack due to vehicles or planes on snow-covered roads or runways were of great interest in many scientific studies (e.g. Blaisdell and others, 1990; Haehnel and Shoop, 2004). However, the majority of these studies merely dealt with the very near surface layers of a relatively compacted snowpack. Field studies on the depth penetration of surface loads, such as skiers, that are relevant for slab avalanche release are rare (Camponovo and Schweizer, 1997; Schweizer and Camponovo, 2001). In fact, only one study exists in which realistic skier stresses were measured in a natural undisturbed snowpack (Schweizer and Camponovo, 2001). The stress transducer setup that was used for their study, however, required significant structural changes to the natural snowpack.

As outlined in Section 1.8, one major objective of this thesis was to measure normal stresses in the snowpack due to realistic surface loads and their variations due to snow temperature changes. For this purpose, a suitable method needed to fulfil the following requirements:

- Measure normal stresses due to surface loads with a sensitivity sufficient to capture the effect of stiffness changes caused by snow temperature variations.
- The entire set-up needed to be portable in the field, since many suitable study sites were only accessible on skis.
- Endure harsh winter field conditions (moisture, below freezing temperatures).
- Minimise effects on snowpack structure due to the intrusive method.

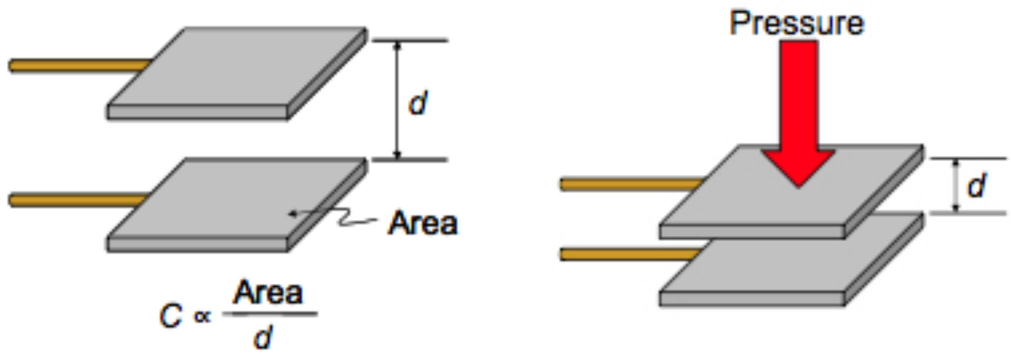

Figure 4.1. Schematic showing the principle of capacitive stress measurement. A decrease of the spacing *d* of the capacitor plates increases the voltage output that is generated between the plates. *C* is the capacitance of the capacitor plates.

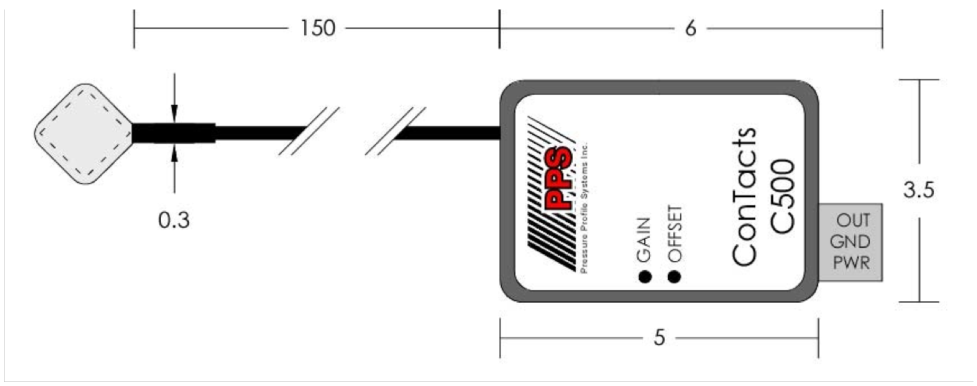

Figure 4.2. Capacitive stress sensor with signal conditioning box (units in cm, stress pad not to scale). (Pressure Profile Systems, 2007).

Figure 4.3. Stress sensor pad (5 cm x 5 cm) mounted on aluminum sheet for insertion into snowpack.

This chapter describes the features and performance of the method that was developed to measure normal stresses in the snowpack.

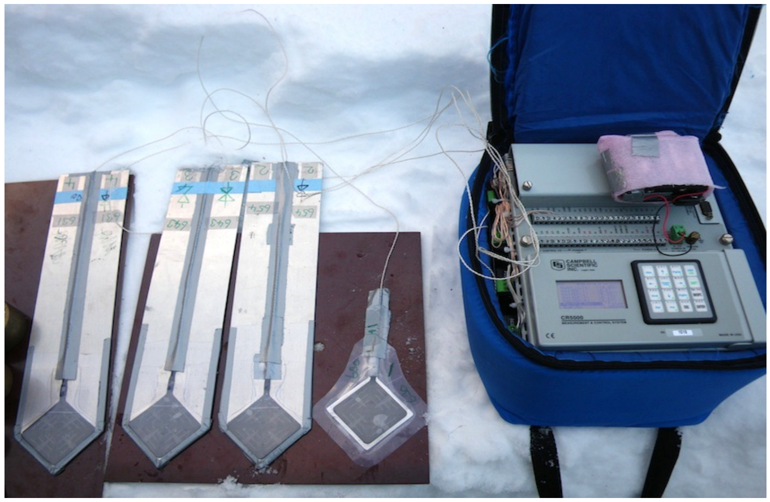

Figure 4.4. Stress measurement set up with Campbell Scientific CR5000 data logger and four stress pads mounted on insertion sheets. The data logger and battery block were kept in an insulated box.

4.2 The stress measurement setup

4.2.1 Stress sensors

To measure the normal stress component in the snowpack due to surface loads, commercial, capacitive (Figure 4.1) stress pads (Figure 4.2, Table 2.1), 5 cm x 5 cm in surface area, were placed horizontally in the natural snowpack. The surface loads applied were static and dynamic forces due to skiers and snowmobiles in outdoor experiments (Chapter 5 and 6) and metal cylinders in cold lab experiments (Chapter 7). The sensors, which were mounted at the tip of a 2 mm thick aluminum sheet (6061 T6) (Figure 4.3) were pushed horizontally into the sidewall of the snow pit (Figure 4.5). Waterproofing of the sensors was necessary with a thin, yet water-resistant plastic adhesive sheet to protect them from moisture. The specific usage of the sensors is described in the methods chapters for each of the experiments (Chapter 5, 6 and 7).

Two sensors were used simultaneously for outdoor experiments during the winter of 2008 with a Campbell Scientific CR1000 data logger (Figure 4.5), and four sensors for outdoor and cold lab experiments in the winter of 2009 with a

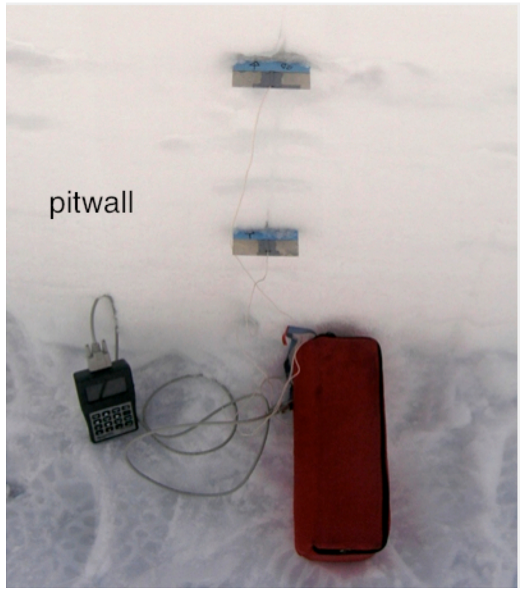

Figure 4.5. Stress measurement setup with Campbell Scientific CR1000 data logger (red container), two sensors and keypad.

Table 4.1. Stress sensor specifications (Pressure Profile Systems, 2007).

Method	*Capacitive*
Sensor thickness	*1 mm (3 mm including insertion sheet)*
Surface area	*25 cm^2 (5 cm x 5 cm)*
Stress range	*13.79 kPa (2 psi) at standard conditions; 6.5 - 10 kPa depending on temperature (-20˚C to 0˚C)*
Temperature range	*-20 to 200˚C*
Response bandwidth	*2 kHz*
Voltage output	*0 – 5 VDC (single ended), 0 – 800 µVDC (half bridge)*
Temperature sensitivity	*Appr. 4.4 µV/˚C*
Sensitivity	*1:200*
Non-repeatability	*<2%*

CR5000 data logger (Figure 4.4). The maximum sampling frequency of the four-sensor CR5000 set up was limited to 11 Hz per sensor due to simultaneous usage of four sensors, signal settling and integration times. The CR1000 set up with two sensors was operated with a sampling frequency of 100 Hz.

Figure 4.6. Stress measurement setup during calibration measurements. The calibration weights were placed on the sensors on a squared aluminum plate with the same dimension of the sensors. Additionally, a squared piece of cellular foam underneath ensured equal distribution of the calibration weight.

4.2.2 Data logger

For both stress measurement setups, Campbell Scientific data loggers were used. Initially, the experiments were run with a CR1000 data logger (Table 4.3). Due to signal interference of the signal conditioning boxes, only two sensors could be used simultaneously in the winter season of 2008. Using a CR5000 (Table 4.3) with switched voltage outputs in half-bridge configuration allowed for operating four sensors simultaneously. Despite the larger dimensions and weight of the CR5000, transport and usage in the field was still reasonable (fits into a 30 – 40 l backpack). The advantage of operating four sensors at the same time outweighed this minor shortcoming. A block of rechargeable AA batteries was kept in an insulation package as the power supply for both setups.

4.2.3 Calibration

The manufacturer provided the sensors with calibration data that were valid for standard, dry laboratory conditions at approximately 20˚C. During the evaluation of

Table 4.2. Technical specifications of stress measurements set ups.

	Setup 1	**Setup 2**
Number of sensors	*2*	*4*
Data logger	*CR1000*	*CR5000*
Measurement	*Single ended*	*Half bridge*
Max. sampling frequency	*100 Hz*	*11 Hz*
Stress range (-20 to 0˚C)	*6.5 to 10 kPa*	*6.5 to 10 kPa*
Voltage output	*5 VDC*	*800 µV*
Accuracy	*±0.18 kPa*	*±0.18 kPa*
Resolution	*0.01 kPa*	*0.01 kPa*
Sensitivity	*0.0028 kPa/mV*	*0.0166 kPa/µV (stand. range); appr. 0.35 kPa/µV (above stand. range)*

Table 4.3. Relevant data logger specification.

	CR5000	**CR1000**
Temperature range	*-25˚C to +50˚C*	*-25˚C to +50˚C*
Voltage input		
Input range	*20 mV*	*5000 mV*
Resolution	*0.67 µV*	*667 µV*
Accuracy	*±0.075 % of reading*	*±0.06 % of reading*
Analog output		
Output range	*±5VDC (4 switched channels)*	*±5VDC*
Resolution	*1.2 mV*	*1.2 mV*
Accuracy	*±10 mV*	*±10 mV*
System power requirements	*11 to 16 VDC*	*9.6 to 16 VDC*
Measurement circuit	*Half bridge*	*Single ended*
Size	*24.7 x 21.0 x 11.4 cm*	*21.6 x 9.9 x 2.2 cm*
Weight	*2.0 kg*	*1.0 kg*
Control	*Built-in keypad and display*	*External keypad via I/O interface*

the measurement method it became obvious that the sensor output strongly depended on sensor temperature. Furthermore, the signal quality was affected bypositioning of the signal conditioning boxes (Figure 4.2) relative to each other and relative to the data logger. Therefore, the sensor boxes were installed around the data logger so that interference was minimal. As well, this installation allowed easy handling and portability of the measurement setup in the field. With this standard setup left in place, the device was re-calibrated for the most likely operating temperatures from -20˚C to 0˚C.

Calibration measurements were carried out for four sensor temperatures for each sensor by placing calibration weights on the sensors in 0.25 kg (0.918 kPa) intervals (Figure 4.6). The calibration was conducted outdoors during early morning while air and snow temperature conditions were most stable. The cold lab that is part of the research facilities at Rogers Pass could not be used for calibration purposes due to temperature fluctuations not acceptable for calibration measurements.

4.2.4 Accuracy

The accuracy of the normal stress values was influenced by a series of random and uncorrelated measurements errors that determined the overall performance of the measurement method. These errors are listed in Table 4.4. According to error propagation theory for adding errors (Bevington and Robinson, 2002) the total absolute error (e_{tot}) was calculated according to:

$$e_{tot} = (e_{conv}^2 + e_{Tcorr}^2 + e_{avg}^2 + e_z^2)^{1/2} \tag{4.1}$$

Table 4.4. Error description of stress measurement method.

Error	*Description*
e_{conv}	*Error due to conversion of voltage output to stress values*
e_{Tcorr}	*Error due to temperature correction*
e_{avg}	*Error due to averaging the stress signal*
e_z	*Error due to manual measurement of sensor depth*

4.3 Performance and evaluation

4.3.1 Temperature dependence

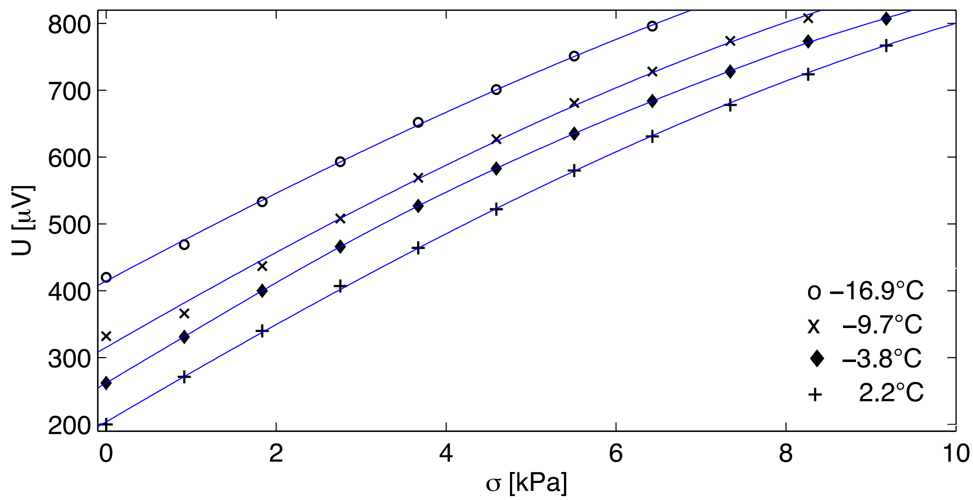

Figure 4.7. Voltage-stress calibration curves for four sensor temperatures. See Table 4.5 for fit statistics.

Depending on temperature, the maximum stress range of the sensors varied between 6.5 kPa and 10 kPa (-20˚C to 0˚C) which was sufficient for normal stresses within the snowpack (below approximately 20 cm depth) due to static and dynamic loads of skiers and snowmobiles. Figure 4.7 shows the stress-voltage calibration curves for the four temperatures for Sensor #643. For temperature correction of the stress signal a linear temperature dependence was assumed according to Figure 4.8. Table 4.6 provides an overview of the fit statistics of the linear fit.

4.3.2 Accuracy

A total absolute error (e_{tot}) of ±0.18 kPa was estimated, which includes the accuracy of the sensor output, temperature correction and errors due to the experimental procedure, such as the manual measurement of the sensor depth (Table 4.7). This translates to an error of ±3.7% relative to the mean range of the sensors. More realistically, the absolute error needs to be related to typical stresses at a given snow depth, for instance due to additional mean stresses of a skier. For approximate skier stresses, this yields a relative accuracy of ±8% at approximately 20 cm snow depth, ±31% at 40 cm, and ±55% at 60 cm (Table 4.7). The error due to the manual snow depth measurement depending on snow depth is given in Table 4.8. Depth of the sensors was measured with an accuracy of approximately 1 cm. Stresses under loads at the snow surface exceeded the maximum range in some cases. As a side effect of operating the sensors in half-bridge configuration with the CR5000 data logger, the sensors could be operated beyond the standard output range, although with lower accuracy and sensitivity (Table 4.2).

4.3.3 Repeatability

The non-repeatability of the sensor output according to the manufacturer is less than 2%. The voltage-stress curves in Figure 4.9 show calibration measurements from March 6 and April 5, 2009 at similar temperatures for the same sensor (#643). These resulted in almost identical regression curves, confirming the repeatability of the method.

Table 4.5. Fit statistics of smoothing spline fit for calibration curves (Figure 4.7) for four temperatures.

Sensor T [˚C]	R^2	SE [µV]
2.2	*0.90*	*2.86*
-3.8	*1.00*	*1.15*
-9.7	*0.99*	*9.82*
-16.9	*0.99*	*4.52*

Table 4.6. Fit statistics of linear fit of temperature dependence of stress sensors (Figure 4.8).

Load [kPa]	R^2	SE [µV]
0.92	*0.96*	*11.08*
2.75	*0.92*	*16.45*
4.59	*0.98*	*6.73*
6.43	*0.96*	*9.30*
8.26	*0.94*	*10.43*

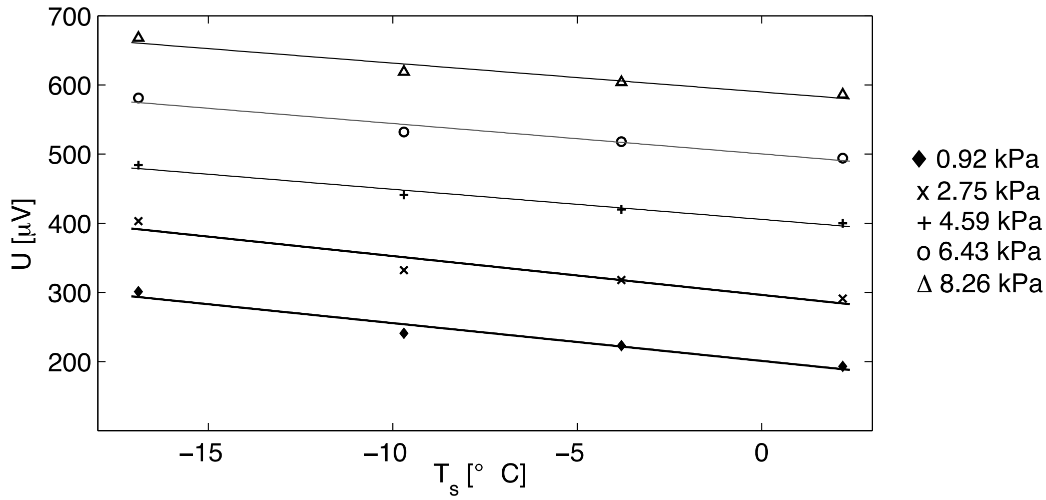

Figure 4.8. Temperature dependence of voltage output for constant loads for four sensor temperatures. Solid lines are linear fits. See Table 4.6 for fit statistics.

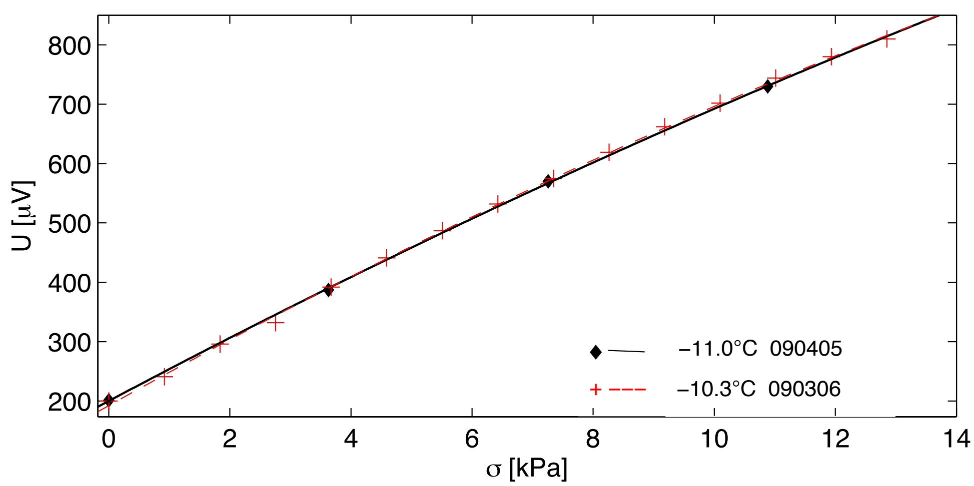

Figure 4.9. Calibration curves from two different calibration measurements with similar temperatures for sensor #643.

4.3.4 Effect of intrusive method

By inserting the sensor sheets into the snowpack, the surrounding snow was slightly compacted. It was assumed that this effect only slightly increased the overall stiffness of the snowpack and was therefore neglected. Nevertheless, the

Table 4.7. Overview of errors of stress measurement method.

Error source (see Table 4.4)	**Absolute error** [kPa]	**Error relative** to mean range of sensors [kPa]	**Error** [%] relative to mean skier stresses 4.5 / 0.66 / 0.36 kPa at 20 / 40 / 60 cm
e_{conv}	*0.08*	*1.45*	*1.7 / 11 / 21*
e_{Tcorr}	*0.18*	*3.35*	*4 / 27 / 50*
e_{avg}	*0.01 – 0.03*	*0.3*	*5*
e_z (at 20 / 40 / 60 cm)	*0.08 / 0.03 / 0.02*	*1.0 / 0.5 / 0.2*	*4.5 / 10 / 10*
e_{tot}	***0.18***	***3.7*** *(40 cm)*	***8 / 31 / 55***

Table 4.8 Error due to manual depth measurement of sensors.

Depth below sensor [cm]	**Typical stress gradient** (due to skier load) [kPa cm^{-1}]	**Typ. stress range** [kPa] (Chapter 5)	**Rel. error** (due to 1 cm reading error of sensor depth) [%]	**Avg. relative error** [%]
20	0.08	1 - 8	1 – 8	4.5
40	0.03	0.17 - 1.15	3 – 17	10
60	0.02	0.12 - 0.61	3 – 17	10

measured values may slightly be higher than in an undisturbed snowpack due to stress concentration around the sensor plates (Schweizer and Camponovo, 2001). The thickness of the aluminum plates (2 mm) was chosen so that the plate did not deflect too much during insertion.

4.3.5 Analysis of stress data

The purpose of the stress measurements was to determine the additional normal stress in the snowpack due to surface loads. Figure 4.10 shows the stress signal during skier loading (standing and knee drops), including stepping on and off the measurement site. The stress spikes during stepping on and off were not considered for analysis, but only mean stress values during static and dynamic loading. To obtain the additional stresses in the snowpack, the initial stress that was measured due to insertion of the sensors in the snowpack and the weight of

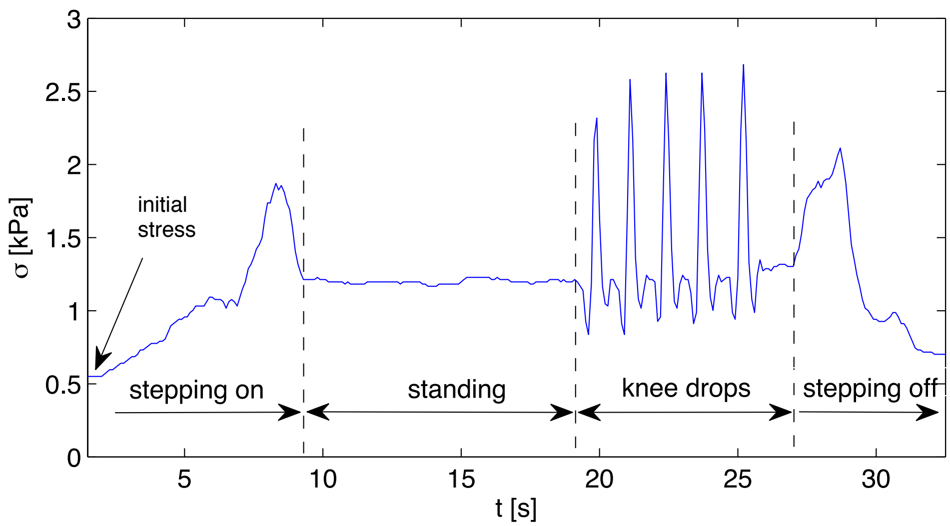

Figure 4.10. Stress signal during an experiment with a skier stepping on, standing, performing five knee drops and stepping off the site.

the snowpack was subtracted. A similar procedure was applied to the snowmobile and cold lab measurements (Chapters 6 and 7). A minimum amount of compaction around the sensors was necessary to ensure proper stress transmission between the snowpack and the sensor pads. For instance, in layers of coarse faceted snow crystals, the insertion of the sensor sheet only destroyed the fragile structure of the ice lattice, but did not create enough initial contact pressure to ensure sufficient stress transmission. In those cases the stress signal was inconsistent and unreliable and was excluded from analysis.

4.4 Summary

The majority of the experiments for this thesis required measuring normal stresses in the snowpack due to surface loads. The method that was developed for this purpose has proven to be field-portable, reliable and functional under harsh snowy winter conditions. Only in rare cases did melting water penetrate the sensor pads or broken connector wires lead to the loss of measurement data or rendered those data unusable.

The capacitive stress pads basically convert the compression of the sensors due to surface loads into a voltage signal, which is proportional to the stress that caused the deformation. The deformation due to surface loads is determined by the stiffness (hardness) of the snowpack, which is highly temperature dependent (see Section 1.3). The stress sensors were able to capture stress changes due these temperature-induced variations of snowpack stiffness (see Section 5.3.4 and Section 7.4).

With the upgrade to four sensors on the CR5000 setup, which all could be operated simultaneously, the time required to measure a full 2D stress profile for example along a ski (Chapter 5) considerably decreased compared to the time requirement of the CR1000 setup with two sensor pads.

The sampling frequency of 11 Hz of the CR5000 setup was sufficient to capture normal stress peaks due to dynamic loads for example due to a skier performing knee bends or jumps.

CHAPTER 5

Normal stresses in the snowpack due to static and dynamic skier loads and the effect of snow temperature

5.1 Introduction

The penetration depth of stresses and deformation into the snowpack due to static and dynamic skier loads has an important impact on the slab avalanche release process (see Sections 1.2 and 1.3). Many factors such as the hardness (stiffness) and temperature of the near-surface layers of the snowpack, the stiffness of the skis and the type of loading (static or dynamic) determine the distribution of skier stresses in the snowpack. This chapter presents the field studies that were conducted on the distribution of normal stresses due to a standing skier and a skier performing knee drops and jumps. A major part of this chapter comprises the effect of snow temperature changes on skier stresses.

5.2 Methods

5.2.1 Experimental set up

To measure the normal stresses due to skier loads, the stress pads as described in Chapter 4 were placed in the side of a pit wall below a skier (Figure 5.1 and 5.1). The sensors were pushed 30 cm into the sidewall of the snow pit, parallel to the snow surface. The measurements in the winter season of 2008 were performed with a Campbell Scientific CR1000 data logger with two stress pads, and the measurements from the winter season of 2009 with a CR5000 data logger, which allowed simultaneous measurements with four stress pads (see Chapter 4).

In Experiments 1, 2, 3, 7 and 8 in the winter of 2009 a snowpack area of approximately 4 x 5 m was skier compacted the previous day to simulate hard slab

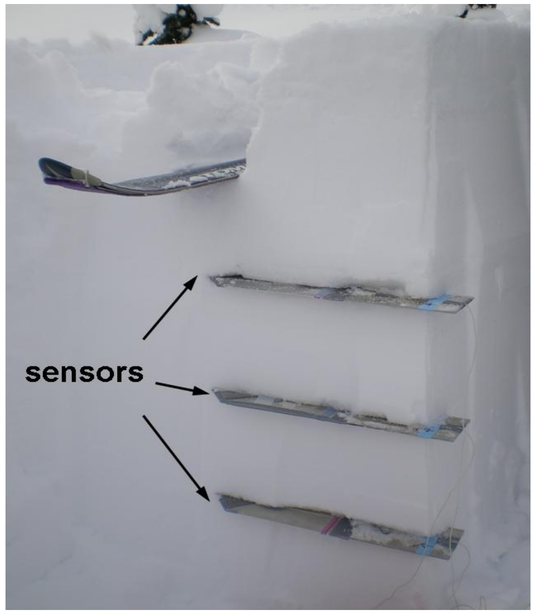

Figure 5.1. After the measurements, the sensors were dug out to determine their distance below the ski. In this photo, the sensors are located at the tip of the insertion plates below the ski.

conditions. The hand hardness of the topmost layer, after skier compaction, was approximately P to P+ (see Table 5.2b).

5.2.1.1 Skier loading

A skier, 30 cm parallel to the pit wall, applied static (standing) and dynamic loads (knee drops and jumps) on the snowpack directly over the sensors (Figure 5.2). See Table 5.2 for the type of loading that was performed for each experiment. In most cases, 185 cm long skis were used and only occasionally were skis of 175 cm length used. The weight of the test skiers ranged from approximately 75 to 90 kg, but was not considered in the analysis of the skier stress data. Within each experiment where the influence of snow temperature effects were investigated the test skier and skis were kept the same. After each single measurement (short horizontal lines in Figure 5.2) the skier walked off the pit wall, the sensors were placed in the new position, and the skier loaded the sensors again. The

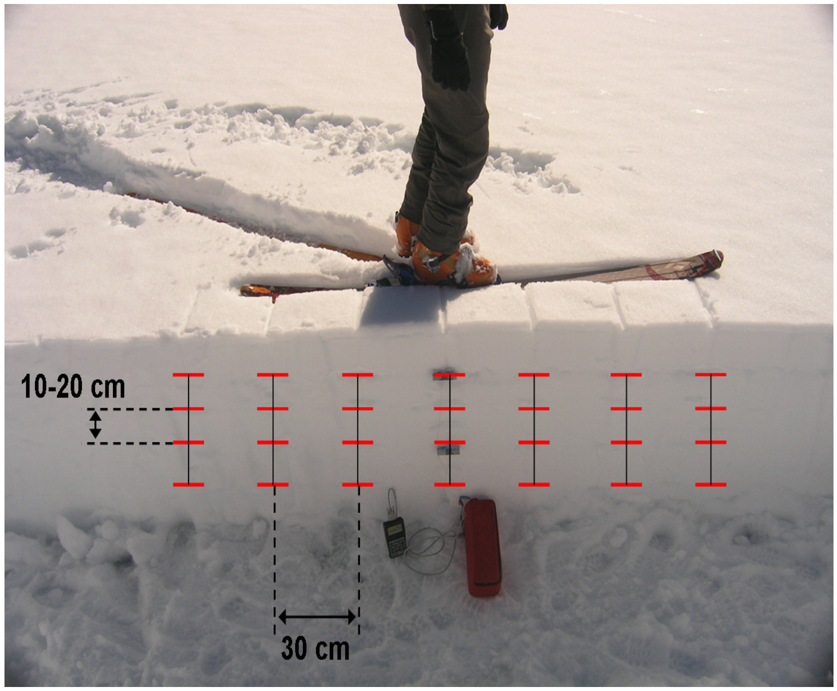

Figure 5.2. Experimental set up for 2D normal stress measurements below a skier. The horizontal lines mark the positions where the sensors were pushed into the pit wall. The red case contains a Campbell Scientific CR1000 data logger with a control-keypad attached.

measurements were performed from bottom to top (10 – 20 cm spacing) to preserve the snowpack above for the following measurements. The middle vertical array was located under the centre of the ski boot. The horizontal spacing between the vertical arrays was 30 cm (Figure 5.2). The centre of the ski boot marks the origin of the horizontal axis (0 cm) in all 2D graphs in Sections 5.3.3 to 5.3.5.

5.2.1.2 Including temperature effects

To determine the effect of snow temperatures changes of the near-surface layers, one set of measurements was conducted in the morning before a warming period and the second set during the maximum of the warming period in the afternoon. Immediately before the second set of measurements the pit wall was moved back by approximately 1 m. Manual temperature profiles were measured to monitor snowpack temperatures in 5 cm vertical spacing. Ski penetration was determined

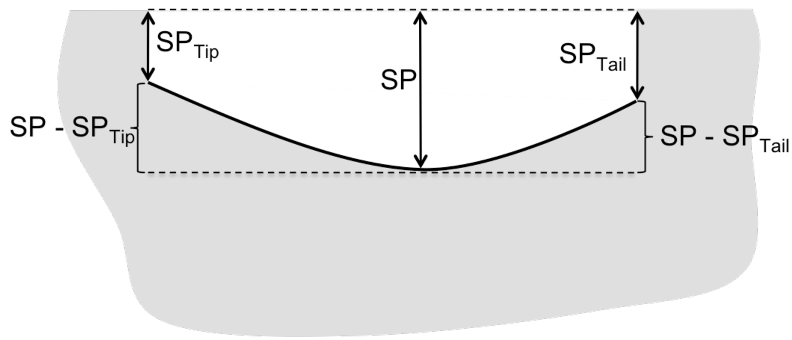

Figure 5.3. Ski penetrations along the ski as a measure for ski bending.

by measuring the depth of the ski track above each vertical array after each set of measurements.

5.2.2 Analysis

The normal stress distribution in the snowpack due to a skier depends on the weight of the skier, the length, width and stiffness of the ski (ski bending), the type of loading (static or dynamic), the stiffness (hardness) of near surface layers and the temperature of near surface layers. To characterise these conditions that were subject to change during an experiment, the following variables were introduced.

T_{avg}: Average snow temperature (mean of T_{surf}, T_{10} and T_{20})

ΔT_{avg}: Mean of changes of T_{surf}, T_{10}, and T_{20} during warming/cooling period

SP: Ski penetration under centre of ski boot

SP_{Tip}: Ski penetration under ski tip

SP_{Tail}: Ski penetration under tail of ski

BI: Bending Index (Figure 5.3):

$$BI = (SP - SP_{Tip}) + (SP - SP_{Tail}) \tag{5.1}$$

ΔBI: Change in BI during warming/cooling

$\Delta\sigma_{40}$: Normal stress changes during warming/cooling relative to initial value at 40 cm snow depth below the centre of the boot

The BI (the sum of the differences in penetration between under the boot and tip and tail, respectively) is a measure of the bending of the ski, which reflects the effect of the skier's weight, the type of loading and the stiffness of the ski and the hardness (stiffness) of the near-surface snow layers. The load distribution along the ski strongly depends on the bending stiffness of the ski. With increasing bending the skier load still peaks under the boot but also spreads more towards the tip and tail of the ski (Lind and Sanders, 2003, p. 65). The higher the BI, the lower the peak stress under the boot and the more the skier load spreads along the ski. Ski penetration was measured as the distance from the undisturbed snow surface to the ski track left behind (Figure 5.3).

Basically, two factors control the normal stress distribution under a skier: snow stiffness and the bending of the ski, while other factors being equal, such as the test skier and the skis. Accordingly, the following classes were defined to describe the temperature effect on the normal stress distribution due to skier loading:

S: Only snow stiffness (hardness) changes (no change in ski bending)

S_B: Temperature effect on snow stiffness overrides influence of ski bending

B_s: Ski bending overrides the temperature effect on snow stiffness

$B+S$: Both factors affect stress change in same direction.

Changes in hand hardness were used to indicate stiffness changes of the upper snowpack layers.

All experiments were split in two groups by average snow hardness of the near-surface layers in soft slabs (SSL, hand hardness F – 4F) and hard slabs (HSL, hand hardness > 1F; see Table 5.1).

5.2.3 Effect of pit wall on stress distribution

To test the influence of the open pit wall on the stress distribution due to skier loads, comparison measurements in an ‘undisturbed’ snowpack were conducted. This ‘full’ snowpack was simulated with the experimental set up shown in Figure 5.4. The sensors were placed 1 m into a 50 cm wide pit wall from about a 2 m long trench. It was assumed this set up is close enough to an ‘undisturbed full’ snowpack. The comparison measurements are available for a standing skier for six cases, and for the loading steps of knee drops and jumps for three cases.

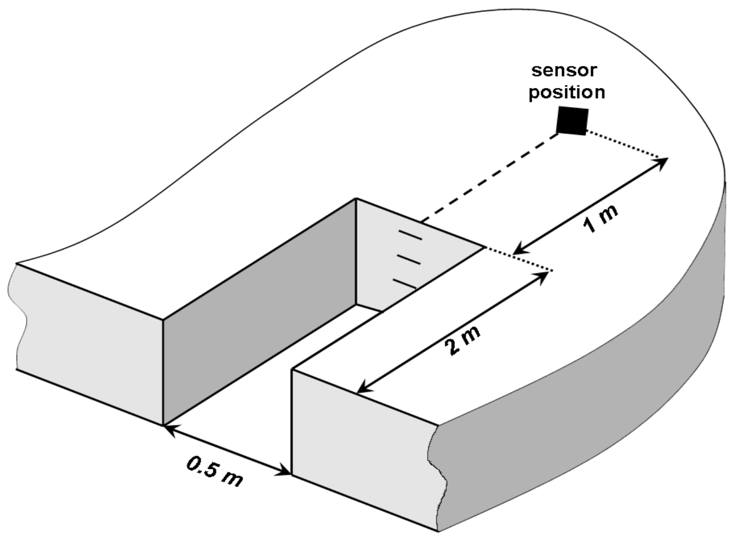

Figure 5.4. This schematic (not to scale) shows the set up which was used to simulated a stress distribution close to a ‘full’ snow pack. The sensors were pushed 1 m into the pit wall at the end of a 2 m long trench. The results of this set up were compared to the standard measurements where the sensors were pushed 30 cm into the pit wall.

5.2.3.1 The problem of stress distribution along a ski

Measuring the stress distribution directly under the ski at the snow surface turned out to be problematic. By placing the sensor plate (3 mm thick) under the skis (in particular on a hard snowpack) the surface was slightly elevated, resulting in unrealistically high stress values.

To estimate the error of this effect the skier load was calculated by integrating over the measured stress distribution along the ski and compared to the known skier load. The measured surface stresses appeared to be too high by a factor of approximately 1.5 – 2. This effect was assumed to only affect the near surface layers. With good confidence, normal stresses measured below the near surface layers were regarded to be sufficiently close to actual values.

5.3 Results

5.3.1 Overview of experiments

In total, 11 experiments were conducted (eight in the winter of 2009 and three in

Table 5.1. Overview of experiments presented in this study. Snow type classification according to ICSSG (Fierz and others, 2009).

	Date	***Location***	***Avg. snow density [kg/m^3] : (upper 50 cm/50-100 cm)***	***Major snow types (upper 50 cm/50-100 cm)***	***Slab conditions[1]***
	2009				
1	Jan 4 – 7	Rogers Pass (backyard)	290 / --	decomposed (2a) / small rounded (3a)	HSL
2	Jan 14/15	Rogers Pass (backyard)	252 / --	mixed forms (3c) / mixed forms (3c)	HSL
3	Jan 15 – 18	Mt. Fidelity (Poetry Flats)	212 / 270	decomposed (2a) / small rounded (3a)	HSL
4	Jan 21/22	Mt. Fidelity (Gopher Butte)	205 / 178	small rounded (3a) / small rounded (3a)	SSL
5	Jan 25	Mt. Fidelity (Gopher Butte)	226 / 194	small rounded (3a) / small rounded (3a)	SSL
6	Feb 21/22	Rogers Pass (backyard)	312 / 328	mixed forms (3c) / mixed forms (3c)	SSL
7	April 4 – 7	Rogers Pass (backyard)	320 / --	polycrystals (6b) / -	HSL
8	April 7/8	Rogers Pass (Poetry Slopes)	241 / 328	polycrystals (6b) / facets (4a)	HSL
	2008				
9	Mar 14/15	Rogers Pass (backyard)	275 / 392	mixed forms (3c) / mixed forms (3c)	HSL
10	Mar 22	Rogers Pass (Mt. Fidelity)	160 / 299	decomposed (2a) / small rounded (3a)	SSL
11	Mar 28	Rogers Pass (pass area)	239 / 393	mixed forms (3c) / mixed forms (3c)	SSL
12	April 2 (12)	Kananaskis (Burstall trailhead)	225 / 300	facets (4a), melt freeze crusts (9e) / depth hoar (5a)	SSL
13	April 11/12	Kananaskis (Burstall trailhead)	292 / 310	facets (4a) / facets, depth hoar(4a, 5a)	SSL

[1] HSL: Hard slab; SSL: Soft slab (Section 5.2.2)

the winter of 2008). Each experiment consisted of up to three warming or cooling periods, during each of which the normal stress distribution due to static and/or dynamic skier loads was measured before and after warming/cooling of the near-surface layers. In sum, 16 warming and six cooling events were available for analysis (Table 5.2). The skier loading steps that were performed for each of the warming and cooling periods are shown in Table 5.2. Table 5.1 provides an overview of experimental conditions of all experiments.

5.3.2 Effect of open snow pit wall on stress distribution

Theoretically, actual stresses in an undisturbed snowpack were expected to be lower since stresses in an undisturbed ‘full’ snowpack spread the skier load more laterally. Therefore, the skier’s weight spreads more laterally over a larger area. The comparison measurements could not confirm this assumption. No consistent and conclusive difference could be found due to the effect of the pit wall for all three types of skier loading (Figure 5.5). Accordingly, for the purpose of the outdoor skier stress experiments the influence of the pit wall was neglected. Although the measured values may be slightly too high compared to a full snowpack this systematic error was assumed to have little influence on the relative stress variation due to temperature changes.

5.3.3 Normal stress distribution under skiers

5.3.3.1 Vertical profiles of normal stress due to static and dynamic skier loads

Figure 5.6 and 5.7 show vertical normal stress profiles for a skier standing and a skier performing knee drops and jumps for the hard and soft near-surface layers (see Section 5.2.2). See Table 5.2 for ski penetration for each experiment. Power law functions describe the non-linear decrease.

$$\sigma\left(z_{eff}\right) = a z_{eff}^{\;b} + c \tag{5.1}$$

with *σ: normal stress*

z_{eff}: *effective snow depth*

a, b, c: coefficients

Table 5.2a. Overview of all skier normal stress experiments: snowpack and temperature conditions that led to normal stress changes. (Part 1)

		Exp ID	*W/C*	*Standing* $\Delta\sigma_{40}$ *[%]*	*Standing* ΔBI	*Knee drops* $\Delta\sigma_{40}$ *[%]*	*Knee drops* ΔBI	*Jumps* $\Delta\sigma_{40}$ *[%]*	*Jumps* ΔBI	*Surface cond.*[1]	T_{avg_S}	T_{avg_E}	ΔT_{avg}	$\Delta T/\Delta t$	*t*
Warming	Stress decreas	13_1	W	-10	4.5	--	--	--	--	w	-6.1	-0.1	6.0	--	31
		13_2	W	-50	2.5	--	--	--	--	m	-0.1	0.0	0.1	--	20
		11	W	-25	1	--	--			d	-8.6	-3	5.6	0.8	7
		6	W	-20	1	-33	+2	-25	+1.5	d	-11.8	-6.6	5.2	--	32
		2_1	W	--	0	+15	0	--	--	d	-2.3	-0.9	1.5	--	28
		1_3	W	-20	0	--	--		--	d	-6.2	-4.5	1.7	--	24.1
		10	W	-30	-5	--	--	--	--	m	-11.6	-3.4	8.2	1.4	6
	Stress increase	7_2	W	200	1.5	120	+2	-40	+3.5	m(c below)	-1.2	-0.9	0.3	--	27
		9_2	W	50	0.5	--	--			m	-2.8	-0.8	1.9	0.4	4.5
		7_1	W	0	0	20	+1	+100	+5.5	m (c below)	-4.9	-1.2	3.7	0.78	4.75
		7_3	(W)	0	0	-80	0	+20	-1.5	m(c below)	-0.9	-0.8	0.1	--	23.5
		8_2	W	25	0	+45	+1.5	--	--	c	-2.3	-0.2	2.2	0.72	3
		1_1	W	25	0	--	--	--	--	d	-11.8	-8.0	3.7	--	29.5
		1_2	W	50	0	--	--	--	--	d	-8.0	-6.2	1.9	--	24.2
		5	W	50	-1	--	--	--	--	d	-15.2	-12.7	2.4	0.6	4
		12	W	40	-2	--	--	--	--	d	-15.7	-4	11.7	1.5	8
Cooling	Stress decr.	3	C	-50	0	--	--	--	--	d	-3.1	-6.3	-3.2	--	27
		7_4	C	-50	-1.5	-30	-3	-60	-4.5	c	-0.8	-3.2	-2.3	0.13	17.3
		2_2	C	-25	0	-20	0	--	--	d	-0.9	-3.1	-2.3	0.13	18
	Stress incr.	8_1	C	0	0	+30	-2	--	--	m	-0.6	-2.3	-1.7	--	20
		9_1	C	50	-2	--	--	--	--	c	-1.2	-2.8	-1.6	0.1	16
		4	C	100	-1.5	--	--	--	--	c	-1.7	-8.6	-6.9	-0.4	18.5

[1] c: crust, d: dry, m: moist, w: wet

Table 5.2b. Overview of all skier normal stress experiments: snowpack and temperature conditions that led to stress changes. (Part 2)

		Exp ID	*W/C*	*Hardness change*		*Density change*	*Width change (0.5 kPa contour at 30 cm)*	*Process*[1] *(see Section 5.2)*
Warming	Stress decrease	13_1	W	0-35 cm: P-1F → 1F-4F 35-50 cm: P	 –	n/a	0.1/40: 115 → 135 (+20%)	B_S
		13_2	W	0-35 cm: 1F-4F → P-4F 35-50 cm: P → 1F+	+ –	240 – 260 326 → 342	0.1/40 cm: 135 → 135 (0)	B_S
		11	W	0-50 cm: 1F/P → 1F/P	0	n/a	n/a	B
		6	W	0-30: 6.5 N – 2N (1 cm^2)	–	n/a	40 cm: 55 → 80 (+40)	B_S
		2_1	W	0-10 cm: P^+ → P 15 -50 cm: 1F → 1F+/P^-	– +	279 – 280, 212 -230	n/a	S
		1_3	W	n/a	n/a		0.4/40 cm:50 → 35 (-40)	--
		10	W	0-25 cm: 4F/1F→ 1F 25-50 cm: p → P	+ 0	n/a	n/a	S_B
	Stress increase	7_2	W	0-10 cm: K → K-; 10-30 cm:1F → P	– +	459 – 466, 308-324	n/a	S_B
		9_2	W	0-15 cm: P → 1F	–	n/a	n/a	S_B
		7_1	W	n/a	n/a	n/a	n/a	(S)
		7_3	(W)	0-10: K- → 1F 10-30 cm: P → 1F+/P-,	– –	466 – 488, 324-333	n/a	S
		8_2	W	0-30 cm: K- → P	–	n/a	n/a	S
		1_1	W	6.5N – 2N	n/a		0.4/40 cm:35 → 60 (+70)	S
		1_2	W	0-15 cm: P^+ → P 15 -50 cm: 1F → 1F+	– +	301 – 336, 240 -270	0.4/40 cm:60 → 50 (-20)	S
		5	W	0-30 cm: 4F+ → 4F 30-60 cm: 1F- → 1F-	– 0	n/a n/a	40 cm: 75 → 85 (+15)	B_S
		12	W	0-25 cm: 4F+ → 1F	+	n/a	n/a	B_S
Cooling	Stress decr.	3	C	0-10 cm: P → P+ below: 1F → 1F	+ 0	N/a	105 → 115 (+10)	S
		7_4	C	0-10 cm: 1F → K, 10-30cm: 1F+ → 1F+	+ 0	N/a		S_B
		2_2	C	N/A	n/a	n/a	45 → 30 (-35) n/a	(S)
	Stress incr.	8_1	C	0-30 cm: 1F → K-	+	n/a	n/a	B_S
		9_1	C	0-15 cm: 4F/1F → P	+	n/a	n/a	B_S
		4	C	0-30 cm: 1F → 4F 30-50 cm P → P	–	192 -189 240-297	40 cm: 75 →105 (+40)	B_S

[1] Interpretation of results

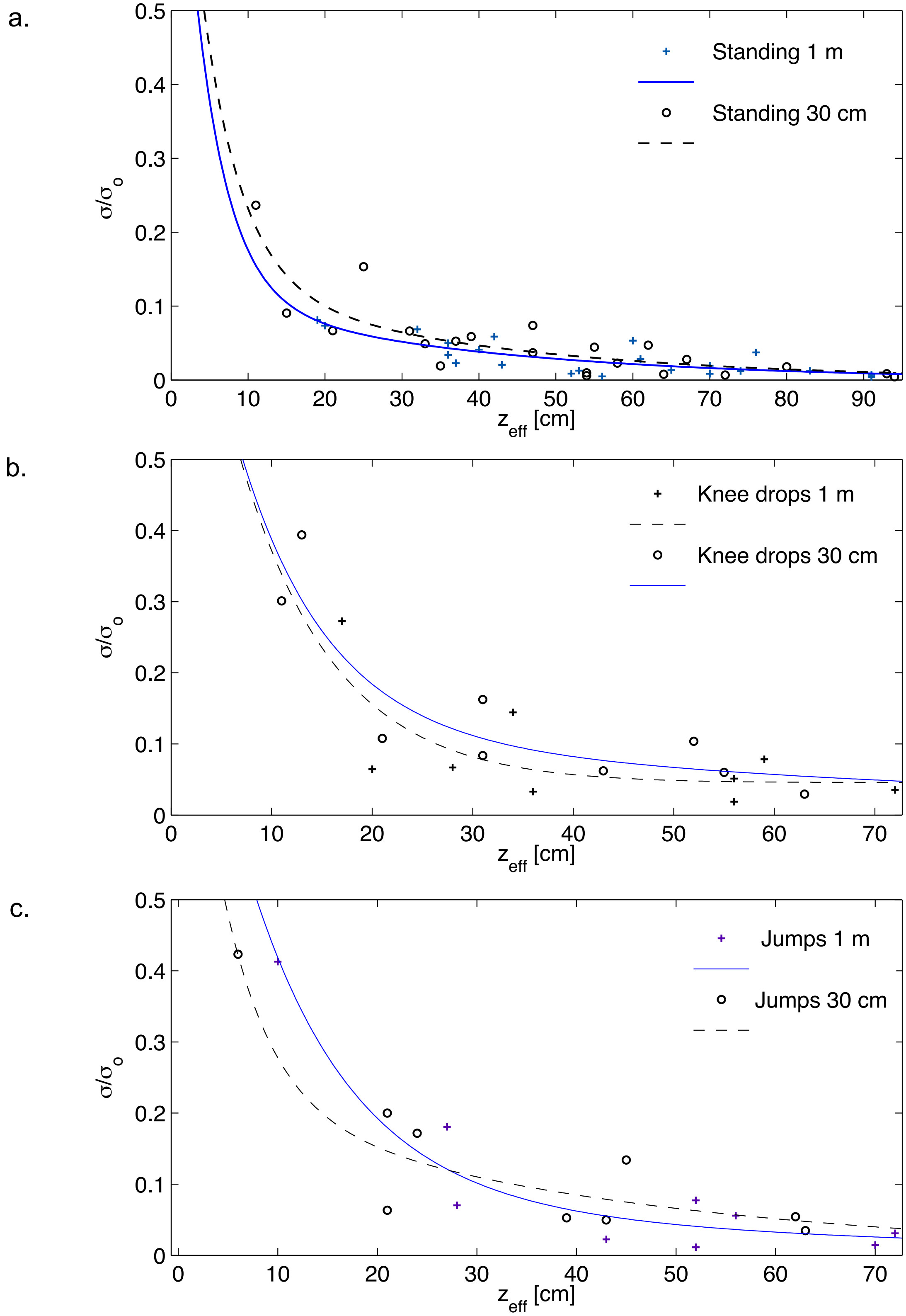

Figure 5.5. Stress profiles due to skier loads 30 cm and 1 m behind the pitwall: **(a)** standing, **(b)** knee drops, **(c)** jumps. Stress values (σ) are normalised to measured surface stresses (σ_o). The solid and dashed lines are power law fits.

a.

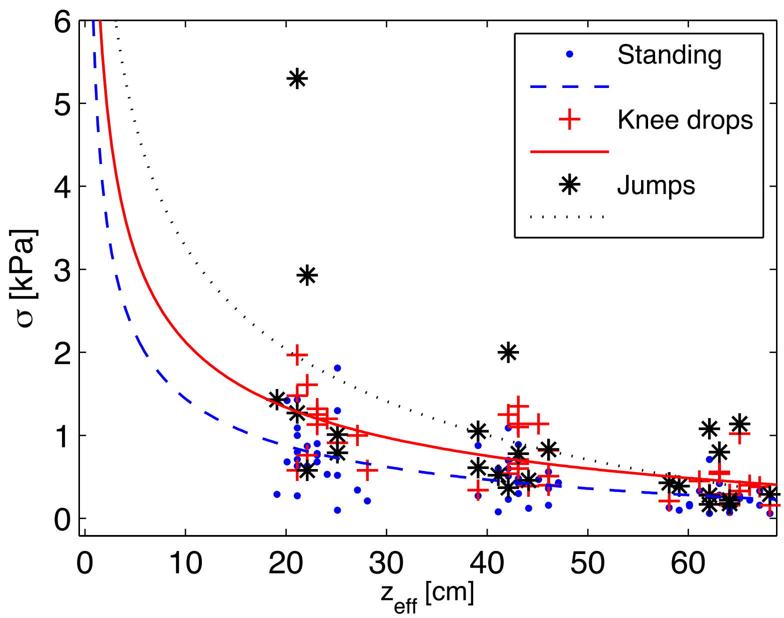

b.

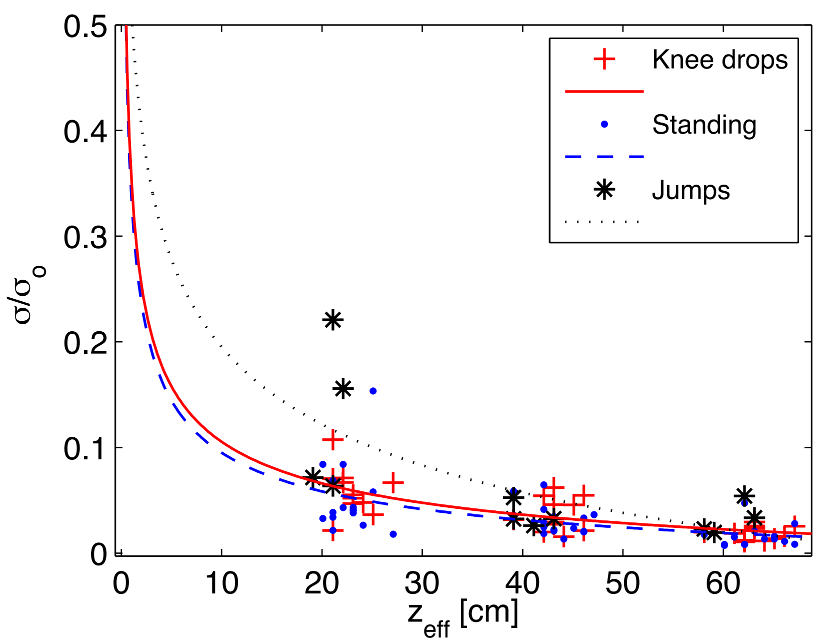

Figure 5.6. Vertical normal stress profiles for static and dynamic skier loading for the skier compacted hard snowpack: **(a)** actual stress values and **(b)** relative to surface stresses.

of σ with snow depth of each of the skier loads. Table 5.3 gives on overview of the fit statistics. For both snowpack conditions, SSL and HSL, the skier stresses relative to the surface values are plotted in Figure 5.6b and 5.7b, respectively.

a.

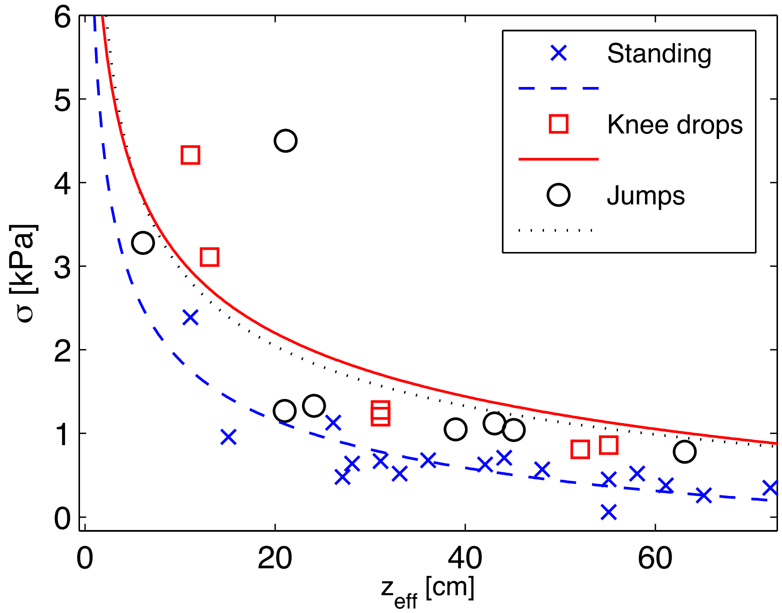

b.

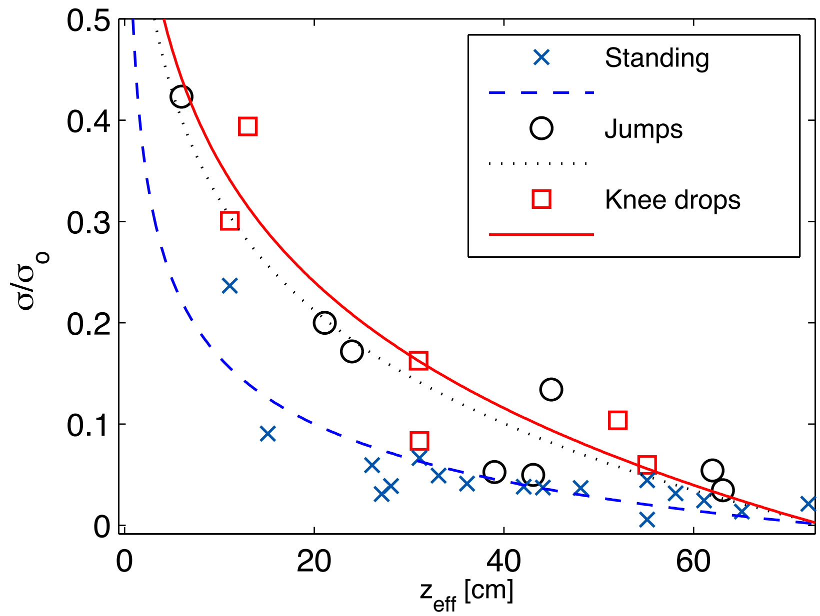

Figure 5.7. Vertical normal stress profiles for static and dynamic skier loading for a soft slab conditions: **(a)** actual stress values and **(b)** relative to surface stresses.

In soft snow (Figure 5.7) the skier stresses decreased slower with depth than those in snowpacks with harder surface layers (Figure 5.6). At 40 cm effective snow depth stresses relative to surface values were all below 5 - 7% in the stiffer

Table 5.3. Fit statistics and coefficients for fits of Figure 5.6 and 5.7.

		R^2	*SE*	*a*	*b*	*c*
HSL	Standing	0.92	2.03	6.01	-0.47	-0.59
(Fig. 5.6a)	Knee drop	0.94	2.28	8.27	-0.44	-0.89
	Jump	0.97	1.16	13.66	-0.26	-4.2
SSL	Standing	0.93	1.81	7.47	-0.34	-1.56
(Fig. 5.7a)	Knee drop	0.99	0.47	10.21	-0.23	-2.88
	Jump	0.98	1.23	32.53	-0.11	-19.84
HSL	Standing	0.99	0.02	0.38	-0.43	-0.04
(Fig. 5.6b)	Knee drop	0.99	0.014	0.41	-0.41	-0.05
	Jump	0.99	0.04	0.94	-0.17	-0.43
SSL	Standing	0.99	0.02	0.76	-0.22	-0.28
(Fig. 5.7b)	Knee drop	0.98	0.05	-1.79	0.07	2.5
	Jump	0.99	0.03	-5.7	0.02	6.36

snowpacks, whereas in softer snow all stresses dropped approximately to 15% and below. In soft snow (Figure 5.7) mean stresses due to knee drops and jumps were fairly similar, but significantly higher, approximately a factor of two to three at a depth between 20 and 60 cm, compared to the static load due to a standing skier. The harder near-surface layers yielded a smaller difference between a standing skier and knee drops than the softer snow. The difference between knee bends and jumps is larger in the case of the harder snow.

5.3.3.2 2D distribution of static and dynamic stresses along skis

A summary of the stress distributions, for snow depths 20 cm, 40 cm and 60 cm, from all 2D experiments is shown in Figure 5.8. The measurements are split up in soft and hard near-surface layers for a standing skier load. The same stress distribution for a skier-performing knee drops on a hard slab is shown in Figure 5.9. Gaussian curves (Equation 5.2) appeared to be the best fit of the mean values of normal stresses of the sensor positions along the ski (Figure 5.10 and 5.11). The fit statistics are given in Table 5.4.

$$\sigma = a e^{-\left(\frac{x-b}{c}\right)^2} \tag{5.2}$$

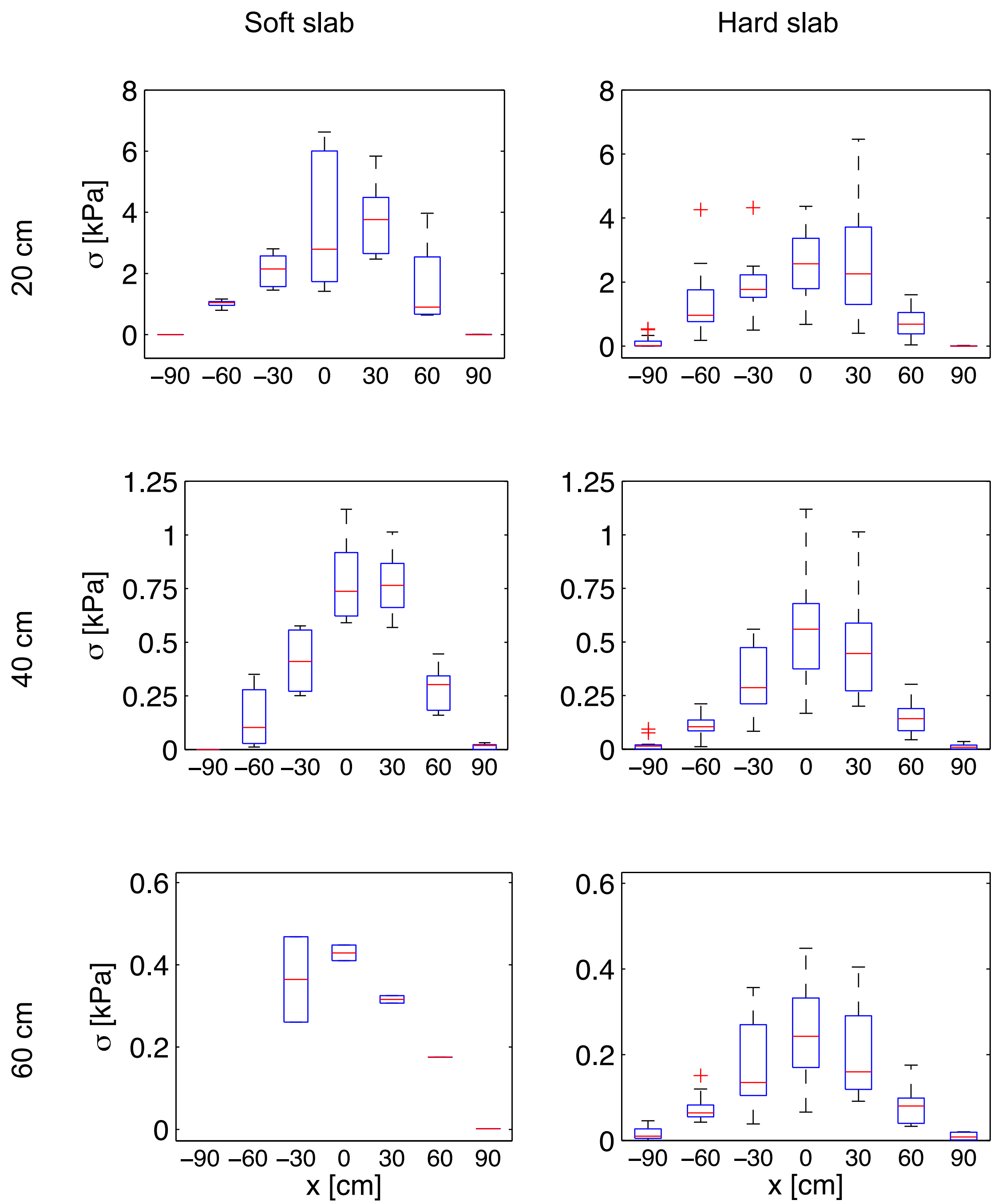

Figure 5.8. Boxplots of normal stresses due to a standing skier under the ski at 20 cm, 40 cm and 60 cm below the snow surface for soft slab (n=8) and hard slab (n=14) conditions (red line: median, edges of blue box: 25th and 75th percentiles, whiskers: most extreme values; red '+': outliers)

with σ: normal stress

x: horizontal distance along ski

a, b, c: coefficients

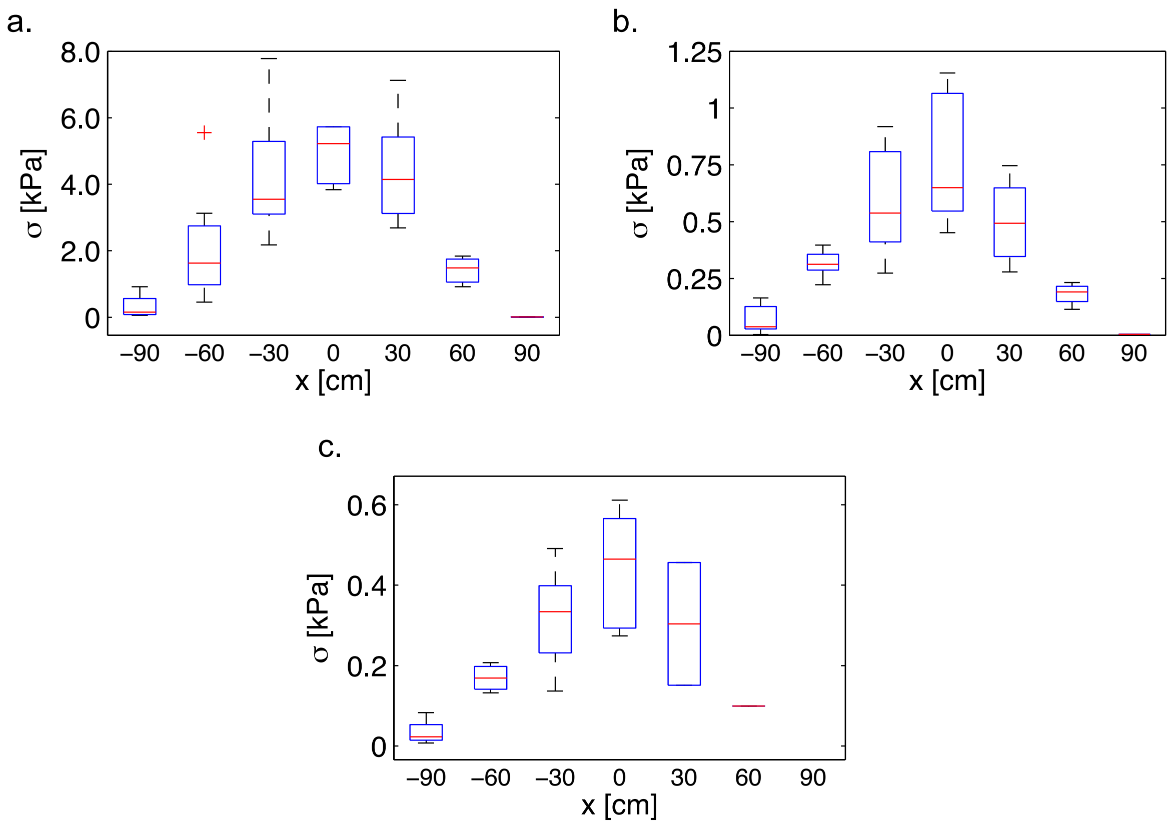

Figure 5.9. Boxplots of skier normal stresses along the ski due to a skier performing knee drops on the hard snow surface, **(a)** 20 cm, **(b)** 40 cm and **(c)** 60 cm below the snow surface. (red line: median, edges of blue box: 25th and 75th percentiles, whiskers: most extreme values; red '+': outliers)

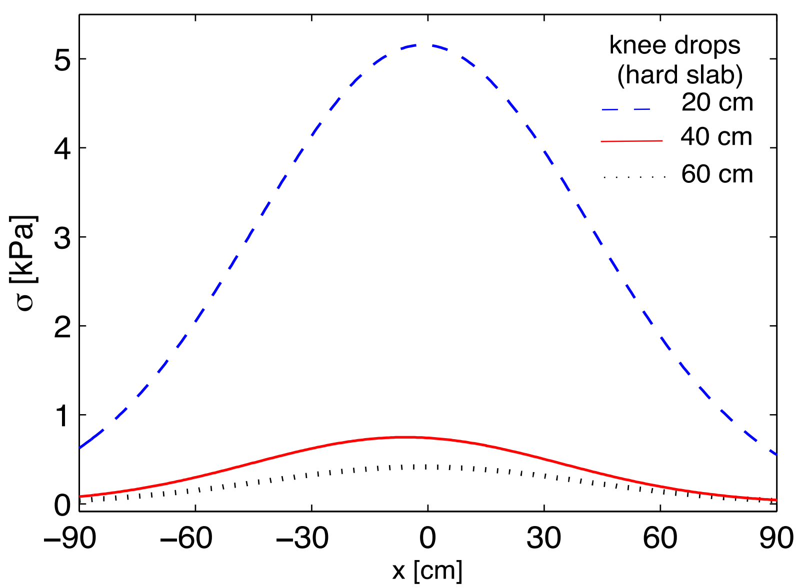

Figure 5.10. Gaussian fits of the medians of the normal stress disribution along a skier according to Figure 5.9.

a.

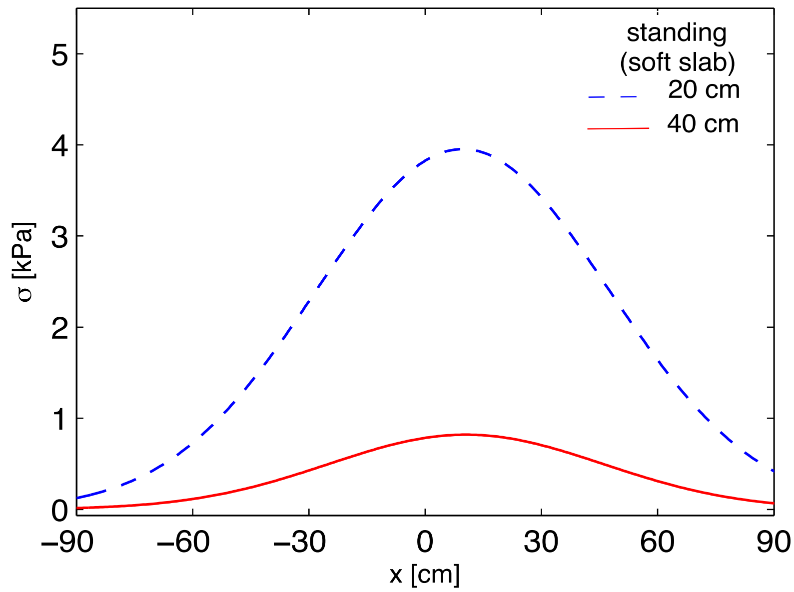

b.

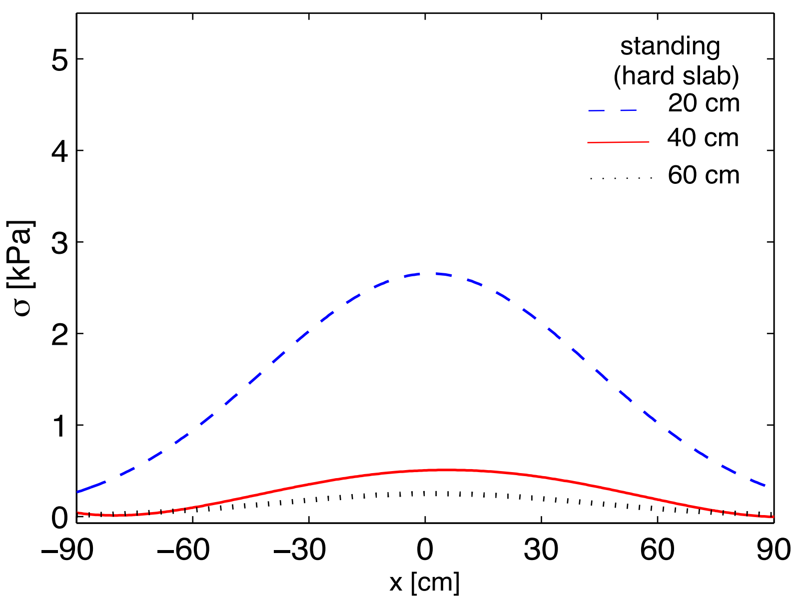

Figure 5.11. Gaussian fits of the medians of the normal stress disribution along a standing skier according to Figure 5.8. **(a)** soft slab and **(b)** hard slab.

At 20 cm, 40 cm and 60 cm depth, peak stresses in the harder snowpack were approximately 20 – 30 % lower compared to the softer snowpack. A skier performing knee bends on the hard snowpack yielded approximately 30 – 40% higher stresses compared to the standing skier load. Additionally, the width of the stress distribution at 20 cm depth increased due to the hardness change approximately 25 %.

Table 5.4. Coefficients and fits statistics for Gaussian fits through medians of Figures 5.11 and 5.12.

	Fig. #	*z [cm]*	*n*	*R^2*	*SE [kPa]*	*a*	*b*	*c*
Standing (SSL)	5.11a	20	5	0.62	1.095	3.95	9.70	53.6
		40	5	0.82	0.132	0.82	10.52	50.18
Standing (HSL)	5.11b	20	19	0.47	0.91	2.65	1.28	60.19
		40	19	0.64	0.14	0.53	6.16	51.21
		60	15	0.56	0.07	0.25	2.24	55.98
Knee drop HSL	5.12a	20	8	0.51	1.56	5.16	-1.31	61.07
		40	8	0.62	0.18	0.75	-5.6	56.55
		60	6	0.57	0.12	0.41	-1.29	58.5
Knee drop HSL	5.12b	0	8	0.75	4.15	22.7	-0.62	59.5
Standing SSL		0	4	0.90	2.04	17.5	5.28	55.53
Standing HSL		0	19	0.75	3.31	17.2	-2.3	57.82

5.3.4 Snow temperature effects on normal stress distribution due to skier loads

In this section, the variations of normal stresses due to skier loads during warming and cooling are presented. The cause of the normal stress change was either the direct temperature effect on stiffness or changing ski bending (see Sections 5.2.2). In the following paragraphs, the numbers in brackets refer to the experiment number in Table 5.2. The effect of varying snowpack stiffness and/or bending of the ski on the stress distribution, as defined in Section 5.2.2, is also given in brackets. Table 5.2 provides an overview of the results of all warming and cooling events.

5.3.4.1 Normal stress decrease due to snowpack warming

Out of all 16 warming events seven yielded reduced normal stresses during warming. In two (Experiment 13_1 and 6) out of the four cases where ski bending increased, stiffness was reduced (B_S). One case (Experiment 13_2) showed increased hardness in the near surface layers and softer less stiff layers below (B+S). Experiment 11 did not yield any detectable changes of hand hardness.

5.3.4.2 Normal stress increase due to snowpack warming

Out of all warming events nine yielded increased normal stresses during warming. In two cases (7_2, 9_2) despite a positive bending index reduced stiffness caused decreasing peak stresses (S_B). Reduced hardness in both cases and a moist snow surface seems to override to bending effect (S_B). In those five cases where ski bending did not change (Experiment 1_1, 1_2, 7_1, 7_3, 8_2,) the stress increase was apparently controlled by reduced hardness/stiffness (S). The two events with reduced bending (Experiment 5 and 12) showed higher hardness (stiffness) in one (Experiment 12), and lower hardness in the other (Experiment 5).

5.3.4.3 Normal stress decrease due to snowpack cooling

In three out of the six cooling periods normal stresses decreased. In Experiments 2 and 3 ski bending was constant and therefore elevated stiffness in the surface layers caused the stress drop (S). The supportive crust that formed during Experiment 7_4 provided sufficient stiffness to override the effect of reduced bending of the ski (S).

5.3.4.4 Normal stress increase due to snowpack cooling

In three out of the six cooling periods normal stresses increased. During all three cases ski bending was reduced and therefore the major factor that determined the stress increase. In Experiment 8_1 and 9_1 decreasing ski bending was the dominating factor over increased hardness of the near-surface layers (B_S), whereas in Experiment 4 softer surface layers worked in the same direction as the bending effect (B+S).

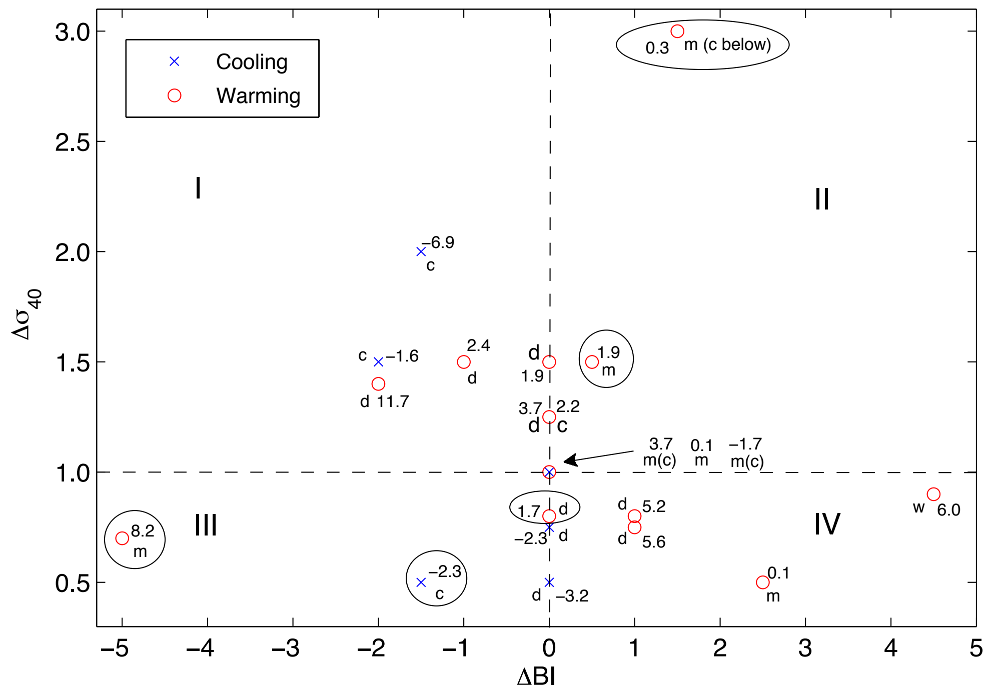

Figure 5.12. Relative normal stress change at 40 cm ($\Delta\sigma_{40}$) below standing skier vs. change of ski bending index (ΔBI) during all warming and cooling events. For each data point the temperature change and surface conditions are given (c = crust, d = dry, m = moist, w = wet)

5.3.4.5 Effect of skier bending on normal stress

Figure 5.12 shows the change of the skier bending index (ΔBI) against $\Delta\sigma_{40}$ for all warming and cooling cases for a skier standing. The graph is divided in four quadrants (I – IV) for interpretation of the effect of ΔBI on normal stress change. Basically, normal stress increased with less ski bending ($\Delta BI<0$, quadrant I) and decreased with increased ski bending ($\Delta BI>0$, quadrant IV). The bending of the skis directly controlled stress changes in these cases. In most cases where the ski bending did not change ($\Delta BI = 0$) stress change was determined by snow temperature and snow stiffness changes. Stress increased in three cases with warming ($\Delta\sigma_{40}>1$) and decreased with cooling in two cases ($\Delta\sigma_{40}<1$).

All cases that yielded an exception from this rule, that either ski bending or temperature controls the stress changes, are marked with a circle. In quadrant III

a.

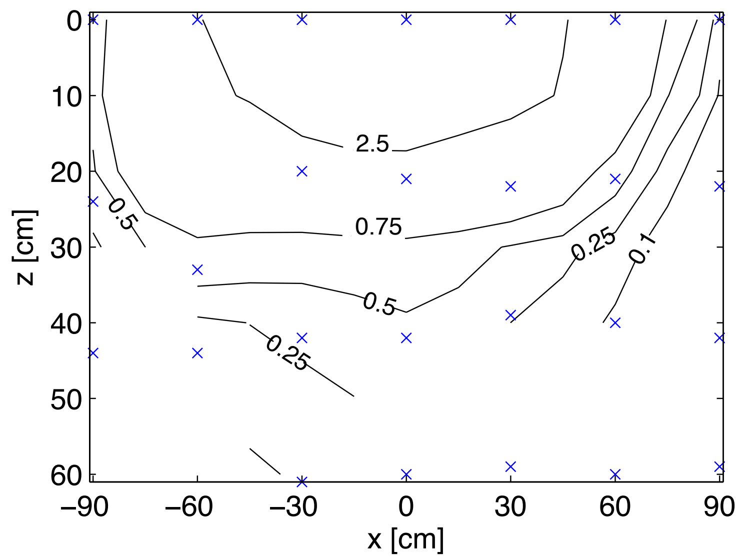
2.5
0.75
0.5
0.25
0.1
z [cm]
x [cm]

b.

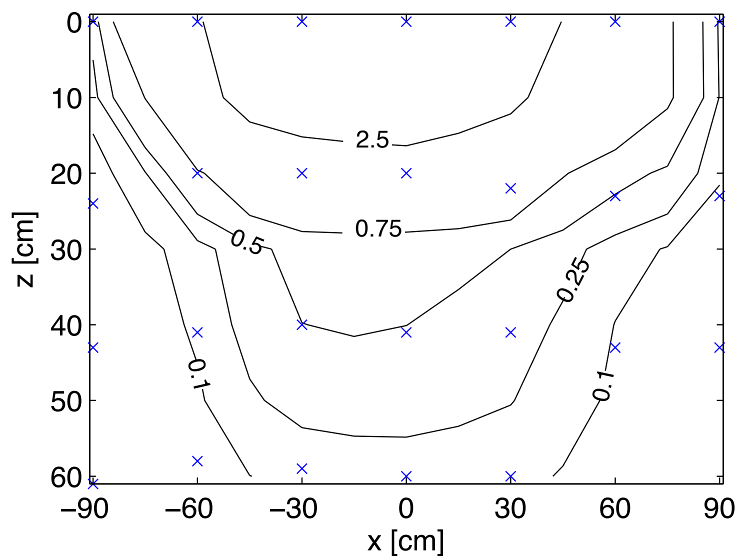
2.5
0.75
0.5
0.25
0.1
z [cm]
x [cm]

c.

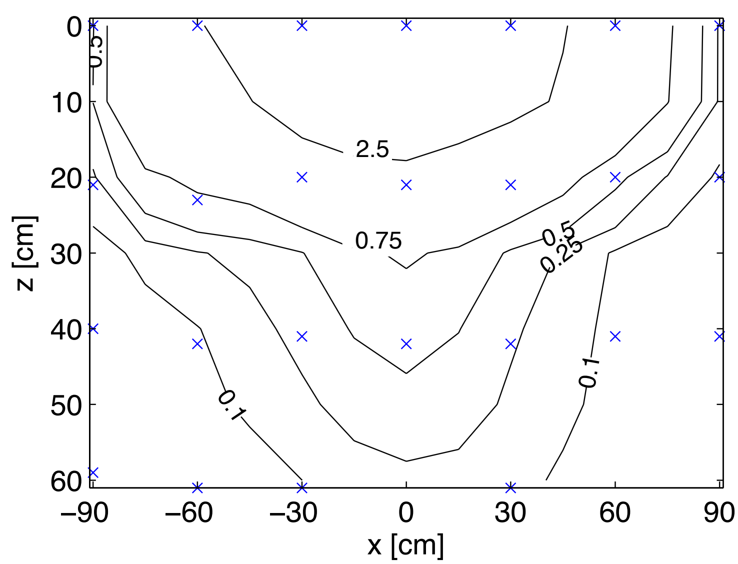
2.5
0.75
0.5
0.25
0.1
z [cm]
x [cm]

d.

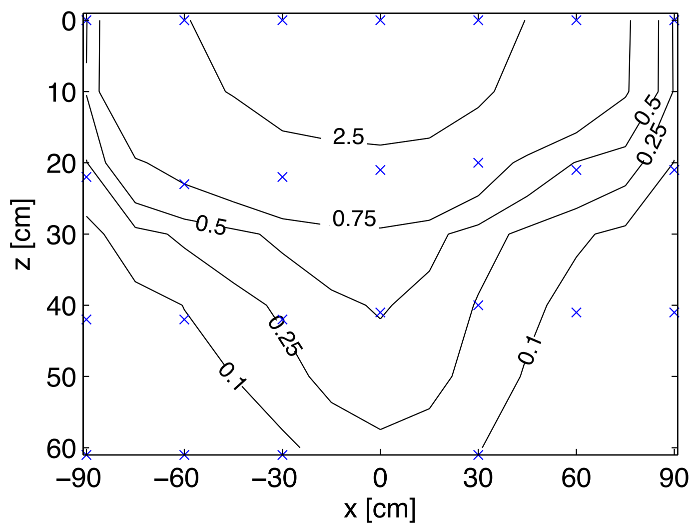

Figure 5.13. Vertical cross-sections of normal stresses along a standing skier for Experiment 1: **(a)** initial stress distribution, **(b)** after Experiment 1_1, **(c)** after Experiment 1_2, **(d)** after Experiment 1_3 (see Table 5.2). Contours are in kPa.

the warming case yielded stress decrease despite a large temperature increase and BI decrease. Snowpack warming to 0˚C (moist surface) may have caused strong settlement and densification, hence higher stiffness and less stress penetration. The cooling case in quadrant III indicates that the temperature drop (-2.3˚C) overrode the fairly small decrease in ski bending (ΔBI=-1). In this case, a crust formed on the snow surface and considerably increased stiffness. Therefore, the skier's weight spread out over a greater length along the ski. The two warming cases in quadrant II provided evidence that warming was the first order effect over increase in skier bending, which was fairly small in these two cases. The high normal stress increase (factor three) of the upper case can be explained by a surface crust the melted with only little warming (0.3˚C). One warming case where ski bending did not change (on negative y-axis) showed stress decrease, although the snowpack in this case remained fairly cold and dry (T_{avg} = -4.5 after warming). Potentially, settlement over the duration of the experiment caused higher hardness (stiffness) that may explain the stress decrease.

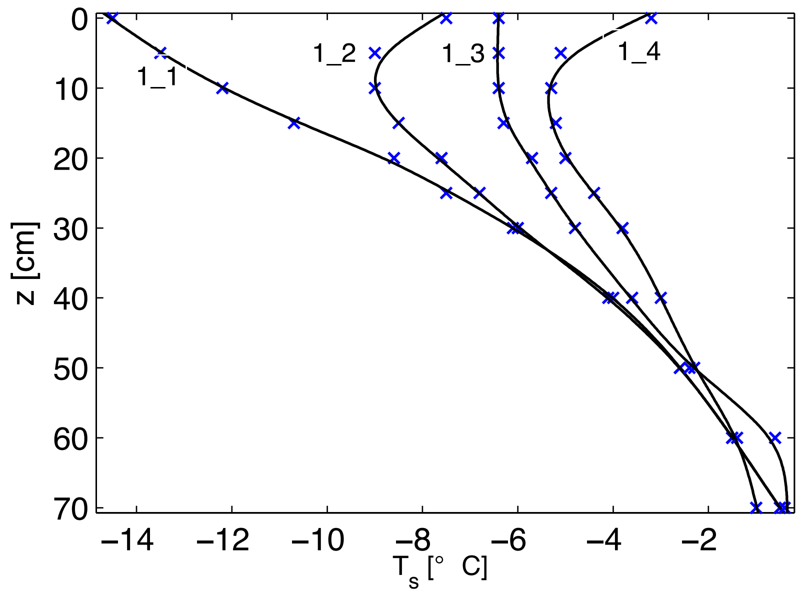

Figure 5.14. Snow temperature profiles for all four time steps of Experiment 1. Numbers (1_1 to 1_4) refer to experiment # in Table 5.2.

5.3.4.6 Width of the stress bulb

The width of the stress bulb (the 0.5 kPa contour at approximately 30 to 40 cm snow depth) changed by approximately 20 – 40% during the temperature changes that were observed in all experiments. The actual width in this depth level ranged from approximately 40 – 130 cm (Table 5.2). No considerable difference in terms of the width-change of the stress bulb was observed between warming and cooling.

5.3.5 Case studies of 2D cross-sections of normal stress along skis

This section presents case studies of the 2D normal stress distribution along the skis and changes due to temperature variations of the near-surface layers. See Appendix A for snow hardness profiles.

5.3.5.1 Case study 1 (Experiment 1)

Figure 5.13 shows a time series of the normal stress distribution during the warming periods of Experiment 1 (see Table 5.2). This experiment was performed on the skier compacted snow surface. Therefore, ski bending and ski penetration did not have any affect on the stress distribution. The measurements were

a.

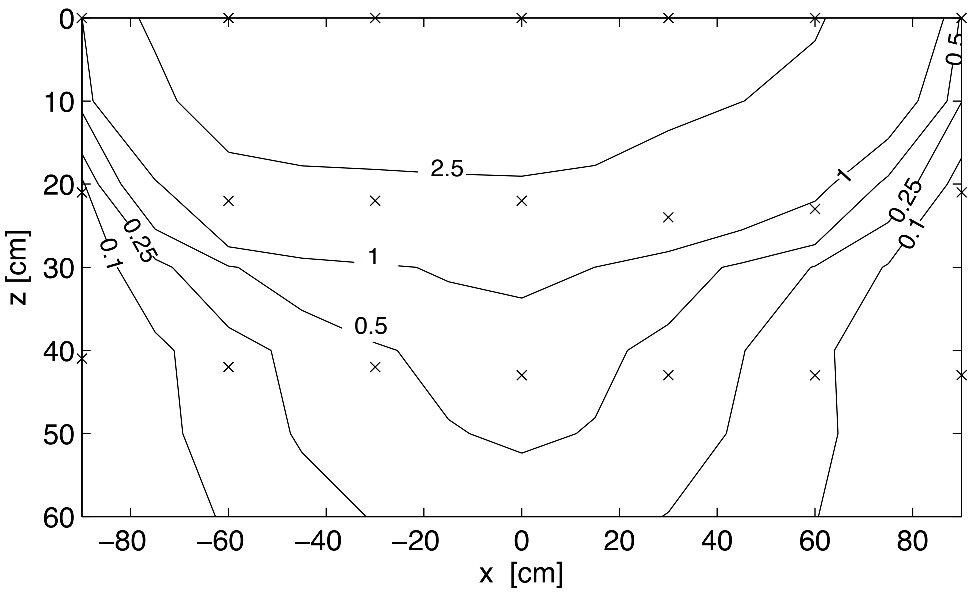

b.

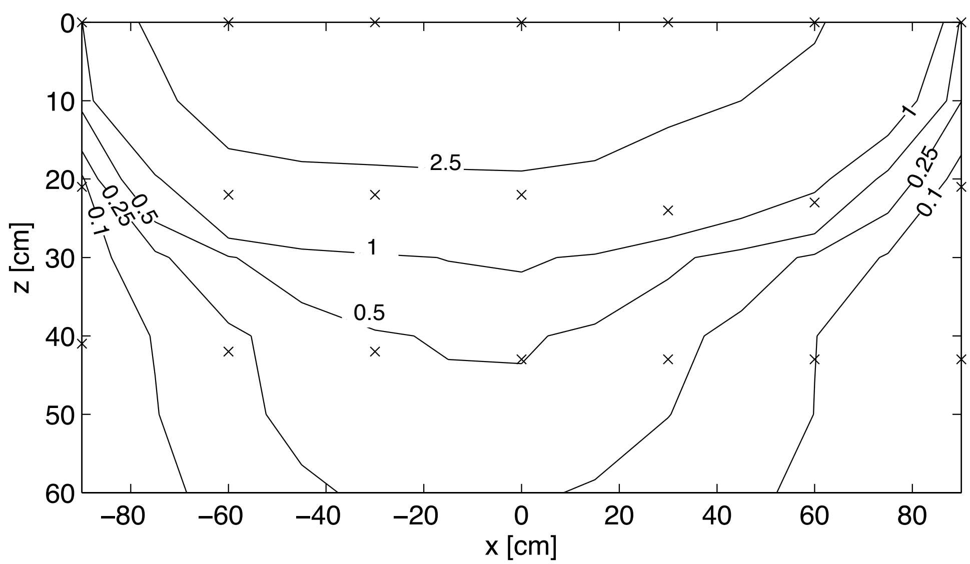

Figure 5.15. Vertical cross-sections of normal stresses along a standing skier from Experiment 2: **(a)** in the afternoon before the cooling (Experiment 2_2), **(b)** early morning after cooling (Experiment 2_3). Contours are in kPa.

conducted over the course of four days. Between each measurement, which was conducted during maximum daytime temperature, the snowpack went through a cooling cycle during the night. The temperature profile for each of the cross-sections is shown in Figure 5.14.

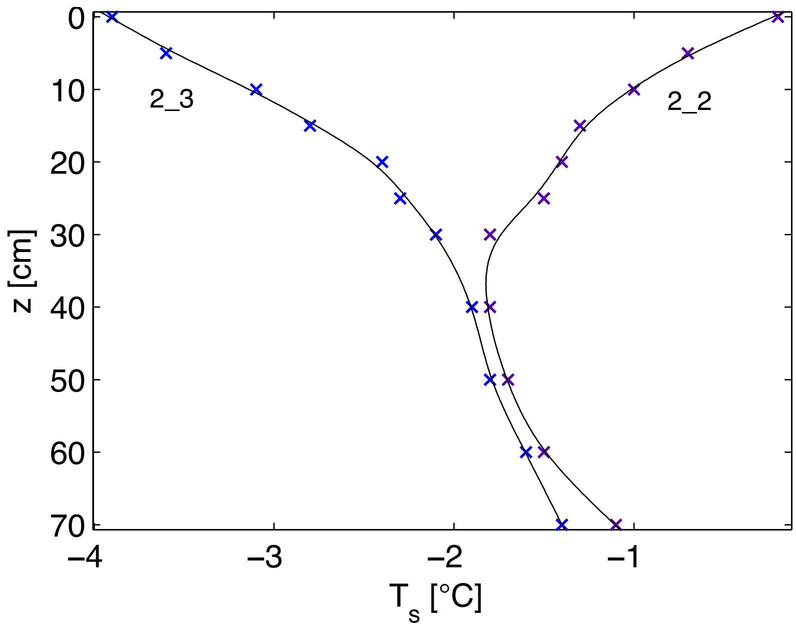

Figure 5.16. Snow temperature profiles for the cooling period of Experiment 2 over 18 h.

After the first warming period (Figure 5.13b) the depth of the 0.5 kPa contour increased from approximately 35 cm to 40 cm. Overall, the shape of the stress bulb between approximately 20 to 40 cm snow depth widened. With the second warming (Figure 5.13c) the stress distribution became slightly deeper but narrower compared to the one before. No significant change 24 h later could be observed (Figure 5.13d). Presumably, slight settlement and densification and metamorphism (*delayed-indirect effects,* see Section 2.2.4) counter-balanced the softening effect of the warmer snow temperatures.

5.3.5.2 Case study 2 (Experiment 2)

This case study examines the stress distribution (Figure 5.15a) after the near surface layers cooled over night during 18 h (Figure 5.15b, ΔTavg=-2.3˚C). The BI in this case was not relevant since the experiment was conducted on hard (skier compacted) near surface layers. With cooling (stiffening) of the near-surface layers the depth of the stress (deformation) penetration considerable decreased. The 0.5 kPa contour lifted by approximately 10 cm from just below 50 cm to below 40 cm.

a.

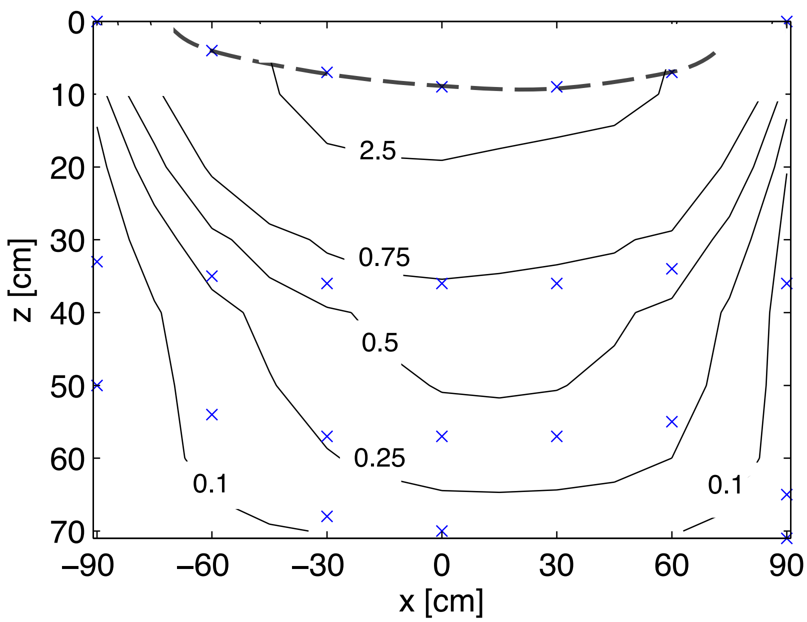

b.

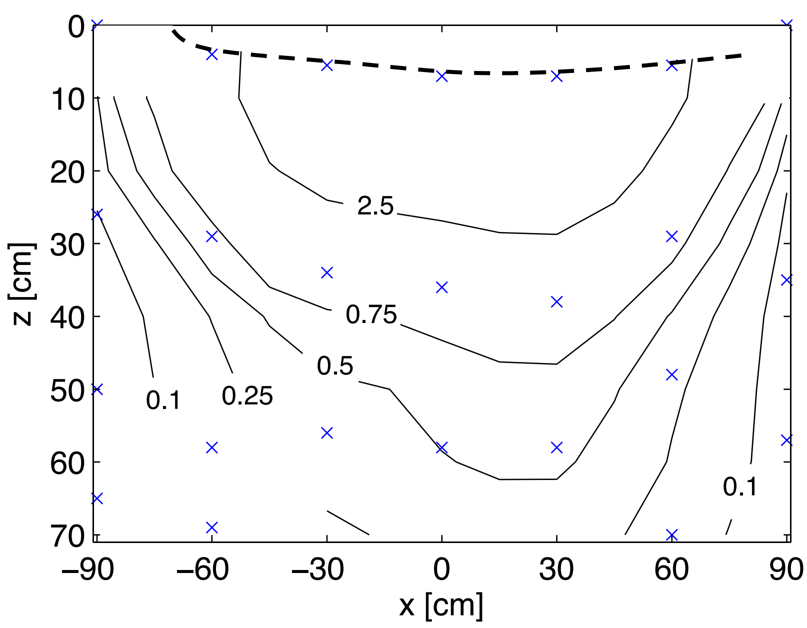

Figure 5.17. Vertical cross-sections of normal stresses along a standing skier from Experiment 4. **(a)** afternoon before the cooling **(b)** early morning after cooling. Contours are in kPa. The dashed line indicates the position of the ski.

The overall shape of the bulb of the normal stress distribution did not undergo any considerable changes.

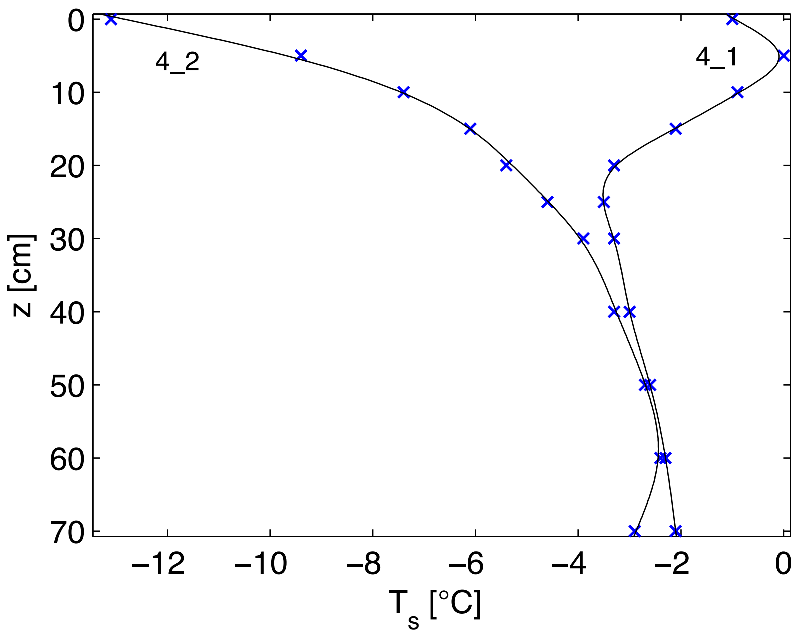

Figure 5.18. Snow temperature profiles for the cooling of Experiment 4.

5.3.5.3 Case study 3 (Experiment 4)

The cooling period of Experiment 4 demonstrates the effect of a change in ski bending due decreased ski penetration on the stress distribution (Figure 5.17). The temperature of the near-surface layers in this case dropped by ΔT_{avg} = -6.9˚C during 18.5 hrs. This experiment was conducted on a natural snowpack.

A ΔBI of -1.5 cm indicates less ski bending after the cooling. The maximum ski penetration decreased from 9 cm to 7 cm. Normal stress at 40 cm snow depth approximately doubled. The width of the stress distribution increased approximately 40%. In this case the effect of the decreased ski bending overrode the cooling effect on stiffness.

5.3.5.4 Case study 4 (Experiment 13)

Figure 5.19 shows the normal stress distribution below a standing skier before and after warming of the near-surface layer by ΔT_{avg} = 6.0˚C. ΔBI = 4.5 indicates a strong influence of the increasing ski bending due to the softening near-surface layers. Despite the strong warming, σ_{40} dropped by approximately 10%. Normal

a.

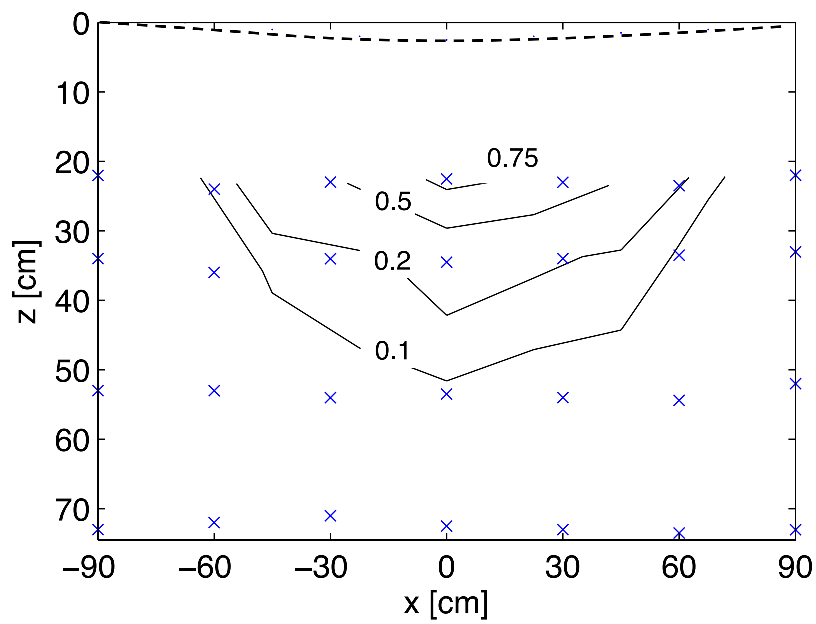

b.

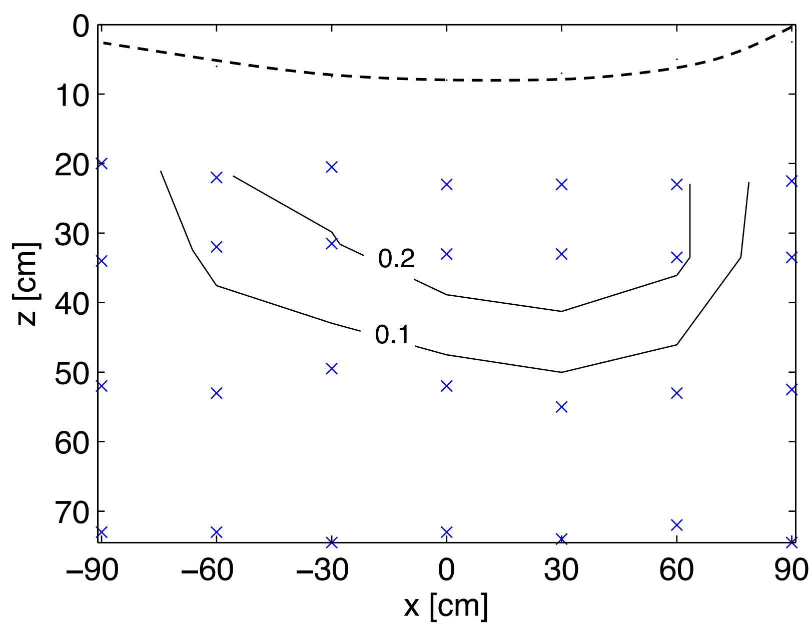

Figure 5.19. Vertical cross-sections of normal stresses along a standing skier from Experiment 13. **(a)** Before and **(b**) after warming of the near-surface layers**.** Contours are in kPa. The dashed line indicates the position of the ski.

stresses of approximately 0.75 kPa at about 20 cm depth below the centre of the boot dropped to just above 0.2 kPa. The overall shape of the stress-bulb appeared to be considerable wider and slightly less deep after the warming and softening of the near-surface layers. In this case, the bending of the ski appeared to be the 1st

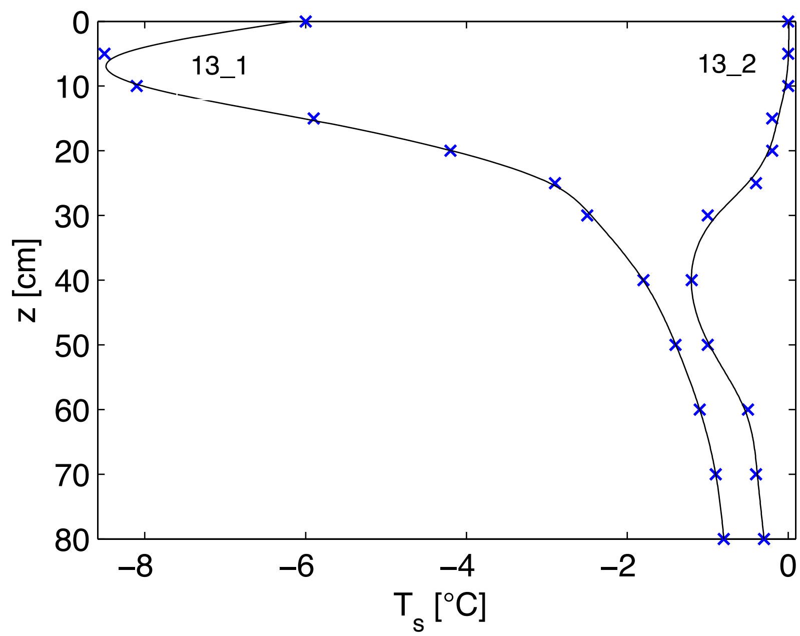

Figure 5.20. Snow temperature profiles of Experiments 13_1 and 13_2.

order effect over the softening effect of warming snow temperatures. The hand hardness of the near-surface layers decreased from approximately 1F – P to 4F – 1F. Furthermore, wetting and moistening of the snow surface likely contributed to softening of the near-surface layers.

5.4 Discussion

5.4.1 Normal stress distribution due to skier loads

Most of the 2D cross-sections of normal stress below a skier showed a characteristic shape. Normal stress directly under the boot was considerably higher or the stress bulb was considerably deeper than closer to the tip and tail of the ski. The bending stiffness of the ski and the actual bending of the ski mainly determine the stress distribution. Figure 5.21 shows the surface stress distribution below two skis of different bending stiffness. The surface stress is concentrated below the boot. The 2D cross sections of normal stress in Figures 5.13 and 5.15 show a

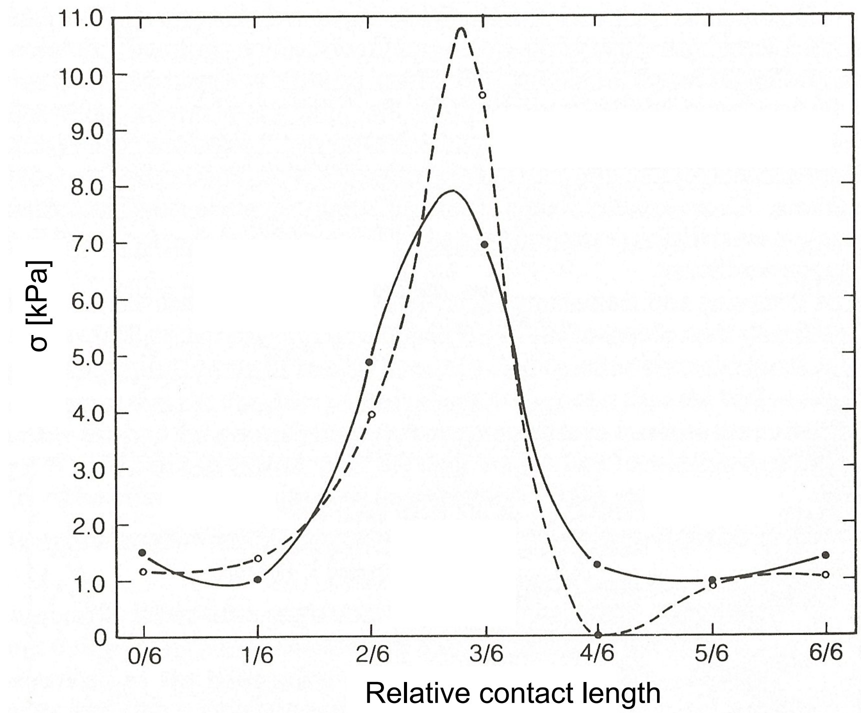

Figure 5.21. Stress distribution on a horizontal surface below two skis of different stiffness for a 356 N load (after Gray and Male, 1981, p.754).

similar stress distribution. These two cases were performed on a hard slab (skier compacted near surface layers) with negligible ski penetration and ski bending. In cases where the stress is distributed more equally (Figure 5.17 and 5.19) the ski bending was larger and therefore the weight of the skier was more equally distributed along the whole length of the ski.

According to Salm's (1977) calculations (Section 2.1) the width of the bulb of the horizontal component of skier-induced stresses is wider than the vertical component of stress (the normal stress measured within this study). Therefore, the width and length of the influence of the skier induced stresses may be larger than estimated in this study by only measuring the vertical normal component of normal stresses.

5.4.2 Snow temperature effects on skier triggering

The findings of this experimental study suggest that two factors mainly controlled the variation of skier normal stresses due to warming or cooling of the near surface layers. Those were the stiffness of the near-surface layers and the bending of the ski. On hard snowpacks where ski penetration was negligible or ski penetration or bending of the ski did not change with changing snowpack temperature, the change in stress penetration due to skier loads was apparently only controlled by the stiffness (hardness) of the snowpack. Generally, softer snowpacks allowed skier stresses to penetrate deeper compared to harder snowpacks. A harder snowpack over a weak layer may prevent surface stresses and deformation from initiating a fracture. This effect is commonly referred to as ‘bridging’ and reduces the likelihood of skier triggering. However, a weak layer below a thick cohesive slab may have high propagation propensity once a fracture is initiated.

If warming near-surface layers softened enough to allow deeper ski penetration, usually stronger bending of the ski occurred. This effect could override the temperature effect on stiffness due to warming (deeper stress penetration). With increasing ski bending, the weight of the skier is distributed more towards the tip and tail of the ski. For example, the increasing bending of the ski can often be observed in a spring-like snowpack while the melt-freeze crust is softening.

The proposed concept by McClung and Schweizer (1999), that stress and deformation penetration increases in warming and softening snow still holds true for hard near-surface layers where ski bending remains constant. This concept is also applicable for loads that do not change their distribution along the snow surface with warming (e.g. explosives, snowmobiles, climbers, cornice fall).

Furthermore, a stress bulb that does not deepen with warming near-surface layers cannot contribute to easier skier triggering, according to the strength-stress stability condition (Schweizer and Jamieson, 2003). Potentially, the widening stress bulb exceeds the critical initial crack size necessary for fracture propagation (see Section 1.4). This critical size appears to be comparable to the order of magnitude of the length of the stress bulb (Figure 5.22). This hypothesis is speculative, since no measurements exist to confirm the critical crack size.

On the other hand, a skier performing downhill turns ‘drives’ the fracture in a potential weak layer. This raises the question if the length of the stress bulb is a valid stability criterion. It is know from experience that re-grouping skiers are able

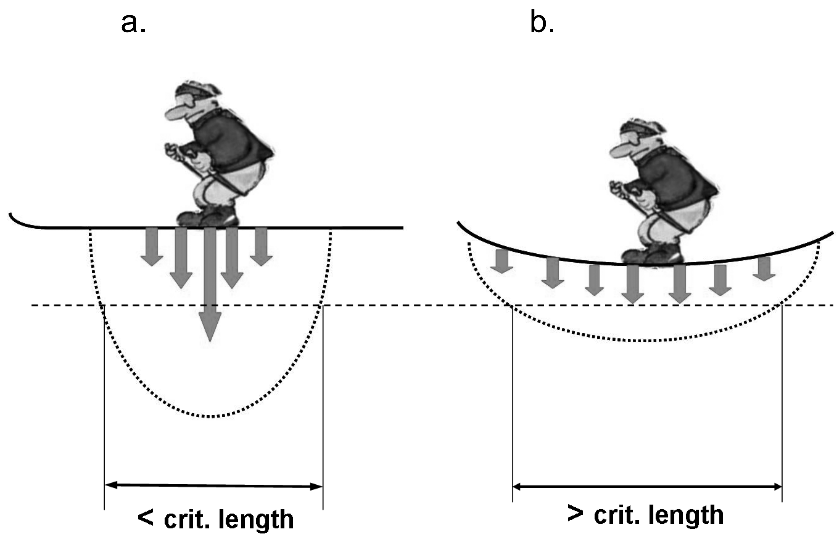

Figure 5.22. Schematic showing the bending of the ski and magnitude of normal stresses before (**a**) and after (**b**) the surface layer warmed up. The widening stress bulb after warming may fracture a weak layer with the necessary critical length for fracture propagation.

to initiate a slab avalanche. In this case, the critical crack size for fracture propagation may have been exceeded.

Schweizer and others (2004) found in lab experiments that the fracture toughness of snow is temperature dependent. Therefore, a warming related change in fracture toughness may be responsible for a change in propagation propensity even though stresses do not change considerably.

The FEM calculations by Wilson and others (1999) yielded shear stress increase in a weak layer by approximately 10 – 50% due to a static skier load during warming of the overlaying slab. Assuming that the additional normal stress due to a skier in level terrain is approximately 1.5 times the shear stress on a 38° slope as in Wilson's study, the normal stress increase during warming of 25 - 50% due to static skier loads found in this study (Section 5.3.4) seems plausible and lies within the same order as Wilson's and others results.

5.4.3 Influence of snow hardness on the dynamic and static response of the snowpack due to skier loads

Snowpack hardness seemed to impact the response of the snowpack due to dynamic skier loading (knee drops and jumps) (Figure 5.6 and 5.7). The negligible difference in normal stress between knee drops and jumps on soft slabs may indicate damping effects of the softer snow (Schweizer and Camponovo, 2001). In contrast, a harder snowpack seemed to transfer the dynamic loads more effectively. Fewer viscous deformation processes absorbed the applied forces on the snow surface.

Primarily, it was the hardness of the near-surface layer that determined the range of absolute values of stresses due to skier loads. The stress variation due warming (short term) or cooling related changes of stiffness were usually more than one order of magnitude less than the stress range set by average hand hardness of the near surface layers. For example, normal stresses in snow layers of 4F – 1F hand hardness were approximately 3 – 4 times (300 to 400%) higher than in snow of P hardness. Stress changes due to typical initial daytime snow temperature changes varied approximately 20 – 50 % of the stress value.

5.5.4. Variation of the skier's weight and skis

The weight of the test skier, and the length, width and stiffness of the skis were kept constant during each experiment. The effect on stress distribution of various types of skis and weight of the skier was not considered. However, it can be assumed that variations of these factors are at least in the same order as stress changes due to temperature induced stiffness variations. The following consideration is intended to estimate the likely range of extreme skier loads. Assuming a skier with 60 kg weight on a relatively long ski (1.70 cm, estimated effective length 90 cm) and a 95 kg skier on relatively short skis (1.80 cm, estimated effective length 100 cm; (Schweizer and Camponovo, 2001)) yields a range of approximately 6.5 kPa to 9.5 kPa for average surface stresses. Presumably, skier stresses in the sub-surface layers due to varying skier surface stresses show the same relative variation of up to 50%, which is within the same order of snow temperature induced normal stress variations (Figure 5.12). Accordingly, if increased skier stresses due to daytime warming can contribute to skier triggering, just the variation in skier stresses due to various skier weights and different ski length and stiffness may have a similar effect.

5.5.5 Weak layer strength compared to skier stresses

The range of maximal skier normal stresses due to knee drops and jumps in a depth between 40 cm and 60 cm, which is the common average depth for skier triggering, was approximately 0.2 to 1.5 kPa (Figures 5.6 to 5.9). This converts to approximately 0.13 to 1 kPa shear stresses on a 38˚ slope. The average shear strength of layers of faceted crystals and surface hoar layers in the first two weeks after burial lie within the same order of magnitude (Zeidler and Jamieson, 2006a,b)

5.5 Summary

The field experiments on the normal stress distribution in the snowpack due to static and dynamic skier loads confirmed the non-linear stress decrease with snow depth in accordance with previous studies (Section 2.1). Softer snow allowed skier-induced stresses to penetrate deeper into the snowpack than stresses in a harder snowpack. Softer near-surface layers, however, appeared to have a dampening effect on dynamic skier loads (knee drops and jumps). Stress transmission in harder snowpack layers seemed more efficient compared to softer layers.

Short-term warming of the near surface layers usually led to deeper stress penetration due to skier loads as long as the bending of the skis did not change. If the bending of the skis increased, with increasing ski penetration in softening near-surface layers, the stress distribution below the ski could widen and become shallower. Bending of the ski resulted in a more equal distribution of the skier load along the ski. In other words, peak stresses directly below the boot decreased and spread out towards the tail and tip of the ski. In general, on hard slabs with negligible ski penetration, changes of skier stress bulb were controlled by the temperature effect on stiffness of the slab. In cases where the ski bending changed, in most cases this became a 1st order effect overriding the direct effect of temperature on stiffness.

Cooling in general increased the stiffness of the near surface layers. If ski bending was constant during snowpack cooling, the skier induced stress bulb widened and became shallower. In some cases, if the ski bending was strong before the cooling and decreased during cooling this could override the direct effect of temperature. In this case, the depth of the stress penetration increased despite a stiffening near-surface layer.

CHAPTER 6

The impact of snowmobiles and skiers on the snowpack

6.1 Introduction

In recent years the number of recreational backcountry users on snowmobiles in North America was on a strong rise and outnumbered skier and snow boarders (CAA, 2010, p. 12). Also the number of avalanche accidents is rising. Snowmobile avalanche fatalities were considerably higher in the past 10 years in Canada compared to all other user groups (Figure 6.1). In responds to this trend many mitigation measures are under way, such as avalanche safety courses (Wood, 2007) and training materials (Jamieson and others, 2007) specifically tailored to snowmobile backcountry users. Furthermore, current research compares the shear stresses within the snowpack due to snowmobiles and skiers (Thumlert and Exner, in prep.). To date, not much knowledge exists on the impact of snowmobiles on the trigger process of slab avalanches that is confirmed by reliable scientific data. Many speculate about additional stresses in the snowpack on potential weak layers. Such speculations range from “snowmobiles float on top of the snow surface and therefore exert less stress on the snow cover” (anonymous snowmobiler) to “no wonder snowmobilers get in trouble with their heavy machines” (anonymous backcountry skier).

At a first glance one might expect a larger stress impact of a snowmobile due to its greater weight compared to that of a skier. On the other hand, the load is distributed over a considerably larger area reducing the load per surface area. At this point, it is not known if the main cause of increased accidents is the higher stress impact or just the fact that the fast paced sport of snowmobiling and ‘high marking’ increases the odds of triggering an avalanche due to more frequent exposure to avalanche start zones. To shed more light on the stress

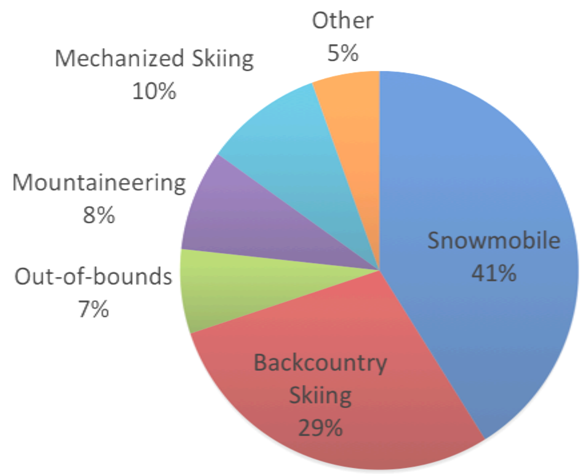

Figure 6.1. Avalanche fatalities in Canada by activity from 2000 to 2010 (April 29); 146 fatalities in total (CAA, 2010).

impact of snowmobiles compared to skier stresses, a field study was undertaken utilizing the stress measurement method described in Chapter 4. The goal of the field study was to measure and compare for the first time dynamic normal stresses exerted on the snowpack by snowmobiles and skiers under selected realistic loading conditions.

6.2 Methods

6.2.1 Experimental set up

The experiments were carried out in the vicinity of Mt. Fidelity weather station at Glacier National Park on three different days in the winter of 2009 (Table 6.1). To ensure comparable and repeatable snowpack conditions a level area of approximately 5 x 4 m was skier compacted to create a stiff and supportive slab in the same way as for the skier stress bulb measurements (Section 5.2). This was done the previous day to allow the slab to strengthen to minimize penetration (indentation) into the snowpack by the skier and snowmobile. The stiff surface layer (pencil hardness) was approximately 10 cm thick overlying a softer snowpack for all three experiments (Table 6.1). The stress sensor sheets were inserted from

Table 6.1. Snowpack conditions of all three experiments.

Exp # (Date)	T_{10} [˚C]	Avg. hardness[1] (slab / 50 cm below)	Major snow types[1] (slab / 50 cm below)	Avg. density [kg/m^3]	Stress profile
Exp 1 (Feb 22)	-11.0	P$^+$ / 4F$^+$ – 1F	Mixed forms / rounds and mixed forms	305 / 210	1D, 2D
Exp 2 (March 23)	-6.2	P$^+$ / 1F – P	Small rounded / small rounded	310 / 250	1D
Exp 3 (March 30)	-6.8	P$^+$/ 1F$^+$/P$^-$	Small rounded / small rounded	302 / 260	1D

[1] According to ICSSG (Fierz and others, 2009)

a trench (max. 50 cm wide) to minimize disturbance of the snowpack (Figure 6.2). On the influence of the open pit wall see Section 5.2.3. The experiments were confined to level terrain.

6.2.2 Procedure

First, the sensors were loaded with a skier standing on both skis (for 15 s) and performing 5 knee drops and then 3 to 5 jumps (Figure 6.2), stopping if the upper stiff layer (slab) broke. After the skier loading steps, the snowmobile was driven with constant slow speed (approximately 2 m/s) across the study site. First with one ski directly above the sensor location (Plane 2 in Figure 6.3), followed by a pass with the sensors below the mid line of the track (Plane 1 in Figure 6.3). Each of the snowmobile passes was repeated two times.

To include dynamic impacts of a jumping or bouncing snowmobile, as usually observed during snowmobile riding, the snowmobile was driven over a bump before the compacted study site to ensure the snowmobile lifted slightly off the ground before impacting the sensor location (Figure 6.4). Two to three jumps were performed until the slab broke too much. After the experiment the sensors were excavated and the exact depth below the snow surface was measured.

6.2.3 The snowmobile

The snowmobile used was a Skidoo Summit 700 (Figure 6.5). For relevant technical specifications see Table 6.2.

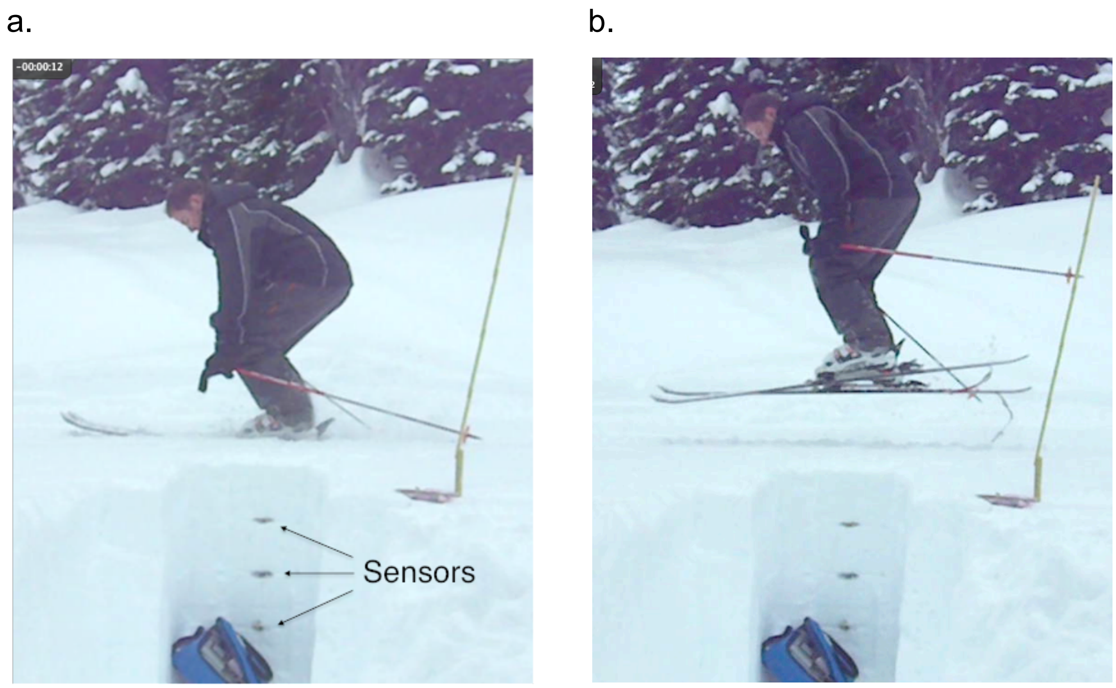

Figure 6.2. Skier jump above the stress sensors on the skier compacted study site.

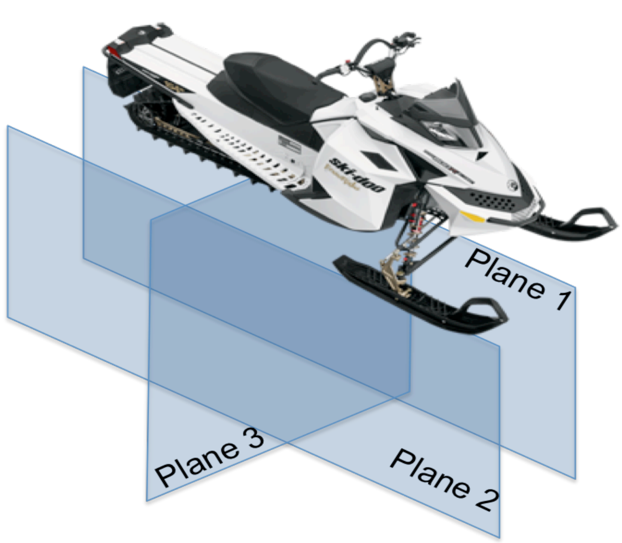

Figure 6.3. Planes along which cross-sections of normal stresses were measured; Plane 1 along mid line of track, Plane 2 along mid line of a skid, and Plane 3 across track where maximum stresses were observed.

a.

b.

c.

d.

Figure 6.4. Sequence of a snowmobile jumping onto measurement site. Note the suspension is fully compressed just above the stress sensor location **(c)**, ensuring high impact on the sensors.

Table 6.2. Relevant snowmobile specifications of the Summit 700.

Dimensions of snowmobile parts in contact with snow surface:	
Track (driving)	38 x 140 cm
Track (jumping)	38 x 150 cm
Skids	13 x 60 cm
Length: back of track – front of skids	250 to 260 cm
Skid stance	100 cm
Weight	310 kg (including rider appr. 80 kg)

6.2.4 Vertical stress profiles

For all three experiments vertical normal stress profiles were measured to a snowpack depth of approximately 90 cm. The vertical spacing of the sensors was approximately 20 – 25 cm (Figure 6.6 and 6.10). During the skier loading steps, stresses were measured below the centre of the ski boot. In the experiments with the snowmobile drive-over the maximum spike in the stress signal was used to compare it against the skier loads. The snowmobile jumps were aimed at landing mid track (lengthwise and across) on the sensor location. For the suitability of the sampling frequency for dynamic loads see Section 2.3.5

6.2.5 2D vertical cross sections

For Experiment 1 cross sections of normal stresses along the skier and snowmobile were measured. The cross sections for loading due a skier standing and performing knee drops were measured in vertical profiles spaced 30 cm along the pit wall, similarly to the method describe in Section 5.2.1 (Figure 5.2). For the snowmobile load, the 2D stress distribution was reconstructed from the time dependent stress signal from one vertical stress profile and the constant speed of the snowmobile that was moving over the sensors. The speed was estimated from the time to move between the two probes with known spacing of 4 m. Time was

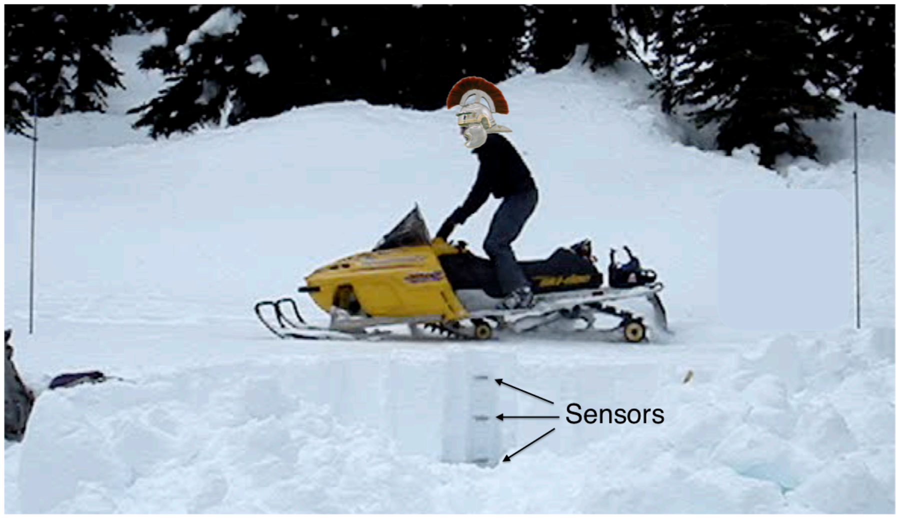

Figure 6.5. Snowmobile driving over measurement site with constant speed between two probes (4 m apart). The pass-over was filmed with a digital camera to estimate snowmobile speed.

estimated from videos taken during the experiments according to the frame count between the probes. With a frame rate of 30 frames per second of the digital camera and a sampling interval of 0.09 s (11 Hz) of the data logger the spacing between each measurement was calculated to 0.189 m. The contours were plotted according to the method described in Section 3.2.

6.3 Results

The following sections present the results of the normal stress distribution below snowmobiles, which were compared to skier stresses. Snowmobile stresses created by a smoothly driving and jumping snowmobile onto the site versus skier stresses due to standing, heavy knee drops and jumps on the same spot are compared. The first section (Section 6.3.1) puts the various loading steps of both skier and snowmobile from all three experiments measured in one-dimensional vertical profiles in perspective. Section 6.3.2 focuses on the two-dimensional stress distribution along and across the snowmobile and skier. In the experiment with the snowmobile, surface stresses were estimated according to the weight of the snowmobile (including rider) and the surface area of the track and skids, since no measured values were available. The measured skier surface stresses were corrected according to the procedure presented in Section 5.2.3.1.

6.3.1 Vertical stress profiles

Vertical stress profiles from all three experiments were plotted for the skier loading steps in Figure 6.6a, and for the snowmobile loading steps in Figure 6.6b. The dashed lines are power law fits for each loading step indicating non-linear stress decrease with depth. The power law fits are shown together in Figure 6.7 (without the data points) for direct comparison of both, the skier and snowmobiler loads with the following inferences:

- *The stress under the snowmobile skis while driving (without bouncing) was comparable to a standing skier.*
- *A jumping skier produced slightly higher stresses than under the track of the smoothly driving snowmobile.*
- *A smoothly driving snowmobile put more stress into the snowpack than the skier knee drops (which is likely comparable to turns while skiing).*
- *The jumping snowmobile stressed the snowpack the most; about twice as much as a jumping skier, and approximately 2 to 4 times more than the skier knee drops.*
- *Skier and snowmobile jumps produced the highest stresses in deeper layers (down to 90 cm).*
- *The jumping (comparable to bouncing) snowmobile produced considerable normal stresses (above 0.5 kPa) close to about 1 m depth.*

6.3.2 Vertical cross sections of normal stresses

6.3.2.1 Normal stress distribution under moving snowmobile

While driving the snowmobile mid track over the sensor positions (Plane 1 in Figure 6.3) the skids with a stance of 1 m passed approximately 50 cm to the left and right of the sensor location. This also reflects in the stress distribution in Figure

a.

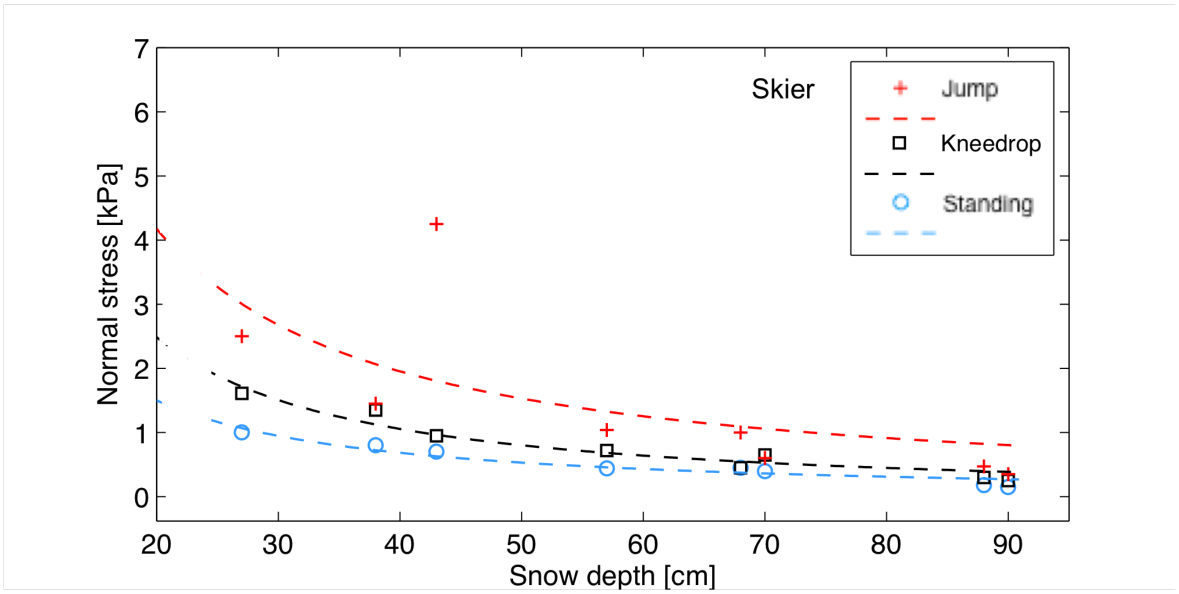

b.

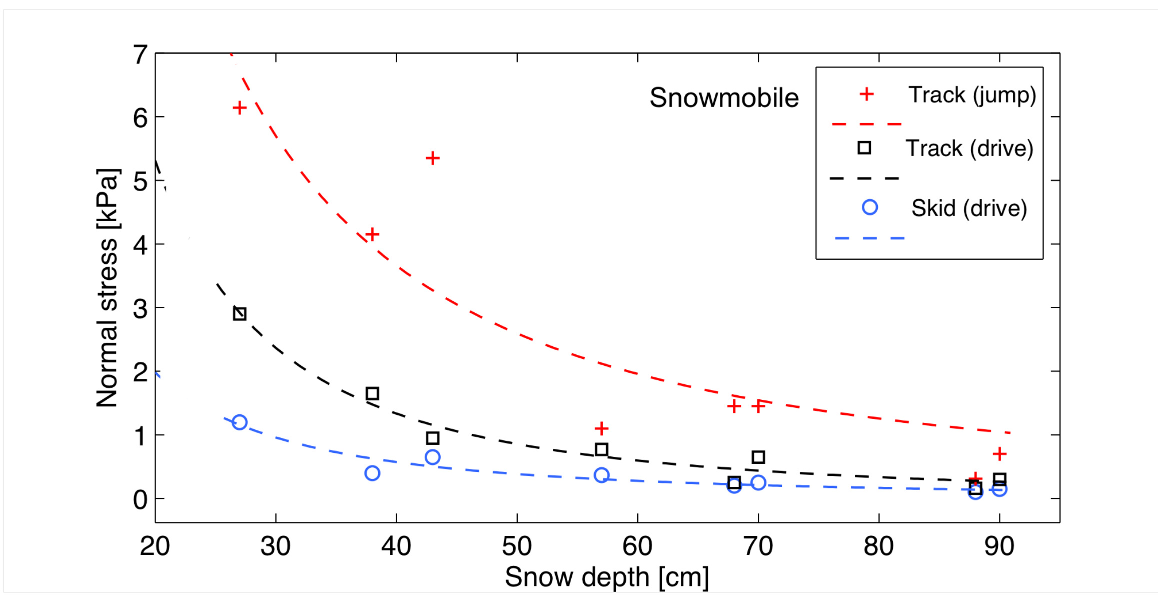

Figure 6.6. Normal stress profiles for all three experiments for **(a)** skier loading and **(b)** snowmobile loading; The dotted lines indicated power law fits.

6.8. The stress maximum under the area where the skids passed on either side appears at approximately 50 cm depth. That is the area where the stress bulb of both skids overlap. The observed pattern only holds true for this cross section along the middle of the track under the snowmobile where the maximum stress appeared.

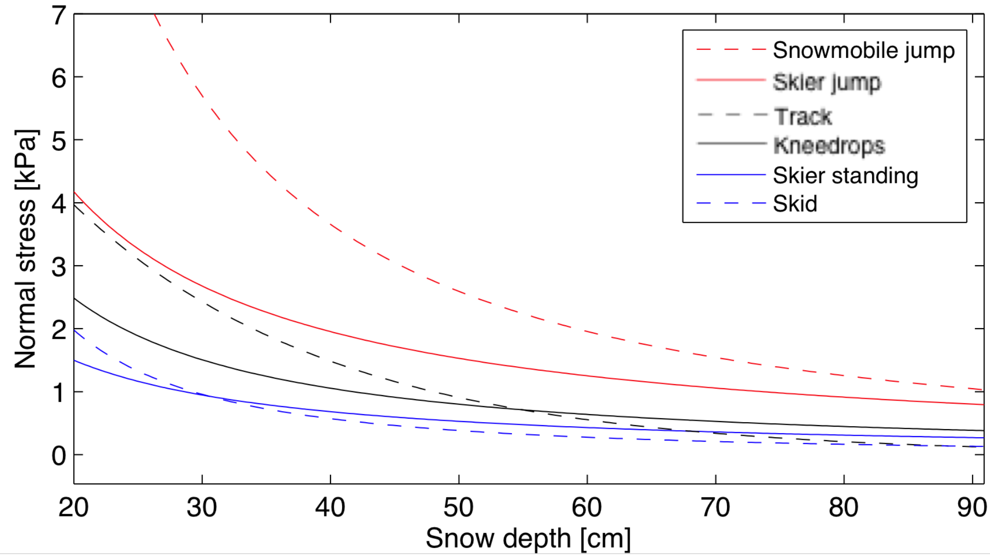

Figure 6.7. The fits for both skier (from Figure 6.6a) and snowmobile loading (from Figure 6.6b) are plotted for comparison.

Figure 6.8b shows the stress distribution during a pass where one of the skids was directly above the sensor location (Plane 2 in Figure 6.3). Stresses under the skids are generally lower than under the track. To draw a more realistic picture of the entire stress distribution the maximum values of both cross sections (Plane 1 and 2) were combined in Figure 6.9.

6.3.2.2 Length of stress bulb along skiers and snowmobiles

The length of the stress bulb under the snowmobile (Figure 6.9) is considerably longer than under skis due to the longer contact area of the snowmobile with the snow surface. The 0.5 kPa contour at about 40 cm depth (Figure 6.9) under the snowmobile is approximately 170 cm, 75 cm under a standing skier, and 1 m during the knee drops (Figure 6.10). The maximum length of the 0.1 kPa contour, which is considered the lower limit of reliable normal stress values, is 220 cm under the snow mobile, 170 cm under the standing skier, and about 180 cm for the knee drops.

a.

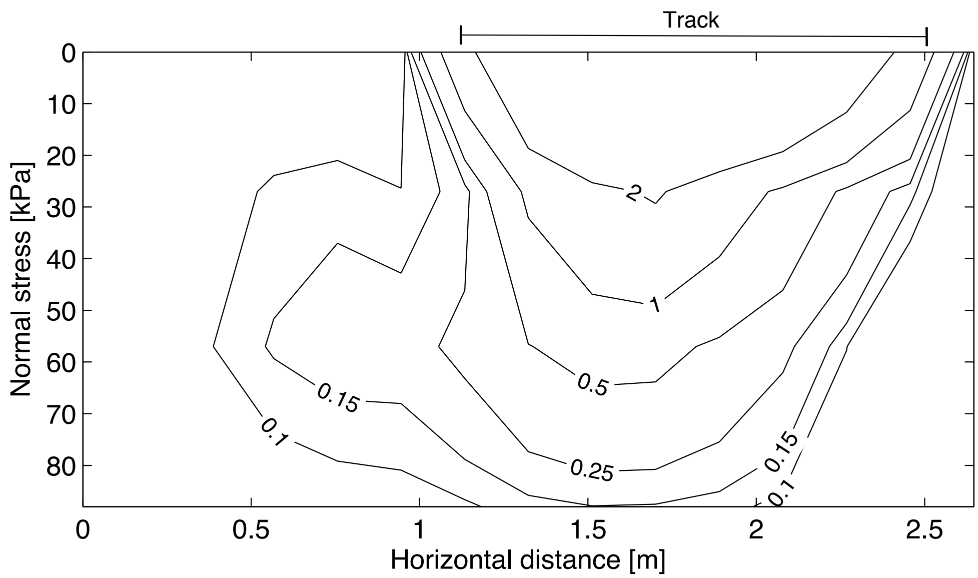

b.

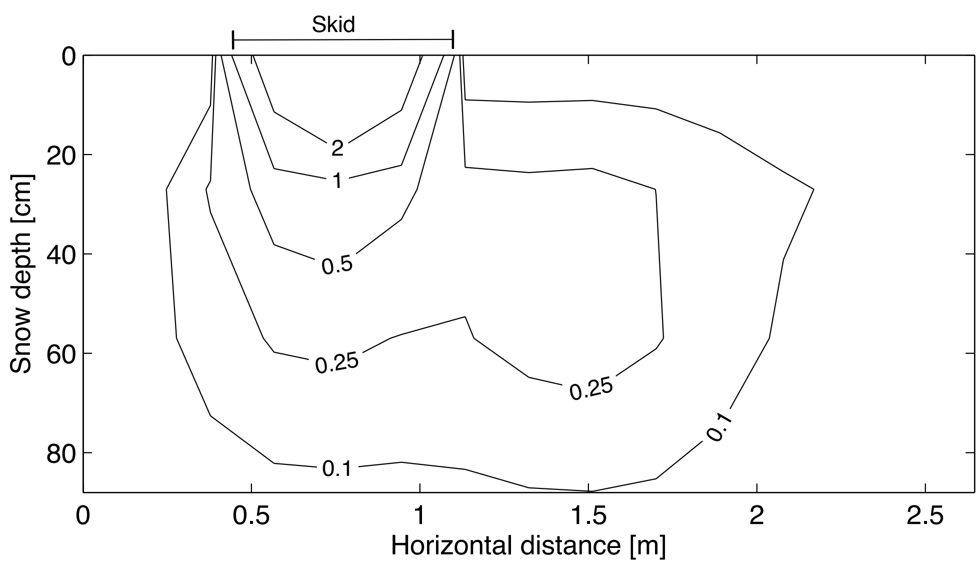

Figure 6.8. Normal stress distribution under the snowmobile: **(a)** along the mid line of the track and **(b)** along a skid. Contours indicate stress values in kPa.

6.3.2.3 Width of stress bulb across snowmobile

Figure 6.11 shows a vertical cross-section across the snowmobile track at the location where the highest stresses were measured. This cross-section was reconstructed from the experiments with the snowmobile passing over the sensors mid-track and with the skid over the sensors. Assuming equal stress distribution

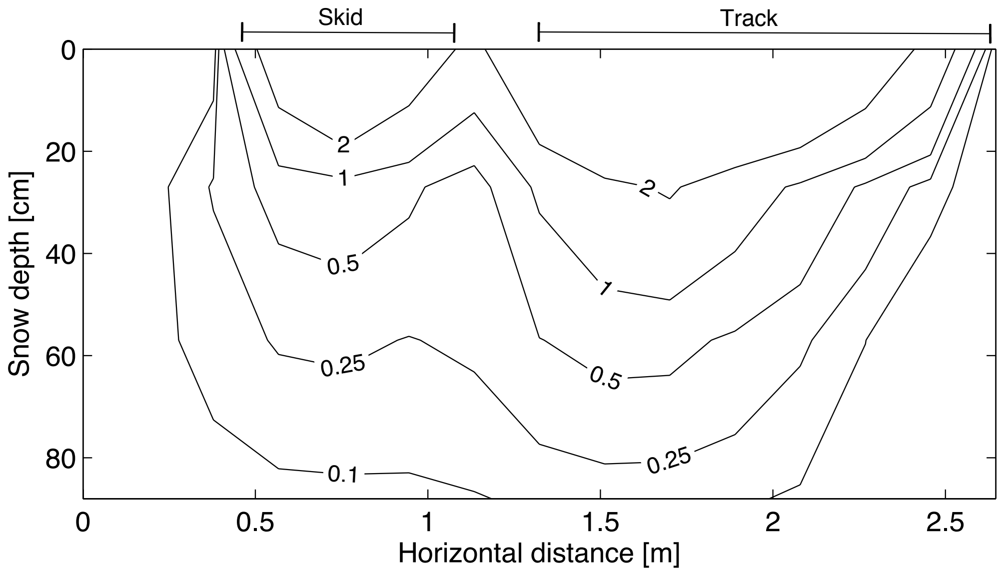

Figure 6.9. The sum of normal stress values of Figure 6.8a and 6.8b combined in one plane. Contours in kPa. Note that the skids and track are off set by approximately 50 cm.

over the surface area of the track and the skids, the surface stress was calculated to 5.6 kPa with the snowmobile specification from Table 6.2.

The width of the stress bulb across the track is about 1 m for the 0.25 kPa contour, which is approximately 5 % of the maximum surface stress (Figure 6.11). The area of influence under the skids is, due to the stance of 1 m, wider than under the track but with substantially lower stress values.

6.3.2.4 Stresses relative to surface loads

The stresses relative to measured surface values are almost identical for the standing skier and a skier performing knee drops (Figure 6.12) indicating the same ratio of stress decrease with depth for both loading cases. Stresses at 30 cm depth reduced to approximately 20 % of the surface values. During the snowmobile drive-over relative stresses were slightly higher compared to the skier loads. Stresses at 30 cm reduced to approximately 35 – 40 %. Stresses under the skier decreased to about 5 % of the surface value at 80 cm depth, whereas the stress under the track of the snowmobile still showed approximately 10 %. The contour lines farther from

a.

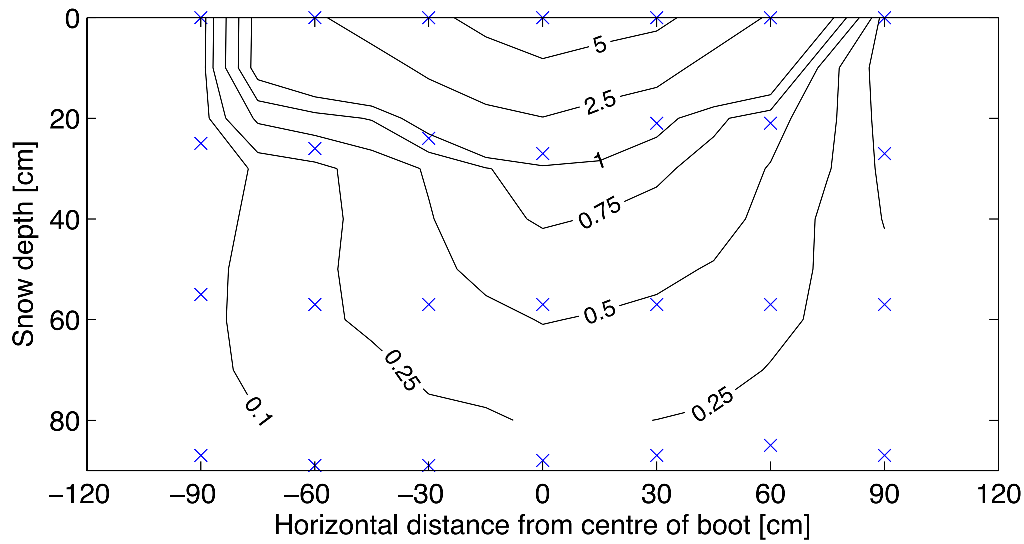

b.

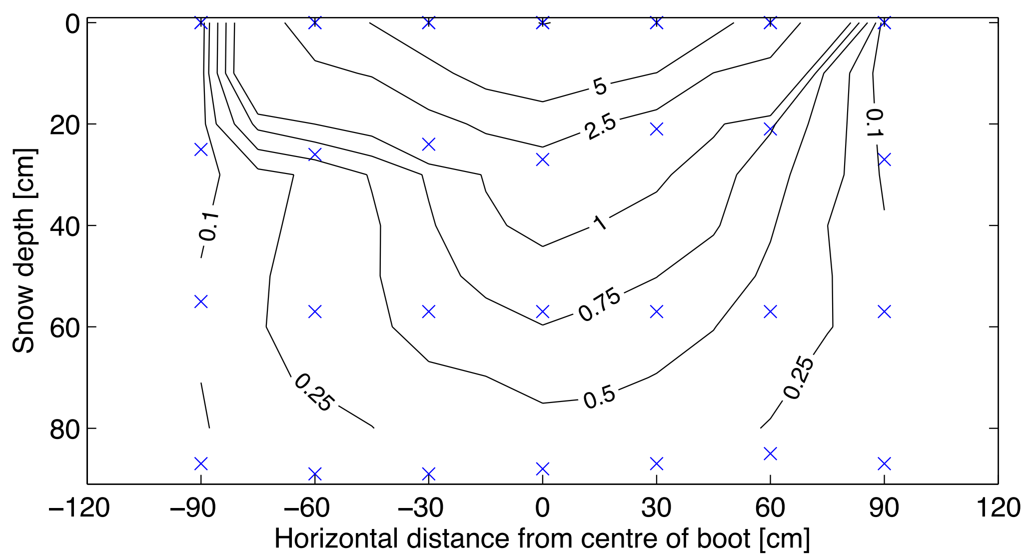

Figure 6.10. Cross sections of normal stress under skis: skier standing on both skis (**a**), and skier performing knee drops (**b**). Contours indicate stress values in kPa. The positions of each stress measurement are indicated by an 'x'.

the centre (0 cm) become less reliable since the measured stresses reach the limit of the accuracy of the stress measurement technique.

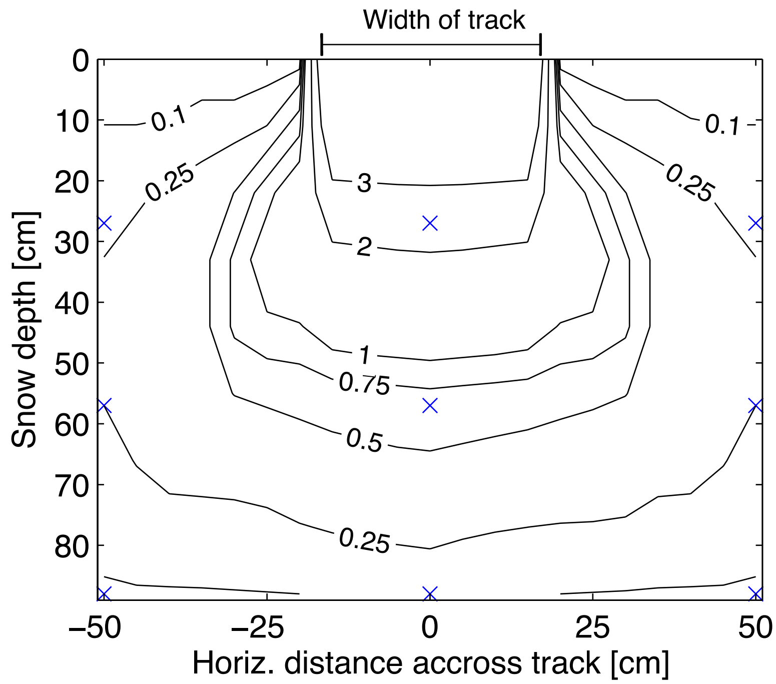

Figure 6.11. Cross-section of normal stresses across snowmobile track according to Plane 3 in Figure 6.3. Surface stresses across the width of the track were estimated to 5.6 kPa. Actual measured data points are indicated by 'x', contours are in kPa.

6.3.2.5 Moving versus standing skier load

In Experiment 2 a skier on both skis was pulled over the study site with constant speed (0.5 m/s). The maximum stress was compared to the stress due to a skier standing over the sensor location for about 15 s. Stresses of the standing skier were about 50 % higher (Table 6.3). The visco-elastic behaviour of snow allows more deformation or stress increase, respectively for loads that are applied over a longer time period.

Table 6.3. Maximum stress at 43 cm depth of a skier standing and pulled on both skis with constant speed (approximately 0.5 m/s) over study site during Experiment 3 for two runs.

Skier load	*Normal stress [kPa]*
Standing skier	0.54 / 0.47
Skier pulled	0.33 / 0.33

a.

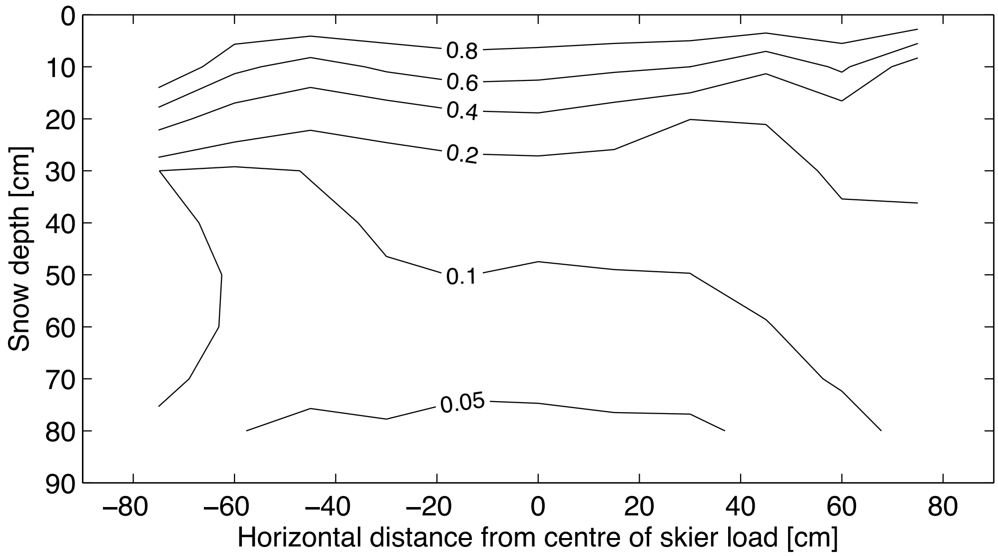

b.

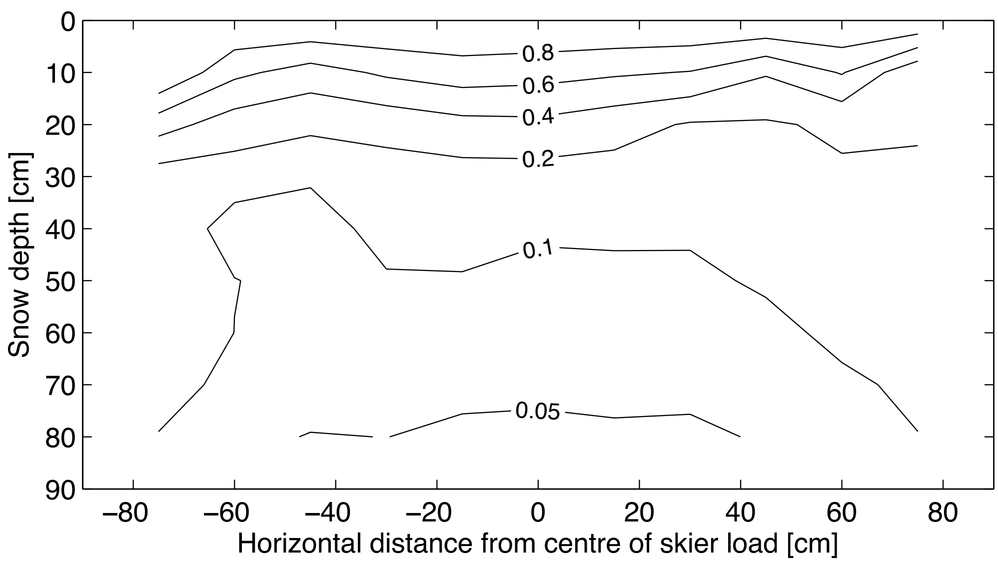

Figure 6.12. Cross sections of normal stress normalized to surface values under skier standing on both skis (**a**), and skier performing knee drops (**b**).

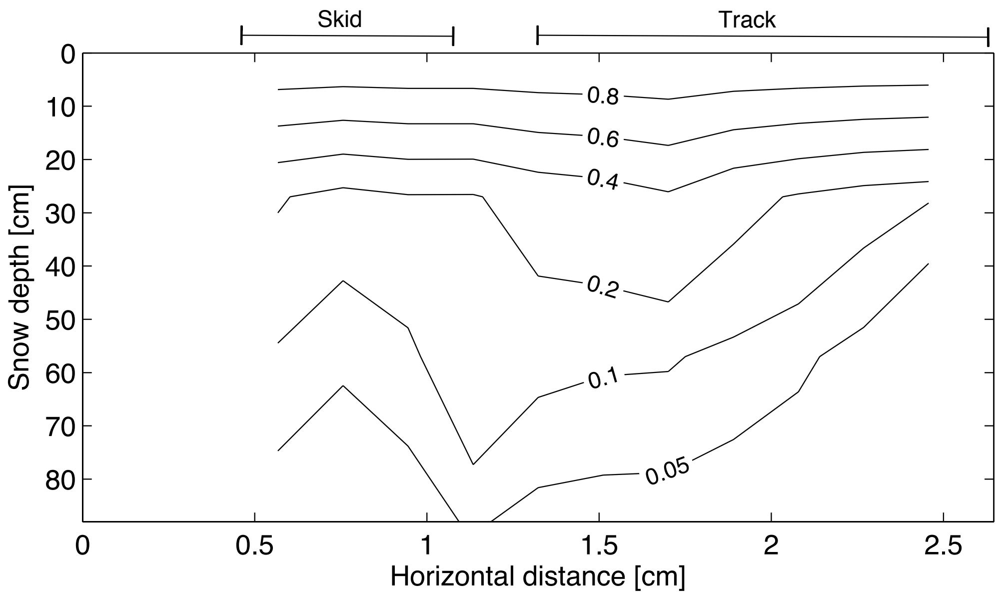

Figure 6.13. Cross section of normal stress normalized to surface stresses below the snowmobile track. No data were available for the blank area on the left.

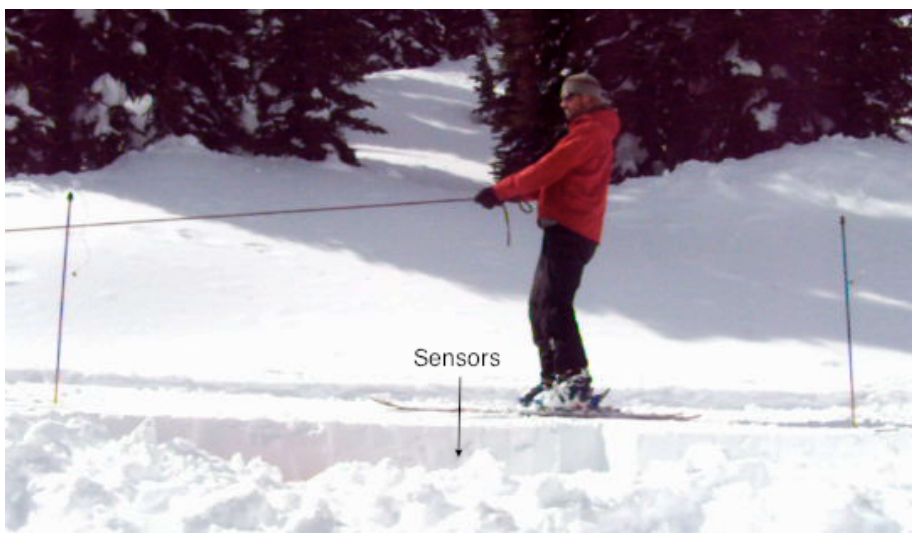

Figure 6.14. Skier pulled with a rope over sensor location.

6.4 Discussion

6.4.1 Depth of stress and deformation penetration

Additional normal stresses and deformation due to snowmobiles penetrate deeper into the snowpack compared to those of skiers. Once a weak layer is buried close to 1 m, the initiation of a fracture by a skier or snowboarder is very unlikely (Schweizer and Lütschg, 2001). Stresses and deformation of a snowmobile may be sufficient to fracture a weak layer up to 1 m depth and beyond (Figures 6.6 and 6.7). In particular the jumping snowmobile seems likely to exert stresses that are sufficient to fracture a weak layer at snow depths where skiers usually do not have any impact. Preliminary results from field studies (Thumlert and Exner, in preparation) showed that the dynamic shear stresses due to snowmobiles are potentially up to five times higher than those of skiers. The shear strength, for example of layers of faceted crystals or buried surface hoar ranges from approximately 1 – 2 kPa after a burial time of about 2 - 3 weeks (Zeidler and Jamieson, 2006a and 2006b). The shear load of the overlying slab on a 38˚ slope is within the same order of magnitude, assuming a slab of approximately 50 – 100 cm with an average density of 200 kg/m^3. The measured additional shear stresses due the jumping snowmobile or skier to a depth of approximately 80 to 90 cm were considerable and might trigger the slab-weak layer combination. The time period after two weeks of burial of a layer is especially critical for triggering by backcountry users since obvious warning signs such as natural avalanche activity tapers off, the ease of triggering decreases, but fracture propagation propensity (avalanche size) increases (Chalmers and Jamieson, 2001).

The normal stresses under the snowmobile decreased less with snow depth compared to those under a skier (Figure 6.12 and 6.13). Even though surface stresses of both, static skier and snowmobile loads are similar with just above 5 kPa, the snowmobile adds the load over a larger surface area causing a more gradual decrease with depth.

6.4.2 Comparison to calculated shear stresses

Based on the measured static normal stresses of a skier and snowmobile, calculated shear stresses for a 38˚ slope yield approximately 0.35 kPa for the skier and 0.6 kPa for the snowmobile. These values are of the same order as calculated static stresses for a linear elastic half space of 0.2 kPa for the skier and 0.5 kPa for the snowmobile (Table 6.4).

Table 6.4. Additional calculated static shear stresses on a 38˚ slope at 50 cm snow depth (After Thumlert and others, 2010)

Surface load	$\Delta\tau$ [kPa]
Snowcat	1.6
Climber	0.9
Snowmobile	0.5
Skier	0.2

6.4.3 How realistic was the snowmobile loading?

The snowmobile drive-over caused stresses and deformation, which are slightly higher than those of a skier performing knee drops. Knee drops are assumed to be comparable to skier down-weighing during a turn (Schweizer and Camponovo, 2001) when many slab avalanches are human-triggered (Harvey and Signorell, 2002). This suggests a smoothly driving snowmobile may be more likely to trigger slab avalanches than a skiers.

The experiment with the jumping snowmobile is most likely closer to the realistic case of a bouncing snowmobile or a track digging deeper into the snowpack when riding with higher speeds on steeper slopes. In particular, during ascending steep slopes the track may dig considerably into the snowpack, which brings the load closer to a potential weakness. Furthermore, during steep ascents it seems plausible that most of the forces are transferred to the snowpack at the back of the track over a smaller surface area. This would concentrate and increase stresses and deformation in the snowpack. According to preliminary results from Thumlert and others (in prep.) the impact of snowmobiles can be up to five times higher than that of a skier with both skiing or riding, respectively over the study site on a slope in undisturbed snow. The dynamic peak stress at a snow depth of approximately 50 cm below the ‘snowmobile jump’ is about three times higher than that of a skier performing knee drops (Figure 6.7). Comparing this to Thumlert and others’ results indicates that the loading step of a ‘snowmobile jump’ may actually underestimate the realistic impact of a snowmobile.

6.4.4 Some speculations on critical crack size

According to calculations for a static skier load (Schweizer and Camponovo, 2001), the maximum width of the stress bulb (10% contour across skis) is approximately 80 cm. The corresponding width of the stress bulb under the snowmobile is slightly wider (Figure 6.11). In addition to higher stress, snowmobiles seem to be more likely to exceed the critical crack length necessary for fracture propagation. A longer stress distribution under snowmobiles might indicate that the critical crack size – as a necessary condition for fracture propagation - is exceeded sooner in comparison to a skier. However, when considering a moving skier or snowmobiler, both can potentially ‘drive the fracture’ lengthwise (Louchet, 2001b), provided there is a sufficiently weak layer. Therefore, the length of the critical crack size may not be the crucial factor distinguishing between the skier and snowmobile slab release process.

6.5 Summary

For the first time, the static and dynamic stress distribution in the snowpack due to a snowmobile was measured in field experiments. This distribution was compared to the stress distribution induced by skier loads on the same study site. Overall, it appeared that snowmobiles stress the snowpack considerably more than other non-motorized backcountry users, such as skiers and snowboarders.

A smoothly driving snowmobile put more stress into the snowpack than a skier performing knee drops, which is likely comparable to turns while skiing. The jumping snowmobile stressed the snowpack the most, with approximately 2 to 4 times more than the skier knee drops. The jumping (comparable to bouncing) snowmobile produced considerable normal stresses (above 0.5 kPa) close to about 1 m depth. The area of impact on the snowpack due to snowmobile loads are is larger compared to skier loads. Snowmobiles may exceed the critical crack size for fracture propagation sooner than that compared to a skier.

CHAPTER 7

Cold lab experiments on the sub-surface normal stress distribution due to surface loads and snow temperature effects

7.1 Introduction

In addition to the outdoor skier and snowmobile stress experiments (Chapter 5 and 6), cold lab experiments were conducted to study the effect of warming and cooling on the sub-surface normal stress distribution due to small static surface loads in a controlled lab environment. During the outdoor skier stress experiments, suitable conditions to study normal stresses and its warming related changes under natural conditions in the field were rare. Meteorological conditions that control the snow surface energy balance such as solar radiation, wind, and clouds cannot be influenced in field studies. The cold lab provided an alternative to conduct a sufficient amount of experiments under controllable temperature conditions in a reasonably timely manner. The main purpose of the cold lab experiments was to learn more about the effect of warming and cooling of the near-surface layers on sub-surface stresses due to static surface loads.

Section 7.2 describes and evaluates the experimental procedure. An overview of the data set and analysis methods is given in Section 7.3. Before the results on temperature effects are presented in Section 7.5, Section 7.4 focuses on results concerning the stress distribution.

7.2 Experimental set up and evaluation

7.2.1 The cold lab

All experiments were conducted during the winter of 2008/09 between January and early April (Table 7.2) in the cold lab at Rogers Pass, BC. Temperature could be adjusted in the range of interest from -25˚C to 0˚C via cooled or heated air that was ventilated into the lab. Warming or cooling related changes in the snowpack most likely take place in this temperature range for the coastal, intermountain and continental snow climates of western Canada (Haegeli and McClung, 2007). Also in other snow covered, populated areas of the world where avalanches are a concern, snowpack temperatures only occasionally drop below -20˚C. The cold lab at Rogers Pass was chosen over other more sophisticated cold labs (for instance at the University of Calgary) due to the proximity to an abundant supply of fresh natural snow.

The radiation balance was basically reduced to a negligible amount of long wave exchange between the snow box and the cold lab walls. Short wave radiation, which is considered the main heat source for rapid warming events (McClung and Schaerer, 2006, p. 39), was negligible in the cold lab. Nevertheless, having control over snowpack temperatures and being able to exclude the transitory influence of clouds and the undesirable cooling effect of turbulent exchange due to winds made up for this shortcoming.

7.2.2 The snow box

For the experiments snow that was taken from a natural snowpack was sieved into a snow box (0.75 x 0.75 x 0.5 m) to ensure uniform snow conditions (Figure 7.1). The snow box was placed into the cold lab at least 24 h before commencement of the experiments to allow the snowpack to adjust to the new temperature conditions. The snow box was built from ½ inch plywood, which thermal properties are similar to snow with a thermal conductivity of 0.13 $W\,m^{-1}K^{-1}$ (Forest Products Laboratory, 1987). Conductivity for snow that was used for the studies with densities between 200 – 350 $kg\,m^{-3}$ ranged from 0.025 – 0.2 $W\,m^{-1}K^{-1}$ (Sturm et al., 1997). The backside of the snow box was removable to access one sidewall of the "snowpack" for push resistance tests and standard snow profiles.

7.2.3 Surface loads

Figure 7.1. Snow box with stem-thermometer inserted on the left, stress transducer plates from the right connected to data logger, and surface load in middle of snow box. Density and push resistance was measured on the open back side.

Cylindrical 1 kg metal weights were placed on a 6 x 6 cm aluminium plate in 1 kg increments in the middle of the snow box (Figure 7.2). The plate was padded with a 0.5 cm thick cellular foam layer to reduce stress concentrations on an uneven snow surface and to keep the snow surface undamaged for following measurements. Depending on snow hardness the surface load was increased up to 4 kg (10.9 kPa). Only surface loads were placed on the snow surface that did not leave any visible imprint on the snowpack to ensure similar snowpack conditions for subsequent loading. Before each experiment the maximal possible load that did not leave any imprint was determined in one of the corners of the snow box, where deformations did not have any influence on the remaining snowpack. Each load was applied for 30 s.

The applied loads (1 – 4 kg or 2.72 – 10.9 kPa) are comparable to a static skier load. Assuming an effective ski length of 1 m (Schweizer and Camponovo, 2001), an average ski width of 0.1 m and a skier weight of approximately 80 kg the expected skier surface stresses calculate to approximately 4 – 8 kPa, depending if

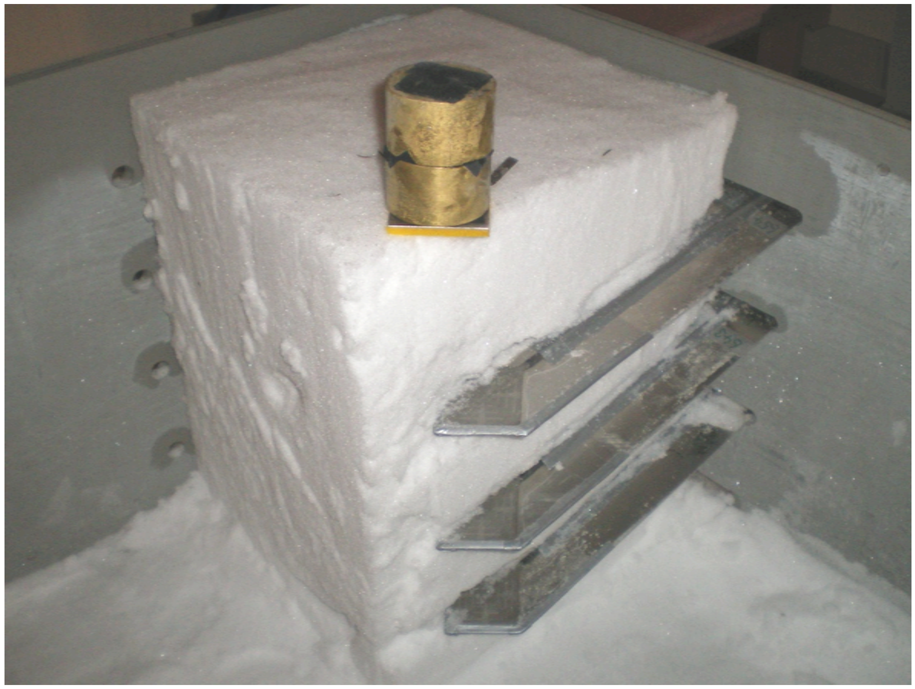

Figure 7.2. Snow box with pressure sensors after excavation after the last round of measurement to determine the actual depth of the stress sensors and thermometer, as both pressure sensors and thermometers obtain measurements near the end of their inserted points.

one or two skis are weighted. However, the resulting stress bulb due to a skier is wider and deeper due to overlapping stresses, which are applied over a much larger surface area.

7.2.4 Normal stress measurements

The stress sensor sheets were inserted into the snow box through slits at the sidewall of the snow box with a 10 cm vertical spacing. The surface stress was calculated from the surface area of the loading plate (6 x 6 cm) and the weight of the cylinders. After the end of each experiment the sensors were dug out and the vertical distance from each sensor to the surface was measured. Sensor output was recorded with a Campbell Scientific CR5000 data logger according to the stress measurement method as described in detail in Chapter 4.

For all experiments vertical normal stress profiles were measured below the centre of the surface load. Additionally for Experiment 7, vertical cross sections

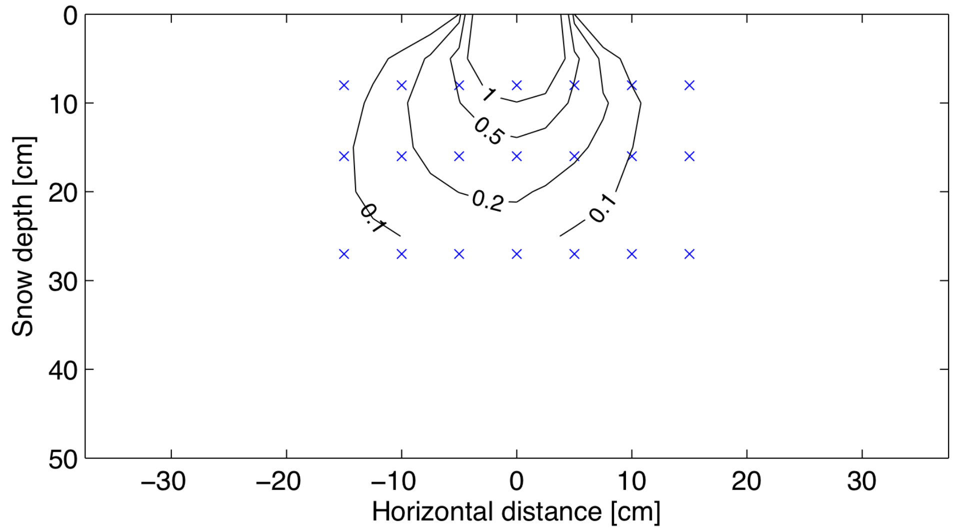

Figure 7.3. Vertical cross section of normal stress over entire snow box below a squared 5.45 kPa (2 kg) surface load. Locations of measured values are indicated by ‘x’. Snow temperature at 10 cm was -6˚C.

were measured by placing the weights in 5 cm increments along a line over the stress sensors, which remained at the same location in the middle of the snow box. The maximum distance from the middle of the snow box was 15 cm in either direction. With these data the 2D cross sections of normal stresses were re-constructed according Section 4.2.

7.2.5 Influence of the snow box walls on pressure distribution

Figure 7.3 shows a cross section of the normal stress distribution over the full dimensions of the snow box due to a 2 kg (5.45 kPa) surface load. The distance of the 0.1 kPa contour from the snow box walls and floor suggests there was little influence on the stress distribution for values greater than 0.1 kPa, which was in the order of the accuracy of the pressure sensors. Accordingly, potential effects of the sidewall and floor were neglected. Higher loads cause a deeper and wider stress bulb and may see more influence of the snow box walls. The results, which are presented in Section 7.4 are based on 2 kg (5.45 kPa) surface loads.

7.2.7 Snow temperature measurement

Handheld Traceable® long-stem thermometers were inserted through holes in the sidewall of the snow box with 10 cm spacing to monitor snow temperatures (Figure 7.1, Table 7.1). The thermometers were positioned as a vertical array close to the surface load. Snow temperatures were recorded manually at every round of measurements after a new snowpack temperature was adjusted. It was aimed for 5˚C intervals when increasing or decreasing air temperature of the cold lab.

Table 7.1. Technical specifications of the Traceable® long-stem thermometers (individually calibrated in 0˚C slush ice).

Range	-50 to 300˚C
Resolution	0.1˚C from -20 to 200˚C
Accuracy	±0.2°C
Stem diameter	3.6 mm
Stem length	28.2 cm

7.2.8 Temperature distribution in snow box

During the experiments the snow box was kept at the cold lab floor ensuring that the major heat exchange took place at the snow surface at the open top of the snow box similar to energy exchange processes of a natural snowpack.

Temperature gradients during warming and cooling experiments were comparable to a natural snowpack (Figure 7.4). The horizontal temperature distribution across the snow box appeared to be fairly uniform (Figure 7.5). This proves that the majority of the energy exchange during cooling and warming actually took place at the snow surface.

7.2.9 Snow hardness measurements

Snow hardness was determined with standard hand hardness tests (see Section 4.1) at the beginning and end of each experiment. The hand hardness test as an intrusive and destructive measurement would have consumed too much space of the snow box if done for each time step. Additionally, after each temperature adjustment vertical profiles of push gauge resistance were determined as

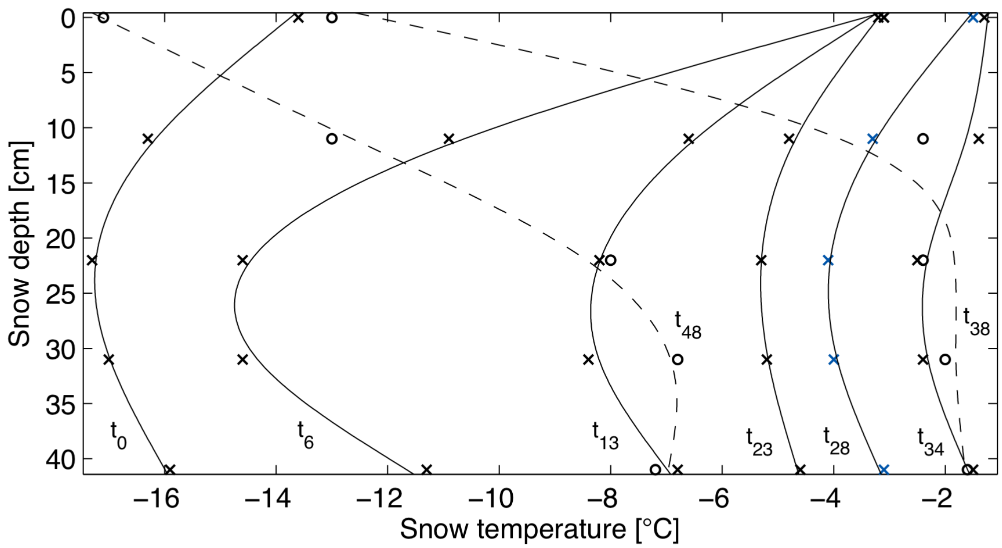

Figure 7.4. Vertical temperature profiles during Experiment 3, which responded to warming (solid lines) and cooling (dashed lines) similar to a natural snowpack; surface temperatures lead the way, lower layers lag behind. t denotes time, in hours, into the experiment.

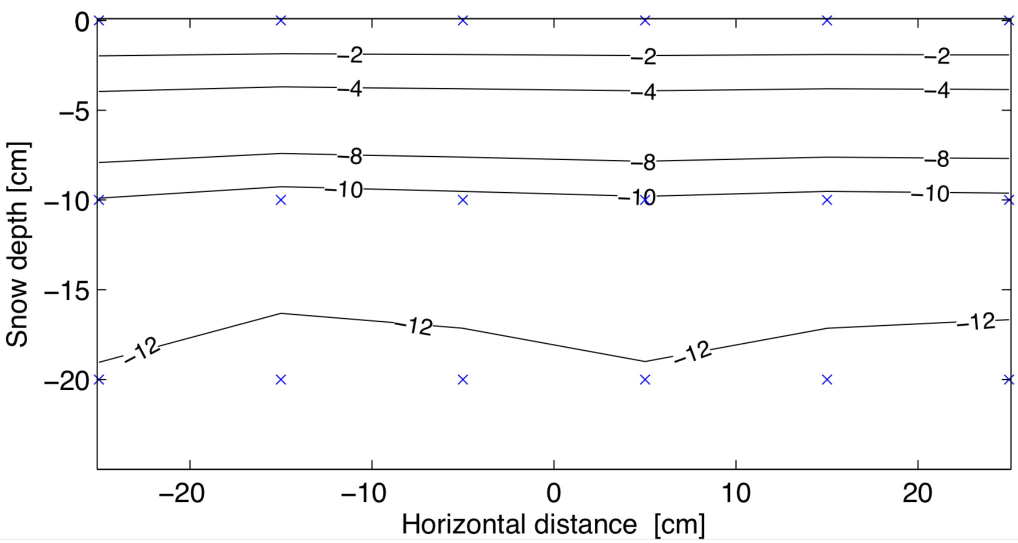

Figure 7.5. Vertical cross section of snow temperature distribution across the middle of the snow box during Experiment 7. Contours in ˚C, location of measured values indicated by ‘x’.

described in Section 4.1.

7.2.10 Experimental procedure

The snow box was filled with natural snow by sieving. After placing the snow box in the cold lab the desired temperatures were set. After the snowpack temperature, between approximately 10 and 20 cm snow depth, was adjusted to the new value the following set of measurements was conducted:

- Normal stress profile (data logger)
- Snow temperature profile (manual)
- Penetration resistance profile (with push gauge, see Section 3.2)
- Surface conditions (moisture content, crusts; according to ICSSG)
- Snowpack height
- Air temperature (approximately in centre of cold lab)

At the beginning and end of each experiment a standard snow profile was recorded (Section 4.1). After each experiment the pressure and temperature sensors were removed and actual depth of the sensor tips below the snow surface was measured.

7.2.11 Comparison of measured to calculated stresses

The cross sections from Experiment 7 (Figure 7.6 a and b) show the characteristic bulb shape of the normal stress distribution. The 0.2 kPa contour line (5% of the surface value) is approximately double the width of the surface load at about 10 - 15 cm below the surface. The stress bulb is approximately 10 – 15 % deeper than wide for all shown contour lines for the given snow hardness of approximately 4F – 1F. Figure 7.6c demonstrates the Boussinesq stress distribution in an elastic, homogeneous, semi-infinite medium due to a vertical point load of 2 kg or 19.6 N, which was calculated according to adapted equations from Das (2008, p. 113):

$$\sigma = \frac{3Q\, z^3}{2\pi\ (z^2 + x^2)^{5/2}} \tag{7.1}$$

with: Q: point load (19.6 N in this case)

z: vertical distance below snow surface [m]

x: horizontal distance [m]

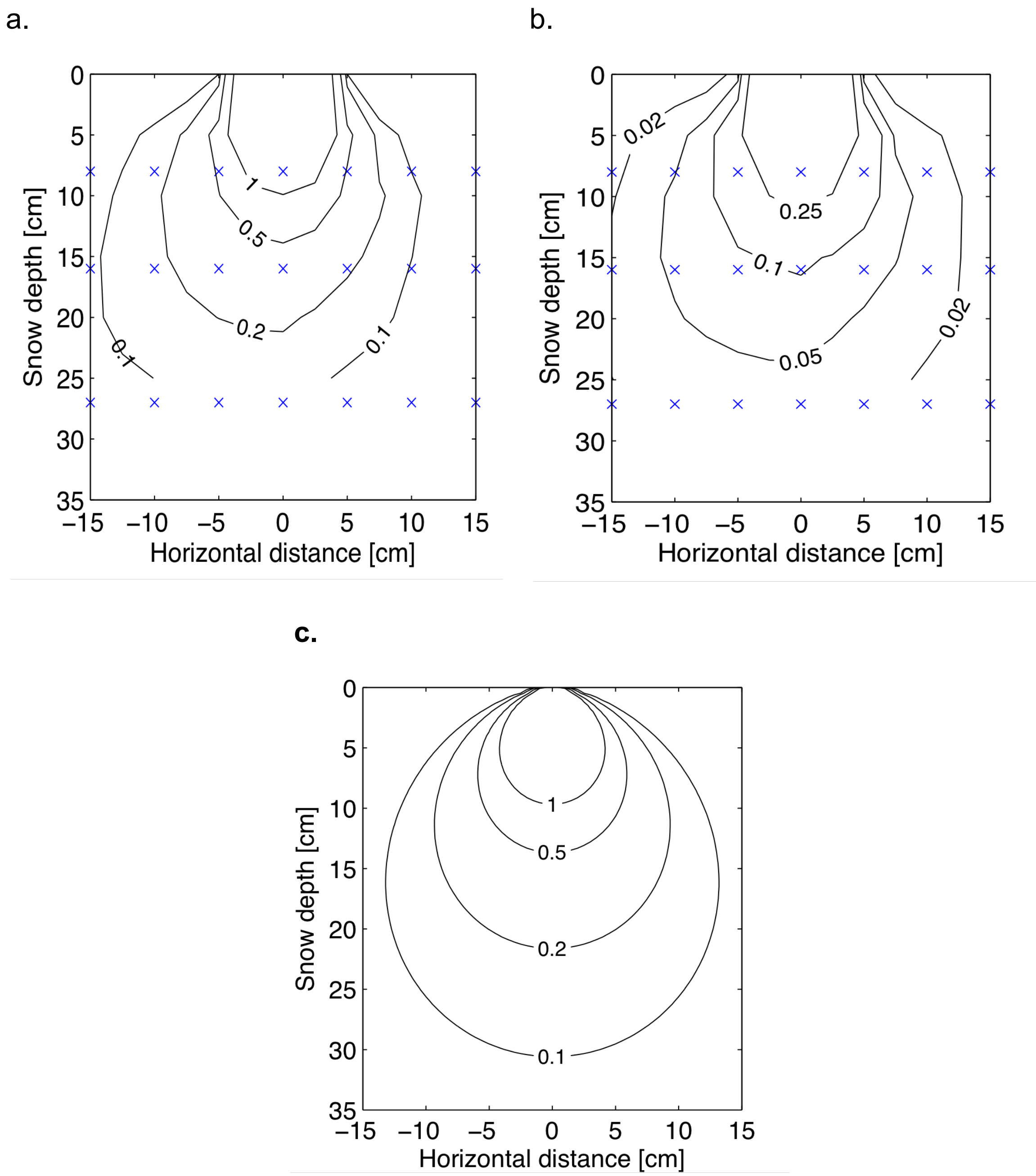

Figure 7.6. Vertical cross sections of normal stresses below a 5.45 kPa (2 kg) surface load of an individual set of measurements from Experiment 5. **(a)** Measured values in kPa; **(b)** normalized values to surface load; location of measured values denoted by 'x'; **(c)** analytical Boussinesq solution for a vertical point load (19.6 N, 2 kg) over a semi-infinite elastic homogeneous medium.

The analytical solution is in fairly good agreement with the measured stresses. The largest differences can be seen in the near surface layers due to the difference in loading – point load versus squared distributed load. Below, in deeper layers, the width and depth of the contour lines are comparable. However, the analytical solution yields slightly higher stresses with increasing depth for the given snow hardness.

7.3 Overview of experiments and analysis

7.3.1 The data set

In total seven experiments were conducted. All experiments started with the coldest snow temperature followed by warming. Cooling followed the initial warming period in three experiments with again subsequent warming in two cases (Table 7.2). The duration of the experiments ranged between 14 and 72 h. The warming periods lasted between 4 h and 21 h, and the cooling events between 7 h and 25 h. Snow hand hardness (see Section 4.1) in Experiments 1 – 4 averaged pencil hardness, whereas average snow hardness in Experiments 5 – 7 was a full step softer (1F hand hardness). During the warming periods snow density and hand hardness increased due to settlement but was always within one full hand hardness step. Due to the sieving process, the initial snowpack in all experiments consisted of a mix of broken and rounded snow particles with densities ranging from 220 – 370 $kg\,m^{-3}$.

All seven experiments were divided in single warming and cooling periods. After an initial and largely inconclusive analysis, longer warming or cooling periods were split up in separate events according to changes of temperature conditions. Additionally, to detect explainable trends it was necessary to group events by the change in normal stress. Figure 7.7 provides an example how Experiment 5 was broken down.

In total, 16 warming and six cooling periods were available for analysis. The initial warming in Experiment 1 (1_1 in Table 7.4) was excluded due to an unreasonable decrease of the stress signal probably caused by insufficient time to allow the snow box to adjust to the new temperature conditions in the cold lab. Also the final cooling in Experiment 7 was excluded (7_4), since an ice layer covered

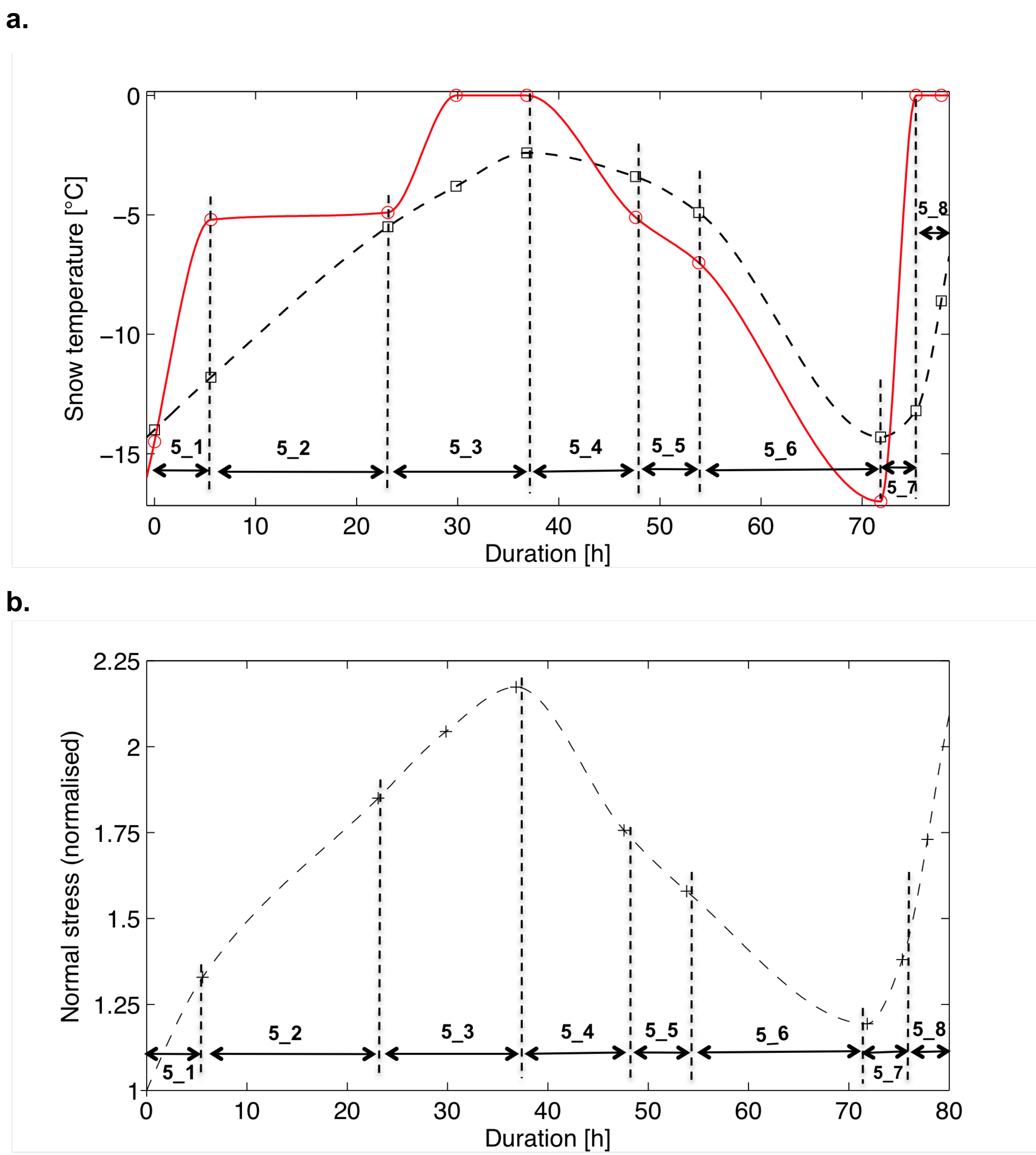

Figure 7.7. Division of Experiment 5 in warming and cooling events. The initial warming period was divided in events 5_1, 5_2 and 5_3, the following cooling in 5_4, 5_5 and 5_6, and the final warming in 5_7 and 5_8. **(a)** Snow temperatures at snow surface (solid red line) and 12 cm snow depth (dashed black line). **(b)** Normal stress at 13 cm snow depth normalized (relative) to initial stress value at beginning of experiment. See Table 7.4 for conditions of the single events.

the pressure sensors after excavation.

In total, three categories of temperature-pressure-change events were analysed:

- Warming with pressure (normal stress) increase (11 cases)
- Warming with pressure decrease (four cases)
- Cooling with pressure decrease (five cases).

Table 7.2. Overview of snowpack conditions of all cold lab experiments.

Exp. #	*Temperature change (W: warming, C: cooling)*	*Max. load [kg]*	*Duration [hrs]*	*Avg. density ρ_s [kg/m^3]*	*Grain type*[1]	*Grain size [mm]*	*Avg. Hardness (top 25 cm)*
1	W	2	14	235	DFbk/RG	0.25	P
2	W	3	14	220	DFbk/RG	0.25 – 0.5	1F/P
3	W/C	3	48	310	DFbk/RG	0.25 – 0.75	P
4	W	4	6.5	370	DFbk/RG	0.25 – 0.75	P
5	W/C/W	4	78	240	DFbk/RG	0.25 – 0.5	1F
6	W	2.5	21	210	DFbk/RG	0.25 – 0.75	1F/P
7	W/C/W	3	48	200	DFbk/RG	0.25 – 0.75	4F/1F

[1] According to Fierz and others (2009): DFbk: Decomposed, broken; RG: rounded grains

7.3.2 Analysis

The normal stress changes relative to the initial values of each warming or cooling at 10 cm depth ($\Delta\sigma_{REL}$) for all three categories were correlated to temperature and snow conditions, referred to as predictor variables (see Table 7.3 for variable definitions) that may have contributed to the stress variations. Due to the low sample sizes the majority of the analysis is based on graphical interpretation of plots of the predictor variables against $\Delta\sigma_{REL.}$ Additionally, the warming cases that showed stress increase were tested for monotonic relationships (Spearman rank correlation).

7.3.2.1 Seeking monotonic trends by splitting predictors at a threshold in cases with stress increase due to warming

The trends and correlations for all 11 cases together of the *warming-stress increase* category do not account for the complex interaction of the predictor variables that affect the stress change. For instance, various temperature ranges, snow hardness, surface conditions, and duration can have a substantial impact on the relationship of the predictor variables with stress changes. After checking for monotonic trends in the complete data set with all 11 cases each predictor variable was divided in two subsets by a threshold value (see Table 7.3) that was selected according to the following criteria:

- Physical relevance: For instance, below approximately -10˚C snow temperature, metamorphic snowpack processes are very slow (McClung and Schaerer, 2006, p. 65); stiffer (harder or denser) near surface layers reduce the depth penetration of surface loads (Schweizer, 1993). Above approximately -7˚C snow temperature mechanical properties (e.g. fracture toughness) of snow appear to change their behaviour (Schweizer and others, 2004; Schweizer and Camponovo, 2002).
- Based on graphical (visual) assessment of the plots to find a reasonable split that two monotonic trends can be assessed within each subset with sufficient sample size of each subset to indicate graphical trends.

Both subsets of each predictor variable were checked for correlation with $\Delta\sigma_{REL}$ again. Further, each variable was split by each of the other variables at the threshold defined in Table 7.3 and each subset was tested for a relation against $\Delta\sigma_{REL}$. For example, T_{max10} was correlated with $\Delta\sigma_{REL}$ for T_{max10} ≥ -7˚C and < -7˚C. Next, T_{max10} was checked for correlation with $\Delta\sigma_{REL}$ for events with T_{min10} < -10˚C and ≥ -10˚C, and so on. This procedure resulted in 121 (11 x 11) predictor–variable–$\Delta\sigma_{REL}$ plots with two sub-sets each, for each of which Spearman rank correlation coefficients were calculated to check for monotonic trends. Additionally, the plots were checked graphically for trends. Those plots that indicated a potential trend are presented in Section 7.4.2. Plots that are not presented were excluded due to:

- Collinearities: For instance the improved correlations in Figure 7.8 cannot be attributed to a direct physical relation to $\Delta\sigma_{REL}$ since high snow temperature differences during warming usually imply low initial snow temperatures and vice versa.

Table 7.3. Definitions of potential predictor variables for relative normal stress change during warming/cooling at 10 cm snow depth and threshold values that were used to divide each variable in two groups for *warming events with stress increase* (see Section 7.4).

	Definition	*Threshold*
Response variable		
$\Delta\sigma_{REL}$	$\Delta\sigma_{REL} = (\sigma_{10}(t)/\sigma_{10}(t{=}0) - 1) \times 100\%$ Change of the normal stress due to (static) surface loads at 10 cm during warming or cooling relative to the stress at beginning of the warming or cooling [%]	
Predictor Variables		
T_{max10}	Max snow temperature (beginning of cooling or end of warming) at 10 cm snow depth [˚C]	-7˚C
T_{min10}	Min. snow temperature (beginning of warming or end of cooling) at 10 cm snow depth [˚C]	-10˚C
T_{max_surf}	Max snow temperature (beginning of cooling or end of warming) at snow surface [˚C]	0˚C (moist/dry)
T_{min_surf}	Min snow temperature (beginning of warming or end of cooling) at snow surface [˚C]	-10˚C
ΔT_{10}	Snow temperature increase/decrease during warming/cooling at 10 cm snow depth [˚C]	4˚C [2]
ΔT_{surf}	Snow temperature increase/decrease during warming/cooling at snow surface [˚C]	10˚C [2]
$\Delta T_{10}/\Delta t$	Warming/cooling rate at 10 cm snow depth [˚C/h]	0.5˚C/h [2]
$\Delta T_{surf}/\Delta t$	Warming/cooling rate at snow surface [˚C/h]	0.5˚C/h [2]
ΔHS	Settlement during warming/cooling [mm]	5 mm
$\Delta HS/\Delta t$	Settling rate [mm/h]	0.5 mm/h
t	Duration of temperature event [h]	10 h
Hand hardness[1]	Hand hardness (only used for sub-dividing of other variables)	1F / P

[1] after ICSSG (Fierz and others, 2009);
[2] According to average values for daytime warming of the near-surface layers these values were chosen to divide the data set.

Table 7.4. Overview of conditions and results of all cold lab experiments split up in single warming (**W**) and cooling (**C**) events. See Table 7.3 for variable descriptions.

Exp #	***W/C***	$\Delta\sigma_{REL}$ ***[%]***	$\Delta T_{sfc}/\Delta t$ *[°C/h]*	$\Delta T_{10}/\Delta t$ *[°C/h]*	*t [h]*	Temp. *range [°C]* *Surf.*	*10 cm*	*ΔHS [mm]*	*Surface Conditions* [1]	*Push resistance change [%]*
1_2	**W**	**+100**	4	2	2	-5/0	-14/-10	n/a	m	n/a
2	**W**	**+100**	2	1.5	14	-25/0	-25/-10	n/a	d	n/a
3_2	**W**	**+10**	0.1	0.25	15	-3/-1.5	-7/-4	11	d	-40
4	**W**	**+30**	2	1	6.5	-14/0	-14/-9	3	m	n/a
5_1	**W**	**+25**	1.5	1	6	-14/-5	-14/-8.5	1	d	n/a
5_2	**W**	**+30**	0.03	0.2	17	-5/-4.5	-8.5/-5	5	d	-25
5_3	**W**	**+15**	0.3	0.3	13	-4.5/0	-5/-1.5	15	m	+20
5_7	**W**	**+15**	5.5	1	3	-17/0	-15/-12	1	m	n/a
5_8	**W**	**+20**	0	1.5	3	0/0	-12/-7	5	m	n/a
6	**W**	**+50**	0.3	0.2	21	-9/-4	-10/-7	13	d	-5
7_1	**W**	**+30**	1	0.4	11	-13/0	-12/-8	1	m	0
(1_1)	**W**	**-30**	4	2	4	-18/-5	-18/-14	n/a	d	n/a
1_3	**W**	**-75**	0	3	4	0/0	-10/-4	10	m/w	n/a
3_1	**W**	**-25**	1	0.5	13	-14/-3	-16/-7	7	d	n/a
3_3	**W**	**-5**	0.25	0.5	6	-1.5/-1.5	-4/-1.5	9	m	+15
7_3	**W**	**-10**	0.5	0.4	12	-5/0	-6/-1.5	2	m (all)	0
3_4	**C**	**-30**	-1	-0.75	14	-1.5/-17	-1.5/-13	1	mfc 2-3cm	+30
5-4	**C**	**-20**	-0.3	-0.2	17	0/-5.1	-1.5/-4	0	mfc 2-3mm	+20
5_5	**C**	**-10**	-0.3	-0.3	7	-5.1/-7	-4/-6	0	mfc 2-3mm	-5
5_6	**C**	**-25**	-0.6	-0.5	18	-7/-17	-6/-15	0	mfc 2-3mm	+10
7_2	**C**	**-10**	-0.2	0.1	25	0/-5	-8/-6	7	mfc	0
(7_4)	**C**	**+10**	-0.5	-0.5	19	0/-10	-1.5/-10	8	mfc	n/a

[1] m – moist, d – dry, w – wet, mfc – melt freeze crust; after ICSSG (Fierz and others, 2009)

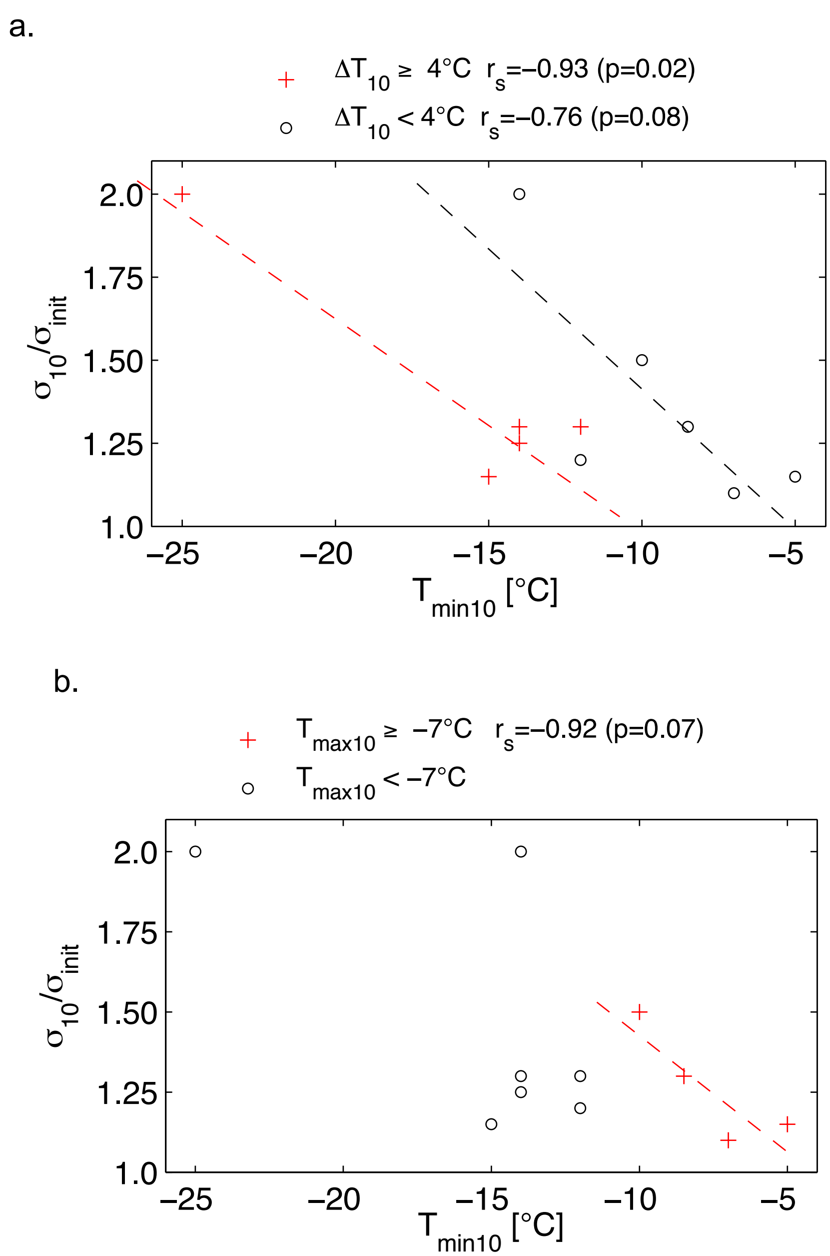

Figure 7.8. Example of artificially improved correlations due to experimental procedure **(a)**, and correlation of predictor variable with $\Delta\sigma_{REL}$ that was excluded from analysis due to collinearity **(b)**. (p-values in brackets)

- Very weak or no graphical trend and/or no statistical significance of Spearman's coefficient ($p > 0.1$). Artificially produced correlations and trends due to the experimental procedure: The improved correlations in Figure 7.8b for example are not directly related to $\Delta\sigma_{REL.}$ Snow temperature was increased in small increments (5˚C). Therefore, lower start temperatures usually coincide with lower end temperatures and vice versa.

7.4 Results

7.4.1 Effects of snow hardness and temperature on pressure distribution

Figure 7.9a displays normal stress values due to a vertical 2 kg (5.45 kPa) square surface load from 37 stress profiles from all seven experiments. The measured normal stresses were normalized with surface stresses. Normal stress decreased non-linearly with snow depth as indicated by a power law fit (solid line). However, a large scatter was observed, which can be explained by varying stiffness, temperature and snow characteristics. Stresses below 20 cm snow depth were reduced to less than 5% of the surface values. The same data set was grouped by average snow hardness in Figure 7.9b. In Experiments 1 – 4 the average snow hand hardness was P (red circles) and 1F in Experiments 5 – 7 (black 'x'). Apparently, snow hardness had a substantial influence on stress decrease with depth. Stresses in softer snow decreased more gradually with depth compared to harder snow. Stresses in the softer (1F) snowpack appeared to be approximately double compared to the pencil-hard snowpack. The power law fits for each hardness group showed accordingly lower scatter compared to the undivided data set (Table 7.5).

Table 7.5. Power law fits of the form $\sigma/\sigma_o = a\,z^b + c$ for all normal stresses normalized to surface values and for stresses grouped by hardness.

	Power law coefficients			*Goodness of fit*[1]	
	a	*b*	*c*	R^2	*SE*
All (Fig. 7.9a)	0.590	-0.174	-0.315	0.994	0.033
1F (Fig. 7.9b)	2.044	-0.571	-1.659	0.996	0.029
P (Fig. 7.9b)	0.314	-0.275	-0.117	0.999	0.014

[1] R^2: Coefficient of determination; SE: Standard deviation

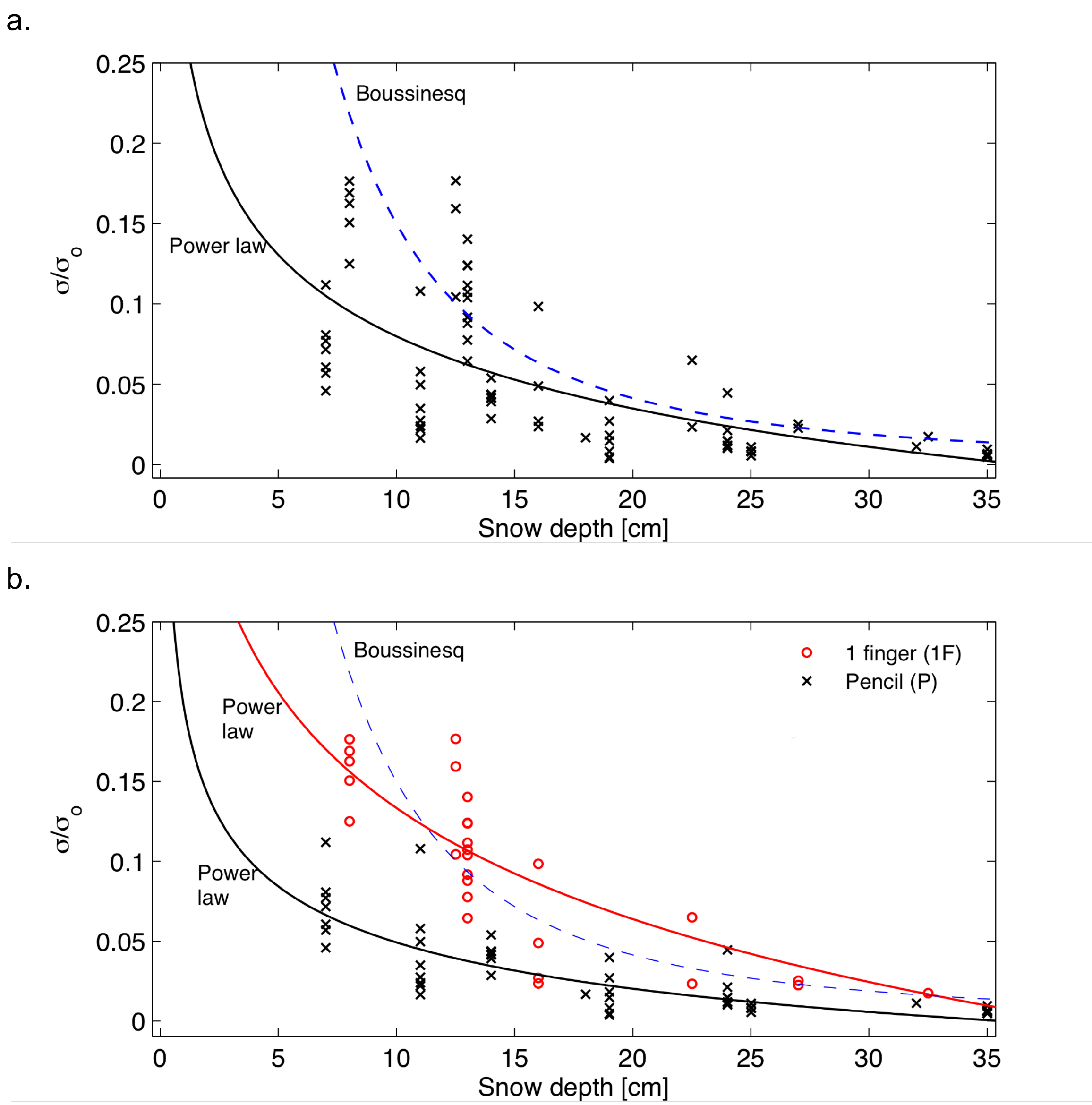

Figure 7.9. Normal stress values (directly below surface load) from 37 stress profiles (all seven experiments), normalized to the 2 kg (5.45 kPa) surface load **(a);** grouped by snow hardness **(b)**. T_{10} ranged from -25 to -1.5˚C. Solid lines are power law fits, the dashed blue line is the analytical Boussinesq solution for a distributed circular load. For better readability the vertical axis is cut off at 0.25.

The blue dashed lines in Figure 7.9 indicate Boussinesq's (1883) solution for normal stresses below the centre of a circular surface load for an elastic homogeneous material. The radius (3.38 cm^2) of the circular load was chosen to match the surface area (36 cm^2) of the square aluminium loading plate. The

Boussinesq stresses were calculated according to Equation 7.2 (Das, 2008, p. 117):

$$\sigma = \sigma_o \left(1 - \frac{z^3}{(b^2 + z^2)^{3/2}}\right) \tag{7.2}$$

with σ_o: uniform surface load per unit area (5.45 kPa in this case)

z: vertical distance below snow surface [m]

b: radius of equivalent circular load [m]

Measured stress values in the softer (1F hardness) snowpack are closer to the Boussinesq solution than are stresses for the harder snow.

Normal stresses at 10 cm snow depth normalized with surface values (σ/σ_o) from 37 profiles from all seven experiments were plotted against snow temperature at 10 cm (T_{10}) and at the snow surface (T_{surf}) (Figure 7.10). Stresses were again separated by snow hardness in two groups similar to Figure 7.8. The hardness difference of approximately one step (1F to P) clearly splits the stress values again in two groups. For the pencil-hard layers, almost all normal stresses remained under 6 % of the surface value. For the 1F-hard snow, values ranged between approximately 6 and 18 %. Overall, the stresses measured at 10 cm snow depth showed less noise (lower standard deviation of fit curves and higher coefficient of determination, Table 7.6).

Stresses in the harder (stiffer) snow stresses slightly increased with warmer temperatures at 10 cm (Figure 7.10b), which is indicated by a linear trend line. The snow surface temperature in the harder snow did not show an obvious trend.

In softer snow, normal stress increased with warmer T_{10} faster than in the pencil-hard snowpack as long as T_{10} remained below approximately -6 to -8˚C. Above this stress peak, decreasing stresses were observed with T_{10} approaching the melting point.

7.4.2 Influences of warming on normal stress

This section presents changes of the normal stress due to surface loads during

a.

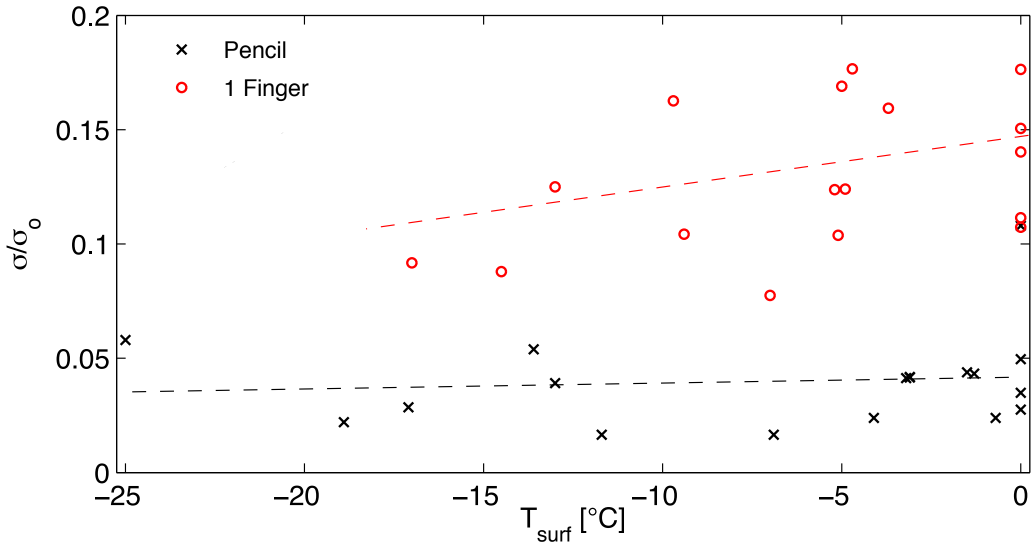

b.

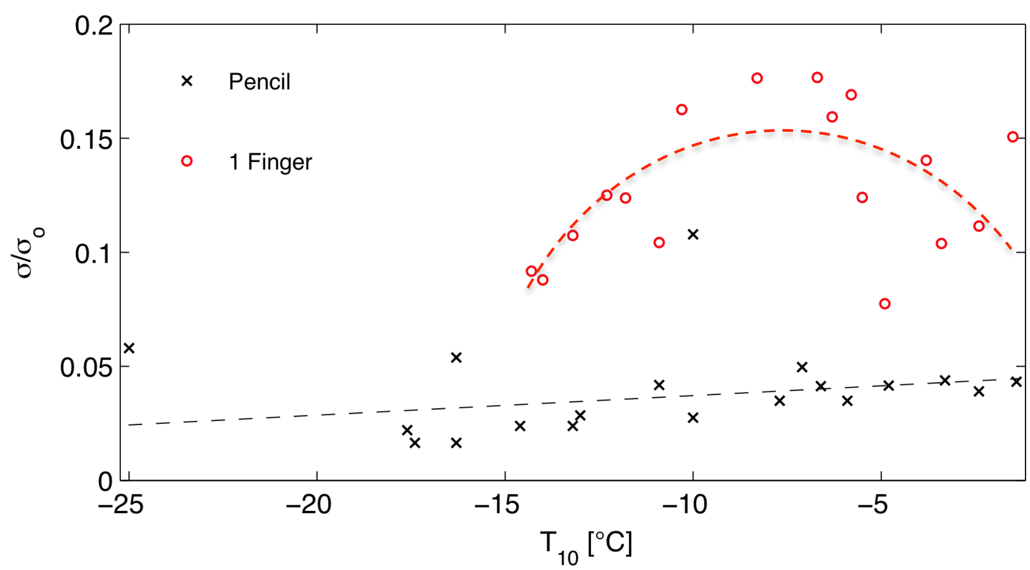

Figure 7.10. Normal stresses at 10 cm snow depth normalized to surface stresses σ_o plotted against snow surface temperatures T_{surf} **(a)** and 10 cm snow temperature T_{10} (**b)** for experiments with pencil hard snow (black x) and one finger hard snow (red circles) with trend lines (dashed).

snowpack warming. Section 7.4.2.1: cases where stress increased with warming; Section 7.4.2.2: warming periods where normal stress decreased.

Table 7.6. Coefficient of determination (R^2) and standard deviation (SE) for fit curves in Figure 7.10. (all linear fits, except the dashed line in 7.10b is a quadratic fit)

	T_{surf} (Fig. 7.10a)		T_{10} (Fig. 7.10a)	
	R^2	SE	R^2	SE
SSL	0.18	0.03	0.34	0.011
HSL	0.013	0.021	0.36	0.0094

The *direct-immediate* and *indirect-delayed* effects of warming to which is referred to in the following sections are defined in Section 2.2.4

7.4.2.1 Normal stress ($\Delta\sigma_{REL}$) increase due to warming

Results of Spearman rank correlation coefficients for predictor variables with increasing $\Delta\sigma_{REL}$ are shown in Table 7.7 and 7.8 for all 11 warming events. The variables are sorted by ascending significance or descending correlations coefficients, respectively.

For the following analysis, two categories were defined that describe the normal stress increase (positive $\Delta\sigma_{REL}$) during warming:

1. The normal stress increase (positive $\Delta\sigma_{REL}$) showed a positive trend ($r_s > 0$; greater stress increase) with increase of the specific predictor variable. In the following this is referred to as *'increase of positive $\Delta\sigma_{REL}$'*
2. The normal stress increase (positive $\Delta\sigma_{REL}$) showed a negative trend ($r_s < 0$; lower stress increase) with increase of the specific predictor variable. In the following this is referred to as *'decrease of positive $\Delta\sigma_{REL}$'*

Variables with the highest correlation coefficients (lowest p-values) were measured or calculated for 10 cm snow depth. The three top ranked variables (T_{min10}, ΔT_{10}, $\Delta T_{10}/\Delta t$) indicated that the positive $\Delta\sigma_{REL}$:

- was reduced (decrease of positive $\Delta\sigma_{REL}$) with warmer initial snowpack temperature (T_{min10})
- increased with larger snow temperature differences and stronger warming rates (increase of positive $\Delta\sigma_{REL}$).

Table 7.7. Spearman correlation (r_s) matrix of all predictor variables during warming where stress increased (n = 11). p-values in brackets.

	$\Delta\sigma_{REL}$	$\Delta T_{surf}/\Delta t$	$\Delta T_{10}/\Delta t$	t	ΔT_{surf}	ΔT_{10}	T_{min_surf}	T_{min10}	T_{max_surf}	T_{max10}	ΔHS/Δt	ΔHS
$\Delta\sigma_{REL2}$	1 (0)											
$\Delta T_{surf}/\Delta t$	0.37 (0.37)	1 (0)										
$\Delta T_{10}/\Delta t$	0.57 (0.14)	0.52 (0.10)	1 (0)									
t	0.17 (0.68)	-0.32 (0.33)	-0.58 (0.06)	1 (0)								
ΔT_{surf}	0.45 (0.26)	0.79 (0.01)	0.34 (0.30)	-0.01 (0.96)	1 (0)							
ΔT_{10}	0.63 (0.09)	0.73 (0.01)	0.51 (0.10)	-0.04 (0.88)	0.82 (0.01)	1 (0)						
T_{min_surf}	-0.42 (0.30)	-0.69 (0.02)	-0.23 (0.48)	-0.01 (0.97)	-0.94 (0.01)	-0.88 (0.01)	1 (0)					
T_{min10}	-0.65 (0.08)	-0.75 (0.01)	-0.73 (0.01)	0.4 (0.21)	-0.77 (0.01)	-0.87 (0.01)	0.78 (0.01)	1 (0)				
T_{max_surf}	0.36 (0.37)	0.33 (0.31)	0.58 (0.06)	-0.19 (0.57)	0.33 (0.31)	0.1 (0.76)	-0.7 (0.81)	-0.31 (0.33)	1 (0)			
T_{max10}	-0.33 (0.43)	-0.84 (0.01)	-0.69 (0.01)	0.46 (0.14)	-0.77 (0.01)	-0.80 (0.01)	0.75 (0.01)	0.96 (0.00)	-0.36 (0.27)	1 (0)		
ΔHS/Δt	-0.13 (0.74)	0.12 (0.71)	0.63 (0.03)	-0.33 (0.31)	0.23 (0.49)	0.15 (0.65)	-0.13 (0.69)	-0.49 (0.12)	0.70 (0.2)	-0.46 (0.15)	1 (0)	
ΔHS	-0.10 (0.79)	-0.42 (0.19)	-0.12 (0.71)	-0.24 (0.47)	-0.26 (0.43)	-0.30 (0.37)	0.19 (0.57)	0.18 (0.59)	0.07 (0.82)	0.19 (0.57)	-0.01 (0.99)	1 (0)

The variables ranked four to six are basically the corresponding properties on the snow surface (ΔT_{surf}, T_{min_surf}, $\Delta T_{surf}/\Delta t$) and indicate the same effect on $\Delta\sigma_{REL}$ but are statically non-significant ($p > 0.1$). Only T_{min10} and ΔT_{10} were statistically significant if values of $p < 0.1$ are accepted.

Table 7.8. Spearman rank correlation coefficients (r_s) and p-values for $\Delta\sigma_{REL}$ during warming periods where stress increased (n = 11).

Variable	r_s	*p*	*Figure #*
T_{min10}	-0.65	0.08	7.11a
ΔT_{10}	0.63	0.09	7.11b
$\Delta T_{10}/\Delta t$	0.57	0.14	7.12b
ΔT_{surf}	0.45	0.26	--
T_{min_surf}	-0.42	0.30	--
$\Delta T_{surf}/\Delta t$	0.37	0.37	--
T_{max_surf}	0.36	0.37	--
T_{max10}	-0.33	0.43	7.11c
t	0.17	0.68	--
$\Delta HS/\Delta t$	-0.13	0.74	--
ΔHS	-0.10	0.79	7.12a

Seeking monotonic trends in subsets that showed stress increase during warming:

The splitting of the predictor variables resulted in some cases in considerable improvement of the correlation coefficients and statistical significance (Table 7.9). In addition, this subdivision revealed some trends between the predictor variables and $\Delta\sigma_{REL}$ that were not apparent in the undivided data set. As in the undivided data set, variables measured or calculated for 10 cm snow depth were most indicative for variations of $\Delta\sigma_{REL}$.

Below, results of the subdivided data sets are presented, which were grouped according to their significance level.

Variables from subsets with $p < 0.05$:

T_{min10}

Figure 7.11a suggests that the colder the snowpack at the beginning of the warming, the more likely the stress increase. In those warming periods that lasted longer than 10 h, T_{min10} showed the strongest (inverse) correlation with positive $\Delta\sigma_{REL}$.

ΔT_{10}

Splitting ΔT_{10} at a threshold of 4˚C showed for both subsets of ΔT_{10} stronger correlations with a positive $\Delta\sigma_{REL}$. (Figure 7.11b). Basically, the larger ΔT_{10}, the higher the increase of positive $\Delta\sigma_{REL}$. The steeper slope of the subset with ΔT_{10} < 4˚C may indicate a faster increase of the positive $\Delta\sigma_{REL}$ before *indirect-delayed* effects cause a slower increase for ΔT_{10} > 4˚C.

T_{max10}

The positive $\Delta\sigma_{REL}$ decreased with warmer snowpack temperatures at the end of the warming. This effect was more apparent when the snowpack at 10 cm

Table 7.9. Spearman rank correlations (r_s) of potential predictor variables with $\Delta\sigma_{REL}$ of subsets. In brackets the range of the variable by which the subset was divided.

Subset		*r_s*	*p*	*n*	*Figure #*
T_{min10}	(t > 10 h)	-0.98	0.007	5	7.11a
ΔT_{10}	(ΔT_{10} > 4˚C)	0.97	0.01	5	7.11b
T_{max10}	(ΔHS > 5 mm)	0.90	0.01	6	7.11c
T_{max10}	(ΔT_{10} < 4˚C)	0.83	0.04	6	7.11d
ΔT_{10}	(ΔT_{10} < 4˚C)	0.83	0.04	6	7.11b
ΔHS	(t < 10 h)	0.88	0.05	5	7.12a
$\Delta T_{10}/\Delta t$	(Pencil hardness)	0.93	0.07	4	7.12b
T_{max10}	(t > 10 h)	0.87	0.07	5	7.12c
$\Delta T_{10}/\Delta t$	(T_{max10} < -7˚C)	0.68	0.10	7	7.13a
ΔHS	(ΔHS/Δt < 5 mm/h)	-0.89	0.11	4	7.13b
T_{min10}	(T_{min10} < -10˚C)	-0.64	0.11	7	7.13c
T_{min10}	(T_{min10} > -10˚C)	0.86	0.13	4	7.13c
t	(ΔT_{10} < 4˚C)	-0.61	0.18	6	7.13d
T_{min10}	(Pencil hardness)	-0.75	0.25	4	7.13e

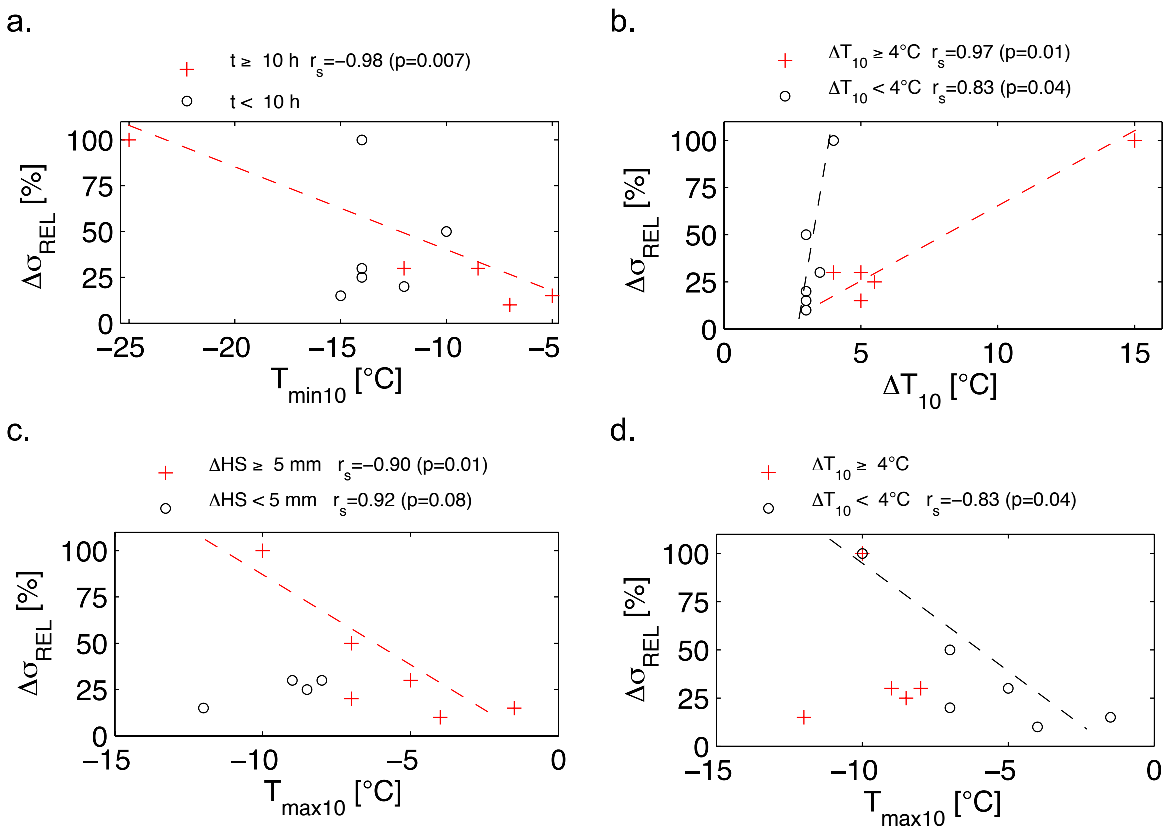

Figure 7.11. Selected subdivided predictor variables that showed significant correlations ($p<0.05$) during warming when normal stress increased. The variables and thresholds by which the data set was split are shown above the plot. The dotted lines indicate linear fits for each subset with $p<0.05$. Spearman coefficients (r_s) and p-values (in brackets) were added for each subset.

warmed up more than 4˚C (Figure 7.11d) and when settlement (ΔHS) of greater than 5 mm occurred (Figure 7.11c).

Variables from subsets with $0.05 \le p \le 0.1$*:*

$\Delta T_{10}/\Delta t$

The harder snow (pencil hardness) showed increasing positive $\Delta\sigma_{REL}$ with higher values of $\Delta T_{10}/\Delta t$ (Figure 7.12b). A weak decreasing trend of the positive $\Delta\sigma_{REL}$ in the softer snow (one finger hardness) even with rising warming rates suggests that softer snow is more susceptible to *indirect-delayed* effects.

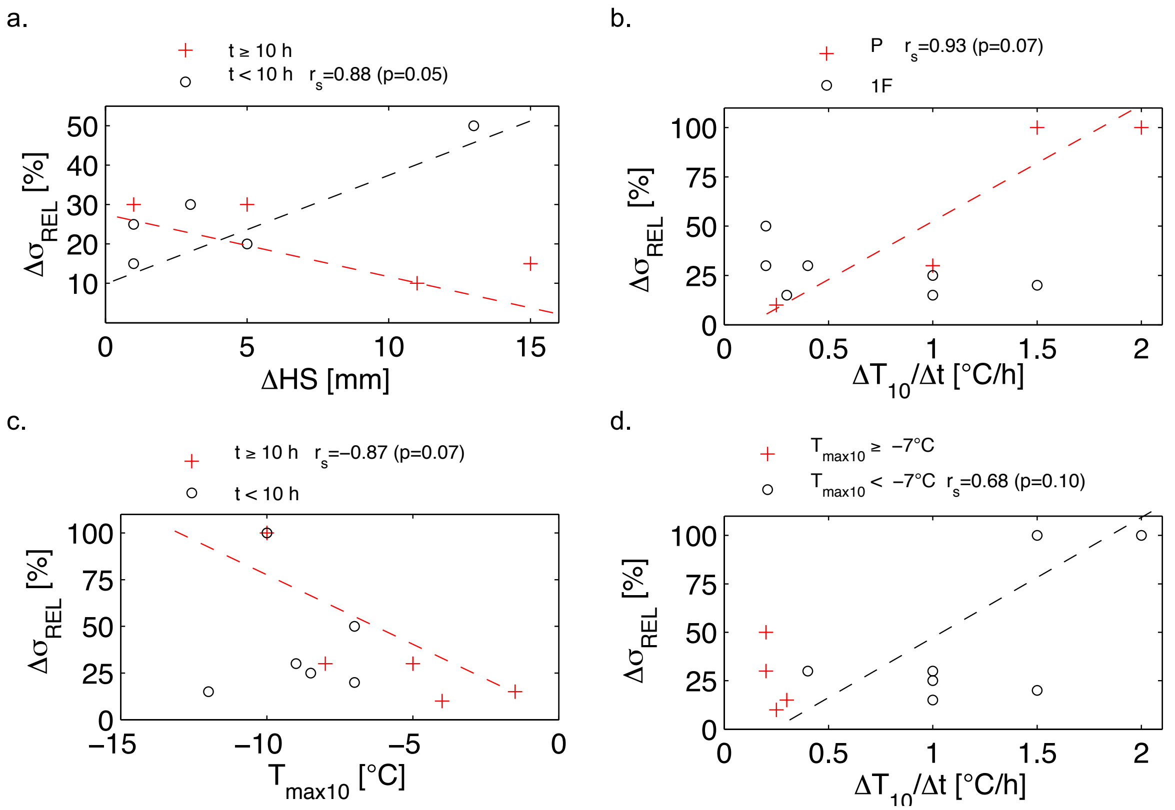

Figure 7.12. Selected subdivided predictor variables that showed significant correlations ($0.05<p<0.1$) for normal stress increase during warming. The variables and thresholds by which the data set was split are shown above the plot. The dotted lines indicate linear fits for each subset with $0.05 \le p \le 0.1$. Spearman's (r_s) coefficient and p-values (in brackets) were added for each subset.

$\Delta T_{10}/\Delta t > 0.5$˚C/h yielded improved correlation coefficients with the increase of positive $\Delta\sigma_{REL}$ as long as maximum snow temperatures (T_{max10}) stayed below -7˚C (Figure 7.12d). For smaller $\Delta T_{10}/\Delta t$ and warmer T_{max10} the positive $\Delta\sigma_{REL}$ tended to decrease; *indirect-delayed* effects seemed to gain importance.

ΔHS

Splitting settlement by longer (>10 h) and shorter (<10 h) durations improved the correlations with the increase of positive $\Delta\sigma_{10}$ (Figure 7.13b). For durations > 10 h the positive $\Delta\sigma_{REL}$ decreased with settlement. Both, settlement and prolonged warming worked against *direct-immediate* effects on stiffness. For t < 10 h the positive $\Delta\sigma_{REL}$ increased although ongoing settlement; *direct-immediate* effects on stiffness appear to override strengthening due to settlement (Figure 12a).

T_{max10}

For longer durations (t > 10 h, Figure 7.12c) of the warming the positive $\Delta\sigma_{REL}$ yielded a decreasing trend with increasing T_{max10}.

7.4.2.2 Normal stress decrease due to warming

During four out of the 15 warming events $\Delta\sigma_{REL}$ decreased by as much as 75%. The conditions and characteristics of the predictor variables for the observed stress decrease during warming are listed below (Figure 7.13):

- Relatively warm end temperatures (T_{max10}> -7˚C) (Fig. 13a)
- Relatively warm initial snow temperatures (>-10˚C in three cases) (Fig. 13b)
- Warming to moist surface (T_{max_surf} = 0˚C) (Fig. 13c)
- Large temperature increase (> 4˚C at 10 cm) (Fig. 13d)
- Relatively high warming rates (> 0.5˚C/h at 10 cm) (Fig. 13e)
- Relatively strong settlement (7 – 20 mm) compared to max. HS of 50 cm (Fig. 13f)
- High settling rates (5 – 25 mm/h) (Fig. 13g)
- Relatively short duration (Fig. 13h)

One case (Experiment 3_1 in Table 7.4; the data points with $\Delta\sigma_{REL}$=-25% in Figure 7.13) indicated more characteristics of the *warming–stress–increase* category with lower initial and end temperatures, and high temperature increase and warming rate. The decrease of stress may be explained by stiffening due to settlement and densification over a fairly long duration (13 h). In this case *indirect-delayed* effects may have overridden the direct softening effect of temperature on stiffness.

7.4.2.3 Summary of warming effects on $\Delta\sigma_{REL}$

Basically, three groups were identified that describe the normal stress change during warming due to surface loads:

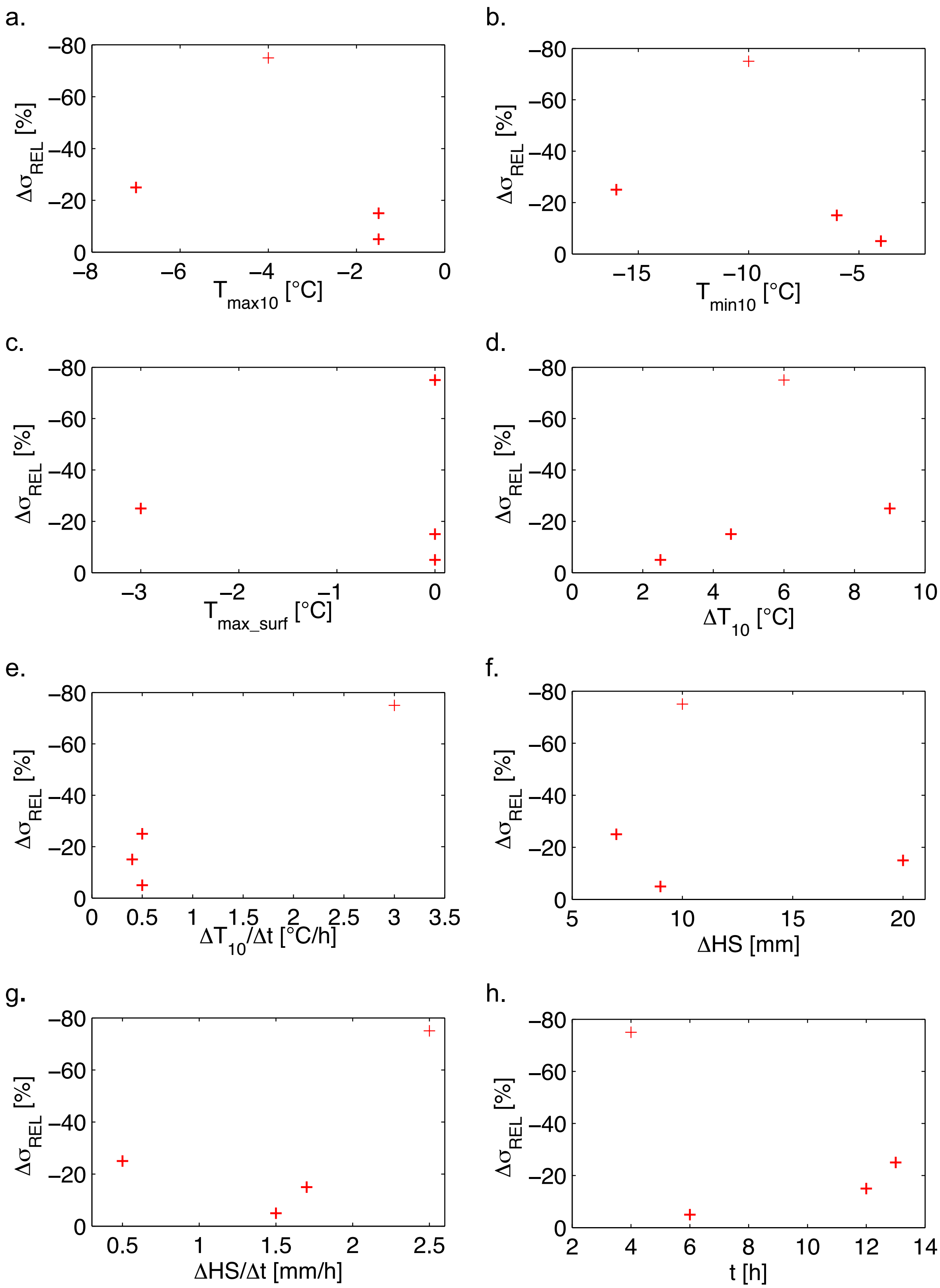

Figure 7.13. Decrease of $\Delta\sigma_{REL}$ during warming (relative to initial value) for various predictor variables. See Table 7.3 for definition of $\Delta\sigma_{REL}$.

Group I *Increase of positive* $\Delta\sigma_{REL}$ *during warming and increasing predictor variable.*

A large snow temperature difference during warming at a high warming rate appeared to have the strongest effect on stress increase for harder snowpack layers. Additionally, low starting and end snow temperatures and shorter durations tend to contribute to this effect on stress.

Group II *Decrease of positive* $\Delta\sigma_{REL}$ *during warming and increasing predictor variable.*

For longer warming durations (> 10 h) and softer snow at warmer initial and end temperatures the positive $\Delta\sigma_{REL}$ appeared to decrease during warming.

Group III *Decrease of normal stress (negative* $\Delta\sigma_{REL}$*) during warming and increasing predictor variable.*

Warming of an already relatively warm snowpack (above approximately -10˚C) by a large temperature increase at high warming rates to a moist snow surface, accompanied by strong settlement and densification may cause decreasing normal stress.

7.4.4 The effect of cooling on $\Delta\sigma_{REL}$

In all five cooling events, $\Delta\sigma_{REL}$ decreased up to 30%. The conditions and characteristics of the predictor variables for the observed stress reduction are listed below:

- Relatively warm initial snow temperature > -7˚C (Fig. 14f and h); (the two cases in Fig. 14h with a moist snow surface ($T_{maxsurf}$ = 0˚C) indicate that a crust formed after cooling)
- Cooling rate up to 0.7 ˚C/h (Fig. 14c)
- No or low settlement and low settling rate (Fig. 14d and e)

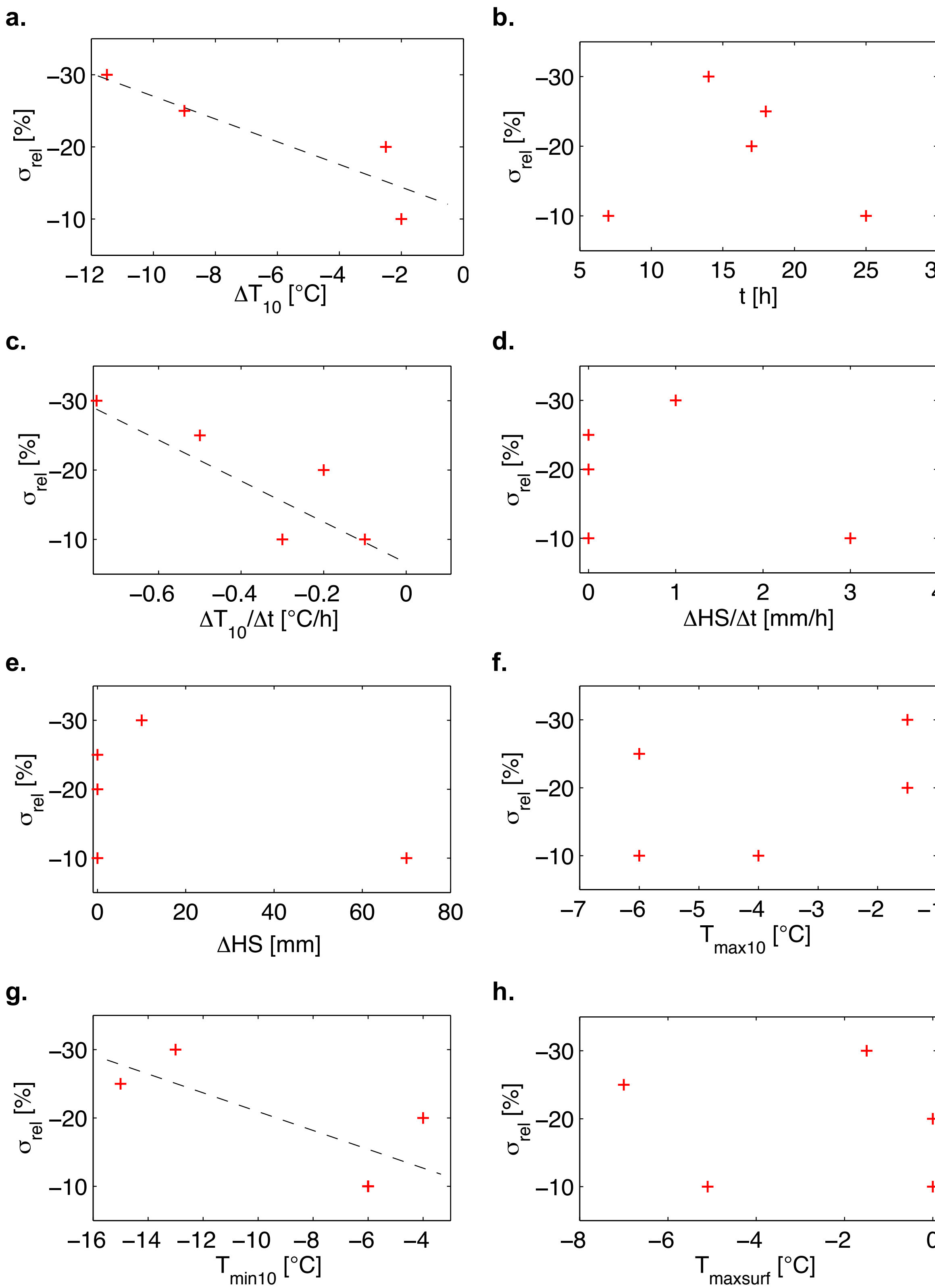

Figure 7.14. Plots of the decrease of $\Delta\sigma_{REL}$ against the predictor variables during cooling. The dashed lines indicate a visual trend that remains if any of the data points is removed. Note, the dashed lines do not indicate statistical significance.

- Snow temperature decrease up to 12˚C and colder end temperatures (a and Fig. 14g)

The trends and pattern that caused stress decrease during cooling can be qualitatively summarized as:

In general, during cooling normal stresses due to surface loads decreased. Larger snow temperature differences and cooling rates, and colder end temperatures caused stresses to decrease by 30%.

7.4.5 Influence of snow temperature on push resistance

The change in push resistance (see Section 4.1) during warming or cooling is plotted against $\Delta\sigma_{REL}$ in Figure 7.15. In most warming cases where stresses increased, push resistance change as an indicator for stiffness change decreased. The one case that showed higher push resistance (stiffness) but yet increased stresses implies that push resistance, in this case is, not necessarily an adequate measure for stiffness when near surface temperatures reach the freezing point, and strong densification comes into play.

In most cooling cases stress decreased and push resistance increased. The only case that exhibited reduced push resistance during cooling can be attributed to a formation of a melt freeze crust on the snow surface responsible for the drop in normal stress. The still reduced stiffness in the near surface layers below the crust may be due to freezing of moist snow without forming stronger bonds during cooling. Less stress during warming and increased push resistance indicates that strengthening due to settlement and densification increased stiffness and therefore reduced normal stresses. Generally, normal stresses increased (up to 50 %) within the same order of magnitude (in terms of percentage change) as push resistance (stiffness) decreased (up to 40 %) and vice versa

7.4.6 Case study: Experiment 5

Experiment 5 was chosen for this case study as an example where normal stresses directly responded to temperature changes of the near-surface layers.

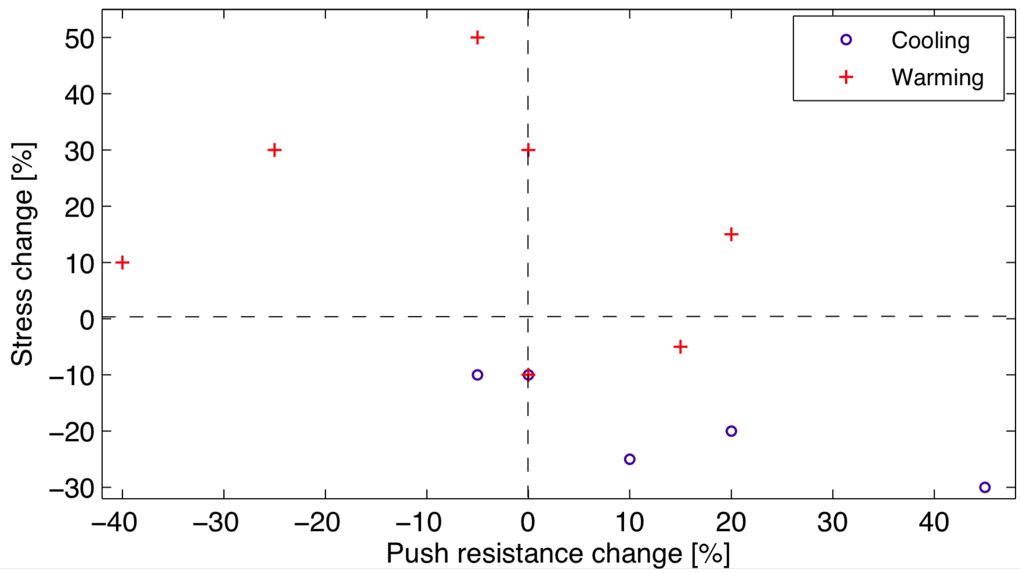

Figure 7.15. $\Delta\sigma_{REL}$ during warming and cooling plotted against push resistance change (relative to initial values before temperature change).

Additionally, this experiment included a second warming phase after cooling that followed the initial warming.

Normal stresses (Figure 7.7b) during the course of Experiment 5 seemed to almost perfectly follow and reacted immediately to snow temperature (Figure 7.7a). Stresses increased with warming, decreased with cooling and again rose with warming almost back to initial values. Snow temperatures reached maximal (minimal) values at the same time when normal stresses reach maximum (minimum) values. Normal stresses followed the snow temperature of the near surface layers (at 13 cm) closer than the snow surface temperature.

7.4.7 Vertical cross sections of normal stress

This section provides an example of the contrary effects of snowpack warming on sub-surface pressure due to surface loads. Figure 7.16 shows vertical cross sections of normal stresses for two warming periods from Experiment 7 between 11 h and 36 h (Exp 7_2), and 36 h and 47.5 h (Exp 7_3) into the experiment. Snow temperature at 10 cm snow depth (T_{10}) rose from -8.0˚C (11 h) to -1.5˚C (47.5 h). T_{10} after 36h was -6˚C. The 0.02, 0.0.5 and 0.1 contour lines indicate a slight

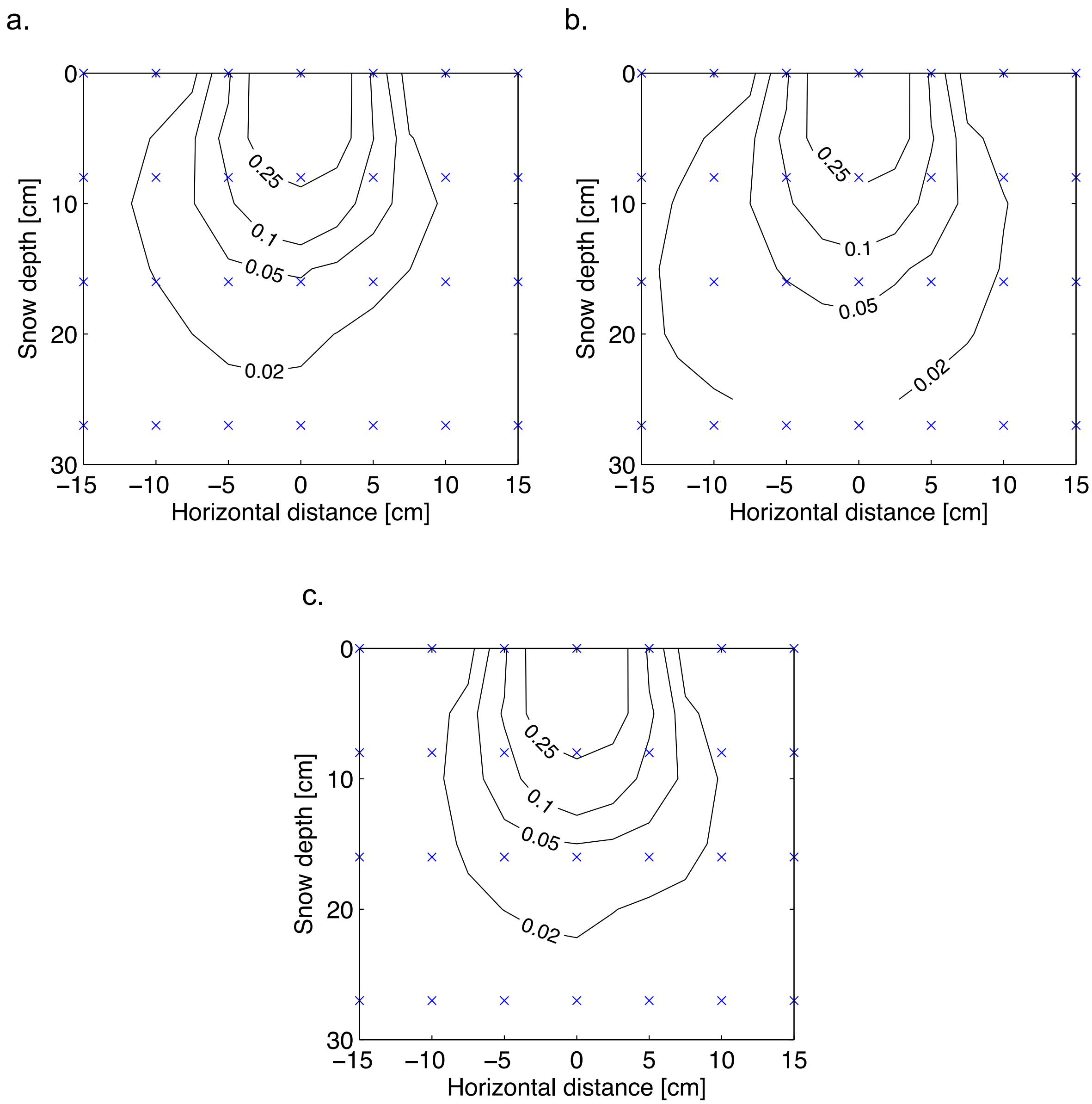

Figure 7.16. Vertical cross-sections of normal stresses (normalised to surface value, 5.45 kPa, 2 kg) from Experiment 7 for **(a**) 11 h, **(b)** 36 h and **(c)** 47.5 h into the experiment.

deepening of the influence of the surface load. The 0.02 contour appeared to be wider after warming (Figure 7.16b). No significant widening of the other contours was observed. With further warming to -1.5˚C at 10 cm (Figure 7.16c) normal stresses decreased to slightly below the initial values at 11 h. The snowpack settled from 36 to 47.5 h by 1.9 cm compared to 0.7 cm from 11 to 36 h (Figure

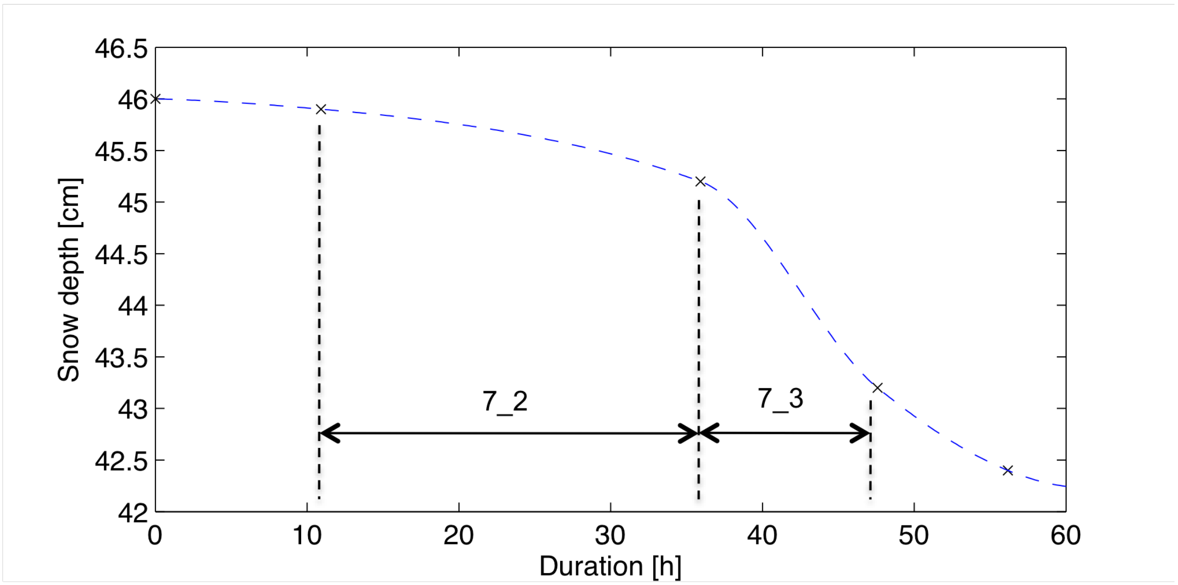

Figure 7.17. Snow height in snow box during Experiment 7 (warming periods 7_2 and 7_3).

7.17). This and an increase of push resistance by 2 – 3 kPa suggest that strengthening of the snowpack reduced the penetration of stress and deformation despite ongoing warming in Exp 7_3.

7.5 Discussion

7.5.1 Validation of correlation analysis

The cold lab experiments yielded results on the snow temperature dependence of the sub-surface pressure due to surface loads without the challenges of snowpack variability and meteorological factors. Further, the effect of ski bending during skier stress experiments, as usually encountered in field studies, was eliminated (see Chapter 5). Nevertheless, the effects of warming and cooling of the near-surface layers on normal stresses in the snowpack due to surface loads appear to have been influenced by a complex interaction of snowpack properties and temperature conditions. Despite the relatively small data set and the number of complicating factors, the cold lab studies provided valuable qualitative insight and to some extent quantitative results.

To have a highly significant correlation within a small data set is quite rare. Hence, to augment the physical discussions significance values of $p \leq 0.1$ were considered. High correlations might occur by chance due to the strong weight of each data point and not due to a physical relationship with the normal stress change (Green, 1991). For example, removing the largest value in Figure 7.11b (red '+') eliminates the indicated correlation (p=0.01). All other subsets in Figure 7.11 and 7.12 still indicated the same trend after each of the points were removed. Plausible physical explanations, however, are consistent with the trends that were found by the correlation analysis and graphical interpretation. For example, the predictor variables ranked four to six for the snow surface (ΔT_{surf}, T_{min_surf}, $\Delta T_{surf}/\Delta t$, Table 7.6) are the same properties ranked one to three 10 cm below the snow surface and indicate the same trend. The larger temperature fluctuations and inaccuracies due to snow surface temperature measurements (Shea and Jamieson, 2011) explain the lower correlation coefficients. Qualitatively, ΔT_{surf}, T_{min_surf}, and $\Delta T_{surf}/\Delta t$ yielded the same relationships with normal stress change as the corresponding variables measured at 10 cm depth.

7.5.2 Temperature dependence of mechanical properties of snow

The findings of the cold lab experiments are in agreement with previous studies that quantified the effect of snow temperature changes on mechanical snowpack properties that determine its stability (see Section 2.2). According to these studies, the stiffness modulus for snow decreases with warming approximately by a factor of two for rising snow temperatures from -20˚C to -2˚C (Section 2.6). A similar decrease of push resistance (Section 7.4.5), which is assumed to be monotonically related the stiffness, contributed to the increase of penetrating stresses up to a factor of two.

According to McClung and Schweizer's hypothesis (1999; Section 2.2.7), warmer, softer snow allows deeper deformation penetration and vice versa. The penetration resistance measurements (Figure 7.15), as an approximation for stiffness, support the direct effect on stiffness due to warming and cooling.

Reuter (2010) measured a decrease of Young's modulus (stiffness) of up to 50% due strong daytime warming of the near-surface layers (T_{10} increased approximately 5 to 7˚C). The observed increase of push resistance with warming (Figure 7.15) of up to 40% is within the same order of magnitude for a comparable increase of T_{10}.

7.5.3 Time dependence of stress response to warming

The cold lab experiments provided quantitative evidence, in support of McClung and Schweizer's hypothesis (Section 2.2.7) that stress penetration due to surface loads generally increases with warming snow temperatures and decreases with cooling. This statement, however, does not hold entirely true for the case of snowpack warming. The influence of *direct-immediate* and *indirect-delayed* effects (see Section 2.2) of warming has opposite effects on the stress and deformation penetration due to surface loads. During rapid warming (< 10 h), at relatively cold initial and end snow temperatures, normal stresses increased according to the considerations of McClung and Schweizer. In this case *direct-immediate* effects were the 1st order effect (Group I in Section 7.4.2.3).

Slower gradual warming (t > 10 h) to higher snow temperatures closer to the melting point may allow micro-structural changes to strengthen the snowpack and therefore decreased deformation and stress penetration. In this case *indirect-delayed* effects overrode *direct-immediate* effects (Group III).

Group II (see Section 7.4.2.3) appeared to be a transitional stage where *indirect-delayed* temperature effects slowly gained importance, but the direct influence of temperature was still dominant. Although, the direct effect on stiffness is the major cause, sintering processes still take place in this short time scale. For instance, Szabo and Schneebeli (2007) pointed out that increased contact pressure between bonds increases bond strength within seconds.

The stress increase in warming period 7_2 is consistent with *direct-immediate* effects, whereas the stress decrease in warming period 7_3 is consistent with *indirect-delayed* effects (Figure 7.16)

According to Experiment 5 (Section 7.4.6), stress increase can occur repeatedly on the same snowpack with repetitive warming. Micro-structural changes did not seem to strengthen the snowpack. Neither, did the second rapid warming to a moist snow surface weaken bonds that formed in the previous warming and cooling. Although snow surface temperatures rose to 0˚C during the warming periods, the temperature changes seemed to happen rapidly enough such that settlement and densification did not reduce the deformation due to the surface load.

7.5.4 The influence of snow hardness on snow temperature induced stress changes

Figure 7.10 suggests that snow hardness influences the order of magnitude of the stress range within which snow temperature changes affect stresses due to surface loads. The larger noise of the stress data in softer snow (Table 7.5 and 7.6) suggests that softer snow is more susceptible to micro-structural changes. The data points in Figure 7.10 contain snow temperatures from the start and the end of warming and cooling periods, which may explain part of the scatter. The lower standard deviation in harder snow indicates that snow stiffness is directly affected by the temperature change. In this case, micro-structural changes take more time to be affected by warming (Section 2.2).

The hardness and snow temperature dependent behaviour of stress transmission in snow is more obvious in Figure 7.10b. The steadily and slightly increasing pressure over a wide temperature range from below -20˚C to close to 0˚C of the harder (pencil hardness) snowpack supports the influence of *direct-immediate* effects as the cause of the stress increase with warming. In this case, micro-structural changes were negligible.

The initial strong stress increase with warming snow temperatures to approximately -8 to -6˚C of the softer snow (1 finger hardness; Figure 7.10b) indicates a high susceptibility of softer snow to *direct-immediate* effects. A thinner ice matrix with fewer and smaller bonds, and a higher surface to volume ratio is more likely affected by *direct-immediate* effects of temperature. The stress decrease at temperatures above approximately -8 to -6˚C suggests that *indirect-delayed* effects of temperature on micro-structural changes start to dominate over *direct-immediate* effects. Again, the thinner ice matrix and lower density makes the softer snow more susceptible to *indirect-delayed* effects for this temperature range. The low sample size and variability of the data points, however, may question this interpretation. On the other hand, fracture toughness in tension decreases with warming to approximately -8˚C; at warmer temperatures the fracture toughness tends to increase (Schweizer and others, 2004; Figure 2.11). This turning point seems to be similar to the one observed in Figure 7.10b. This normal stress behaviour proposes decreasing stiffness with warming approximately to -8˚C and increasing stiffness at warmer snow temperatures. This corresponds with the temperature dependence of fracture toughness, found by Schweizer and others, since stiffness and toughness are directly proportional according to Equation 1.2. Furthermore, the effective elastic shear modulus decreases with warming snow temperatures to approximately -6˚C (Figure 2.11). Above -6˚C the shear modulus tends to decrease faster towards 0˚C. This change of the temperature-dependent behaviour of the shear modulus and fracture toughness at approximately the same temperature range as the change of normal stress in Figure 7.10b supports the temperature dependence of normal stresses in softer snow as suggested by the dashed trend line in Figure 7.10b.

7.6 Summary

The cold lab studies yielded for the first time systematic climate controlled, experimental results on the sub-surface normal stress distribution due to static surface (point) loads and the influence of warming and cooling. Theoretical concepts were confirmed by experimental data. Generally, warming (cooling) reduced (increased) snow stiffness and normal stresses due to the surface loads increased (decreased). Furthermore, the effect of warming of the near surface layers on normal stress changes was refined and to some extent quantified. Snow temperature variations, similar to those as observed in the near-surface layers of a natural snowpack during the course of a day, yielded relative normal stress variation between -30% to 80% of the initial value before warming or cooling, respectively.

7.6.1 Stress distribution

Normal stress due to static surface loads decreased non-linearly with snow depth. Greater decrease with depth was observed in softer snow. Snow hardness (stiffness) at the beginning of the warming effects the order of magnitude to which normal stress due to surface loads is transferred. Normal stress changes due to short-term snow temperature variations occurred well within this set range by initial snow hardness. One hand hardness step (1F to P) corresponds to a factor two in stress difference. The ratio of the width to the depth of the stress bulb was about equal. The depth, however, was slightly larger than width for relatively soft snow (4F - 1F hardness).

7.6.2 Temperature effects on stress (Table 7.10)

- Three groups were identified that describe the normal stress change due to warming of the near-surface layers:
  - Group I: Rapid warming, starting at colder snow temperatures and a harder snowpack (pencil) led to an *increase of the positive normal stress change* ($\Delta\sigma_{REL}$)[1]. *Direct-immediate* effects of temperature dominated.
  - Group II: Slower more gradual warming at generally higher snowpack temperatures led to a *decrease of the positive normal stress change* ($\Delta\sigma_{REL}$)[1]. *Direct-immediate* effects of temperature still dominate, but *indirect-delayed* effects showed more influence.
  - Group III: Warming to moist snow surface with strong settlement and densification led to normal stress decrease. *Indirect-delayed* effects of temperature dominate over *direct-immediate* effects.

- *Direct-immediate* effects of snow cooling generally caused decreasing normal stresses. [1]

Table 7.10. Effect of snow temperature changes on normal stress due to surface loads. The *direct-immediate* and *indirect-delayed* temperature effects are defined in detail in Section 2.2.4.

Snow temp. change	**Warming** (rapid, colder, harder snow)	**Warming** (slower, softer, warmer snow)	**Warming** (moist, strong settlm.)	**Cooling** (for all conditions)
	⬇	⬇	⬇	⬇
Normal stress response	Strong increase	Less increase	Decrease	Decrease
Dominating effect	Direct-immediate	Direct-immediate (Ind.-Del.)	Indirect-delayed	Direct-immediate

[1] see Section 7.4.2.1 for explanation

CHAPTER 8

The effect of daytime warming on snowpack creep

8.1 Introduction

Snowpack creep on slopes is believed to strengthen the snowpack under most circumstances due to settlement and densification (McClung and Schaerer, 2007, p.75). Deformation rates are typically well below critical values necessary for ductile to brittle transition, by approximately two orders of magnitude (see Section 2.2.8). Nevertheless, experience and observation showed (Section 2.2.1) that instabilities can develop in rare cases during rapid solar warming. The exact mechanism, however, that causes these instabilities is not fully understood. Presumably, solar heating of the near-surface layers increased the layer parallel deformation rate above a critical value for ductile to brittle transition.

To shed more light on the effect of rapid near-surface solar warming, the creeping motion of the snowpack, on vertical up-slope snow pit walls, was monitored with digital photography during the transition from cold morning temperatures to rapidly rising air temperatures due to direct solar radiation. Experimental conditions were chosen that were similar to those cases where ski guides observed rapidly developing instabilities (Section 2.2.1). In those cases, the first warming of low-density storm snow on steep east to south-east facing slopes was assumed to cause instability. Two field experiments that closely matched those conditions are presented in this chapter.

8.2 Methods

8.2.1 Experimental set up

Approximately 5 cm long toothpicks were inserted slope-parallel in the near-surface layers of a down-slope pit wall with a vertical spacing of approximately 3 - 4 cm (Figure 8.1). The tips of the toothpicks were coloured black for better contrast to the surrounding snow. To monitor the movement of the toothpick tips, which were assumed to follow the creeping motion of the snowpack, a digital camera was mounted on a tripod at a distance of approximately 1.5 m, viewing the toothpick profile perpendicularly from the side. Time-lapse images were taken with a frame rate of four images per hour. The camera was set up just after dawn, while air and snowpack temperatures, and therefore snow creep, were still at their minimum.

For length scale reference an avalanche probe with the centimetre-scale facing the camera, was pushed into the snowpack next to the tooth pick profile (Figure 8.1). To analyse the movement of the toothpick tips reliable reference points were necessary. An aluminium post (3 m x 4 cm diameter) with black markers along its length was rammed vertically into deeper, consolidated layers of the snowpack. Snow creep of those deeper layers, and therefore the movement of the pole was assumed to be negligible compared to the displacement of the toothpicks in the near-surface layers for the relatively short duration of the experiments (few hours).

Direct solar radiation and air temperature was measured at the nearby weather station (see Section 3.2.4)

8.2.2 Analysis

8.2.2.1 Image analysis

The movement of the toothpick tips from frame to frame was determined with help of Mathwork Matlab's Image Processing Toolbox functions. The *'impixel'* tool enabled the user to select each toothpick and reference point manually and provided pixel coordinates in x and z-direction. The pixel coordinates of the centre of each toothpick tip and reference point were selected on an enlarged image to improve selection accuracy (Figure 8.1). The centre of the same toothpick from frame to frame was selected with an accuracy of ±1 pixel. This converts to an accuracy due to the manual selection process of ±0.141 mm and ±0.135 mm for Experiment 1 and Experiment 2, respectively. See Table 8.1 for pixel to distance conversion for each experiment.

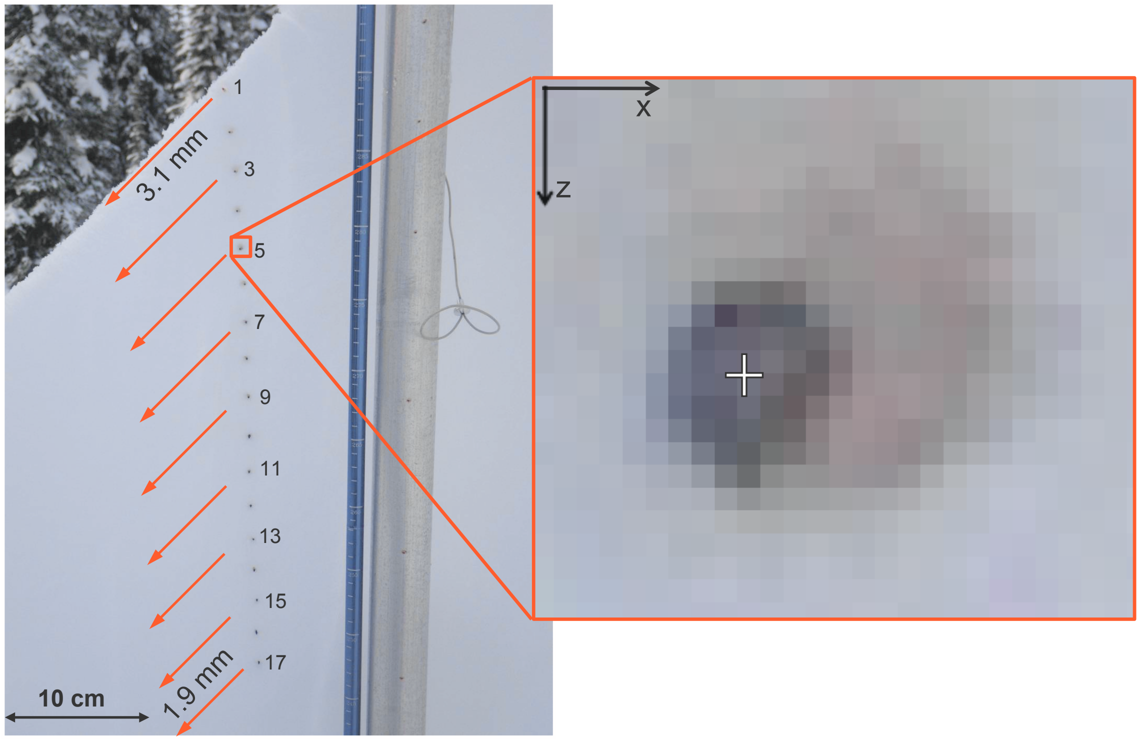

Figure 8.1. Total layer-parallel displacement during Experiment 1 from 6:15 to 9:15 (red arrows; not to scale). The displacement decreased from maximum values of 3.1 mm close to the surface to 1.9 mm at the lowest measured profile point. The pixel coordinates of the centre of each toothpick were manually selected in enlarged images. The white cross on the right image is the 'pixel selection cursor tip'.

From the varying distance of the toothpick tips to the reference points from frame to frame the relative motion of the toothpick tips was calculated. To decrease the error due to the manual pixel selection process the relative pixel position was determined from multiple reference points (six in Experiment 1 and five in Experiment 2; Table 8.1). With help of the scale on the avalanche probe, the 5 cm interval approximately in the middle of the toothpick profile, the pixel-displacement of the toothpicks was converted into a length scale in mm. See Table 8.1 for the conversion factor from pixel to mm for each of the experiments. The resulting vertical profile for each time step was smoothed by a moving average over three profile points.

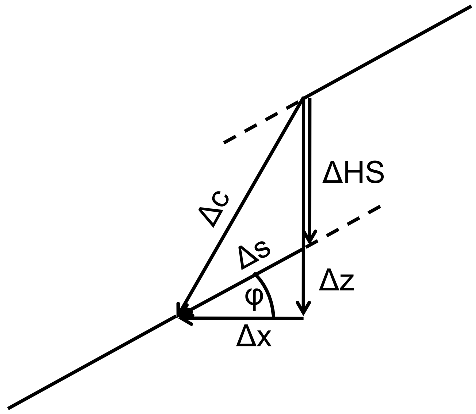

Figure 8.2. Diagram showing total creep Δc, measured vertical (Δz) and horizontal (Δx) displacement and calculated slope parallel displacement (Δs) and settlement (ΔHS) for each toothpick.

8.2.2.2 Definitions

The total creep (Δc) of each profile point (toothpick) per each 15 min interval was determined from the measured vertical (Δz) and horizontal (Δx) displacement. Vertical settlement (ΔHS) and slope parallel displacement (Δs) was calculated according to the following equations:

$$\Delta s = \Delta x / \cos\varphi \tag{8.1}$$

$$\Delta HS = \Delta z - \Delta x \cdot \tan\varphi \tag{8.2}$$

with φ: slope angle

8.2.2.3 Calculation of shear rates

Slope parallel shear rate ($\dot{\tau}$) was approximated by the change of slope parallel displacement speed with depth between adjacent profile points (Figure 8.3). The shear rate plays an important role during the slab avalanche release process (Section 1.2).

$$\dot{\tau} = \frac{v_n - v_{n+1}}{z_n - z_{n+1}} = \frac{\Delta v}{\Delta z} \tag{8.3}$$

with v_n, v_{n+1}: slope-parallel creep speed at snow depth z_n and z_{n+1}, respectively

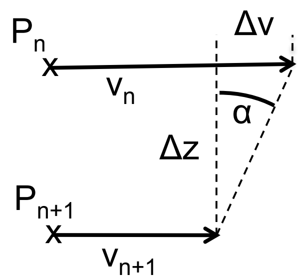

Figure 8.3. Diagram showing the slope-parallel displacement speed between two adjacent profile points.

8.3 Results

8.3.1 Overview of experiments

Two experiments are presented (Table 8.1) that yielded a measurable change of snowpack creep with increasing insolation and rising air temperatures. In both experiments the recent storm snow was exposed for the first time to direct solar radiation. Both experiments were set up on an east-facing slope in a forest opening at approximately 1900 m. The total snow height was approximately 315 - 330 cm, which is about average for this time of year and elevation in an area with a transitional snow climate (McClung and Schaerer, 2006, p. 23). Typically, hand hardness increases gradually with depth to about finger to pencil hardness in the mid and lower snowpack, which usually consists of rounded grains (Fierz and others, 2009).

Prior to Experiment 1, 30 cm of dry snow fell in the previous 72 h and 12 cm of those fell during the previous night. The storm snow above the crust at 15 cm depth in Experiment 2 also accumulated the previous night. For details about hand hardness, grain size and type, and density in the top 50 cm of the snowpack, where the toothpicks were placed see Table 8.1. Initial snowpack temperatures ranged from -6 °C at the surface to -4 °C at a depth of 50 cm in Experiment 1. Cooler snowpack temperatures were observed at the beginning of Experiment 2, ranging from -11˚C at the surface to -8˚C at 40 cm depth.

Table 8.1. Overview of snowpack creep experiments.

	Experiment 1	**Experiment 2**
Date	21 March 2009	1 April 1 2009
Duration	6:15 – 9:15 (6:15 – 18:00, only ∆HS)	5:45 – 10:45
Cold/warming period	6:15 - 7:30/7:30 - 9:15	6:00 - 7:30/7:30 - 10:30
Aspect	East	East
Slope angle	45˚	48˚
Avg. density of near surface layers	70 - 90 kg/m^3	75 - 80 kg/m^3 (above crust) 120 – 200 kg/m^3 (below)
Number of vertical ref. points	6	5
Distance: Surface to 1st toothpick	0.8 cm	3.3 cm
Images resolution	72 dpi	72 dpi
Pixel to length-scale conversion factor	0.141 mm/pixel	0.135 mm/pixel

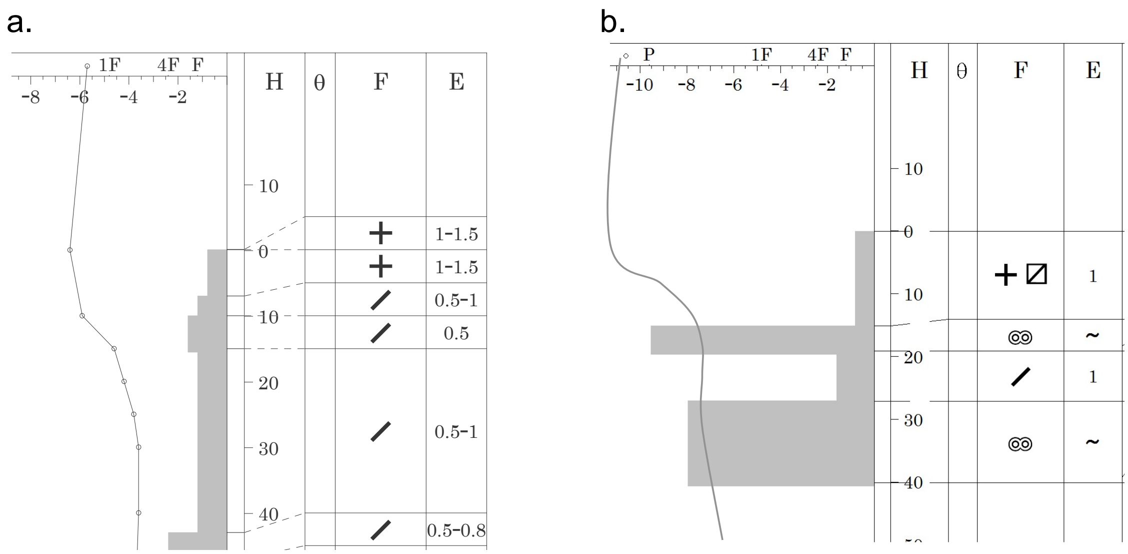

Figure 8.4. Snow and temperature profiles (solid line) of the upper snowpack of **(a)** Experiment 1 and **(b)** Experiment 2 (see Fierz and others, 2009 for hand hardness classification).

8.3.2 Experiment 1 - March 21

Figure 8.5 shows half-hourly creep profiles relative to the initial profile at 6:15 (solid lines) and trajectories of every odd-numbered toothpick tip (dotted lines).

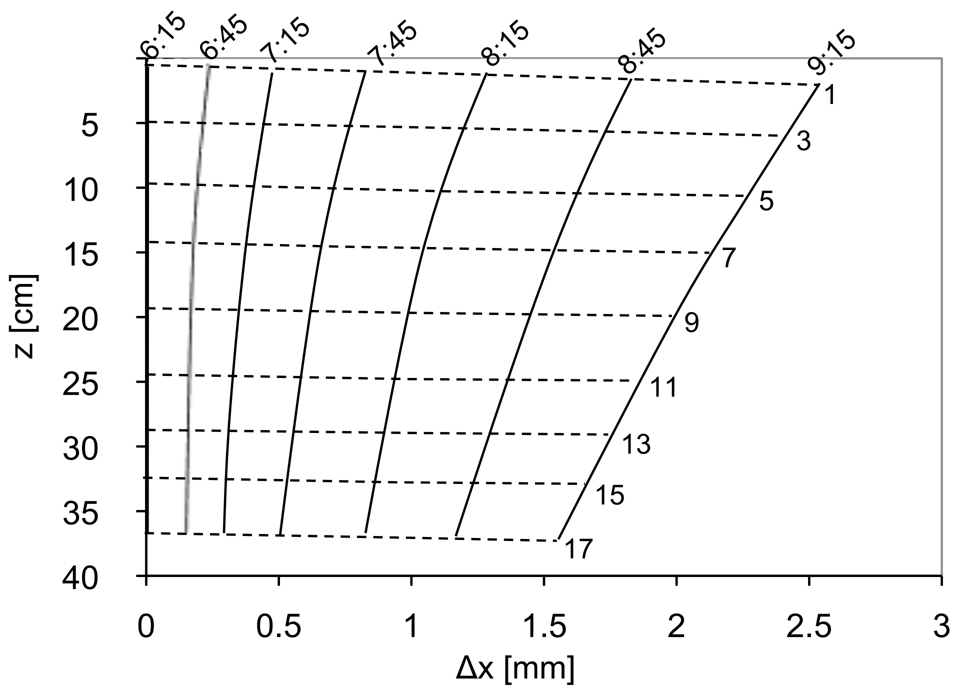

Figure 8.5. Half-hourly creep profiles (solid lines) and trajectories (dashed lines) of odd-numbered profile points (Figure 8.1) of Experiment 1 relative to initial profile at 6:15. (Δx: horizontal displacement)

Figure 8.6. After 9:15 the toothpicks started to melt into the snowpack in irregular patterns and were useless for creep analysis.

Weather and snowpack conditions only allowed high-resolution creep measurements until 9:15. After this time with penetrating solar radiation and rising air temperatures close to 0˚C the toothpicks started to melt adjacent snow and did not follow the natural creep of the snowpack (Figure 8.6). Total vertical settlement,

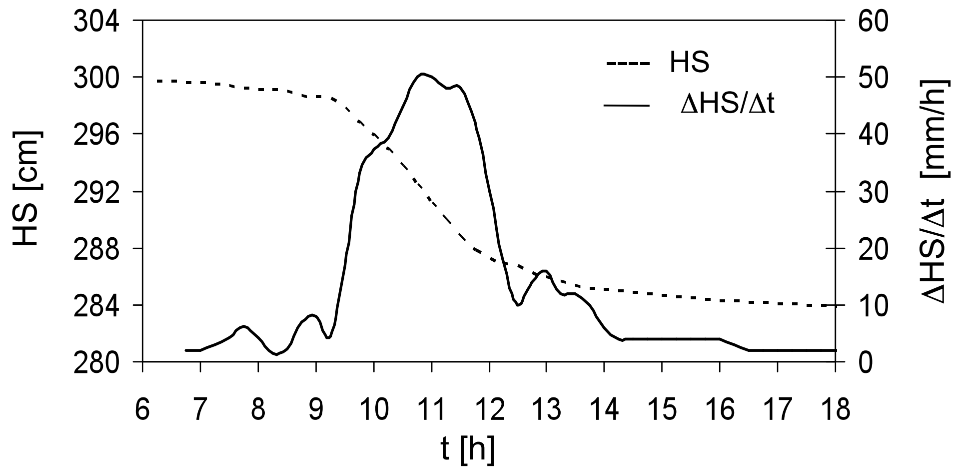

Figure 8.7. Total snow height HS (dashed line) and settlement rate (solid line) during the course of the day of March 21.

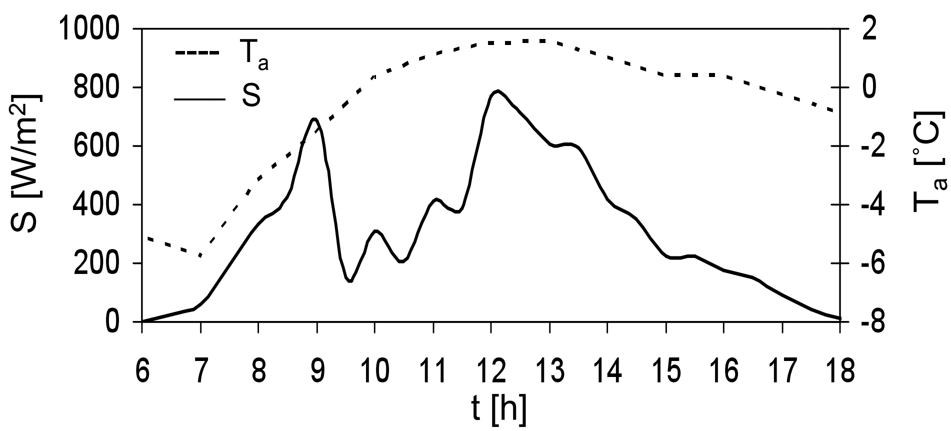

Figure 8.8. Air temperature (dashed line) and direct solar radiation (solid line, averaged over 30 min) on March 21.

however, could still be determined over the full duration of the experiment until 6 pm (Figure 8.7). For further analysis the cold period was defined from 6:15 to 7:30 and the warming period from 7:30 to 9:15, based on the increase of horizontal displacement in Figure 8.5.

8.3.2.1 Settlement

Figure 8.7 shows the change in total snow depth (HS) and settling rate (ΔHS/Δt, measured at the snow surface) during the course of Experiment 1. The snowpack settled a total of 16 cm by the end of the experiment at 6 pm. Settling rates

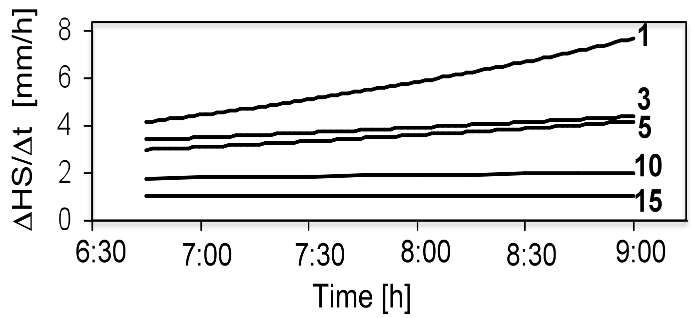

Figure 8.9. Vertical settling rate on various depth levels on March 21. The numbers on the right refer to selected profile points in Figure 8.1 and Figure 8.5.

increased from initially 2 mm/h to 8 mm/h from the coldest morning temperatures before sunrise with increasing solar radiation and air temperatures until 9:15 (Figure 8.8). The variations in settling rate between 6:45 and 9:15 were due to alternating shading and insolation of the study site by sparse trees while the sun was still at low angles early morning.

Measured solar radiation did not reflect the variations since the radiometer was located in a nearby weather station with unobstructed sky view. After 9:15 settling rate rapidly increased to maximum values of 50 mm/hr, followed by a strong reduction to 15 mm/h until 12:30 pm. After 12:30 pm settling rates reduced to 2 mm/h with the sun leaving the east facing study site in the early afternoon. Although thin, high clouds reduced insolation between 9:00 and 12:00, air temperatures rising close to 0˚C and the remaining solar input were sufficient to cause the high settling rates after 9 (Figure 8.7).

A closer look at the settling rate between 6:45 and 9:00, the time period for which detailed creep data are available (Figure 8.9), reveals a depth dependence of settling rate gain over time. Settling rate of the top layer (profile point #1) doubled with daytime warming from 4 mm/h to 8 mm/h. In deeper layers (profile points #3 and #5), a rise of approximately 1 mm/h was observed, whereas the deepest layers (#10 and #15) remained fairly constant during the observation period until 9:15.

The total settlement for each profile point decreased with snow depth

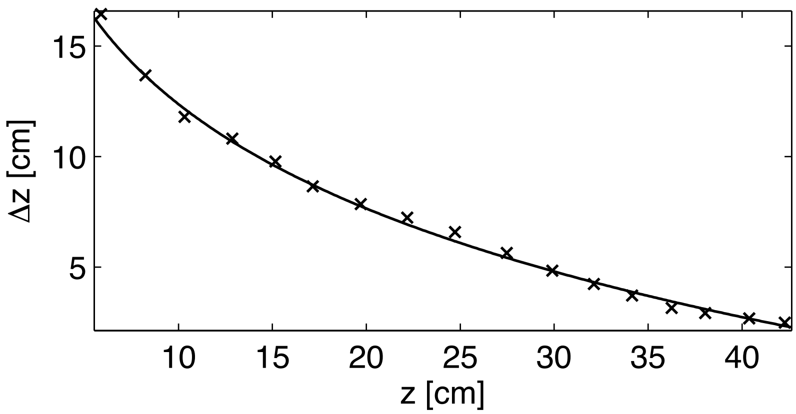

Figure 8.10. Total settlement for each profile point (toothpick) during Experiment 1 from 6:15 to 18:00. The solid line is a power law fit.

(Figure 8.10). Basically, the near surface layers showed stronger settlement than layers below. The decrease of settlement with snow depth was approximated by a power law fit of the form $\Delta HS = -88.19 \cdot z^{0.058} + 127.5$ (R^2=0.99, SE=0.43).

8.3.2.2 Slope parallel displacement

Until 9:15 the total slope parallel displacement (Δs) ranged from 1.6 mm at the bottom of the profile (profile point 17) to 2.5 mm close to the snow surface (Figure 8.1 and 8.5). The total displacement decreased gradually with depth to about 40 cm. After approximately 7:15 the horizontal displacement accelerated considerably (Figure 8.5 and Figure 8.11) with increasing solar energy input (Figure 8.8). Until this point, available direct solar radiation accumulated to approximately 2 MJ m^{-2}.

In contrast to settling rates, slope parallel creep rate increased until 9:00 at all measured depth levels, although the velocity gain in lower layers was less (Figure 8.5 and Figure 8.11). At the top layer (profile point 1), creep rate rose from 0.9 mm/h to 1.3 mm/h. The increase gradually decreased with depth, with a gain at the lowest point (#15) from 0.6 mm/h to 0.75 mm/h.

8.3.2.3 Slope parallel shear rate

During the case study of March 21, shear rates ($\dot{\tau}$) increased in all measured depth levels with exposure to the early morning sun and rising air temperature until

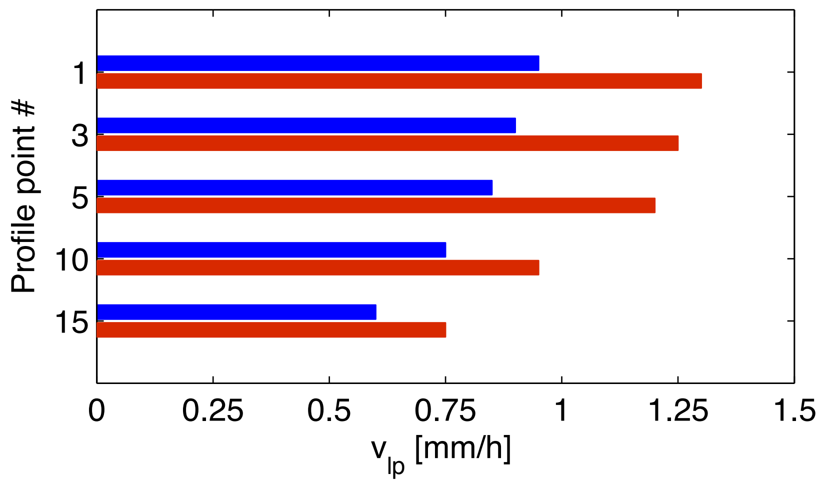

Figure 8.11. Slope parallel creep rate on various depth levels for the cold period (blue) and warming period (red). The numbers on the right refer to selected profile points in Figure 8.1 and 8.5.

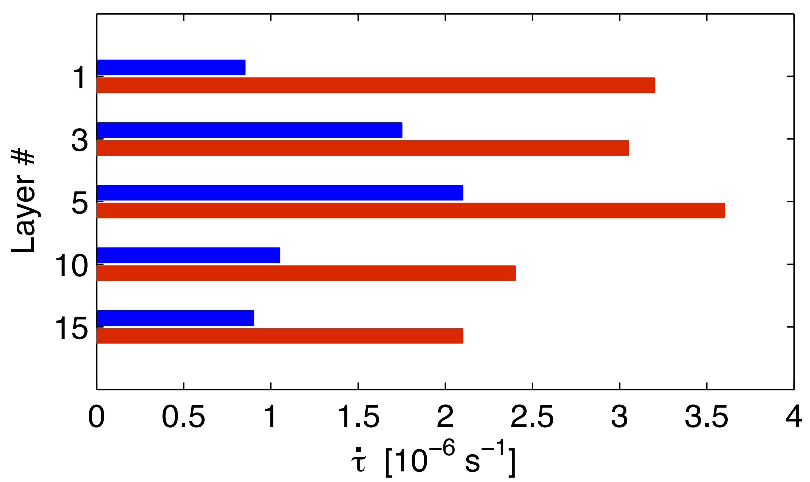

Figure 8.12. Slope parallel deformation rate on various depth levels during Experiment 1 for the cold period (blue) and warming period (red). The numbers on the right refer to selected profile points in Figures 8.1 and 8.5. Estimation of $\dot{\tau}$ according to Equation 8.3.

9:00 (Figure 8.12). A clear dependence on depth could not be observed, although the strongest increase was observed at layers close to the surface (from 0.8 to $3.25 \cdot 10^{-6}$ s^{-1}). In all other (deeper) layer to approximately 34 cm snow depth (profile point 15) shear rate rose by a factor of approximately 1.5 – 2.5 to values of 2 – $3.5 \cdot 10^{-6}$ s^{-1}.

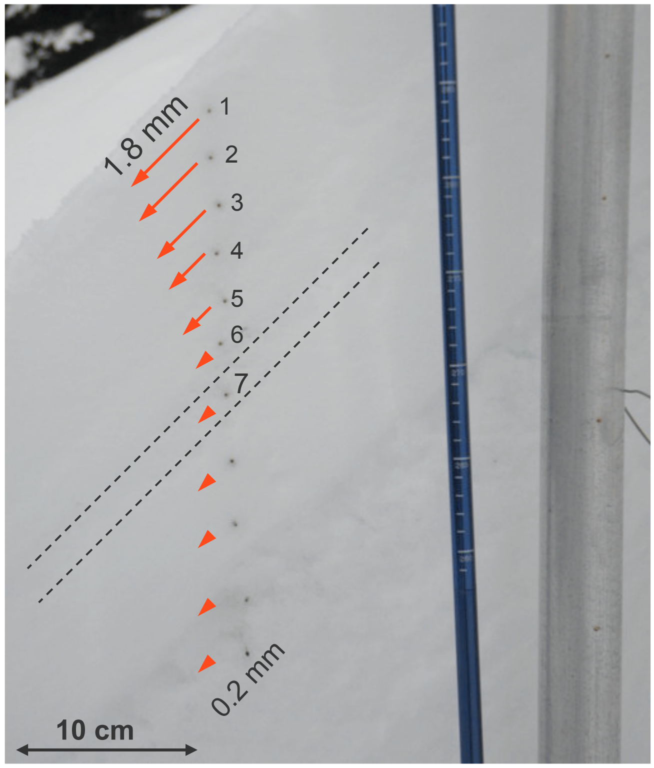

Figure 8.13. Total layer-parallel displacement during Experiment 2 from 5:45 to 10:30 (red arrows; not to scale). The dashed lines indicate the position of the crust.

8.3.3 Case study April 1 – Experiment 2

8.3.3.1 Slope parallel displacement

Figure 8.13 shows the total slope parallel displacement (Δs) for each profile point (red arrows) during Experiment 2 from 5:45 to 10:30. The total displacement rapidly decreased from the surface (approximately 1.8 mm) to just above the crust (indicated by the dashed parallel lines) to below 0.2 mm. The crust acted as a barrier that apparently impeded the creeping motion to deeper layers.

The slope parallel displacement speed (v_{lp}) of the near surface layers (mean displacement of the top two profile points #1 and #2) increased between 7:30 and 8:30 by a factor of three to four from approximately 0.2 to 0.3 mm/h to up to 0.7 to 0.8 mm/h with increasing energy input due to solar radiation (Figure 8.14). After 9:00, v_{lp} gradually decreased. Until approximately 7:30 absorbed direct solar radiation was not sufficient for a considerable increase of v_{lp}.

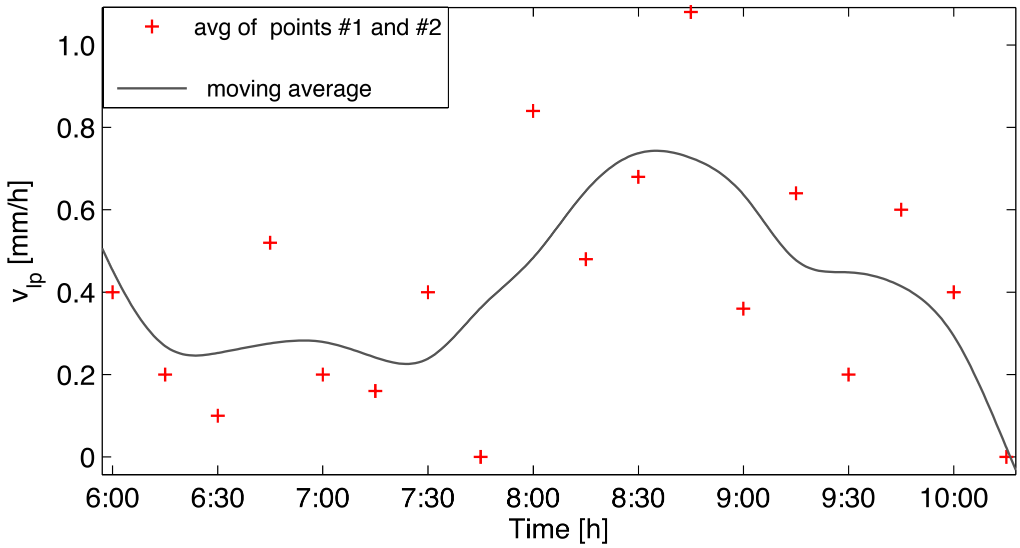

Figure 8.14. Average layer parallel displacement rate (v_{lp}) of top two profile points (#1 and #2; red '+') of Experiment 2. The solid line indicates the moving average over five data points.

Figures 8.15a and 8.15b demonstrate the snow-depth dependence of $\dot{\tau}$ and v_{lp}. Average values were calculated for the cold period (blue bars) until 7:30 and the warming phase from 7:30 to 9:30 (red bars). The cold and warming period was defined according to the average of v_{lp} of the near surface layers (Figure 8.14). In all depth levels down to the top of the crust at 15 cm the slope parallel displacement increased by approximately a factor of three to four. Actual values increased from approximately 0.2 to 0.8 mm/h in the near surface layers (#1 and #2) from to cold to the warming phase. With increasing depth towards the layer just above the crust, displacements speeds decreased (cold and warm) to less than a tenth of the surface value.

8.3.3.2 Shear rate

For the layer above the crust shear deformation rates ($\dot{\tau}$) were calculated for each layer between two adjacent profile points according to Equation 8.3 (Figure 8.3). Shear rates were lowest in the top layer with approximately $0.2 \cdot 10^{-6}$ s^{-1} and increased to approximately $2.5 \cdot 10^{-6}$ s^{-1} at about 10 cm below the snow surface (Figure 8.15b). Maximum values closer to the crust were slightly lower. Shear rates

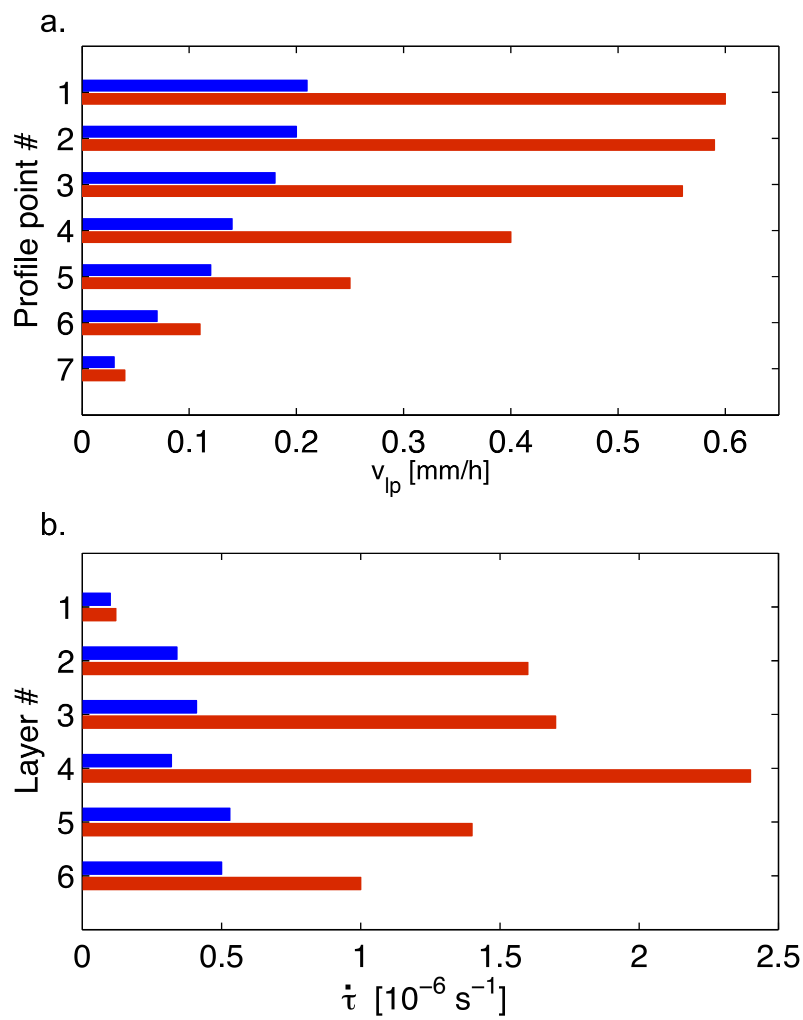

Figure 8.15. Slope parallel displacement rate of toothpicks **(a)** and shear deformation rate **(b)** of layers above the crust in Experiment 2, during the cold period (blue) and the warming (red). Layer 1 is the layer between profile point 1 and 2, Layer 2 between profile point 2 and 3, and so on.

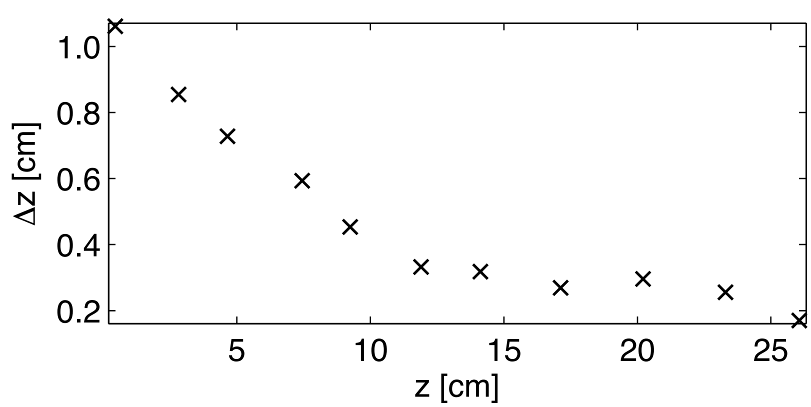

Figure 8.16. Total settlement (Δz) of each profile point during Experiment 2 from 5:45 to 10:45 .

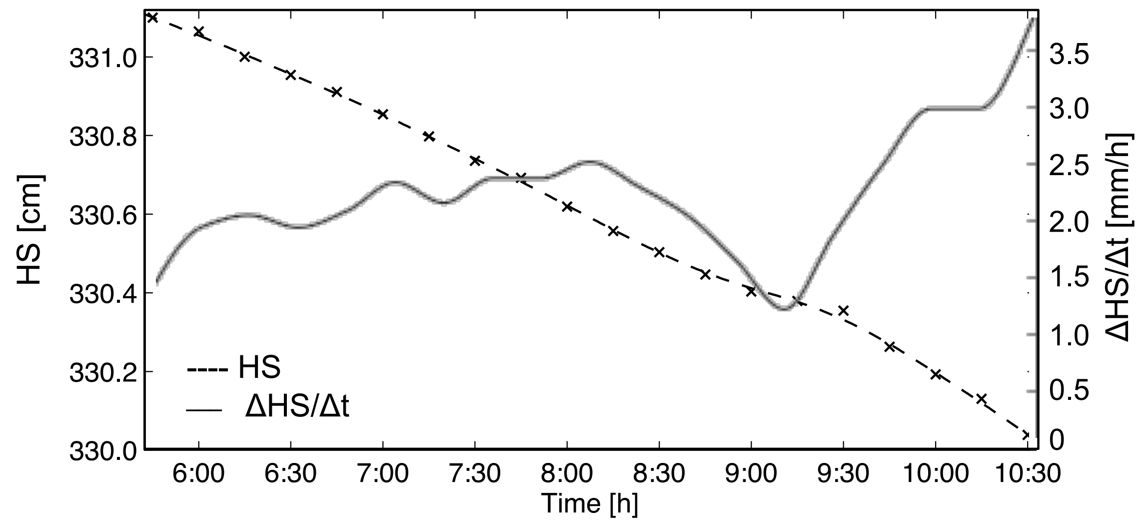

Figure 8.17. Total snow height (HS) and settling rate during Experiment 2.

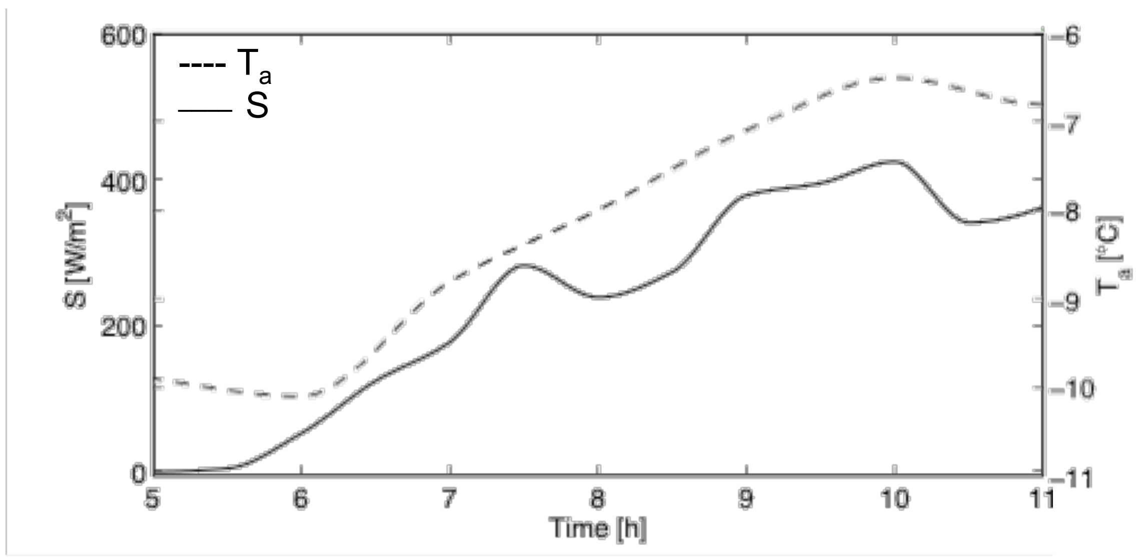

Figure 8.18. Air temperature (T_a) and incoming short wave radiation (S) between 5:00 and 11:00 during Experiment 2 from a nearby weather station.

from the cold to the warming period increased approximately four to five fold. In the top-most layer, however, $\dot{\tau}$ did not show any considerable increase.

8.3.3.3 Settlement

Total settlement during Experiment 2 (Figure 8.16) gradually decreased from just above 1 cm at the surface to approximately 0.3 cm just above the crust. Below the crust only a slight decrease of settlement with depth was observed. The low-density snow above the crust was more susceptible to settlement with warming. Below the crust snow with higher density and strength only experienced minor settlement.

Figure 8.17 shows the change of HS (settlement) and settling rates during the course of the experiment until 10:45. Settling rate slightly increased during daytime warming until approximately 8:15 from about 2.0 to 2.5 mm/h. After, until 9:15, settling rate dropped to approximately 1 to 1.5 mm/h, followed by a considerable increase to above 3.5 mm/h.

Until about 7:30 to 8:30, approximately the time when creep (settlement and slope parallel displacement) accelerated due to warming, approximately 1.25 MJ $m^{-2}$of direct solar energy were available. Maximum direct insolation until this point reached approximately 275 Wm^{-2}.

8.4 Discussion

8.4.1 Settlement

The creep measurements during March 21 (Experiment 1) exhibited accelerating vertical settlement and slope parallel displacement with daytime warming in the morning on a steep east-facing slope with low density, dry storm snow (before 9:00). Air temperatures rising above 0 °C, penetrating solar radiation, low density snow and rising liquid water content may explain the strong and rapid increase of vertical settlement rate after 9:15. Conway and others (1996) pointed out that when liquid water is present, capillary forces cause shrinkage of the snowpack independently of gravity. The irregular melting pattern around the toothpicks (Figure 8.6) hints at the presence of liquid water. Conway and others measured creep rates, mostly due to settlement, up to 90 mm/h with the onset of rain.

Experiment 1 provided clues that only the near-surface layers increased settling rate and settlement due to warming. This could potentially lead to a denser layer developing over a softer colder layer underneath. Consequences on snowpack stability are addressed in Section 9.3.

8.4.2 Ductile to brittle transitions

Depending on snow properties, critical deformation rates in shear for brittle fracture usually ranges from 10^{-4} to 10^{-3} s^{-1} (see Section 1.2). The formation of micro cracks in tension was reported to start between 10^{-6} and 10^{-5} s^{-1} by Narita (1983). Compared to those values, the measured increase in shear rate on March 21 suggests failure initiation may be possible with a pre-existing weak layer. Furthermore, stress concentration at the interface of snowpack layers with different hardness, density or grain size usually causes higher shear rates (Habermann et al., 2007). Reiweger and Schweizer (2010) reported up to 10 to 100 times higher shear rates on the micro-scale due to stress concentration on weak buried surface hoar layers. Larger stresses may concentrate, in particular, at the perimeter of an existing flaw (Section 1.4.2)

8.4.3 Depth of warming effect

The maximum snow depth that is actually warming up due to daytime warming is approximately 20 cm (Armstrong and Brun, 2008, p. 39). According to Experiment 1 (Section 8.3.2) layer-parallel displacement and deformation also increased in deeper layers although the warming front did not reach these layers. During snowpack creep the accelerated slope-parallel motion of the upper layers is transferred to deeper layers. The depth of near-surface layers in Experiment 1 that actually warmed up is assumed to be less than this 20 cm since the warming period only lasted for 3 h. The deepest profile point at approximately 37 cm still showed considerable acceleration during warming. The maximum snow depth, therefore, that was indirectly affected due to warming is likely deeper. Natural slab releases due to warming have been observed up to a slab depth of approximately 50 cm (McClung and Schaerer, 2006, p.38).

8.4.4 Creep behaviour in Experiment 2

Settling rate ($\Delta HS/\Delta t$; Figure 8.17) and slope parallel creep speed (v_{lp}; Figure 8.14) in Experiment 2 both showed an increasing trend in response to near-surface warming. After approximately 8:15 to 8:45 both velocity components decreased. Potentially, a nearby tree shaded the study site temporarily. The decreasing air temperatures (Figure 8.18) between 7:30 and 8:00 and the relatively slow increase of insolation suggest that the high thin clouds may have contributed to the delay in warming and therefore caused the decrease of v_{lp} and $\Delta HS/\Delta t$. The nearby weather station was not affected by shading due to trees. Higher viscosity due to settlement and densification, potentially contributed to the decrease of creep.

With ongoing input of solar radiation and warming of the near-surface layers, $\Delta HS/\Delta t$ considerably increased after approximately 9:15 until the end of the experiment, whereas v_{lp} decreased. No plausible explanation could be found for this contrary behaviour.

Two data points in Figure 8.14 yielded v_{lp} values of 0 mm/h. Both points occurred during already low displacement speeds, which were approximately within the order of magnitude of the resolution of the centroids of the toothpick tips (Section 8.2.2.1).

8.5 Summary

For the first time, short-term (daytime) creep of the near-surface layers of a fresh low-density snowpack was monitored with digital photography during the first solar warming in the morning hours.

- Slope-parallel shear and displacement rate increased with short-term warming up to a factor of four.
- The strongest warming-induced settlement took place in the near surface layers of the snowpack.

- Acceleration of the slope-parallel displacement speed was observed below the top layer that is directly affected by the warming front. In other words, the layers below are indirectly affected by warming since the accelerated displacement is transferred to lower layers.
- Slope parallel shear strain rate due to warming increased sufficiently to potentially reach the limit for ductile to brittle transition (basal fracture initiation) if a weak layer were present.
- At approximately 1 to 2 MJ m^{-2} of available direct solar radiation, snowpack creep accelerated on a steep east-facing slope. This equals approximately 1.5 to 2 h of insolation directly after sunrise.

CHAPTER 9

Conclusions

The objective of this thesis was to conduct field experiments to enhance the understanding of the human-triggered and spontaneous slab avalanche release process including warming effects. As outlined in Chapter 2, the work that was conducted for this thesis was divided in two main topics:

1. Stresses in a layered snowpack due to surface loads.
2. Impacts of warming of the near-surface layers on snowpack stability.

In this chapter the conclusions that were drawn from the field and cold lab experiments are summarized and put into context with respect to practical and relevant questions regarding the slab avalanche release process:

- Does skier-triggering become more likely with daytime warming of the near-surface layers?
- Are snowmobiles more prone to trigger slab avalanches than skiers?
- Does snowpack creep due to near-surface warming accelerate and contribute to instability?

9.1 Stress measurement technique

To collect field data to address the first two questions a method was developed to measure normal stresses in a natural snowpack due to surface loads (Chapter 4). This method worked reliably under harsh winter conditions, was field-portable, and minimized the impact on the snowpack due to the insertion of the sensors. The sensitivity of the sensors was sufficient to capture the normal stress changes that were caused by slab stiffness variations of the near-surface layers due to daytime warming (Section 5.3.4 and 7.4.2).

9.2 Normal stress due to surface loads

9.2.1 Stress decrease with depth

Normal stress under skiers, snowmobiles and metal cylinders decreased with depth, approximately following power law functions (Sections 5.3.3, 6.3.1 and 7.4.1). Concerning skier-triggering, it appeared unlikely that layers below approximately 80 cm to 100 cm depth would be substantially affected by static or dynamic skier forces. The weak layer strength at this depth is typically larger than the skier stresses.

9.2.2 Snowmobiles

Stresses in the snowpack due to snowmobiles could initiate a fracture in weak layers beyond 1 m snow depth (Section 6.3.1). The spinning track contributed to this effect. Furthermore, the area that was affected by a snowmobile was considerably larger compared to that of a skier (Section 6.3.1). Consequently, the area in a weak layer that is fractured due to a down-weighting snowmobile may more likely exceed the critical size for fracture propagation compared to a down-weighting skier. The common interpretation of snowpack stability tests, such as the Compression Test and the Rutschblock Test (CAA, 2007) with regard to the ease of fracture initiation likely needs to be revised for snowmobile loads.

9.2.3 Effect of slab hardness on static and dynamic surface loads

The ‘bridging’ effect of harder (stiffer) layers over a weak layer appeared to contribute to stability of the slab/weak layer combination in two ways:

1. Stresses due to surface loads tended to spread out more laterally within the slab (Section 5.3.3 and 7.4.1). Consequently, the strain rate in the weak layer due to surface loads is less likely to exceed the critical strain rate threshold for ductile to brittle transition.

2. Less slope-parallel strain rate on weak layers due to snowpack creep was observed. In particular during daytime warming, harder (stiffer) slabs transferred less of the slope-parallel component of the accelerated strain rate due to creep to deeper layers.

Stress transmission of higher dynamic skier loads with a shorter impact time (jumping skier) on harder near-surface layers appeared to be more effective compared to softer snow layers. In relatively soft near-surface layers, approximately less than 1F to P, the higher dynamic force due to jumping did not penetrate deeper than a skier load due to knee drops (Section 5.3.3.1). It appeared that in softer snow, damping effects absorbed some of the energy input due to dynamic surface loads.

9.3 Temperature effects on slab stability

During the initial stages of the fieldwork for this thesis it became clear that days with directly measurable snowpack stability changes due to warming were infrequent. Due to the challenge of collecting sufficient data in a reasonably timely manner, the experiments were altered to more repeatable ones, which were not as dependent on natural weather and snowpack conditions.

Even after these changes, directly measurable evidence of decreasing stability due to the effect of near-surface warming was still rare. Most indications stemmed from experience and observations. Apparently, many factors need to act together for surface warming to cause instability, such as a slab/weak layer system that is susceptible to warming effects and suitable temperature conditions (Schweizer and Jamieson, 2010; McClung, 1996)

9.3.1 Temperature effect on human triggering

With warming of the slab, generally, the ease of initiation of a fracture in an underlying weak layer due to a skier increased as long as ski penetration and the bending of the ski did not change during warming. This appears to be the case on slabs with approximately 1F to P hardness and harder (Section 5.3.4.3).

Warming and softening of the near-surface layers, however, did not necessarily promote instability, since skier-induced stresses did not always penetrate deeper due to the effect of the bending skis and the resulting distribution of the skier's weight along the ski. This effect likely gained importance in relatively soft snow layers less than approximately 1F to P hardness (Section 5.3.4.2). On the other hand, the lengthening stress bulb may initiate a fracture in the weak layer that is beyond the critical length for fracture propagation, although peak stresses are reduced. These considerations on snowpack stability, however, do not take into account the warming induced acceleration of the slope-parallel shear strain rate, which may cause instability by itself (Section 8.3.2.2 and 8.3.3.2) without any external forces due to a skier. If this effect does not directly cause slab release it may set the stage for easier skier (human) triggering.

During cooling, stresses and deformation due to skiers, or in general due to surface loads, decreased (Sections 5.2.4.4 and 7.4.4). Additionally, layer-parallel creep slowed down with cooling snow temperatures (Section 8.3.3.2). Decreasing bending of the skis due to stiffening near-surface layers during cooling, however, in some cases caused higher peak stresses (Section 5.3.4.4).

9.3.2 Temperature effect on natural slab release

Daytime warming of the near-surface layers appeared to contribute to instability of natural slab avalanches. The layer-parallel shear strain rate increased in the weak layer. Also, layers below the warming front were affected (Section 8.3.2.3). Consequently, the peak shear stress along the perimeter of a deficit zone may reach critical values for ductile to brittle transition and self-propagation (Section 1.4.2) of the initial deficit zone. This process may explain natural slab release as often observed during the first exposure to solar radiation after a storm.

9.4 Limitation and future research

All skier and snowmobile experiments were concerned with measuring normal stresses and were conducted in level terrain. Shear stresses were not measured.

Snow stiffness changes due to warming and cooling were indirectly derived from hand hardness measurements and push gauge measurements in all experiments of this thesis. Snowpack stability changes due to warming were not directly measured due to the challenges of their infrequent occurrence.

The following list provides objectives for future research:

- Conduct a FEM analysis on the effect of the rigid stress sensor plate on snowpack stiffness.
- Measure shear stresses due to skier and snowmobiles on a slope and include effects of temperature changes of the slab. Ideally, realistic loading is applied, such as a skier skiing downhill or falling, and a snowmobile riding uphill on a steep slope including the effect of a digging track.
- Determine the susceptibility of various slab weak layer combinations to stability changes due to warming.
- Directly measure and quantify stability changes due to surface warming. A suitable stability test appears to be the Propagation Saw Test (Reuter and Schweizer, 2001) or the Extended Column Test (Simenhois and Birkeland, 2008). Ideally stability decrease can be verified by slab avalanche release.
- Measure the temperature effect on creep of the near-surface layers on various slope angles that are relevant for backcountry users (approximately 25 – 45°) for various slab and weak layer systems of different stiffness.
- Include direct stiffness measurements of the slab. The snow penetrometer SnowMicroPen (Reuter, 2010) appears to be a suitable device to measure slab stiffness changes due to near-surface warming.
- As a long-term goal, develop a model to predict the stability trend due to daytime warming which is based on the initial snowpack structure and the daily weather forecast as input parameters.

CHAPTER 10

Discussion of applications

10.1 Overview of effects of near-surface warming on various slab and weak layer combinations

This section summarises the effect of near-surface warming on snowpack stability with regard to the initial snowpack conditions before the warming (Table 10.1). This summary is derived from the results of this thesis, other published work (Section 2.2), and empirical knowledge and observations (Section 2.2.1).

Table 10.1. Overview of the warming effect on potential snowpack stability changes for various snowpack conditions.

Weak layer (WL)	Initial snow (slab) above WL	Warming event	Stability trend
No WL	Cold low density	Rapid (solar)	Temporary decrease, then increase
	Any other	Any other	Increase
Shallow WL (less than 60 to 80 cm)	Loose (non-cohesive)	Mild conditions or warming	Decrease with settlement in slab (increased cohesion)
	Cohesive	Rapid	Decrease
		Slow, gradual	Increase (over longer time period)
Deep WL (>80 to 100 cm)	Cohesive	Daytime warming (rapid or gradual)	Usually no change
		Multiday warming (as one of other factors)	Decrease

The effect of surface warming on snowpack stability cannot be generalized since it is depends on many factors such as the temperature range, warming rate, thickness and cohesiveness of the overlying slab, and type and depth of the weak layer. All these factors determine the susceptibility of the slab and weak layer as a mechanical system to warming induced stability changes (McClung, 1996). In particular, for the timing of warming induced slab avalanche releases no general rules of thumb can be formulated due to the number of complicating factors, the interaction of which is still poorly understood (Schweizer and Jamieson, 2010). Natural loading due to snowfall, rain and redistribution due to wind in combination with warming are not addressed here.

In general, as long as the snowpack is mostly dry and no weak layer is present daytime warming does likely not cause instability. In most cases when temperature changes cause decreasing stability a slab/weak layer combination was already present that only requires a trigger. In those cases, warming, and in particular, the effect of direct solar radiation, can rapidly contribute to instability.

In the following paragraphs the bolded header at the beginning describes the initial snowpack conditions before the warming:

No pre-existing WL: Usually, if no pre-existing weak layer is present under most warming conditions the snowpack gains strength due to settlement, rounding and growing bonds between snow grains (McClung, and Schaerer, 2006, p. 75). In rare cases, when cold low-density snow is exposed to strong solar radiation, the near surface layers can settle into a reactive slab that sits on top of still colder low-density snow (Section 9.3.2). In those incidents where ski guides reported deteriorating stability (cracking, whumpfing or slab release) of a dry snowpack within hours during intense solar radiation (see Section 2.2.1), increased creep rates may have contributed to the critical conditions (Figure 10.1). Settlement only increased in the near surface layers, whereas slope parallel strain rate increased in deeper layers (Section 8.3). In other words, settling and stiffening of the near surface layers and increased strain rate on a potentially pre-existing weak layer below may actually create a reactive slab/weak layer system. Presumably, rapid solar warming and settlement stiffened the near surface layer and turned it into a releasable slab. A buried, subtle storm snow layer may have turned into a reactive sliding surface with the stiffening slab on top. With ongoing warming this temporary stage of instability probably stabilizes subsequently due to strengthening of the storm snow layer. Stability appears to decrease over a few hours, but with ongoing

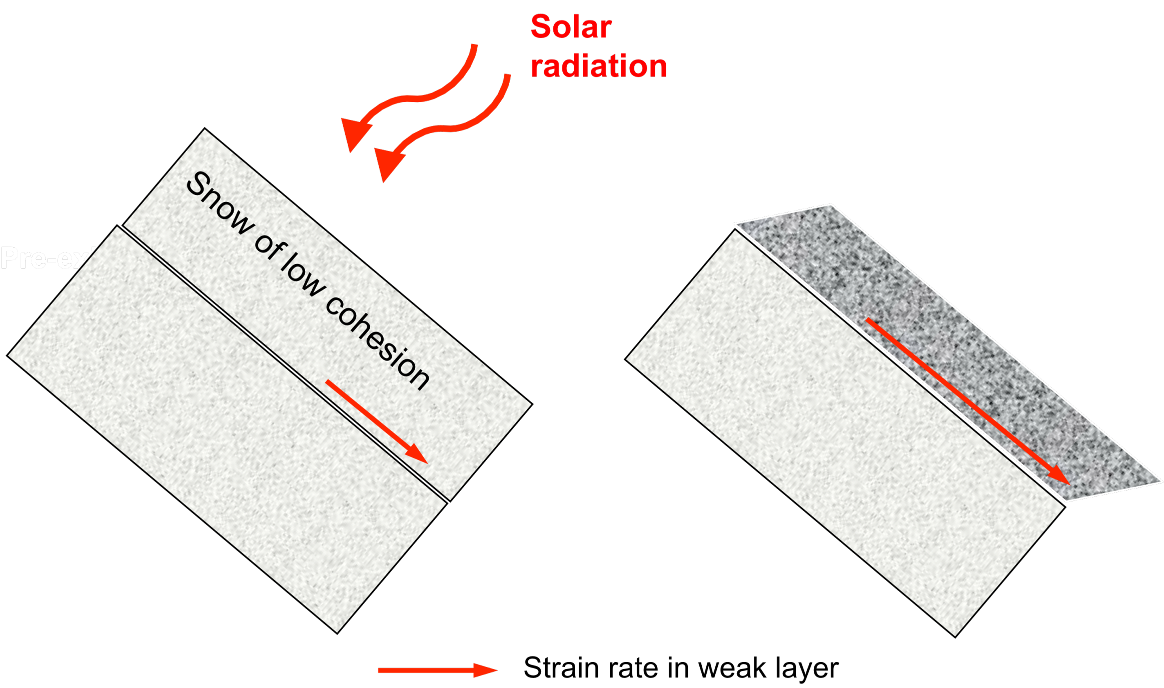

Figure 10.1. 2D diagram of cold low-density snow settling into a potentially reactive slab due to solar warming while slope parallel strain rate increases.

settlement the slab/weak layer system likely gains strength again. In this case, it is typically the first exposure to solar radiation that can cause rapid stability decrease due to strain rate increase in the weak layer.

Loose snow over WL: In case of an already existing weak layer that is only covered by loose, low density snow the snowpack is initially stable. This snow lacks cohesiveness (stiffness) to transmit stresses and propagate an initiated weak layer fracture. With ongoing settlement, faster at temperatures above approximately -10˚C to -7˚C, a slab builds on top of the weak layer and stability decreases. Subsequently, with prolonged warming and the warming front penetrating deeper into the snowpack the weak layer likely gains strength and stability increases.

Slab over WL: In case of a shallow slab, within the range of skier-triggering to approximately 60 to 80 cm, that is already overlying a weak layer, rapid warming contributes to instability. Prolonged or slow gradual warming over days likely strengthens and stiffens the slab/weak layer system.

Deep slab instability: Deep weak layers, below approximately 80 to 100 cm depth, are usually not directly affected by daytime warming. The warming trend likely needs to last for multiple days to warm up enough of the slab and indirectly increase shear strain rate in deeper weak layers. In many cases multiday-warming and loading due to precipitation and redistribution by winds go hand in hand to release deep slabs (Jamieson and others, 2000). In many cases, slab thickness in the start zones appears to be quite variable. Most likely the fracture is initiated in those thinner areas, for example in wind affected or in weaker zones that consist of faceted layers and depth hoar (Logan, 1993).

10.2 Effect of daytime warming of the near-surface layers on natural slab release

When initially low-density snow above the weak layer increases stiffness, forces can be transmitted laterally in the slab and the localized weak layer fracture may propagate. Both propagation models that were introduced in Section 1.4.2, deficit zone model and bending/collapse model, require a stiff slab to drive the fracture laterally.

Decreasing stiffness of an initially relatively stiff slab increases the releasable strain energy that becomes available for fracture propagation during the fracture process. This applies for both, the deficit zone model and the collapse model (Section 1.4.2).

10.3 Time scale of direct-immediate and indirect-delayed effects on stability

Immediate effects of warming that contribute to instability (Section 2.2.4) can occur on a time scale from less than an hour to a few hours depending on the depth of the weak layer. Rapid direct-immediate changes generally decrease stability before delayed micro-structural changes typically cause a strengthening of the snowpack and promote stability over one or more days. (Sections 5.3.4.2 and 7.4.2.3).

The cold lab experiments (Section 7.4.2.2) suggest that during relatively short-term warming to 0˚C of surface temperatures and moistening of the surface snow, strong settlement and densification normal stresses due to local surface loads tend to decrease. In this case, despite the short-term warming, delayed effects likely strengthen the near-surface layers. Regardless, the potential increase of slope parallel shear strain rate may still be the crucial factor that promotes instability.

References

Abe, O., 2001. Creep experiments and numerical simulations of very light artificial snowpacks. *Annals of Glaciology*, 32, 39–42.

Armstrong, R.L. 1980. An analysis of compressive strain in adjacent temperature-gradient and equi-temperature layers in a natural snow cover. *Journal of Glaciology*, 26(94), 283–289.

Bader, H.P., Salm B., 1990. On the mechanics of snow slab release. *Cold Regions Science and Technology*, 17, 287–300.

Bakermans, L., Jamieson, B., 2009. SWarm: A simple regression model to estimate near-surface snowpack warming for backcountry avalanche forecasting. *Cold Regions Science and Technology*, 59(2-3), 133–142.

Bevington, P.R., Robinson, D.K., 2002. Data reduction and error analysis for the physical sciences, 3rd Ed., McGraw-Hill, 336 pages.

Birkland, K., Schweizer, J., Jamieson, B., 2009. Fracture propagation: Recent research and implications. *The Avalanche Review*, 27 (4), 28–29.

Blaisdell, G.L., Richmond, P.W., Shoop, S.A., Green, C.E., Alger, R.G., 1990. Wheels and tracks in snow: validation study of the CRREL shallow snow mobility model. *CRREL Report No. 90-9.* U.S. Army Cold Regions Research and Engineering Laboratory, Hanover, NH.

Borstad, C., McClung, D. M., 2008. Slab fracture at 1900 frames per second - experimental methods. *Proceedings of the International Snow Science Workshop*, Whistler, B.C. Canada, 21-27 September, 2008, 22–24.

Boussinesque, J., 1885. Application des potentiels à l'étude de l'équilibre et du mouvement des solides élastiques. Gauthier-Villars, 721 pages.

Bucher, E., 1948. Contribution to the theoretical foundations of avalanche defense construction. *Snow, Ice and Permafrost Research Establishment,* Translation 18, 1956, 99 pages.

Burmister, D.M., 1945. The general theory of stresses and displacements in layered systems I, II, III. *Journal of Applied Physics*, 16, 89–96, 126–127, 296–302.

Camponovo, C., Schweizer J., 1997. Measurements on skier triggering. *Proceedings of the International Snow Science Workshop*, Banff, AB, Canada, 100–103.

Canadian Avalanche Association (CAA), 2007. Observation Guidelines and Recording Standards for Weather, Snowpack and Avalanches. *Canadian Avalanche Association*, Revelstoke, BC, Canada, 88 pages.

Canadian Avalanche Association (CAA), 2010. Fatality statistics. Retrieved from http://www.avalanche.ca/cac/about/media/Fatality_Statistics, August 2011.

Canadian Avalanche Association (CAA), 2011. Technical avalanche hazard analysis. Retrieved from http://www.avalanche.ca/cac/bulletins/latest/north-columbia, June 2011.

Chalmers, T.S., Jamieson, B., 2001. A snow-profile-based forecasting model for skier-triggered avalanches on surface hoar layers in the Columbia Mountains of Canada. *Cold Regions Science and Technology,* 33, 163–177.

Chandel, C., Srivastava, P. K., Upadhyay, A., 2007. Estimation of rheological properties of snow subjected to creep. *Defense Science Journal*, 57 (4), 539–547.

Colbeck, S.C., 1991. The layered character of snow covers. *Reviews of Geophysics, 29*(1), 81–96.

Colbeck, S.C., 1997. A review of sintering in seasonal snow. *CRREL report 97-10*, U.S. Army Cold Regions Research and Engineering Laboratory, Hanover, NH, 11 pages.

Colbeck, S.C., 1998. Sintering in a dry snow cover. *Journal of Applied Physics,* 84(8), 4585–4589.

Conway, H., 1998. The impact of surface perturbations on snow-slope stability. *Annals of Glaciology,* 26, 307–312.

Conway, H., Wilbour, C., 1999. Evolution of snow slope stability during storms. *Cold Regions Science and Technology,* 30(1-3), 67–77.

Curtis, J.O., Smith, F.W., 1974. Material property and boundary condition effects on stresses in avalanche snowpacks. *Journal of Glaciology*, 13(67), 99–108.

Das, B.M., 2008. Advanced soil mechanics. Taylor and Francis, 567 pages.

Davis, R.E., Elder, K., Howlett, D., Bouzaglou, E., 1999. Relating storm and weather factors to dry slab avalanche activity at Alta, Utah, and Mammoth Mountain, California, using classification and regression trees. *Cold Regions Science and Technology,* 30(1-3), 79–89.

de Quervain, M.R., 1966. Problems of avalanche research. *International Association of Hydrological Sciences Publication 69* (Symposium at Davos, 1965. Scientific Aspects of Snow and Ice Avalanches), 1–8.

Exner, T., 2006. The effect of warming on dry snow slab avalanches: Results from avalanche accident statistics and surveys. *Course project report ENCI 753*, Department of Geoscience, University of Calgary, 15 pages.

Exner, T., Jamieson, B., 2008. Can solar warming contribute to dry slab avalanches?, *Avalanche.ca - The Journal of Canada's Avalanche Community*, 84, 70–73.

Exner, T., Jamieson, B., 2008. The effect of snowpack warming on the stress bulb below a skier. *Proceedings of the International Snow Science Workshop*, Whistler, Canada, 415–420.

Exner, T., Jamieson, B., 2009. The effect of daytime warming on snowpack creep. *Proceedings of the International Snow Science Workshop*, Davos, Switzerland, 271–275.

Fierz, C., Armstrong, R.L., Durand, Y., Etchevers, P., Greene, E., McClung, D.M., Nishimura, K., Satyawali, P.K., Sokratov, S.A., 2009. The International

Classification for Seasonal Snow on the Ground. IHP-VII Technical Documents in Hydrology N°83, IACS Contribution N°1, UNESCO-IHP, Paris, 79 pages.

Föhn, P.M.B, 1987. The stability index and various triggering mechanisms. In: B. Salm and H. Gubler, eds., Avalanche Formation, Movement and Effects. International Association of Hydrological Sciences, Publication No. 162, 195–211.

Forest Products Laboratory, 1987. Wood Handbook: Wood as an Engineering Material. *USDA Agricultural Handbook No. 72*, U.S. Govt. Print. Off. Washington, DC.

Fukuzawa, T., Narita, H.,1993. An experimental study on the mechanical behavior of depth hoar under shear stress. *Proceedings of the International Snow Science Workshop*, Breckenridge, Colorado, U.S.A.,171–175.

Gallardo, R. L., 2003. Nieve y avalanchas, una blanca historia de riesgos en montaña. *Literatura y Lingüística Nº14*, doi: 10.4067/S0716-5811200300-1400020, 307 pages.

Gauthier, D.M., 2007. A practical field test for fracture propagation and arrest in weak snowpack layers in relation to slab avalanche release. PhD thesis, Dept. of Civil Engineering, University of Calgary, Canada. 302 pages.

Green, S. B., 1991. How many subjects does it take to do a regression analysis? *Multivariate Behavioral Research, 26*, 499–510.

Grey, D. M., Male, D. H., 1981. Handbook of snow. Pergamon, 765 pages.

Gubler, H., 1977. Artificial release of avalanches by explosives. *Journal of Glaciology*, 19(81), 419–429.

Habermann, M., Schweizer J., Jamieson J.B., 2008. Influence of snowpack layering on human-triggered snow slab avalanche release. *Cold Regions Science and Technology*, 54(3), 176–182.

Harvey S., Signorell, C., 2002. Avalanche accidents in backcountry terrain of the Swiss alps: New investigations of a 30 year database. *Proceedings of the International Snow and Science Workshop*, Penticton, B.C., Canada, 449–455.

Haegeli, P., McClung, D., 2007. Expanding the snow-climate classification with avalanche-relevant information: initial description of avalanche winter regimes for southwestern Canada. *Journal of Glaciology*, 53(181), 266–276.

Haehnel, R. B., Shoop, S. A., 2004. A macroscale model for low density snow subjected to rapid loading. *Cold Regions Science and Technology*, 40, 193–211.

Haynes, F. D., 1978. Effect of temperature on the strength of snow and ice. Department of the Army, Cold Regions Research and Engineering Laboratory*, CRREL Report 78–27*, Hanover, New Hampshire.

Heierli, J., Zaiser, M., 2008. Failure initiation in snow stratifications containing weak layers: Nucleation of whumpfs and slab avalanches. *Cold Regions Science and Technology*, 52, 385–400.

Hirashima, H., Abe, O., Sato, A., Lehning, M., 2008. Implementation of depth hoar factor into the SNOWPACK model. *Proceedings of the International Snow Science Workshop*, Whistler, B.C., Canada. 970–977.

HeliCat Canada Association, 2002. Analysis of socio-sconomic benefits of helicopter and snowcat skiing in British Columbia. HeliCat Canada Associaiton, Report prepared by Brent Harley and Associates, Vernon, BC, 48 pages.

Hoeller, P., 1998. Snow stability and its variation in course of time. *Proceedings of the International Snow Science Workshop*, Sunriver, OR, 474–477.

Hogarth, R.M., 2001. Educating intuition. *The University of Chicago Press*, Chicago, U.S.A., 357 pages.

International Commission for Alpine Rescue, 2010. Retrieved from http://www.ikar-cisa.org/eXtraEngine3/WebObjects/eXtraEngine3.woa/wa/menu?id=298&lang=en, June 2011.

Jamieson, J. B., 2000. Backcountry Avalanche Awareness. Canadian Avalanche Association, 7th edition, Revelstoke, Canada, 78 pages.

Jamieson, J. B., 2006. Formation of refrozen snowpack layers and their role in slab avalanche release. *Review of Geophysics*, 44, RG2001, doi:10.1029/2005RG000176.

Jamieson, J. B., Geldsetzer, T., Stethem, C., 2000. Case study of a deep slab instability and associated dry avalanches. *Proceedings of the International Snow Science Workshop*, Big Sky, Montana, 101–108.

Jamieson, J. B., Johnston, C. D., 1998. Refinements to the stability index for skier-triggered dry slab avalanches. *Annals of Glaciology*, 26, 296–302.

Jamieson, J. B., Haegeli, P., Schweizer, J., 2009. Field observations for estimating the local avalanche danger in the Columbia Mountains of Canada. *Cold Regions Science and Technology,* 58, 84–91.

Jamieson, J. B., Haegeli, P., Gauthier, D., 2010. Avalanche accidents in Canada 1996 – 2007, *Canadian Avalanche Association*, 5, 427 pages.

Jamieson, J. B., Svederus, D., Zacaruk, D., 2007. Sledding in avalanche terrain. *Canadian Avalanche Association*, 50 pages.

Jamieson, J. B., Stethem, C., 2002. Snow avalanche hazards and management in Canada: Challenges and progress. *Natural Hazards,* 26, 35–53.

Jamieson, J. B., Schweizer, J., Shea, C., 2009. Simple calculations of risk for backcountry skiing. *Proceedings of the International Snow Science Workshop*, Davos, Switzerland, 336–340.

Johnson, B, Jamieson J. B., Johnston C.D., 2000. Field data and theory for human-triggered "whumpfs" and remote avalanches. *Proceedings of the International Snow Science Workshop,* Big Sky, Montana, 208–214.

Johnson, J. B., 1980. A model for snow-slab failure under conditions of dynamic loading. *Journal of Glaciology*, 26(94), 245–254.

Johnson, B. C., Jamieson, J. B., Stewart, R. R., 2004. Seismic measurement of fracture speed in a weak snowpack layer. *Cold Regions Science and Technology*, 40(1-2), 41–45.

Jones, A., Jamieson, J. B., Schweizer, J., 2006. The effect of slab and bed surface stiffness on the skier-induced shear stress in weak snowpack layers. *Proceedings of the International Snow Science Workshop*, Telluride, CO, 157–164.

Jones, A., Jamieson, J. B., 2001. Meteorological forecasting variables associated with skier-triggered dry slab avalanches. *Cold Regions Science and Technology,* 33, 223–236.

Jordan, R. E., Albert, M., Brun, E., 2008. Physical processes within the snow cover and their parameterization. *In: R.L. Armstrong, Brun E., Snow and climate: physical processes, surface energy exchange and modeling.* Cambridge University Press, Cambridge, U.K., 12–69.

Kaps, P., Moessner, W., Nachbauer, W., Stenberg, R., 2000. Pressure distribution under a ski during carved turns. *2nd International Congress on Skiing and Science (ICSS)*, St. Christoph am Arlberg, Austria, E. Mueller, R. Roithner, W. Niessen, Ch. Raschner, H. Schameder, (Editors), 1–18.

Keeler, C.M., 1969. The growth of bonds and the increase of mechanical strength in a dry seasonal snowpack. *Journal of Glaciology*, 8(54), 441–450.

King, J.C., Pomeroy, J.W., Gray, D.M., Fierz, C., Föhn, P.M.B., Harding, R.J., Jordan, R.E., Martin, E., Plüss, C., 2008. Snow–atmosphere energy and mass balance. *In: R.L. Armstrong, Brun E., Snow and climate: physical processes, surface energy exchange and modeling.* Cambridge University Press, Cambridge, U.K., 70–124.

Kirchner, H., Michot, G., Narita, H., Suzuki, T., 2001. Snow as a foam of ice: plasticity, fracture and the brittle-to-ductile transition. *Philosophical Magazine A,* 81, 2161–2181.

Kirchner, H., Michot, G., Schweizer, J., 2002. Fracture toughness of snow in shear and tension. *Scripta Materialia*, 46(6), 425–429.

LaChapelle, E.R., 1980. The fundamental processes in conventional avalanche forecasting. *Journal of Glaciology*, 26(94), 75–84.

Lind, D., Sanders, S.P., 2003. The physics of skiing. Springer. 266 pages.

Lipson, C., Sheth, N. J., 1973. Statistical design and analysis of engineering experiments. McGraw-Hill, 518 pages.

Logan, N., 1993. Snow temperature patterns and artificial release, *Proceedings of the International Snow Science Workshop.* Breckenridge, Colorado, 37–46.

Louchet, F., 2001a. Creep instability of the weak layer and natural slab avalanche triggering. *Cold Regions Science and Technology*, 33 (2-3), 141–146.

Louchet, F., 2001b. A transition in dry-snow slab avalanche triggering modes. *Annals of Glaciology*, 32, 285–289.

Marshall, H. P., Pielmeier, C., Havens, S., Techel, F., 2010. Slope-scale snowpack stability derived from multiple Snowmicropen measurements and high-resolution terrestrial FMCW radar surveys. *Proceedings of the International Snow Science Workshop*, Squaw Valley, CA,102–109.

Meyer, S.L., 1975. Data analysis for scientists and engineers. Wiley. 513 pages.

McClung, D.M., 1979. Shear fracture precipitated by strain softening as a mechanism of dry slab avalanche release. *Journal of Geophysical Research*, 84(87), 3519–3526.

McClung, D. M., 1981. Failure characteristics of alpine snow in slow deformation. *Mechanics of Structured Media,* Proceedings of the International

Symposium on the Mechanical Behaviour of Structured Media, Ottawa, Canada, May 18-21,1981 Part A, Elsevier Scientific Publishing Company, Amsterdam, 409–418

McClung, D. M., 1984. Empirical corrections to snow creep pressure equations. *Canadian Geotechnical Journal*, 21 (1), 191–193.

McClung, D.M., 2002a. The elements of applied avalanche forecasting, Part I: The human issues, *Natural Hazards,* 25, 111–129.

McClung, D.M., 2002b. The elements of applied avalanche forecasting, Part II: The physical issues and the rules of applied avalanche forecasting, *Natural Hazards,* 26, 131–146.

McClung, D. M., 2003. Size scaling for dry snow slab release. Journal of Geophysical Research, 108(B10), 2465, doi:10.1029/2002JB002298, 1–12.

McClung, D.M., J. Schweizer, 1999. Skier triggering, snow temperatures and the stability index for dry-slab avalanche initiation. *Journal of Glaciology*, 45(150), 190–200.

McClung, D., 2009. Dry snow slab quasi-brittle fracture initiation and verification from field tests. *Journal of Geophysical Research*, 114, F01022, doi:10.1029/2007JF000913.

McClung, D. M., 2011. The critical size of macroscopic imperfections in dry snow slab avalanche initiation. *Journal of Geophysical Research.*, *116*, F03003, doi:10.1029/2010JF001866.

McClung, D. M., Schaerer, P. A., 2006. The Avalanche Handbook. The Mountaineers, Seattle, Washington, U.S.A., 342 pages.

Mellor, M., Smith, J. H., 1966. Creep of snow and ice. CRREL, Research Report 220, Hanover, New Hampshire, 14 pages.

Mellor, M., 1975. A review of basic snow mechanics. *Snow Mechanics Symposium, Proceedings of the Grindelwald Symposium,* April, 1974, International Association of Hydrological Sciences, Washington, D.C., Publication No. 114, 251–291.

Munter, W., 2009. 3x3 Lawinen, Risikomanagement im Wintersport. Pohl & Schellhammer, Garmisch-Partenkirchen, Germany, 230 pages.

Olagne, X., McClung, D. M., 1990. Nonlinear formulation of snow creep. *Cold Regions Science and Technology*, 19, 1–18.

Palmer, A.C. , Rice J.R. 1973. The growth of slip surfaces in the progressive failure of over-consolidated clay. *Proc. Roy. Soc.* Lond. A . 332, 527-548.

Pedrenko, V.F., Withworth, R.W., 1999. Physics of ice. Oxford University Press, New York. 373 pages.

Petrovic, J.J., 2003. Review – Mechanical properties of ice and snow. *Journal of Material Sciences*, 38, 1–6.

Perla, R.I., 1976. Slab avalanche measurements. *Proceedings of the 29th Canadian Geotechnical Conference*, Canadian Geotechnical Society, Vancouver, B.C., Part VII, 1–15.

Perla, R.I., Ommanney, C.S.L., 1985. Snow in strong or weak temperature gradients. Part I: Experiments and qualitative observations. *Cold Regions Science and Technology*, 11, 23–35.

Piziali, R.L., Mote Jr, C.D., 1972. Snow ski as a dynamic system. *Journal of Dynamic Systems, Measurement & Control*, 94 (G2), 133–138.

Podolskiy, E.A., Sato, A., Komori, J., 2009. Avalanche issue in Western Himalaya. *SEPPYO - Journal of the Japanese Society of Snow and Ice*, 71(6), 498–502.

Pressure Profile Systems, 2007. http://www.pressureprofile.com/UserFiles/file/PPS%20_ConTacts_Specsheets_08_18_10.pdf, retrieved, April, 2012.

Reiweger, I., Schweizer, J., 2010. Failure of a layer of buried surface hoar, *Geophysical Research Letters*, *37*, L24501, doi:10.1029/2010GL045433.

Reuter, B., 2010. The effect of surface warming on snowpack stability. MSc thesis, University of Innsbruck, Austria, Faculty of Geo- and Atmospheric Sciences, 78 pages.

Reuter, B., Schweizer, J., 2011. The effect of surface warming on snow slab stiffness and fracture propagation propensity in avalanche snowpacks. *Geophysical Research Abstracts,* Vol. 13, EGU2011-13929, 2011 EGU General Assembly.

Richmond, D., 2000. What research we would like to see. *Proceedings of the International Snow Science Workshop,* Big Sky, Montana, 592–594.

Roch, A., 1966. Les Variations de la Resistance de la Neige. *Proceedings of the International Symposium on Scientific Aspects of Snow and Ice Avalanches*, Gentbrugge, Belgium, International Association of Hydrological Sciences, 86–99.

Salm, B., 1977. Snow forces. *Journal of Glaciology,* 19(81), 67–99.

Schweizer, J., 1993. The influence of the layered character of snow cover on the triggering of slab avalanches. *Annals of Glaciology,* 18, 193–198.

Schweizer, J., 1998. Laboratory experiments on shear failure of snow. *Annals of Glaciology,* 26, 97–102.

Schweizer, J., 1999. Review of dry snow slab avalanche release. *Cold Regions Science and Technology*, 30(1-3), 43–57.

Schweizer, J., Camponovo, C., Fierz C., Föhn, P.M.B. 1995a. Skier-triggered slab avalanche release - some practical implications. *Proceedings of the International Symposium at Chamonix*, 30 - 3 June 1995: The Contribution of Scientific Research to Snow, Ice and Avalanche Safety. Association Nationale pour l'Etude de la Neige et des Avalanches. Grenoble.

Schweizer, J., Schneebeli, M., Fierz, C., Foehn, P. M. B, 1995b. Snow mechanics and avalanche formation: Field experiments on the dynamic response of the snow cover. *Surveys in Geophysics,* 16, 621–633.

Schweizer, J., Camponovo, C., 2001a. The skier's zone of influence in triggering slab avalanches. *Annals of Glaciology*, 32, 314–320.

Schweizer, J., Camponovo, C., 2002. The temperature dependence of the effective elastic shear modulus of snow. *Cold Regions Science and Technology*, 35, 55–64.

Schweizer, J., Jamieson, J.B., 2001. Snow cover properties for skier triggering of avalanches. *Cold Regions Science and Technology*, 33, 207–221.

Schweizer, J., Jamieson, B., 2010. On surface warming and snow instability. *Proceedings of the International Snow Science Workshop*. Squaw Valley, CA, 619–622.

Schweizer, J., Jamieson, J. B., Schneebeli, M. 2003. Snow avalanche formation. *Reviews of Geophysics*, 41(4), 1016, doi:10.1029/2002RG000123.

Schweizer J., Lütschg M. 2001. Characteristics of human triggered avalanches. *Cold Regions Science and Technology*, 33, 147–162.

Schweizer, J., Michot, G., Kirchner O.K., 2004. On the fracture toughness of snow. *Annals of Glaciology*, 38,1–8.

Schulson, E. M., 1999. The structure and mechanical behavior of Ice. *JOM – Journal of the Minerals, Metals and Materials Society*, 51(2), 21–27.

Scott, N., Yoneyama, T., Kagawa, H., Osada, K., 2007. Measurement of ski snow-pressure profiles. *Sports Engineering*, 10, 145–156.

Shea, C., Jamieson, B., 2011. Some fundamentals of handheld snow surface thermography. *The Cryosphere*, 5, 55–66.

Sigrist, C., 2006. Measurement of fracture mechanical properties of snow and application to dry snow slab avalanche release. Ph.D. thesis, Swiss Federal Institute of Technology, Zurich, Switzerland, 139 pages.

Simenhois, R., Birkland, K., 2008. Extended column test results during surface warming: Does surface warming affect fracture propagation potential? *Proceedings of the International Snow Science Workshop*, Whistler, British Columbia, 26–35.

Sinha, N.K., 1978a. Short-term rheology of polycrystalline ice. *Journal of Glaciology.* 21(85), 457–473.

Sinha, N.K., 1978b. Rheology of columnar-grained ice. *Exp. Mech*., 18 (12), 464–470.

Smith, F. W., 1972. Elastic stresses in layered snow packs. *Journal of Glaciology*, 11 (63), 407–414.

Smith, M., Jamieson, J.B., 2008. Observation and modeling of buried melt-freeze crusts. *Proceedings of the International Snow Science Workshop,* Whistler, BC, Canada, 170–178.

Spear, K. E., Visco, S., Wuchina, E.J., Wachsman, E. D., 2006. High temperature materials. *Interface*, The Electrochemical Society, 15 (1), 48–51.

Statham, G., Haegeli, P., Birkeland, K. W., Greene, E., Israelson, C., Tremper, B., Stethem, C., McMahon, B., White, B., Kelly, J., 2010. The North American public avalanche danger scale. *Proceedings of the International Snow Science Workshop,* Squaw Valley, California, 117–123.

Sturm, M., Holmgren, J., Konig, M., Morris K., 1997. The thermal conductivity of *seasonal* snow. *Journal of Glaciology*, 43 (143), 26–41.

Szabo, D., Schneebeli, M., 2007. Sub-second sintering of ice. *Applied Physics Letters*, 90, 4 pages.

Thumlert, S., 2010, Avalanche initiation through localized dynamic loading. *Course report ENCI 753*, Dept. of Civil Engineering, University of Calgary, Canada,18 pages.

Trautman, S.M., Custer G.C., Birkeland K.W., 2004. Investigations of wet snow instability in the intermountain climate zone. *Proceedings of the International Snow Science Workshop,* Jackson Hole, Wyoming, USA, 19-24 September.

Tremper, B., 2008. Staying alive in avalanche terrain. The Mountaineers Books, Seattle, 318 pages.

van Herwijnen, A., Heierli, J., 2009. Measurement of crack-face friction in collapsed weak snow layers. *Geophysical Research Letters*, *36*, L23502, doi:10.1029/2009GL040389.

Voitkovsky, K. F., Bozhinsky, V. N., Golubev, M. N., Laptev, M. N., Zhigulsky, Slesarenko, Y. Y., 1975. Creep-induced changes in structure and density of snow. *Structure*, 114, 171–179.

Wilson, A., Schweizer, J., Johnston, C., Jamieson, J. B., 1999. Effects of surface warming on a dry snowpack. *Cold Regions Science and Technology*, 30, 59–64.

Wood, A., 2007. New standards for snowmobile operators. *Avalanche.ca – Journal of the Canada's avalanche community*, Canadian Avalanche Association, 81, 72 pages.

Zeidler, A., Jamieson, J. B., 2006a. Refinements of empirical models to forecast the shear strength of persistent weak snow layers PART A: Layers of faceted crystals. *Cold Regions Science and Technology*, 44, 194–205.

Zeidler, A., Jamieson, B., 2006b. Refinements of empirical models to forecast the shear strength of persistent weak snow layers PART B: Layers of surface hoar crystals. *Cold Regions Science and Technology*, 44, 184–193.

Appendix Snowpack profiles of Chapter 5

a.

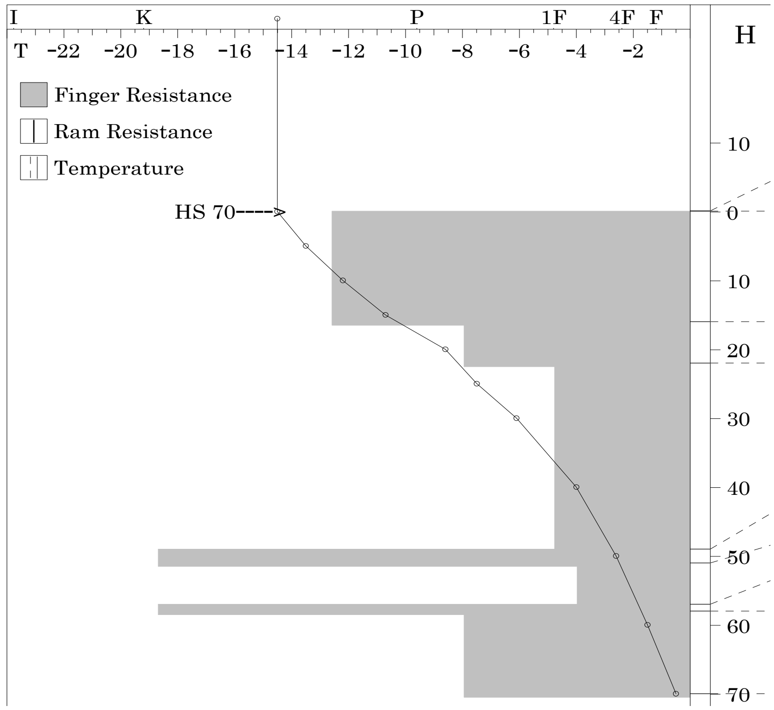

b.

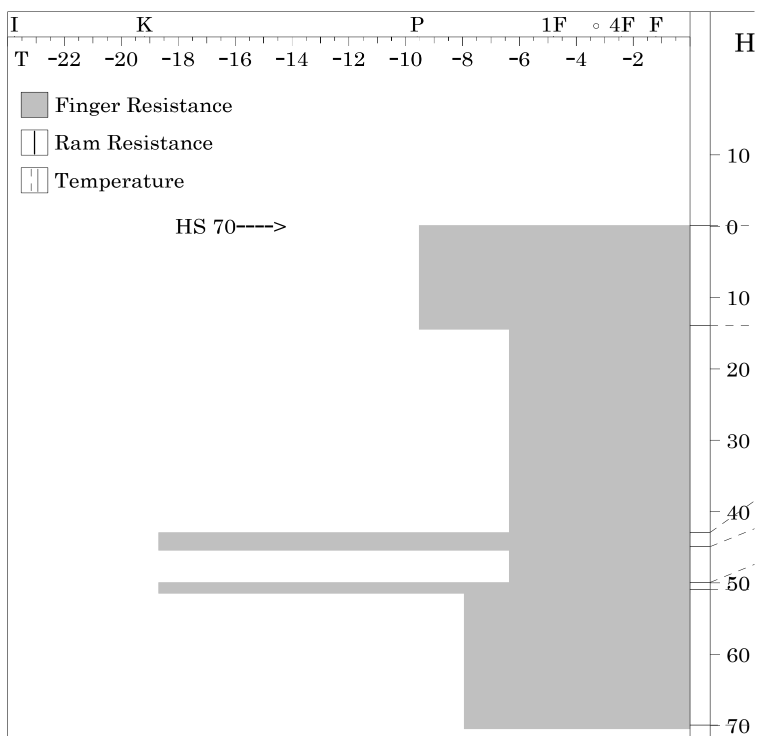

Figure A.1. Snowpack profiles of **(a)** Experiment 1_1 and **(b)** Experiment 1_4 in Chapter 5.

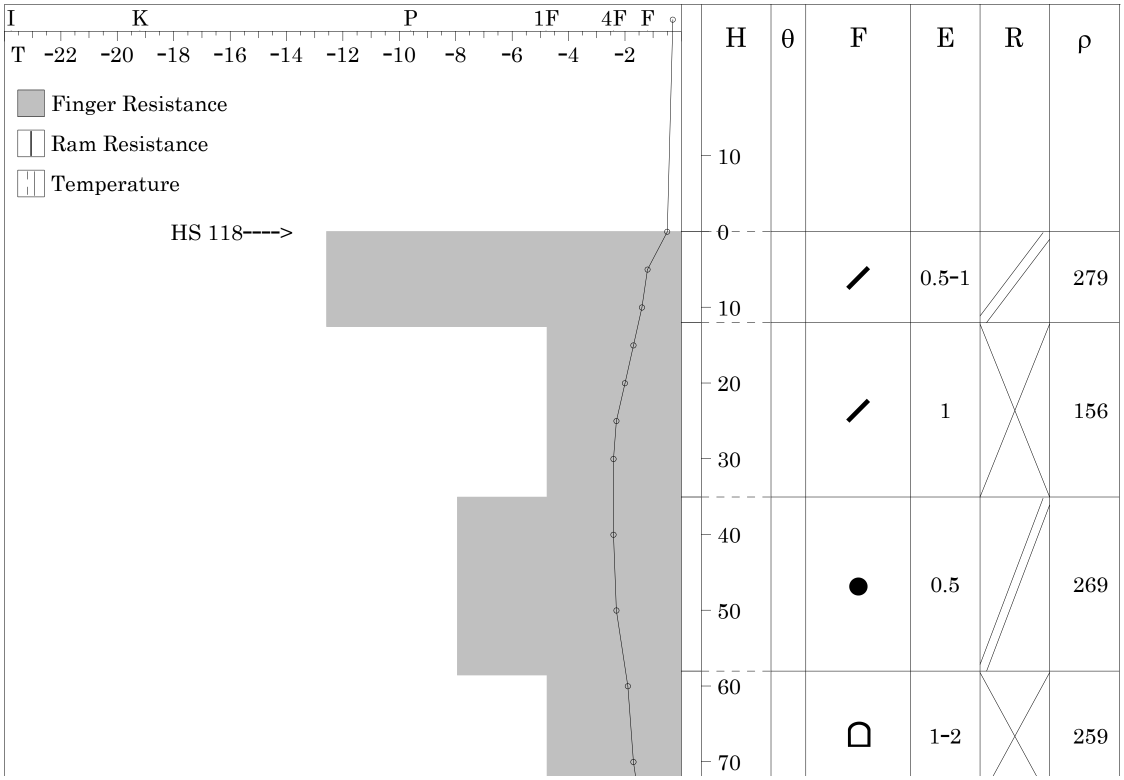

Figure A.2. Snowpack profile at the end of the cooling of Experiment 2 in Chapter 5.

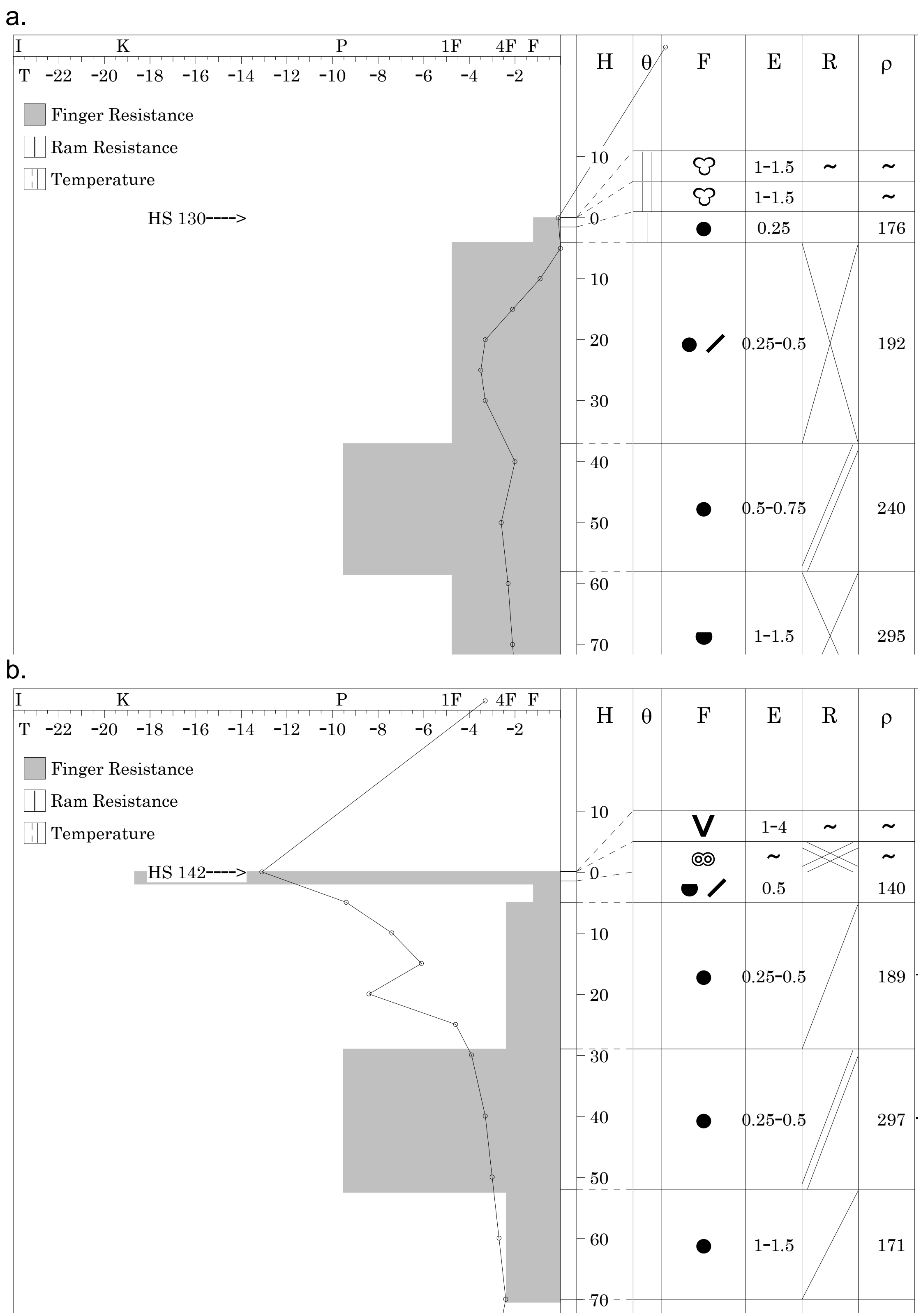

Figure A.3. Snowpack profiles for **(a)** Experiment 4_1 and **(b)** Experiment 4_2 in Chapter 5

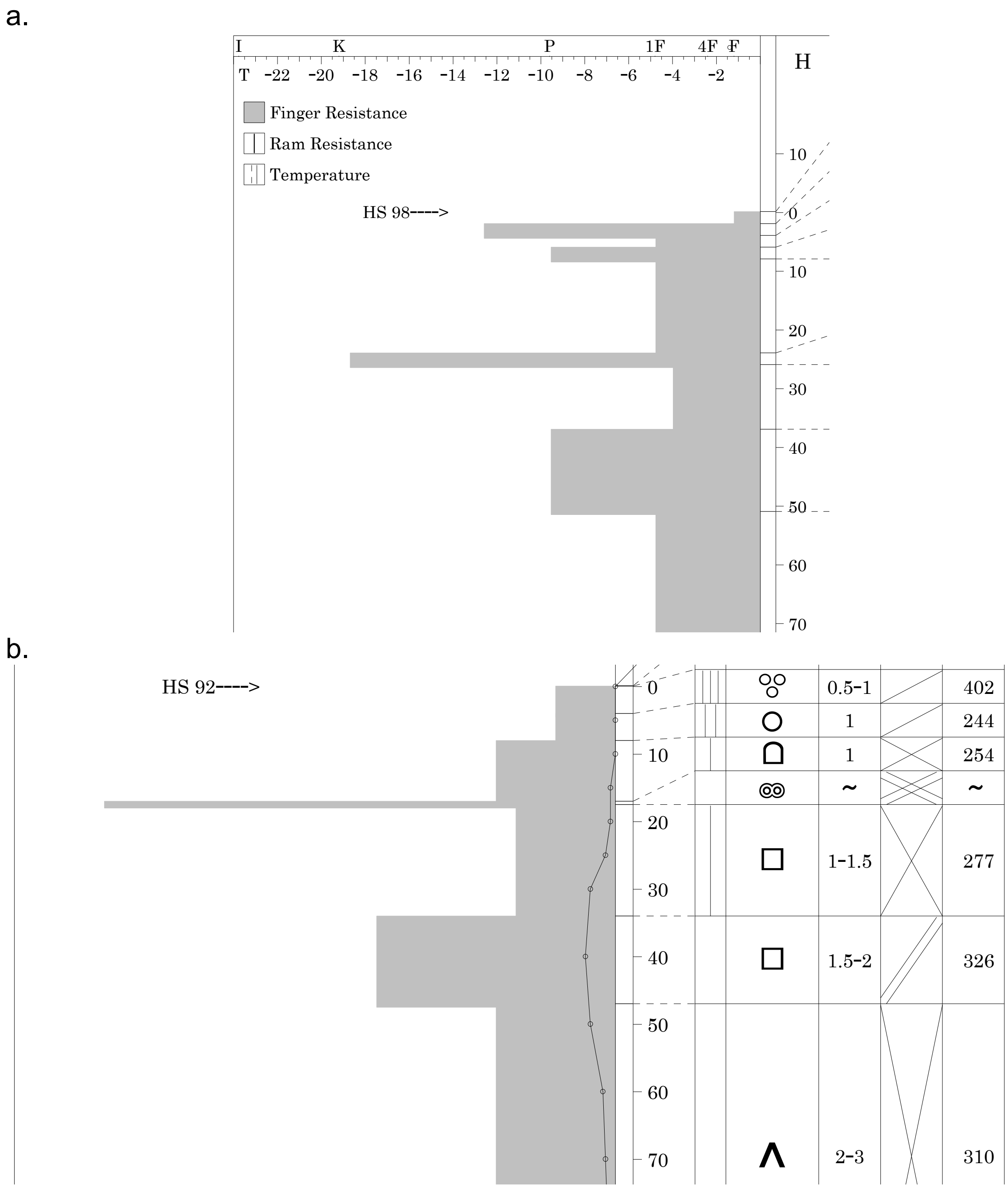

Figure A.4. Snow profiles of **(a)** Experiment 13_1 and **(b)** Experiment 13_2 in Chapter 5.